IAEA
International Atomic Energy Agency

INDC International Nuclear Data Committee

Translations of Selected Papers published in

Jadernye Konstanty (Nuclear Constants) 1, 2001

Translated by the IAEA

December 2002

Selected INDC documents may be downloaded in electronic form from
http://www-nds.iaea.org/reports-new/indc-reports/
or sent as an e-mail attachment.
Requests for hardcopy or e-mail transmittal should be directed to *services@iaeand.iaea.org*
or to:
Nuclear Data Section
International Atomic Energy Agency
Vienna International Centre
PO Box 100
A-1400 Vienna
Austria

Printed by the IAEA in Austria

December 2002

CONTENTS

NEUTRON CONSTANTS AND PARAMETERS

INVESTIGATION OF THE ^{93}Nb NEUTRON CROSS-SECTIONS IN RESONANCE ENERGY RANGE

Yu.V.Grigoriev, V.Ya.Kitaev, B.V. Zhuravlev,V.V.Sinitsa,
Institute of Physics and Power Engineering,Obninsk, Russia

S.B.Borzakov,H.Faikov-Stanchik[*], G.Ilchev, Zh.V.Mezentseva , Ts.Ts.Panteleev
Frank Laboratory of Neutron Physics, JINR, Dubna, Russia

G.N.Kim
University of Science and Technology, PAL, Pohang, Korea

The results of gamma-ray multiplicity spectra and transmission measurements for ^{93}Nb in energy range 21.5 eV-100 keV are presented. Gamma spectra from 1 to 7 multiplicity were measured on the 501 m and 121 m flight paths of the IBR-30 using a 16-section scintillation detector with a NaI(Tl) crystals of a total volume of 36 l and a 16-section liquid scintillation detector of a total volume of 80 l for metallic samples of 50, 80 mm in diameter and 1, 1.5 mm thickness with 100% ^{93}Nb. Besides, the total and scattering cross-section of ^{93}Nb were measured by means batteries of B-10 and He-3 counters on the 124 m, 504 m and 1006 m flight paths of the IBR-30. Spectra of multiplicity distribution were obtained for resolved resonances in the energy region E=30-6000 eV and for energy groups in the energy region E=21.5 eV-100 keV. They were used for determination of the average multiplicity, resonance parameters and capture cross-section in energy groups and for low-laying resonances of ^{93}Nb. Standard capture cross-sections of ^{238}U and experimental gamma-ray multiplicity spectra were also used for determination of capture cross-section ^{93}Nb in energy groups. Similar values were calculated using the ENDF/B-6 and JENDL-3 evaluated data libraries with the help of the GRUKON computer program. Within the limits of experimental errors there is observed an agreement between the experiment and calculation, but in some groups the experimental values differ from the calculated ones.

Introduction

Niobium is widely used material in the atomic reactors. It is in all energy reactors as ligature part of construction materials and as the fission product of a fuel. In connection with this, the measurements of neutron capture, scattering and total cross-sections for the ^{93}Nb and its self-shielding coefficients in resonance energy range are necessary because of theirs insufficient accuracy. Recently, we already carried out the measurements of the transmissions and self-indication functions for obtaining the average resonance parameters of ^{93}Nb in the energy range 0.465 – 200 keV [1]. Until now, it is essential to study the neutron capture cross-section, a resonance self - shielding effect and their temperature dependence. Now we have started the ^{93}Nb neutron capture and total cross-section measurements within 21.5 eV – 100 keV resonance energy region.

Experimental technique

The measurements of the neutron capture and total cross-sections were carried out on the 121 m (124 m) neutron flight paths of the IBR-30 (W = 10 kW, f = 100 Hz, τ = 4 μsec) with 16-section liquid scintillation detector of volume 80 l (the neutron ^{10}B detector) (setup Parus) and on the 501 m (503 m) ones with 16-section NaI(Tl) detector of volume 36 l (setup Romashka) [2] and with the neutron ^{3}He detector also. The general scheme of the multisectional liquid detector is given in Fig. 1.

The holes of the lead collimators in front of the liquid and NaI(Tl) γ-detectors were 70 mm and 60 mm diameter. The B$_4$C filters were placed in the beam for removing of recycled neutrons with the energy less than 0.8 eV (121 m) and 13 eV (501 m). Two metallic niobium samples with thickness of 1 mm and 1.5 mm and with the 50 mm and 80 mm diameters were used as the radiator samples in the liquid and NaI(Tl) detectors. The U$_3$O$_8$ powder with uranium-238 (99.999%) and by weight of 3.86 g, contained in the aluminum tank with the 46 mm inside diameter and the metallic disc of ^{238}U with the 80 mm diameter and the 0.25 mm thickness, were served as the standard radiator as well.

---

[*] Permanent address: University of Lodz, Lodz, Poland
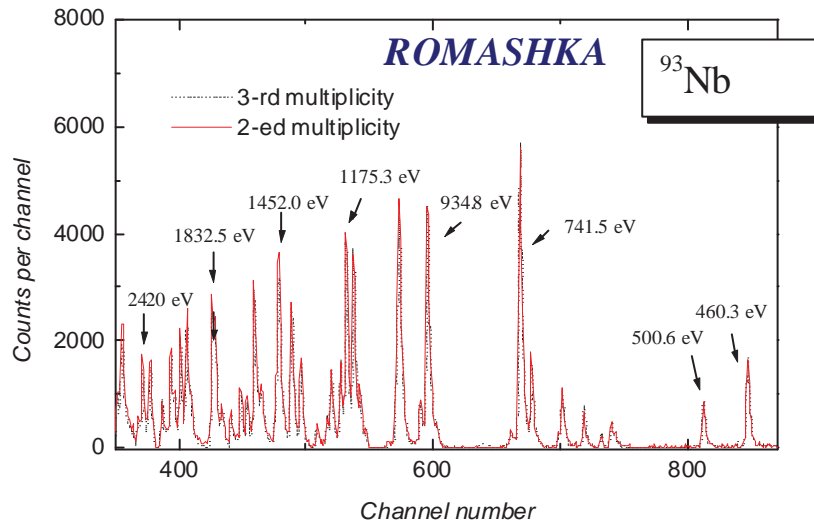
Fig. 1. The time-of-flight spectra of γ-ray coincidence summed from the 2^{ed} to 3rd multiplicity for ^{93}Nb inside "Romashka" on 501 m. (The time channel width – 2 μsec)

The detector had a new lead shielding with thickness of 10 cm. The shape of the lead shielding was changed. The neutron detector consists of a battery of three boron counters SNM-13 which were placed into a polyethylene disc 100 mm in diameter and 15 mm in thickness, was placed at 124 m from the IBR-30 fuel core. One ^{3}He neutron counter of SNM-18 type was placed after Romashka on 503 m flight paths. The liquid and NaI(Tl) detectors operated in the multiplicity coincidence spectrometry conditions. Figs. 2 and 3 show typical apparatus time-of-flight spectra. The background components from natural radioactivity are great, and the effect to background ratio for the liquid detector in third multiplicity spectrum is 100% in a best case. The background for the boron helium neutron detectors are 5-10%. The SNM-12 and SNM-18 counters were used as monitors.

Fig. 2. The multiplicity spectra of γ-ray coincidence for ^{93}Nb different s-and p-resonances

Fig. 3. The average multiplicity spectra for ^{93}Nb different s-resonances

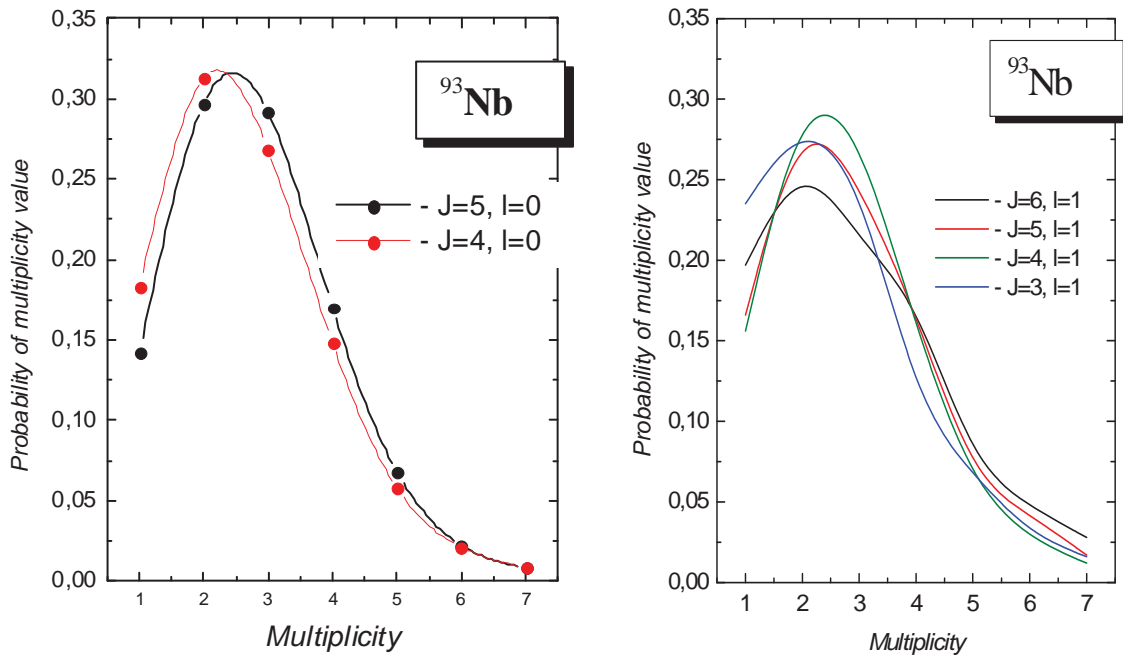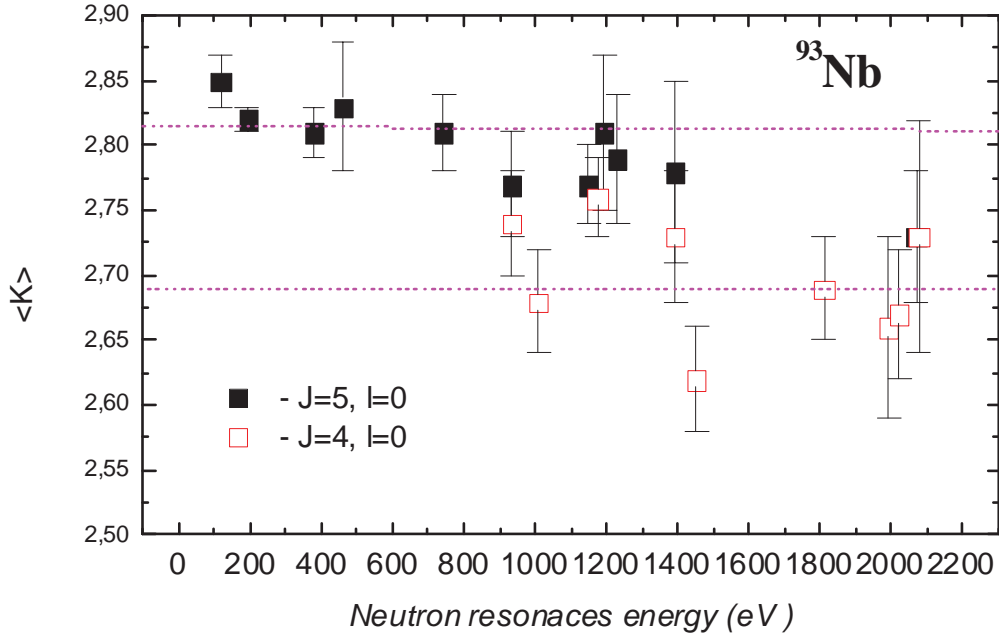## The processing technique and the results of measurements

Some runs of measurements were performed with the help of the liquid (n,γ) – detector (121 m) having used in turn the ^{93}Nb radiator sample and ^{238}U one. The measurements with the neutron boron detector (124 m) were carried out, when the niobium and uranium radiator samples in liquid detector were absent. After the background components had been subtracted and the time-of-flight spectra had been brought mutual monitor coefficient, one determined the quantity pulses in the energy groups of the BNAB constants system [3] over the energy region of 20 eV – 10 keV. Analogous measurements were carried out on the 501 m, 503 m and 1006 m flight paths by means the NaI(Tl) detector and the neutron helium detector. The integral counts within the energy groups are connected with a neutron flux and the neutron capture cross - section for the thin ^{238}U and ^{93}Nb samples of the following relations:

$$N_c^U / M^U = S^U n^U <\sigma_c>^U \varepsilon^U(E)\varphi(E), \quad N_c^{Nb} / M^{Nb} = S^{Nb} n^{Nb} <\sigma_c>^{Nb} \varepsilon^{Nb}(E)\varphi(E), \tag{1}$$

where: M^U and M^{Nb} are the monitor coefficients for the U and Nb, S^U and S^{Nb} are the areas , n^U and n^{Nb} are the thickness of radiator samples, $\varepsilon^U(E)$ and $\varepsilon^{Nb}(E)$ are the gamma - rays efficiencies of registration , $\varphi(E)$ is a neutron flux.

If to suppose that the gamma-rays efficiency of registration for the uranium and niobium samples is the same, one may get from relations (1) the expression to determine a capture cross -section according to a known ^{238}U capture cross-section:

$$<\sigma_c>^{Nb} = <\sigma_c>^U M^U S^U n^U N_c^{Nb} / M^{Nb} S^{Nb} n^{Nb} N_c^U \tag{2}$$

The mentioned liquid detector made it possible to define the time-of-flight spectra for 16 multiplicities of coincidences. However, due to an influence of scattered neutrons in the first three multiplicities, the summary spectrum corresponds to the sum of multiplicities from fourth to seventh. A neutron capture was not already observed with the eighth multiplicity spectrum.

After the grouping of total spectra was being done, and the ^{93}Nb - group capture cross-section, according to formula (2), was being determined. The group capture cross-sections for the ^{93}Nb and ^{238}U were obtained by the calculation with help GRUKON program [3] on the basis of the estimated data of various libraries also.

The experimental and calculated values of the group neutron capture cross-sections for niobium-93 and uranium-238 are shown in Table 1. The experimental errors of the capture cross-sections are about 7-10%. It is seen

from Table 1 that within the limits of experimental errors an agreement between the experiment and calculation is observed, but in the group 17 an experimental value is larger than calculated one.

The total transmissions were measured on two ^{93}Nb filter samples with thickness of 0.005784 at/b and 0.0074294 at/b. The group transmissions and observed cross - sections were determined by following formulas:

$$T_t(n, E, \theta) = _{\Delta E}\int \varphi(E)\varepsilon(E)e^{-\sigma(E,\theta)n}dE/_{\Delta E}\int \varphi(E)\varepsilon(E)dE = (N_s - F_s)M/(N_{o/b} - F_{o/b}),$$
$$\sigma_t^{ob} = (-\ln T_t)/n \tag{3},$$

where: $\varphi(E)$ is the neutron flux, $\varepsilon(E)$ is the detector efficiency, σ_t is the total cross-section, n is the thickness of the filter sample, E is the neutron energy , θ is the temperature of the filter sample, N_s and $N_{o/b}$ are the detector counts with sample and without it, F_s and $F_{o/b}$ are the detector backgrounds, M is the monitor coefficient, σ_t^{ob} is the observed total cross-section.

The group total cross-sections were obtained by extrapolating the observed experimental ones to zero thickness of the filter sample, i. e. by multiplication of the observed cross-sections by the calculated coefficients of the self-shielding:

$$<\sigma_t>^{exp} = K_{sh}\sigma_t^{ob}(n), K_{sh} = <\sigma_t>^{cal}/\sigma_t^{cal}(n) \tag{4},$$

where: $<\sigma_t>^{exp}$ and $<\sigma_t>^{cal}$ are the experimental and calculated group total cross-sections, $\sigma_t^{ob}(n)$ and $\sigma_t^{cal}(n)$ are the experimental and calculated the group observed total cross-sections for the filter sample n at/b thick.

The experimental and calculated group total and capture cross-sections for niobium-93 uranium-238 are shown in Table 1.

Table 1.

The experimental and calculated neutron capture cross-sections of the ^{93}Nb and ^{238}U

N_{gr}	E_{gr}(keV)	$<\sigma_c>^{Nb}$ (b)	$<\sigma_c>^{Nb}$[4]	$<\sigma_c>^{U}$[4]	$<\sigma_t>^{Nb}$(b)	$<\sigma_t>^{Nb}$[4]
9	100±46.5	-	0.155	0.262	9.32±0.72	9.06
10	46.5±21.5	-	0.272	0.445	9.23±0.71	8.16
11	21.5±10.0	-	0.441	0.597	8.47±0.73	7.30
12	10.0±4.65	-	0.648	0.814	9.11±0.81	9.27
13	4.65±2.15	-	1.099	1.24	9.21±0.82	11.12
14	2.15±1.0	1.53±0.15	2.758	1.70	10.4±0.97	11.57
15	1.0±0.465	1.19±0.11	1.090	3.32	7.5±0.06	7.81
16	465±215 eV	1.69±0.10	1.995	4.55	-	8.28
17	215±100	3.00±0.07	3.058	20.3	-	9.19
18	100±46.5	0.16±0.02	0.147	16.6	-	5.88
19	46.5±21.5	0.89±0.36	0.413	54.2	-	6.29
20	21.5±10	-	0.061	0.84	-	6.03

The group transmissions and cross-sections are averaged over Fermi spectrum. The experimental uncertainties of transmissions are 0.2-0.5%, the errors of the total cross-sections are 2-10%. The total transmissions are usually measured at $n\sigma_t = 0.2$-0.4. This leads to underestimating the average group cross- sections by 20-40% in the region of unresovled resonances, if the correction for the resonance self-shielding of the averaged cross-sections is not introduced.

The resonance parameters. The time-of-flight spectra with multiplicities from 2 to 5 were summarized to obtain the radiative cross-section σ_γ of ^{93}Nb. The program MINUIT was used for the fitting of resonance parameters.

Detector count in the *i*-th channel is presented by the next formulae:

$$N_i = \Phi_n S\int\int \frac{\sigma_\gamma}{\sigma_t}(1 - \exp(-n\sigma_t))f_D(E,E')R(t,t'(E))dE'dt' \cdot \varepsilon \cdot t_m , \tag{5}$$

where Φ_n is the flux density, S – is the sample area, σ_t is the total cross-section, ε - detector efficiency, t_m – measurement time. The detector counts is presented as a double integral from Breit-Wigner cross-section with Doppler and resolution functions. This method was described in [6]. The Doppler function is taken in the form:

$$f_D = \frac{1}{\Delta_D \sqrt{\pi}} \exp(-((E - E')/\Delta_D)^2), \tag{6}$$

where Δ_D is the Doppler width, $\Delta_D = 2[Ek\theta/(A+1)]^{1/2}$, k – the Boltzmann constant, θ - the sample temperature, A- atomic weight. The resolution function is connected with pulse form of the IBR-30.

Because resonance widths less considerably than distance between resonances, the radiative capture is negligible between resonances and this intervals were used to determine a background. The background is described as a polynoum function of the energy.

Table 2.

The resonance parameters of ^{93}Nb

E_r, (eV)	$\Gamma_{n,}$ (meV)	Γ_γ (meV)	$\Gamma_{n,}$ (meV) [4]	Γ_γ (meV) [4]
35.85	0.143±0.068	228±30	0.107±0.010	166±30
42.15	0.11±0.04	163±25	0.084±0.008	173±30
94.14	0.45±0.12	194±30	0.314±0.020	170±60
105.65	0.62±0.13	167±30	0.450±0.020	163±60
118.77	5.8±0.33	172±17	3.80±0.16	132±14
193.6	39.5±3.6	320±60	41.0±1.2	125±12

The energy interval, which correspond to time resolution of the installation, is calculated by the formulae $\Delta E = 2\Delta t E/t$. This interval is shown on Fig. 4. together with Doppler width as function of neutron energy. The points correspond to the resonance radiative widths for ^{93}Nb.
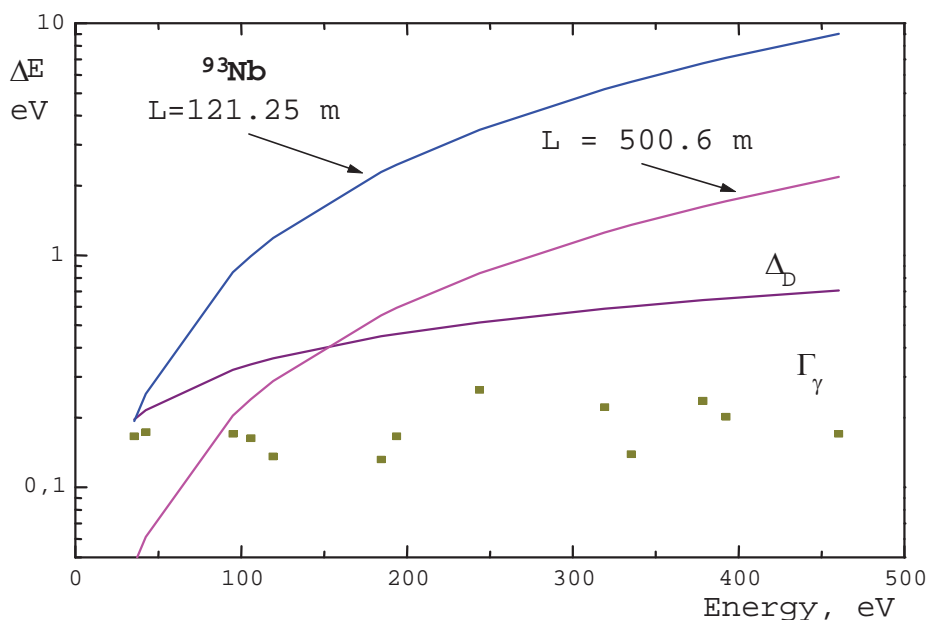

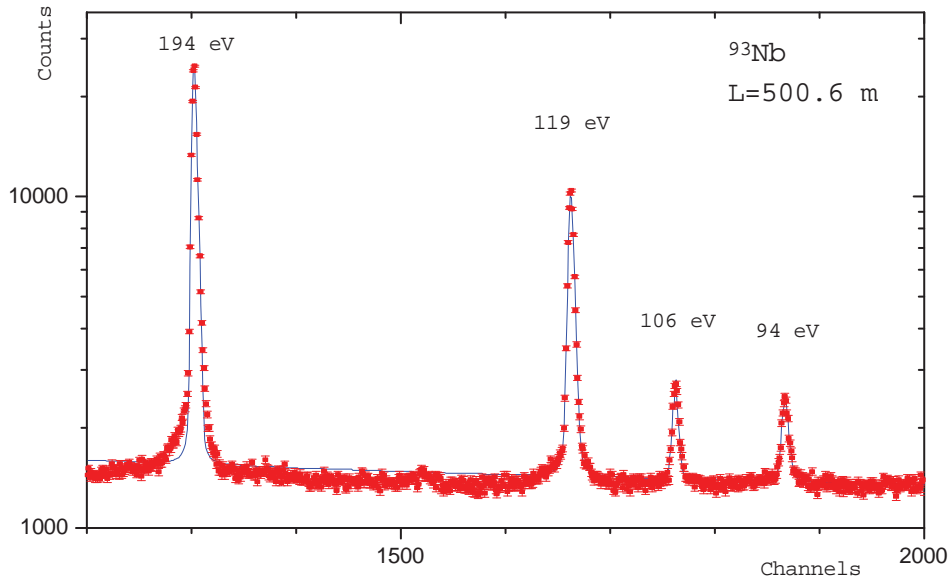Fig. 4. The energy resolution of spectrometers

Fig. 5. The experimental and calculated time-of-flight spectra with ^{93}Nb

Conclusion

The measurements of the neutron capture cross-sections and transmissions were carried out and using them the group total cross-sections of the ^{93}Nb in the 20 eV – 100 keV energy region were determined. The analogous integral characteristics for the ^{93}Nb were obtained on the basis of the evaluated data of ENDF/B-6 and JENDL-3. The experimental and calculated cross-sections have agreement within limits of the experimental errors but ones different in 14,16 energy groups for capture cross-sections .

In the future, we intend to continue the work in this direction to determine self-indication functions in neutron capture and on their base to define the resonance self-shielding factors.

References

1. Grigoriev Yu.V.,Vertes P. Average resonance parameters for Nb-93 and natural tungsten. Nuclear Data for Science and Technology (1988 Mito). Japan, p. 623-626, 1988.
2. Grigoriev Yu.V, Kitaev V. Ya., Sinitsa V.V., Faikov – Stanzcyk H. Investigation of a resonance self – shielding effect in the α value of ^{235}U, ^{239}Pu in energy range 4.65 –2150eV. ISSIN-7, Dubna, May 13-16, 1999, p.
3. Sinitsa V.V. Program for calculating the group constants using the library of evaluated neutron data. VANT, ser. Yadernye Konstanty, v.5(59), p.34, 1984.
4. Rose P.F., Dunford C.K. ed. ENDF-102. Data Formats and Procedures for the Evaluated Nuclear Data File. Report BNL, Upton, New York, 11973, USA, 1988.
5. Shibata K. et al. Japanese Evaluated Nuclear Data Library. Version JENDL-3. Rep. JAERI 1319, 1990.
6. Borzakov S.B. et al. Phys. At. Nucl., v.62, p.872, 1999.

01-11405 (132)   [2]
<u>Translated from Russian</u>

UDC 621.039.514

THE *TENDL* NEUTRON DATA LIBRARY AND THE *TEND1038* 38-GROUP NEUTRON CONSTANT SYSTEM

S.N. Abramovich, V.P. Gorelov, A.A. Gorshikhin,
A.N. Grebennikov, V.I. Il'in, N.A. Krut'ko, G.G. Farafontov

Russian Federal Nuclear Centre - All-Russia Scientific Research Institute for Experimental Physics, Sarov, Russia

THE TENDL NEUTRON DATA LIBRARY AND THE TEND1038 38-GROUP NEUTRON CONSTANT SYSTEM. The library contains neutron data for 103 nuclei – i.e. for 38 actinide nuclei (from ^{232}Th to ^{249}Cm), 26 fission fragment nuclei and 39 nuclei in structural and technological materials. The 38-group constants were obtained from TENDL. The high-energy group boundary is 20 MeV. The energy range below 1.2 eV contains 11 groups. Temperature and resonance effects were taken into account. The delayed neutron parameters for 6 groups and the yields of 40 fission fragments were obtained (light and heavy, stable and non-stable). The fast neutron features of spherical critical assemblies were calculated using constants from TEND1038.

References [1] and [2] presented the results from the first stage of the setting up of the Transmutation Evaluated Neutron Data Library (TENDL). Neutron data were established for 38 actinides from ^{232}Th to ^{249}Cm and for 20 fission fragments. The TENDL library is intended for use in solving applied transmutation tasks. The setting up of TENDL was prompted by the lack of neutron data for certain nuclei in the data libraries available to us. Where neutron characteristics for a particular nucleus were available in several libraries, we gave preference to the version of the neutron data whose neutron interaction characteristics were closest to the recommended values.

The setting up of the TENDL library was pursued through ISTC (International Science and Technology Center) project No. 1145-99. This paper presents the results of the selection for TENDL of neutron data for neutron-absorbing fission fragments and for nuclei in structural and technological materials. In addition, the TEND1038 38-group neutron constant system is presented which is based on the neutron data from TENDL.

1. The TENDL neutron data library

By comparison with the list of fragments from Ref. [1], the list of fragments identified was extended: it was decided to remove the nuclei ^{113}Cd, ^{155}Gd and ^{157}Gd from the groups of light and heavy poison fragments and to consider their build-up and annihilation separately. Conversely, neutron-induced intensive burnup of ^{113}Cd, ^{155}Gd and ^{157}Gd is not taken into

account. The primary component in the ^{113}Cd formation chain is the ^{113}Pd fragment, in the ^{155}Gd formation chain it is the ^{155}Sm fragment, and in the ^{157}Gd formation chain it is the ^{157}Sm fragment. For ^{113}Cd account must be taken of the formations of ^{113}Ag^m and ^{113}Ag, for ^{155}Gd of ^{155}Eu, and for ^{157}Gd of ^{157}Eu.

For ^{113}Ag, owing to the lack of data, it was proposed that the neutron characteristics from ENDF/B-6 for the similarly unstable nucleus ^{111}Ag be used in TENDL. For ^{157}Gd, the neutron data from ENDF/B-6 will be used in TENDL. When selecting neutron data for the nuclei ^{113}Cd, ^{155}Eu, ^{155}Gd and ^{157}Gd, the neutron radiative capture cross-sections at the thermal point (E=0.0253 eV) and the radiative capture resonance integrals (from 0.5 eV to 10 MeV) from several neutron data collections (BROND-2 (Russia), ENDF/B-6 (US), JENDL-3.2 (Japan), JEF-2 (European Union)) were compared with the results of measurements or with recommended data. On the basis of this comparison, it was decided to use data from the JEF-2 library for ^{113}Cd in TENDL, data from the ENDF/B-6 library for ^{155}Eu, and data from the JENDL-3.2 library for ^{155}Gd and ^{157}Gd. Owing to a lack of data, neutron interaction with ^{113}Pd, ^{113m}Ag, ^{155}Sm and ^{157}Sm must be disregarded. The relatively short half-lives of these nuclei provide some justification for this.

Neutron data for possible non-fissile components of fuel, and of structural and technological materials (39 nuclei from ^{1}H to ^{209}Bi inclusive) were selected for entry in TENDL. In doing so, we compared the absorption and scattering cross-sections at the thermal point and absorption resonance integrals from the BROND-2, ENDF/B-6, ENDL-82 (USA), CENDL-2 (People's Republic of China), JENDL-3.2 and JEF-2 neutron data libraries with the recommended values.

Table 1 gives a full list of the 103 nuclei for which neutron data have been included in TENDL, following completion of the setting up of the library.

Table 1

List of nuclei from TENDL

No.	Nucleus	Neutron data selected	No.	Nucleus	Neutron data selected
Actinides					
14	^{235}U	ENDF/B-6	33	^{244}Cm	JENDL-3
15	^{236}U	ENDF/B-6	34	^{245}Cm	JENDL-3
16	^{237}U	ENDF/B-6	35	^{246}Cm	JENDL-3
17	^{238}U	JENDL-3	36	^{247}Cm	ENDF/B-6
18	^{239}U	ENDL-82	37	^{248}Cm	ENDL-82
19	^{237}Np	ENDF/B-6	38	^{249}Cm	JENDL-3
Fission fragments					
39	^{90}Sr	ENDF/B-6	52	^{135}Xe	ENDF/B-6
40	^{90}Y	ENDF/B-6	53	^{135}Cs	ENDF/B-6
41	^{93}Zr	ENDF/B-6	54	^{137}Cs	ENDF/B-6
42	^{99}Tc	ENDF/B-6	55	^{149}Pm	ENDF/B-6
43	^{107}Pd	ENDF/B-6	56	^{149}Sm	ENDF/B-6
44	^{113}Ag	ENDF/B-6	57	^{151}Sm	BROND-2

№	Nucleus	Neutron data selected	№	Nucleus	Neutron data selected
45	^{113}Cd	JEF-2	58	^{155}Eu	ENDF/B-6
46-48	"eslpf" *)	ENDF/B-6	59	^{155}Gd	JENDL-3.2
49	^{126}Sn	ENDF/B-6	60	^{157}Eu	ENDF/B-6
50	^{129}I	ENDF/B-6	61	^{157}Gd	JENDL-3.2
51	^{135}I	ENDF/B-6	62-64	"eshpf" **)	ENDF/B-6
Components of fuel and of structural and technological materials					
65	^{1}H	ENDF/B-6	84	Fe	ENDL-82
66	^{2}D	BROND-2	85	Ni	CENDL-2
67	^{3}T	BROND-2	86	Mo	JENDL-3.2
68	^{3}He	BROND-2	87	Cr	ENDL-82
69	^{4}He	BROND-2	88	^{55}Mn	ENDF/B-6
70	^{6}Li	BROND-2	89	Si	JEF-2
71	^{7}Li	ENDF/B-6	90	S	CENDL-2
72	^{9}Be	JENDL-3.2	91	^{31}P	JENDL-3.2
73	^{10}B	CENDL-2	92	^{59}Co	JENDL-3.2
74	^{11}B	ENDF/B-6	93	Cu	JENDL-3.2
75	C	BROND-2	94	^{27}Al	JENDL-3.2
76	^{14}N	JENDL-3.2	95	Ti	JENDL-3.2
77	^{16}O	JENDL-3.2	96	^{93}Nb	JENDL-3.2
78	^{19}F	ENDF/B-6	97	Cd	ENDF/B-6
79	^{23}Na	JENDL-3.2	98	Pb	CENDL-2
80	Cl	ENDF/B-6	99	^{209}Bi	ENDF/B-6
81	Zr	ENDF/B-6	100	^{51}V	JENDL-3.2
82	^{40}Ar	JENDL-3.2	101	^{181}Ta	BROND-2
83	W	ENDF/B-6	102	Ga	JENDL-3.2
			103	Hf	CENDL-2

Notes:

*) "eslpf" - effective stable light poison fragment; three versions of its neutron characteristics were obtained by averaging the neutron characteristics from ENDF/B-6 for $^{72-74, 76}$Ge, ^{75}As, $^{77, 78, 80, 82}$Se, $^{79, 81}$Br, $^{80, 82-84, 86}$Kr, ^{85}Rb, $^{86-88}$Sr, ^{89}Y, $^{90-92, 94}$Zr, ^{93}Nb, $^{95-97, 100}$Mo, $^{98, 99, 101, 102, 104}$Ru, ^{103}Rh, $^{105, 106, 108, 110}$Pd, $^{107, 109}$Ag, $^{110-112, 114}$Cd and ^{115}Sn; the cumulative yields of these fragments per fission of ^{233}U or ^{235}U, or ^{239}Pu by thermal neutrons were used as the proportions for the averaging;

**) "eshpf" - effective stable heavy poison fragment; three versions of its neutron characteristics were obtained by averaging the neutron characteristics from ENDF/B-6 for $^{117-120, 122, 124}$Sn, $^{121, 123}$Sb, $^{124-126}$Te, ^{127}I, $^{128-131}$Xe, ^{133}Cs, $^{132, 134-138}$Ba, ^{139}La, $^{140, 142}$Ce, ^{141}Pr, $^{143-146, 148, 150}$Nd , $^{147, 148, 150, 152, 154}$Sm, $^{151, 153}$Eu, $^{156, 158, 160}$Gd, ^{159}Tb, $^{160-164}$Dy, ^{165}Ho and $^{166, 167}$Er; the cumulative yields of these fragments per fission of ^{233}U or ^{235}U, or ^{239}Pu by thermal neutrons were used as the proportions for the averaging.

Reference [2] recommended using the BROND-2 neutron data evaluation for ^{240}Pu in TENDL. However, this evaluation does not go up to a neutron energy of 20 MeV and we therefore declined to use it. After comparing the radiative capture and fission cross-sections at the thermal point 0.0253 eV and the radiative capture and fission resonance integrals for ^{240}Pu from various evaluated data libraries with the recommended values, we selected the JENDL-3 neutron data evaluation for ^{240}Pu.

Initially, for ^{1}H, the BROND-2 neutron data evaluation was proposed for use in TENDL. However, after calculating k_{eff} for critical assemblies containing layers of water or polyethylene, it was decided to replace the BROND-2 evaluation with the ENDF/B-6 evaluation.

The data from TENDL are stored in ENDF/B text format and in binary form. These data may be used as source data when generating constants for transmutation problems. They are for stationary target nuclei. The text format can be used for the preparation of multigroup constants. The binary format facilitates browsing of the archive.

The NDX program manager is used to browse the TENDL binary archive. It is implemented in the Win32 environment (Windows 95, 98 and Windows NT 4.0 operating systems) in two modules - NDX.EXE and NDX_NT.DLL. The NDX program itself is implemented in the Borland Delphi 4.0 programming environment. The NDX_NT.DLL module, which reconstructs the resonance cross-sections and calculates the resonance integrals, is implemented in the Watcom Fortran 10.6 environment. The NDX program allows the required information to be extracted from the archive in either tabular or graphical form. Its user interface consists of a main window and special data presentation windows. The main window provides a convenient means of selecting the isotope and then accessing the data on it. In addition, the main window gives some general reference information.

2. The TEND1038 38-group neutron constant system

The neutron data from the TENDL library were used to prepare the TEND1038 38-group neutron constant system. The RMK program from the BEND archive program package [3] was used to calculate the multigroup constants. The calculation was carried out in two stages. In the first stage, the data from TENDL were recalculated to take account of the thermal motion of nuclei. If for some nuclei in a specific cross-section energy region resonance parameters were given, the special RECONR program first calculated the energy dependence of the cross-sections in that region. In the second stage, multigroup neutron constants were calculated which were entered in a special archive. The methodology for calculating multigroup constants in a medium comprising stationary nuclei is set out in Ref. [4]. The generalization for moving nuclei is published in Ref. [5].

Table 2 gives the boundaries of the groups E_j and $E_{j+1,}$ which were adopted in TEND1038. The grouping was based on the ABBN-64 [6] 26-group constant system. The boundaries of groups 5-26 from Table 2 correspond to this grouping.

In calculating the multigroup constants, linear averaging of the neutron data was performed. As in Ref. [6], when averaging the neutron data "standard" neutron flux energy spectrum shaper were used inside individual groups. These weighting functions do not convey the features which should occur as a result of the resonance structure of the cross-sections.

A constant was used as the "standard" weighting function for groups 1-4. The ^{252}Cf spontaneous fission neutron spectrum was used as the "standard" weighting function for groups 5-7. In the 2.5 MeV $\geq E \geq E_F(T)$ neutron energy interval, the "standard" weighting function took the form of normalized Fermi distribution. Here $E_F(T)$ is the Fermi matching energy and T is the temperature of the medium. The normalization ensures the equality of the Fermi distribution and the Maxwellian distribution with temperature T where $E=E_F(T)$.

The matching energy $E_F(T)$ was determined using the approximation from Ref. [7]

$$E_F(T)=7T.$$

The lower boundaries of groups i = 27-32 are equal to the values of $E_F(T)$ for the temperatures 2000, 1500, 1000, 600, 400 and 300 K.

In the $E_F(T) \geq E \geq 0$ energy interval, the Maxwellian distribution for the neutron flux was used as the "standard" weighting function. The lower boundaries of groups i = 33-37 are equal to the energies at which the distribution maximum occurs for temperatures of 1500, 1000, 600, 400 and 300 K respectively.

Table 2

Group boundaries in the TEND1038 system

Number of group j	E_j	E_{j+1}	Number of group j	E_j	E_{j+1}
1	20 MeV	17.5	20	465 eV	215
2	17.5	14.1	21	215	100
3	14.1	13.9	22	100	46.5
4	13.9	10.5	23	46.5	21.5
5	10.5	6.5	24	21.5	10
6	6.5	4	25	10	4.65
7	4	2.5	26	4.65	2.15
8	2.5	1.4	27	2.15	1.205
9	1.4	0.8	28	1.205	0.904
10	0.8	0.4	29	0.904	0.603
11	0.4	0.2	30	0.603	0.362
12	0.2	0.1 MeV	31	0.362	0.241
13	100 keV	46.5	32	0.241	0.181
14	46.5	21.5	33	0.181	0.129
15	21.5	10	34	0.129	0.086
16	10	4.65	35	0.086	0.052
17	4.65	2.15	36	0.052	0.034
18	2.15	1 keV	37	0.034	0.026
19	1000 eV	465	38	0.026	0

When taking into account the resonance features in the energy dependence of the cross-sections, we used the dilution cross-section formalism of I.I. Bondarenko [6]. The group constants were calculated for the following set of dilution cross-sections σ_0: ∞, 10^4, 10^3, 10^2, 10, 1, 0 barns. For each of the values of T above, and for T=0, group constants were calculated for all the values of σ_0 given.

Unlike Ref. [6], we do not use resonance self-shielding factor formalism when recording multigroup cross-sections. For each pair of values of T and σ_0, values are given in the archive for all multigroup constants for a specific reaction for a specific nucleus, and not only for multigroup cross-sections.

In the ENDF/B format, the different reactions are assigned MT numbers. TEND1038 contains multigroup constants for reactions with MT numbers in the range 2-133. The excitation processes of isolated levels and a continuum of levels for inelastic neutron scattering are combined in one inelastic scattering process with the number MT=4.

The influence of the thermal motion of nuclei on the energy spectra and the angular distribution of secondary neutrons was taken into account only for elastic scattering on light nuclei from ^{1}H to C inclusive, starting from an incident neutron energy of 5 eV. For reactions whose thresholds are above the resonance region, the group constants were calculated only using the "standard" weighting functions ($\sigma_0 = \infty$). These functions were also used to calculate the group constants for nuclei whose cross-sections do not have resonance features in the 0-20 MeV energy region. The thermal motion of target nuclei was not taken into account for some threshold reactions whose thresholds are rather high.

For reactions involving neutron emission, the group angular distribution of the neutrons is described in a P_5-approximation for all nuclei except ^{1}H. For scattering on ^{1}H, a P_{15}-approximation is used.

TENDL does not contain data on the number of prompt fission neutrons for ^{232}Pa, ^{239}Np, $^{236,\ 242-244}$Pu and ^{247}Cm. Therefore, for these nuclei the group numbers for prompt fission neutrons were determined as the differences between the group numbers for the total fission neutron yield and corresponding group numbers for delayed neutrons.

For ^{238}Pu and $^{241,\ 242}$Am$^{g,\ m}$ in BROND-2, when describing secondary neutron spectra from the reactions (n,2n) and (n,3n), a format is used which cannot be processed by the RMK program for calculating multigroup constants from the BEND archive [4]. For this reason, the multigroup constants for the reactions (n,2n) and (n,3n) for ^{238}Pu and $^{241,\ 242}$Am^m were prepared using the ENDF/B-6 library, and for ^{242g}Am using the JENDL-3.2 library.

The total numbers of delayed neutrons per fission event in the energy groups and the total spectra of delayed neutrons were calculated using the "standard" weighting functions not taking into account thermal motion of fissile nuclei. In TEND1038, it is assumed that the total spectrum of delayed neutrons is not dependent on the energy of the neutrons inducing fission. Six groups of precursor fragments were examined. The decay constants λ_d of the groups of

delayed neutron precursor fragments and the relative proportions a_d of these groups in TEND1038 are not dependent on T, σ_0 or the energy group number.

TENDL did not contain:

- data on the numbers of delayed neutrons for $^{232, 233}$Pa, ^{239}Np, ^{232}U, $^{236, 238, 242-244}$Pu and ^{247}Cm;

- λ_d values for ^{233}Th, ^{232}Pa, ^{239}U, $^{238, 239}$Np, $^{236, 238, 240, 242-244}$Pu and $^{247, 248}$Cm;

- a_d values and delayed neutron spectra data for ^{233}Th, $^{231-233}$Pa, $^{232, 239}$U, $^{238, 239}$Np, $^{236, 238, 240, 242-244}$Pu, ^{242}Am, $^{244g, 244m}$Am, and $^{242-249}$Cm.

Thus, when preparing TEND1038:

- for ^{233}Th, the same λ_d, a_d values and delayed neutron spectra data were used as for ^{232}Th;

- for ^{231}Pa, the a_d values and delayed neutron spectra data from ENDF/B-6 were used;

- for ^{232}Pa, the λ_d values and absolute delayed neutron yields data from JENDL-3.2 were used, but the same a_d values and delayed neutron spectrum as for ^{231}Pa;

- for ^{233}Pa, absolute delayed neutron yield data were used as for ^{232}Pa, and the same a_d values and delayed neutron spectrum as for ^{231}Pa;

- for ^{232}U, the absolute delayed neutron yield values, a_d values and delayed neutron spectrum were taken from ENDF/B-6;

- for ^{239}U, the same λ_d, a_d values and delayed neutron spectrum data were used as for ^{238}U;

- for ^{238}Np, the λ_d, a_d values and delayed neutron spectrum data from ENDF/B-6 were used;

- for ^{239}Np, the λ_d values and absolute delayed neutron yield data from JENDL-3.2 were used, but the same a_d values and delayed neutron spectrum as for ^{238}Np;

- for ^{236}Pu, the λ_d values and absolute delayed neutron yield data from ENDF/B-6 were used, but the same a_d values and delayed neutron spectrum as for ^{238}Pu;

- for $^{238, 242}$Pu, the λ_d values and absolute delayed neutron yield data, a_d values and delayed neutron spectrum from ENDF/B-6 were used;

- for ^{243}Pu, the absolute delayed neutron yield data from ENDL-82 were used, but the same λ_d, a_d values and delayed neutron spectrum as for ^{242}Pu;

- for ^{244}Pu, the same λ_d, a_d values and delayed neutron spectrum were used as for ^{242}Pu, but the same absolute delayed neutron yield value as for ^{243}Pu;

- for ^{242g}Am, the same a_d values and delayed neutron spectrum data were used as for ^{242m}Am;

- for $^{244g,\,244m}$Am, the same a_d values and delayed neutron spectrum data were used as for ^{243}Am;

- for ^{242}Cm, the a_d values and delayed neutron spectrum data from ENDF/B-6 were used;

- for $^{243,\,244}$Cm, the same a_d values and delayed neutron spectrum data were used as for ^{242}Cm;

- for ^{245}Cm, the a_d values and delayed neutron spectrum data from ENDF/B-6 were used;

- for ^{246}Cm, the same a_d values and delayed neutron spectrum data were used as for ^{245}Cm;

- for ^{247}Cm, the λ_d values and absolute delayed neutron yield data from JENDL-3.2 were used, but the same a_d values and delayed neutron spectrum as for ^{245}Cm;

- for ^{248}Cm, the λ_d values from JENDL-3.2 were used, but the same a_d values and delayed neutron spectrum as for ^{245}Cm;

- for ^{249}Cm, the same a_d values and delayed neutron spectrum were used as for ^{245}Cm.

For ^{238}U in JENDL-3, when describing the delayed neutron spectra, a format is used which cannot be processed by the RMK program for calculating multigroup constants from the BEND archive [3]. For this reason, the a_d values and delayed neutron spectrum for ^{238}U were taken from ENDF/B-6.

We note that, when preparing the delayed neutron data in ENDF/B-6, an error was discovered in the energy dependence of the total number of delayed neutrons per fission of ^{233}U: as of the energy E=14 MeV, the number of delayed neutrons is too high by a factor of 10. In addition, for ^{232}Th in JENDL-3, instead of the correct value $a_1 = 0.034$ [8] an erroneous value of 0.0124 is given. As a result, the sum of all the a_d values is not 1. These errors have been corrected in TENDL.

The group fission fragment yields per fission event in TEND1038 are not dependent on T or σ_0. For all the actinides and fragments in Table 1, the fragment yield values from Ref [1] were used as the source data, as well as additional data from ENDF/B-6. The "eslpf" and "eshpf" yields from Ref. [1] were corrected to take account of other fragments identified. The yield values from Ref. [1] for the short-lived fragments ^{83m}Kr, ^{90m}Y, ^{99m}Tc, ^{103m}Rh, ^{107m}Pd, ^{135m}Cs, ^{137}Ba^m, ^{135}Te, ^{135}Xe^m and ^{149}Nd were also used. The yields for the short-lived fragments ^{113}Pd, ^{113m}Ag, ^{155}Sm and ^{157}Sm are as in ENDF/B-6. When making practical use of these values, the following must be done:

- from the "eslpf" yield, subtract the sum of the numbers of delayed neutrons from precursor fragment groups 1 and 6 per fission event for the same actinide; in the equation, as regards the "eslpf" concentration, introduce a source which is equal to the sum of the numbers of precursor decays for groups 1 and 6;

- from the "eshpf" yield, subtract the sum of the numbers of delayed neutrons from precursor fragment groups 2-5 per fission event for the same actinide; in the equation, as regards the "eshpf" concentration, introduce a source which is equal to the sum of the numbers of precursor decays for groups 2-5.

This is based on the conclusions on precursor identification from Ref. [8].

The group calorific values were calculated for each reaction, i.e. the energies which are released in one event of the reaction with MT number initiated by neutrons of group j on the nucleus k. Here, we assumed that γ-rays, charged particles, fission fragments and recoil nuclei lose their energy locally.

The calorific value $q_{r,k,j}$ is the energy released in one event of the reaction r initiated by neutrons of group j on the nucleus k. The group calorific value of the reaction r on any nucleus may be calculated using the formula (nucleus index not given)

$$q_{r,j} = \frac{\int\limits_{E_{j+1}}^{E_j} q_r(E)\ \sigma_r(E,T)\ \phi(E)\ dE}{\int\limits_{E_{j+1}}^{E_j} \sigma_r(E,T)\ \phi(E)\ dE} \ .$$

Integration is performed within the boundaries of the group with the index j.

For a fission reaction, the function $q_f(E)$ is written in the form

$$q_f(E) = Q_f + E - \nu_{pf}(E)\int\limits_0^\infty E'\cdot\xi_{pf}(E \Rightarrow E')\,dE' - \nu_{delf}(E)\int\limits_0^\infty E'\cdot\xi_{delf}(E \Rightarrow E')\,dE'$$

Here, $Q_{f,k}$ is the energy of a reaction involving fission of a nucleus by neutrons, which is assumed to be independent of the energy of the incident neutron; $\nu_{pf}(E)$ and $\nu_{delf}(E)$ are the number of prompt and delayed neutrons per fission of the nucleus by neutrons with energy E; $\xi_{pf}(E \Rightarrow E')$ and $\xi_{delf}(E \Rightarrow E')$ are the normalized spectra of prompt and delayed fission neutrons. The values of $Q_{f,k}$ should take account of the kinetic energy of the fission fragments, the kinetic energy of fission neutrons, the energy of prompt and delayed γ–rays and the energy of delayed β-particles (minus the contribution of β-decays with half-lives of more than a year [9]).

For other reactions the expression for $q_r(E)$ takes the form

$$q_r(E) = Q_r + E - \nu_r \overline{E}_r(E) \ .$$

Here Q_r is the energy of the reaction r (for elastic scattering this value is zero); ν_r is the number of secondary neutrons, which does not depend on E; $\overline{E}_r(E) = \int\limits_{all\ E'} E'\xi_r(E \Rightarrow E')\ dE'$ is the energy which is removed by the secondary neutron from the zone of the reaction r initiated by a neutron with energy E (integration is performed for all values of E' which, for a fixed value of E, do not

break the laws of conservation); $\xi_r(E \Rightarrow E')$ is the spectrum of secondary neutrons from the reaction r.

We shall look separately at the threshold reactions involving emission of neutrons where Q_r < 0 and $v_r \neq 0$. For the reaction (n,2n), for example, the expression for $q_{2n}(E)$ takes the form

$$q_{2n}(E) = Q_{2n} + E - 2\overline{E}_{2n}(E)_{\text{F}}.$$

Here, $\overline{E}_{2n}(E) = \int\limits_0^{E-U_{2n}} E' \xi_{2n}(E \Rightarrow E') \, dE'$; $U_{2n} = -\dfrac{\overline{A}+1}{\overline{A}} Q_{2n}$ is the threshold of reaction (n,2n), so the cross-section of the reaction $\sigma_{2n}(E) \equiv 0$ at $E \leq U_{2n}$; $\overline{A}$ is the target nucleus mass in neutron masses.

$\overline{E}_{2n}(E)$ can be calculated analytically using the evaporation model for $\xi_{2n}(E \Rightarrow E')$. According to this model the expression for the spectrum is written in the form

$$\xi_{2n}(E \Rightarrow E') = \sum_{m=1}^{2} a_m(E) \; \xi_m(E \Rightarrow E'),$$

where

$$\sum_{m=1}^{2} a_m(E) = 1,$$

$$\xi_m(E \Rightarrow E') = \frac{E' \; \exp[-E'/T_m(E)]}{N_m(E)}, \quad 0 \leq E' \leq E - U_{2n} - E_{m-1}(E),$$

$$N_m(E) = T_m^2(E)\left\{1 - \left[1 + \frac{E - U_{2n} - E_{m-1}(E)}{T_m(E)}\right] \; \exp\left[-\frac{E - U_{2n} - E_{m-1}(E)}{T_m(E)}\right]\right\},$$

$$E_m(E) = 2T_m(E) - \frac{T_m(E)}{N_m(E)} \cdot \left[E - U_{2n} - E_{m-1}(E)\right]^2 \exp\left[-\frac{E - U_{2n} - E_{m-1}(E)}{T_m(E)}\right],$$

and $E_0(E) \equiv 0$.

If $a_1(E) \equiv a_2(E) \equiv 0.5$, then $q_{2n}(E) = Q_{2n} + E - E_1(E) - E_2(E)$.

If $a_1(E) \equiv 1$, $a_2(E) \equiv 0$, then $q_{2n}(E) = Q_{2n} + E - 2E_1(E)$.

It can be demonstrated that the following holds

$$\lim_{E \Rightarrow U_{2n}} E_m(E) = 0,$$

i.e.

$$q_{2n}(U_{2n}) = -Q_{2n} / \overline{A}.$$

That the temperatures $T_m(E)$ are correctly evaluated is borne out by the fact that for all values of $E \geq U_{2n}$ the following holds

$$q_{2n}(E) = Q_{2n} + E - E_1(E) - E_2(E) > 0 \ , \ (a_1(E) \equiv a_2(E) \equiv 0.5)$$

or

$$q_{2n}(E) = Q_{2n} + E - 2E_1(E) > 0 \ , \ (a_1(E) \equiv 1, \ a_2(E) \equiv 0).$$

If the corresponding inequality holds, then for the groups j in which the group cross-sections $\sigma_j^{(2n)}$ are non-zero, q_{2nj} will be positive. If the function $q_{2n}(E)$ is positive and monotonic, then

$$q_{2n,j} \geq -Q_{2n} / \bar{A} \, .$$

The Q_{2n} and U_{2n} values, and the $T_m(E)$ values at the nodes of the reference grid for E and the $a_m(E)$ values at the nodes of its reference grid for E are given in the neutron data libraries. Let us consider the simplest way of correcting these data in the event of negative values of $q_{2n}(E)$. As calculations have shown, this may occur at the node of the reference grid for E closest to U_{2n}. To ensure that $q_{2n,j}$ is positive, in this case we must ignore this node and its corresponding T_m values (or value). This approach may also be used for tabular representation of $\xi_{2n}(E \Rightarrow E')$ on the reference grid of E values.

Let us consider two simple methods for evaluating $q_{2n,j}$ where $q_{2n}(E)$ is positive. The first method is as follows. By means of linear interpolation using the $q_{2n}(E)$ values at the nodes of the reference grid for E, we determine the $q_{2n}(E_j)$ values at the boundaries of the groups of multigroup approximation under examination. Then we evaluate the $q_{2n,j}$ values using the formula

$$q_{2n,j} \approx \begin{cases} \dfrac{q_{2n}(E_j) + q_{2n}(E_{j+1})}{2}, & E_j > E_{j+1} > U_{2n}, \\[2mm] \dfrac{q_{2n}(E_j) - Q_{2n} / \bar{A}}{2}, & E_j > U_{2n} \geq E_{j+1}. \end{cases}$$

In the second method, when $\mathbf{E_j > E_{j+1} > U_{2n}}$, the $q_{2n,j}$ values can be evaluated using the following formula (proposed by G.A. Goncharov)

$$q_{2n,j} = Q_{2n} + \bar{E}_j - 2\sum_i \bar{E}_i \ \xi_{j \Rightarrow i}^{(n,2n)} \, .$$

Here $\bar{E}_j = \dfrac{m_n \bar{v}_j^2}{2}$ is the effective kinetic energy of the neutrons in group j;

$$\bar{v}_j = \cfrac{\displaystyle\int_{E_{j+1}}^{E_j} \varphi(E)\,dE}{\displaystyle\int_{E_{j+1}}^{E_j} \left[\sqrt{2E/m_n}\right]^{-1} \varphi(E)\,dE} \quad \text{is the mean rate of motion of the neutrons in group j;}$$

m_n is the neutron mass.

When $E_j > U_{2n} > E_{j+1}$ and, in particular, when $E_j, < U_{2n}$ using the latter formula for the $q_{2n,j}$ calculations can yield a negative value. Therefore, when j meets these conditions we propose proceeding as follows: if $q_{2n,j-1} > 0$, assume that **Error! Objects cannot be created from editing field codes.**; using linear interpolation determine $q_{2n}(E_j)$ using $q_{2n}(\bar{E}_{j-1})$ and $q_{2n}(U_{2n})$,

$$q_{2n}(E_j) = -Q_{2n}/\bar{A} + [q_{2n,j-1} + Q_{2n}/\bar{A}] \cdot \frac{E_j + (\bar{A}+1)Q_{2n}/\bar{A}}{\bar{E}_{j-1} + (\bar{A}+1)Q_{2n}/\bar{A}} \ ;$$

then subtract $q_{2n,j}$ using the formula

$$q_{2n,j} = -Q_{2n}/\bar{A} + [q_{2n,j-1} + Q_{2n}/\bar{A}] \cdot \frac{E_j + (\bar{A}+1)Q_{2n}/\bar{A}}{2\left[\bar{E}_{j-1} + (\bar{A}+1)Q_{2n}/\bar{A}\right]} \ .$$

If $q_{2n,j-1} < 0$, then for the recalculation of $q_{2n,j-1}$ and the calculation of $q_{2n,j}$ we propose using the formulae:

$$q_{2n,j-1} = -Q_{2n}/\bar{A} + [q_{2n,j-2} + Q_{2n}/\bar{A}] \cdot \frac{E_{j-1} + E_j + 2(\bar{A}+1)Q_{2n}/\bar{A}}{2\left[\bar{E}_{j-2} + (\bar{A}+1)Q_{2n}/\bar{A}\right]} \ ;$$

$$q_{2n,j} = -Q_{2n}/\bar{A} + [q_{2n,j-2} + Q_{2n}/\bar{A}] \cdot \frac{E_j + (\bar{A}+1)Q_{2n}/\bar{A}}{2\left[\bar{E}_{j-2} + (\bar{A}+1)Q_{2n}/\bar{A}\right]} \ .$$

This procedure may be extended if $q_{2n,j-2} < 0$ too.

Let us now assume the following holds

$$E_1 > U_{2n} > E_2 \ .$$

We can attempt to calculate the calorific value $q_{2n,1}$ using the formula

$$q_{2n,1} = Q_{2n} + \bar{E}_1 - 2\sum_{i'} \bar{E}_{i'} \ \ \xi_{1\Rightarrow i'}^{(n,2n)} \ .$$

If $q_{2n,1} < -Q_{2n}/\bar{A}$ and, in particular, $q_{2n,1} < 0$, then for the recalculation of $q_{2n,1}$ we propose using the expression

$$q_{2n,1} = -\frac{Q_{2n}}{\bar{A}}\left[1+\frac{E_1-(\bar{A}+1)\left|Q_{2n}\right|/\bar{A}}{2\left|Q_{2n}\right|/\bar{A}}\right].$$

The proposed methods for evaluating $q_{2n,j}$ are more accurate the narrower the width of group $\Delta E_j = E_j - E_{j+1}$. We also used similar methods when examining the reactions (n,3n), (n,4n) and other threshold reactions involving emission of neutrons.

If several r' processes combine in the r process, its group calorific values should be calculated using the formula

$$q_{r,j} = \frac{\sum_{r'} q_{r',j}\sigma_j^{(r')}}{\sum_{r'} \sigma_j^{(r')}}.$$

This is how we calculated the group calorific values of the process MT=4.

The energies of the reactions Q_r for each nucleus and the Q_f values for each actinide are contained in TENDL. These values, with a small exception, were used when calculating group kerma factors.

The Q_f values for ^{232}Th, $^{233, 235}$U, ^{237}Np and $^{239, 240, 241}$Pu from TENDL agree with the data from Ref. [9]. For ^{236}U and ^{238}U we used the Q_f values from this study: $Q_f(^{236}$U$)$ = 191.6 MeV, $Q_f(^{238}$U$)$ = 193.8 MeV. For ^{237}U we used the same Q_f value as for ^{236}U; for ^{239}U we used the same Q_f value as for ^{238}U; for $^{238, 239}$Np we used the same Q_f value as for ^{237}Np.

When calculating the group constants for individual nuclei in a medium of given composition and at a given temperature, a formalism for taking account of resonance and heterogeneous effects which is well known from the reference literature can be used (for example, see Refs [6], [9] and [10]). This formalism has been incorporated in the program for calculating the group constants for a medium used at the All-Russia Scientific Research Institute for Experimental Physics.

TEND1038 is stored in both text format and in binary form. The text format allows TEND1038 to be used for numerical solution of the neutron transport equation using the programs available at the All-Russia Scientific Research Institute for Experimental Physics. The binary archive facilitates browsing of the archive. It saves disk memory and time when selecting data from the archive. The GX program manager was developed to work with data from the binary archive. The program has a graphic multi-window user interface and runs in an MS-DOS environment on IBM/AT-compatible PCs. The program allows the user to browse the archive data in both text (tabulator) and graphical form. The graphics system includes a set of utilities (overlay of graphs, scaling, taking the logarithm, selection of viewing angle, removal of numerical values from graph, etc.).

The information on the "standard" weighting functions used in preparing the TEND1038 constants is contained in the archive in a single TEXT comment section for the whole constants system. This section contains a text table of energy values for reactions with MT numbers in the range 2-113 for all the nuclei indicated in Table 1 of this paper. These values were used when calculating group calorific values of the reactions. The group boundaries, group neutron velocities and corresponding group kinetic neutron energies are given in the GVUE section which covers the entire constant system.

There is also a TEXT comment section for the constants for each nucleus. This indicates the half-life, decay product, mass number and library of neutron data used for TENDL. It may also contain additional information. For each actinide this section gives values for the parameters of the 6 groups of delayed neutrons λ_d and a_d, and for the group yields of the fission fragments listed in Table 1. It also gives the group yields and half-lives of the short-lived fragments ^{83m}Kr, ^{90m}Y, ^{99m}Tc, ^{103m}Rh, ^{107m}Pd, ^{113}Pd, ^{113m}Ag, ^{135m}Cs, ^{137m}Ba, ^{135}Te, ^{135m}Xe, ^{149}Nd, ^{155}Sm and ^{157}Sm, and indicates their decay products.

There are no neutron data for these last mentioned nuclei. Reference [1] proposes ignoring neutron interaction processes with these nuclei when solving the equations for fuel composition kinetics, because of the shortness of their half-lives. An approximation for prompt decay of isomer fragments, and the short-lived primary fragments ^{113}Pd, ^{135}Te, ^{149}Nd, ^{155}Sm and ^{157}Sm can also be used. In this approximation, the yields of these nuclei should be added to the yields of their decay products. Also, in the ^{113}Cd formation chain the ^{113}Pd yield should be added to the ^{113}Ag yield; to this sum 64% of the ^{113m}Ag yield should be added, and 36% of the ^{113m}Ag yield should be added to the ^{113}Cd yield.

To check the TEND1038 38-group constants for some nuclei, the following characteristics were calculated for spherical models of fast critical assemblies from an international handbook [11]:

- k_{eff} - the effective multiplication factor taking into account prompt and delayed fission neutrons;

- k_p - the effective multiplication factor taking into account only prompt fission neutrons;

- λ - the prompt fission neutron time constant;

- central spectral indices (i.e. the ratios of the cross-sections of different processes in different nuclei, each of which is average with respect to the neutron flux spectrum in the central region of the assembly).

The multigroup neutron transport equation was solved using the MNRSN program from the BEND archive [3] in an S_{32}-approximation using the S_n method from Ref. [12] employing a radial grid uniform within each region of the assembly with, as a rule, a pitch of $\Delta r \approx 0.2$ cm. The eigenvalues were determined with a methodological error of 10^{-5} using a direct procedure of successive approximations with corrections [13]. The spectral indices were calculated for the

neutron spectrum in the central region of an assembly with a radius of 0.5 cm. The dilution cross-section formalism of I.I. Bondarenko [6] was used to account for resonance and heterogeneous effects. The constants used corresponded to the average assembly temperature $\approx$ 300 K.

Increasing the thickness of reflectors made of light materials slows down convergence in Δ r. Therefore, in such cases, the calculations were made for a value of $\Delta r \approx 0.1$ cm, or even $\Delta r \approx$ 0.05 cm if the buffer capacity of the MNRSN program for solving the transport equation allowed. In H_2O or polyethylene reflectors, account was taken of the hydrogen chemical bond using the model from ENDF/B-6.

The value of β - the effective fraction of delayed neutrons, λ_0 - the prompt neutron time constant in the critical state taking account of prompt and delayed neutrons, and l - the lifetime of prompt neutrons, were calculated using the following formulae [8]:

$$\beta = (k_{eff} - k_p)/k_{eff} ;$$

$$\lambda_0 = \frac{\lambda}{1 - (k_{eff} - 1)/(\beta k_{eff})} ;$$

$$l = \beta/|\lambda_0|$$

If, in the calculations, $k_p = 1$ and $k_{eff} = \dfrac{1}{1 - \beta}$, then to calculate λ_0 using the above formula we must change the assembly model so that the following holds

$$k_{eff} < \frac{1}{1 - \beta} .$$

We can, for example, limit ourselves to a value of $k_{eff} = 1.0001$. This can be achieved by reducing the thickness of the reflector or, in assemblies without a reflector, reducing the external radius of the core. Such changes have virtually no influence on the neutron spectrum, especially at the centre of the core.

Table 3 compares the calculated and experimental values of k_{eff}. Apart from the spherical assembly models in Ref. [11], k_{eff} was calculated for 3 spherical models of fast neutron critical assemblies from Ref. [14]. These assemblies were given the names 1Ni, 2Ni and 3Ni. Assembly 1Ni had a Ni reflector 3.15 cm thick, and assemblies 2Ni and 3Ni had an internal lining of Ni 7.75 cm thick in 2Ni and 4.6 cm thick in 3Ni.

Table 4 compares the calculated and experimental or evaluated values of β, $|\lambda_0|$, l and the central spectral indices.

Table 3

k$_{eff}$ values for standard spherical models of critical assemblies

Name of assembly [11]	Core	Reflector (thickness in cm)	Calculation: TEND1038, S$_{32}$, δ k$_{eff}$=10^{-5},Δr ≈ 0.2 cm	Experiment [11]
Hmf1/1 [1]	^{235}U(94%)	-	0.99946	1±0.0010
Hmf1/2 [2]	^{235}U(94%)	-	0.99929	1±0.0010
Hmf2	^{235}U(94%)	^{238}U(20.32)	0.99537	1±0.0030
Hmf3-1	^{235}U(94%)	^{238}U(5.08)	0.99122	1±0.0050
Hmf3-3	^{235}U(94%)	^{238}U(10.16)	0.99418	1±0.0050
Hmf3-8	^{235}U(94%)	WC(4.826)	1.01017	1±0.0050
Hmf3-11	^{235}U(94%)	WC(16.51)	1.01272	1±0.0050
Hmf3-12	^{235}U(94%)	Ni(20.32)	1.02627	1±0.0050
1Ni, /14/	^{239}Pu+^{235}U(90%)	Ni(3.15)	1.00037	1±0.0010 [14]
2Ni, /14/	^{235}U(90%)+^{235}U(36%)	Ni(7.75) [3]	1.00210	1±0.0014 [14]
3Ni, /14/	^{235}U(90%)	Ni(4.6) [3]	1.00371	1±0.0032 [14]
Hmf18	^{235}U(90%)	-	1.00006	1±0.0014
Hmf19	^{235}U(90%)	C(3.45)	1.00693	1±0.0028
Hmf20	^{235}U(90%)	CH$_2$(1.45)	1.00122 [4]	1±0.0028
Hmf21	^{235}U(90%)	Fe(9.7)	1.01127	1±0.0024
Hmf22	^{235}U(90%)	Al(3.9)	0.99365	1±0.0019
Hmf27	^{235}U(90%)	Pb(3.25)	1.00329	1±0.0025
Hmf28	^{235}U(94%)	^{238}U(18.0086)	0.99610	1±0.0030
Hmf29	^{235}U(90%)	^{238}U(2.7)	1.00217	1±0.0020
Hmf32-3	^{235}U(94%)	^{238}U(4.42471)	0.99640	1±0.0017
Hmf32-4	^{235}U(94%)	^{238}U(1.73482)	0.99819	1±0.0017
Hmf41-1	^{235}U(94%)	Be(4.69903)	1.00964 [4]	1.0013±0.0030
Hmf41-2	^{235}U(94%)	Be(11.78559)	1.00990 [4]	1.0022±0.0043
Hmf41-3	^{235}U(94%)	C(5.08002)	1.00200	1.0006±0.0029
Hmf41-6	^{235}U(94%)	C(20.32001)	1.00567	1.0006±0.0045
Imf3	^{235}U(36%)	-	1.00488	1±0.0017
Imf4	^{235}U(36%)	C(3.2)	1.01016	1±0.0030
Imf5	^{235}U(36%)	Fe(8.25)	1.01963	1±0.0021
Imf6	^{235}U(36%)	Al(11.75)	1.00104	1±0.0023
Imf8	^{235}U(36%)	^{238}U(3.25)	1.00682	1±0.0018
Imf9	^{235}U(36%)	CH$_2$(5.75)	0.98494 [5]	1±0.0053
Mmf1	^{239}Pu+^{235}U(94%)	-	0.99769	1±0.0016
Mmf2-1	^{239}Pu+^{235}U(94%)	^{238}U(18.9230)	0.99909	1±0.0042
Mmf2-2	^{239}Pu+^{235}U(94%)	^{238}U(18.8722)	0.99911	1±0.0044
Mmf2-3	^{239}Pu+^{235}U(94%)	^{238}U(18.7452)	0.99925	1±0.0048
Mmf7-1	^{239}Pu+^{235}U(94%)	Be(24.0)	1.01065 [4]	1±0.0045
Mmf7-2	^{239}Pu+^{235}U(94%)	Be(16.2)	1.01330 [4]	1±0.0023
Mmf7-3	^{239}Pu+^{235}U(94%)	Be(8.67)	1.00875 [4]	1±0.0028
Mmf7-4	^{239}Pu+^{235}U(94%)	Be(5.6)	1.00720 [4]	1±0.0028
Mmf7-5	^{239}Pu+^{235}U(94%)	Be(2.74)	1.00355	1±0.0032
Mmf7-6	^{239}Pu+^{235}U(94%)	Be(1.36)	1.00091	1±0.0035
Mmf9	^{239}Pu+^{235}U(90%)	-	0.99830	1±0.0010

Name of assembly [11]	Core	Reflector (thickness in cm)	Calculation: TEND1038, S_{32}, δ $k_{eff}=10^{-5}$, $\Delta r \approx 0.2$ cm	Experiment [11]
Mmf10	$^{239}Pu+^{235}U(90\%)$	-	0.99842	1±0.0009
Pmf1	^{239}Pu	-	0.99825	1±0.0020
Pmf2	$^{239}Pu(20\%^{240}Pu)$	-	1.00145	1±0.0020
Pmf5	^{239}Pu	W(4.699)	1.01158	1±0.0013
Pmf6	^{239}Pu	$^{238}U(19.6088)$	0.99436	1±0.0030
Pmf8	^{239}Pu	$^{232}Th(24.57)$	1.00923	1±0.0006
Pmf9	^{239}Pu	Al (7.9248)	0.99873	1±0.0027
Pmf10	^{239}Pu	$^{238}U(4.1275)$	0.99557	1±0.0018
Pmf11	^{239}Pu	$H_2O(25.4)$	0.98807	1±0.0010
Pmf18	^{239}Pu	Be(3.6881)	1.00258 [4]	1±0.0030
Pmf22	^{239}Pu	-	0.99643	1±0.0021
Pmf23	^{239}Pu	C(2.35)	0.99833	1±0.0020
Pmf24	^{239}Pu	$CH_2(1.55)$	1.00095 [4]	1±0.0020
Pmf25	^{239}Pu	Fe(1.55)	0.99638	1±0.0020
Pmf26	^{239}Pu	Fe(11.9)	1.01091	1±0.0024
Pmf27	^{239}Pu	$CH_2(5.58)$	0.99514 [5]	1±0.0022
Pmf28	^{239}Pu	Fe(19.65)	1.01518	1±0.0022
Pmf29	^{239}Pu	-	0.99501	1±0.0021
Pmf30	^{239}Pu	C(4.49)	1.00248	1±0.0021
Pmf31	^{239}Pu	$CH_2(3.69)$	0.99691 [4]	1±0.0021
Pmf32	^{239}Pu	Fe(4.49)	0.99861	1±0.0020
Pmf35	^{239}Pu	Pb(3.15)	1.00068	1±0.0016
Pmf36	^{239}Pu	$CH_2(2.3)$ [6]	1.00496 [4]	1±0.0034
Pmf39	^{239}Pu	Al(4.25)	0.98749	1±0.0022
Pmf40	^{239}Pu	Cu(1.6)	0.99882	1±0.0039
Pmf41	^{239}Pu	$^{238}U(20.98)$	1.00004	1±0.0016
Umf1	^{233}U	-	0.99436	1±0.0010
Umf2-1	^{233}U	$^{235}U(1.2217)$	0.99714	1±0.0010
Umf2-2	^{233}U	$^{235}U(1.9888)$	0.99966	1±0.0011
Umf3-1	^{233}U	$^{238}U(2.3012)$	0.99611	1±0.0010
Umf3-2	^{233}U	$^{238}U(5.3086)$	0.99793	1±0.0010
Umf4-1	^{233}U	W(2.4384)	1.00644	1±0.0007
Umf4-2	^{233}U	W(5.7912)	1.00979	1±0.0008
Umf5-1	^{233}U	Be(2.0447)	0.99808	1±0.0009
Umf5-2	^{233}U	Be(4.1961)	1.00053 [4]	1±0.0006
Umf6	^{233}U	$^{238}U(19.9136)$	0.99606	1±0.0014

Remarks: 1)   layered model with gaps;
2)   homogeneous sphere, "Godiva";
3)   Internal region;
4) $\Delta r \approx 0.05$ cm;
5) $\Delta r \approx 0.1$ cm;
6)   layer of Cd 0.05 cm thick between the core and the reflector

Table 4

Values of β, $|\lambda_0|$ (10^7 s^{-1}), l (10^{-9} s) values and the central spectral indices for standard spherical models of critical assemblies

Name of assembly [11]	Value	Calculation: TEND1038, S_{32}, $\delta k_{eff}=10^{-5}$, $\Delta r \approx 0.2$ cm	Experiment [11]
Hmf1-1	β	0.0065	0.0065₉ [8]
	$\sigma_f(^{237}Np)/\sigma_f(^{235}U)$	0.810	0.837±0.013
	$\sigma_f(^{238}U)/\sigma_f(^{235}U)$	0.162	0.1647±0.0018
	$\sigma_f(^{239}Pu)/\sigma_f(^{235}U)$	1.377	1.402±0.025
	$\sigma_f(^{233}U)/\sigma_f(^{235}U)$	1.588	1.59±0.03
Hmf1-2	β	0.0065	0.0065₉ [8]
	$|\lambda_0|$	0.113	0.111±0.002
	L	5.75	6.04 [8]
	$\sigma_f(^{237}Np)/\sigma_f(^{235}U)$	0.810	0.837±0.013
	$\sigma_f(^{238}U)/\sigma_f(^{235}U)$	0.162	0.1647±0.0018
	$\sigma_f(^{239}Pu)/\sigma_f(^{235}U)$	1.377	1.402±0.025
	$\sigma_f(^{233}U)/\sigma_f(^{235}U)$	1.588	1.59±0.03
Hmf28	β	0.0067	0.0072[1]) [8]
	$|\lambda_0|$	0.0037	0.038±0.002
	L	18.1	18.2 [8]
	$\sigma_f(^{237}Np)/\sigma_f(^{235}U)$	0.758	0.76±0.01
	$\sigma_f(^{238}U)/\sigma_f(^{235}U)$	0.149	0.149±0.002
	$\sigma_f(^{239}Pu)/\sigma_f(^{235}U)$	1.355	1.37±0.02
	$\sigma_f(^{233}U)/\sigma_f(^{235}U)$	1.586	0.16±0.003[2])
Pmf1	β	0.0018	0.0019₄ [8]
	$|\lambda_0|$	0.0623	0.064±0.001
	L	2.9	3.0 [8]
	$\sigma_f(^{238}U)/\sigma_f(^{235}U)$	0.211	0.2173±0.0023
	$\sigma_f(^{233}U)/\sigma_f(^{235}U)$	1.576	1.578±0.027
	$\sigma_f(^{237}Np)/\sigma_f(^{235}U)$	0.948	0.962±0.016
	$\sigma_f(^{239}Pu)/\sigma_f(^{235}U)$	1.421	1.448±0.029
Pmf2	$\sigma_f(^{238}U)/\sigma_f(^{235}U)$	0.206	0.206±0.003
	$\sigma_f(^{237}Np)/\sigma_f(^{235}U)$	0.93	0.92±0.02
Pmf6	β	0.0029	0.0027₇[3]) [8]
	$|\lambda_0|$	0.0293	0.0214±0.0005
	L	9.9	12.1 [8]
Pmf8	β	0.0021	-
	$|\lambda_0|$	0.0188	0.0197±0.001
	L	11.2	-
	$\sigma_f(^{238}U)/\sigma_f(^{235}U)$	0.192	0.195±0.003
	$\sigma_f(^{237}Np)/\sigma_f(^{235}U)$	0.883	0.92±0.02
	$\sigma_f(^{232}Th)/\sigma_f(^{238}U)$	0.26	0.26±0.01
	$\sigma_{n,\gamma}(^{238}U)/\sigma_f(^{235}U)$	0.069	0.083±0.003
	$\sigma_{2n}(^{238}U)/\sigma_f(^{238}U)$	0.047	0.053±0.003
	$\sigma_{n,\gamma}(^{232}Th)/\sigma_{n,\gamma}(^{238}U)$	1.23	1.2±0.06
	$\sigma_{2n}(^{232}Th)/\sigma_{2n}(^{238}U)$	1.21	1.04±0.03

Name of assembly [11]	Value	Calculation: TEND1038, S_{32}, $\delta k_{eff}=10^{-5}$, $\Delta r \approx 0.2$ cm	Experiment [11]
Umf1	β	0.0029	0.0029$_0$ [8]
	$|\lambda_0|$	0.106	0.100±0.002
	L	2.74	2.82 [8]
	$\sigma_f(^{237}Np)/\sigma_f(^{235}U)$	0.975	0.977±0.016
	$\sigma_f(^{238}U)/\sigma_f(^{235}U)$	0.217	0.2131±0.0023
Umf6	β	0.0037	0.0035$_5$[3) [8]
	$|\lambda_0|$	0.037	0.027 [8]
	L	10.0	13.1 [8]

Remarks: 1)   the calculated evaluation from Ref. [8] is 0.0069$_4$;

2)   there appears to be an erroneous value in Ref. [11]; 1.6±0.3 would be correct;

3)   calculated evaluation.

Conclusion

We have presented the results of the work to complete the setting up of the TENDL neutron data library. The library contains data on the characteristics of neutron interaction with 103 nuclei: 38 actinide nuclei from ^{232}Th to ^{249}Cm, 26 fission fragments, and 39 nuclei which are non-fissile components of fuel and structural and technological materials.

The data from TENDL are stored in ENDF/B text format and in binary form. They are for stationary target nuclei. These data may be used as source data when generating constants for transmutation problems. The text format can be used for the preparation of multigroup constants. The binary format facilitates browsing of the archive. The NDX program manager can be used to browse the TENDL binary archive. This program allows the required information to be extracted from the archive in either tabular or graphical form.

The TEND1038 38-group neutron constants are presented, which are based on the data from TENDL. The upper boundary of the grouping is 20 MeV. There are 11 groups in the <1.2 eV energy region. Temperature dependence and resonance effects are taken into account. For reactions involving emission of neutrons, the group angular distribution of secondary neutrons for all nuclei, except ^{1}H is described in the P_5-approximation. The angular distribution of neutrons scattered on ^{1}H is described in the P_{15}-approximation. The excitation processes of isolated levels and a continuum of levels for inelastic scattering are combined in one inelastic scattering process. Data are included on the parameters of 6 groups of delayed neutrons and the yields of 40 stable and unstable fission fragments. The group calorific values of the reactions were calculated.

TEND1038 is stored in both text format and binary form. The text format allows TEND1038 to be used for numerical solution of the neutron transport equation using the programs available at the All-Russia Scientific Research Institute for Experimental Physics. The GX program manager was developed to work with data from the binary archive. The program allows the user to browse the archive data in both text (tabular) and graphical form.

In checking the TEND1038 constants we limited ourselves to describing the characteristics of standard spherical models of fast neutron critical assemblies from the international handbook Ref. [11] and from Ref. [14]. The cores of these assemblies contained ^{235}U(~90%), ^{235}U(36%), ^{233}U and ^{239}Pu. There was either no reflector, or an H_2O, CH_2, Be, C, Al, Fe, Ni, Cu, WC, W, Pb, ^{232}Th or ^{238}U reflector.

The TEND1038 constant system can be used to solve transmutation problems for waste from the nuclear power sector. This system can also be used to solve traditional nuclear power problems. The TENDL database can be used to perform calculations using the Monte Carlo method, and when preparing multigroup constant systems with significantly more than 38 groups.

References

1. Abramovich S.N., Gorelov V.P., Gorshikhin A.A., et al., Database for numerical modelling of build-up of fragments in power reactor fuel, Voprosy atomnoj nauki i tekhniki, Ser.: Matematicheskoe modelirovanie fizicheskikh protsessov, No. 3, pp. 40-61, 1996.

2. Abramovich S.N., Gorelov V.P., Grebennikov A.N., et al., Recommendations for the selection of neutron nuclear data for numerical modelling of actinide build-up processes in power reactor fuel, Voprosy atomnoj nauki i tekhniki, Ser.: Matematicheskoe modelirovanie fizicheskikh protsessov, No. 3, pp. 62-70, 1996.

3. Grebennikov A.N., Farafontov G.G., The BEND evaluated neutron data archive: Principles for the organization of the archive and the program package for working with archive data, Voprosy atomnoj nauki i tekhniki, Ser.: Matematicheskoe modelirovanie fizicheskikh protsessov, No. 2, pp. 65-70, 1994.

4. Goncharov G.A., Gorelov V.P., Ivannikova V.N., et al., Algorithms for calculating group constants for the energy-angular distribution of scattered neutrons in a medium of stationary nuclei, Voprosy atomnoj nauki i tekhniki, Ser.: Matematicheskoe modelirovanie fizicheskikh protsessov, No. 1, pp. 38-70, 1991.

5. Gorelov V.P., Goncharov G.A., Farafontov G.G., Accounting for thermal and directed movement of nuclei in a medium in multigroup neutron calculations, Voprosy atomnoj nauki i tekhniki, Ser.: Teoreticheskaya i prikladnaya fizika, No. 2, pp. 18-23, 1990.

6. Abagyan L.P., Bazazyants N.O., Bondarenko I.I., Nikolaev M.N., Group constants for reactor calculations, Moscow, Atomizdat, 1964 [in Russian].

7. Gorelov V.P., Grebennikov A.N., Il'in V.I., et al., Numerical modelling of the energy dependence of the neutron flux in a polyethylene block with a fast neutron source, Voprosy atomnoj nauki i tekhniki, Ser.: Yadernye konstanty, No. 2, pp. 39-51, 1998.

8. G. Robert Keepin, Physics of Nuclear Kinetics, Massachusetts - Palo Alto - London: Addison-Wesley Publishing Company, Inc., 1965.

9. Abagyan L.P., Bazazyants N.O., Nikolaev M.N., Tsibulya A.M., Group constants for reactor and shielding calculations, Handbook, edited by M.N. Nikolaeva, Dr. of Physical and Mathematical Sciences, Moscow, Ehnergoizdat, 1981 [in Russian].

10. Luk'yanov A.A., Slowing down and absorption of resonance neutrons, Moscow, Atomizdat, 1974 [in Russian].

11. International Handbook of Evaluated Criticality Safety Benchmark Experiments, Nuclear Energy Agency, Organization for Economic Co-Operation and Development, Paris, NEA/NSC/DOC(95)03, September 1999 Edition.

12. Carlson B., Bell, J., Solution of the transport equation using the S_n method, in nuclear reactor physics: selected pages by foreign scientists, edited by A.I. Lejpunskij and V.S. Fursov, Moscow, Press of the State University for the use of nuclear energy to the Council of Ministers of the USSR, 1959, p. 408 [in Russian].

13. Gorelov V.P., Grebennikov A.N., Farafontov G.G., Yudintsev, V.F., Speeding up convergence of iterations in the direct procedure for determining the eigenvalues of the neutron transport equation by successive approximations, Voprosy atomnoj nauki i tekhniki, Ser.: Matematicheskoe modelirovanie fizicheskikh protsessov, No. 3, 1992, p. 81-85.

14. Kuvshinov M.I., Gorelov V.P., Egorov V.P., Il'yin V.I., Measurements of Critical Parameters of ^{239}Pu and ^{235}U Spherical Assemblies, which contain Nickel as a Reflector and a Filler of the Central Cavity, for the Purpose of Nuclear Data Testing, Report INDC(CCP)-421, IAEA Nuclear Data Section, IAEA, Vienna, December 1999.

01-11405 (131)   [003]

<u>Translated from Russian</u>

UDC 539.163

RESOLVED RESONANCE PARAMETERS FOR ^{236}Np

G.B. Morogovskij, L.A. Bakhanovich
Radiation Physics and Chemistry Problems Institute
Belarus National Academy of Sciences

RESOLVED RESONANCE PARAMETERS FOR ^{236}Np. Multilevel Breit-Wigner parameters were obtained for fission cross-section representation in the 0.01-33 eV energy region from evaluation of a ^{236}Np experimental fission cross-section in the resolved resonance region.

This paper completes a cycle of papers in which multilevel Breit-Wigner resonance parameters are obtained based on the measurements of Danon et al. [1]. The previous papers [2, 3] give parameter sets for ^{238}Np and ^{232}Pa nuclei.

There are no resonance parameters in the only existing file of evaluated ^{236}Np nuclear data (JENDL-3.2 [4]), which gives cross-sections in the 10^{-5} eV-20 keV region as a point curve based on the $\sigma_f(E)$ measurements in [5]. However, the σ_f^{2200} and the fission cross-section group constants calculated using the file in [4] differ from the corresponding values given in [5]: in the 0.465-46.5 eV energy range, the differences range from 0.2% for the 2.15-4.65 eV group to 14.6% for the 21.5-46.5 eV group. The remaining cross-section types in this file were obtained theoretically.

Danon et al. [1] have obtained Breit-Wigner parameters up to 22.08 eV based on their fission cross-section measurements in the 0.01 eV-11 keV energy range. A comparison of the $\sigma_f(E)$ cross-section reconstructed according to these parameters, taking the energy resolution and temperature into account, with the measurements in [1] shows that, at the very least, these parameters require improvement. In the present paper we have, through analysis of the experimental data in [1] and evaluation of σ_f^{2200}, obtained multilevel Breit-Wigner parameters which reproduce the fission cross-section curve in [1] more precisely and over a wider energy range.

The $\sigma_f(E)$ curve measured in [1] gives, according to the authors' evaluation, σ_f^{2200} =3007 ± 90 b, whereas calculation from the parameters in [1] gives a σ_f^{2200} of 3142.3 b, which is substantially greater than in [5], where σ_f^{2200} =2770±260 b. Our evaluation of the $\sigma_f(E)$ curve in [1] in the thermal region gives σ_f^{2200} =2983.04±82.95 b, which is somewhat closer to the value in [5] with which the authors of [1] compare their measurements. Using the σ_f^{2200} value we obtained for [1] with the thermal fission cross-section value from [5] and the measurements for

E=0.0253 eV in [6,7,8] gives a weighted average σ_f^{2200} =2764.74±60.14 b, which is very close to the value in [5]. We took this weighted average value as the evaluated thermal fission cross-section. The normalization factor used for the experimental measurements in [1] when calculating the resonance parameters was K_N=2764.74/2983.04=0.92682.

In [1] the authors identified 23 resonances for the fission cross-section in the 0.01-22 eV energy range and one background resonance with E_r=-1.41 eV, 2 $g\Gamma_n$= 2.624 meV and Γ_f=7.006 eV, required to describe the fission cross-section curve in the energy range up to 2 eV, with approximately 75% of the σ_f^{2200} value being the contribution of this resonance. The clearly non-physical Γ_f values (12 times larger than the $<\Gamma_f>$ calculated for the remaining resonances) and Γ_n^0 (8 times larger than the $<\Gamma_n^0>$ for the remaining resonances) of the background resonance were needed by the authors to describe the $\sigma_f(E)$ curve in the 0.4-0.6 eV and 0.8-1.8 eV energy ranges for values of the resonance energies and resonance parameters taken in [1].

Our calculations showed that agreement between the experimentally measured and the calculated fission cross-section values in the 0.01-22 eV energy range is improved considerably by:

1.   Changing the energies of a number of resonances (see Table 1);

Table 1

E_r, eV [1]	-1.41	0.20	0.70	2.67	3.07	11.95	12.72	17.88	20.28	22.08
E_r, eV changed	-0.80	0.22	0.685	2.64	3.10	11.91	12.82	17.53	20.27	22.13

2.   Assuming that the resonance E_r=9.62 eV [1] is a doublet, and replacing it by two others: E_r=9.31 eV and E_r= 9.89 eV;

3.   Adding resonances with the following energies: 0.85, 1.55, 10.95, 18.24 and 20.87 eV;

4.   Excluding resonances with the following energies: 2.39, 2.8, 3.38 and 12.36 eV [1];

5.   Calculating new parameter values for all the resonances.

From analysis of the experimentally measured fission cross-section in [1] we can, with some confidence, identify 12 resonances in the 22.5-33.5 eV energy range and calculate their parameters, enabling good reproduction of the measured $\sigma_f(E)$ curve up to 33 eV.

Since the parameters of all the resonances were calculated on the basis of the fission cross-section alone, and the resolution of the experiment was low, a large uncertainty arises in obtaining the Γ_γ values for each resonance. $<\Gamma_\gamma>$=40 meV was used as additional information in calculating the radiation widths. Two additional resonances with energies 0.85 eV and 1.55 eV enabled good description of the fission cross-section curve in the 0.4-0.6 eV and 0.8-1.8 eV

energy intervals with purely physical values for the background resonance parameters: E_r=-0.80 eV, $g\Gamma_n$=0.303 meV, Γ_f=900 6 meV and Γ_γ=40.0 meV.

Table 2 gives the resolved resonance parameters up to 33.35 eV obtained in the present study. For ease of comparison, the $\sigma_f(E)$ values calculated using those parameters were renormalized to the experimental data in [1] using the renormalization factor K_R=1/K_N. The results of comparison of the measured fission cross-section in [1] with calculations based on the parameters obtained in [1], which are also given in Table 2, are as follows:

1.   In the 0.5-20 eV energy range, the resonance fission integral, calculated from the experimental measurements in [1] as the sum of the resonance integrals for each resonance, is 1116.82 b. Calculation according to the authors' parameters in [1] gives a value of 1165.21 b, which is 4.3% greater, with a mean deviation in the region of one resonance of 7.6%. The I_f (0.5-0 eV) obtained according to our data with renormalization is 1117.28 b, which is virtually the same as the calculation based on the measurements in [1], with a mean deviation in the region of one resonance of 1.9%. The average experimental error in the 0.01-20 eV range is 12.66%, the mean deviation from the experiment of the cross-sections calculated according to the Ref. [1] parameters is 12.61%, and the mean deviation from the Ref. [1] experiment of the cross-sections calculated according to our parameters is 11.05%;

2.   The value of the resonance fission integral for the 0.5-33 eV range was 1171.77 b for the experiment in [1] and 1173.27 b for the Table 2 parameters with renormalization, which is a difference of 0.13% with a mean deviation in the region of one resonance of 1.66%. The average experimental error in the 0.01-33 eV range is 12.87%, and the mean deviation from the experiment in [1] of the cross-sections calculated according to our parameters with renormalization is 9.63%.

Therefore we can claim that our set of resonance parameters is better than the parameters in [1]; it reproduces the $\sigma_f(E)$ curve measured experimentally in [1] and, in addition, the resolved resonance region was significantly expanded.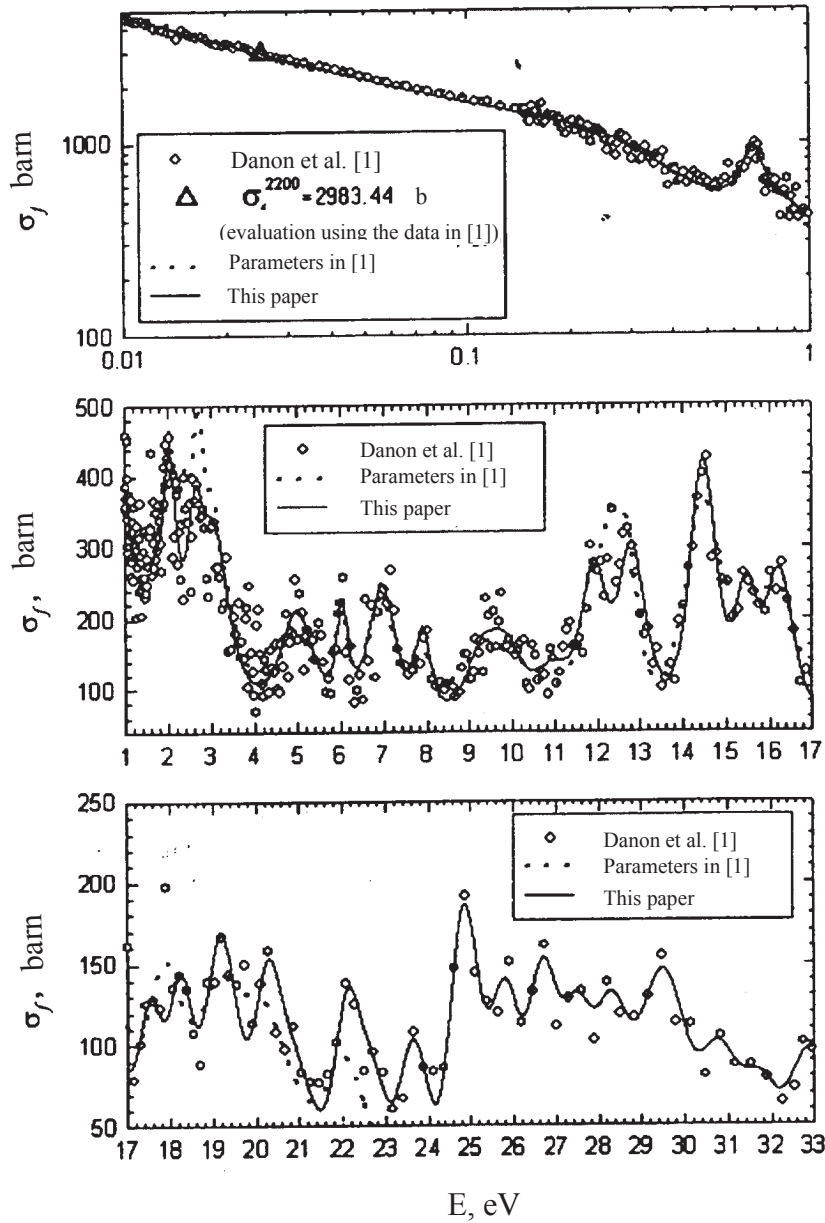 Fig. 1 show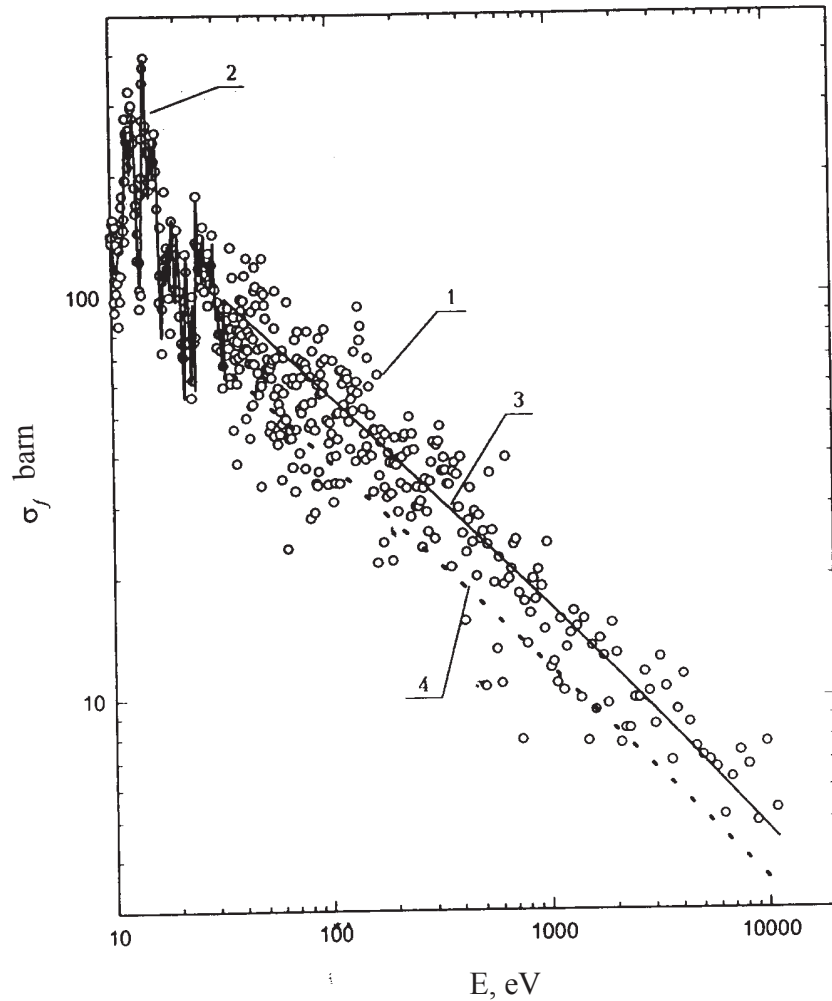s a comparison of the experimental fission cross-sections with the fission cross-sections calculated from both sets of parameters in the 0.01-33 eV energy range; the cross-sections obtained from the parameters in Table 2 were renormalized as described above for ease of comparison.

The resonance fission integral calculated from the Table 2 parameters in the 0.5-33 eV energy range is 1087.41 b, which is approximately 200 b larger than the corresponding resonance integral for the data in [5]. At the same time, the fission cross-section values measured in [5] in the 0.0253-0.3 eV energy range are in good agreement with the $\sigma_f(E)$ values obtained from the Table 2 resonance parameters. One reason for divergence in the resonance integrals is that, judging by the figures in [1 and 5], no resonance with E_r= 0.7 eV was observed, but its contribution to the I_f value is approximately 80 b. Also, the resonance fission integral in [5] was calculated from experimental data from which resonances may have been missing given the low energy resolution of the experiment in [5]. On the other hand, the fission cross-sections of all the nuclei experimentally measured in [1] systematically exceed the earlier measurements, but the authors of [1] cannot explain this discrepancy precisely.

Table 2

Resonance parameters for ^{236}Np

Eγ, eV	J	Γ_n, meV	Γ_γ, meV	Γ_f, meV
-0.800	6.5	0.56322	40.00	900.600
0.220	5.5	0.05287	40.15	398.410
0.685	6.5	0.03345	33.60	68.818
0.850	5.5	0.09537	41.53	505.320
1.550	5.5	0.13916	47.85	860.140
2.030	6.5	0.15822	38.02	354.520
2.640	6.5	0.16453	41.76	408.720
3.100	5.5	0.55053	43.71	833.270
4.990	5.5	0.70601	41.85	957.520
6.030	6.5	0.20081	36.04	210.100
6.960	6.5	0.82132	46.02	719.920
7.900	5.5	0.35117	38.00	318.890
9.310	5.5	0.78277	45.24	953.490
9.890	6.5	0.69524	49.53	949.750
10.950	6.5	0.50059	36.08	874.330
11.910	5.5	1.52328	48.13	582.030
12.820	6.5	1.63501	43.11	583.180
14.480	6.5	2.76176	42.29	521.190
15.470	5.5	1.16510	39.75	290.440
16.250	6.5	1.99346	42.59	557.650
17.530	5.5	0.70893	37.24	299.390
18.240	5.5	0.87711	39.65	287.230
19.200	6.5	1.55662	42.88	558.300
20.270	6.5	0.91292	39.81	302.100
20.870	5.5	1.11456	42.97	768.980
22.130	5.5	1.27196	37.21	212.770
22.730	6.5	0.52873	34.53	141.710
23.650	5.5	1.13774	36.76	184.760
24.850	5.5	2.42428	35.48	150.030
25.800	6.5	1.64335	44.23	156.640
26.700	5.5	2.85567	32.05	35.502
27.500	6.5	2.66723	40.00	26.888
28.300	6.5	2.50194	40.00	27.081
29.500	5.5	4.37710	46.79	901.660
30.830	6.5	1.78772	32.79	35.422
31.750	5.5	2.07220	33.01	35.214
32.800	6.5	1.87924	29.35	38.457
33.350	6.5	0.85809	40.00	197.500

The thermal data derived from Table 2 using the value R=9.89 fm are as follows:

$$\sigma_t^{2200} = 2970.30 \text{ b} \qquad \sigma_f^{2200} = 2764.74 \text{ b} \qquad g_f = 1.01695$$

$$\sigma_n^{2200} = 10.59 \text{ b} \qquad \sigma_\gamma^{2200} = 194.97 \text{ b} \qquad g_\gamma = 1.03222$$

The mean resonance parameters for the 0-33 eV energy range are:

$$<\Gamma_n^0> = 0.30018 \text{ meV} \qquad <\Gamma_\gamma> = 40.00 \text{ meV}$$

$$<\Gamma_f> = 419.717 \text{ meV} \qquad <D> = 0.9309 \text{ eV}$$

The fission cross-section calculated according to these parameters is in agreement with the $\sigma_f(E)$ curve in [1] in the 33-10000 eV region (see Fig. 2), although it is even somewhat higher than the mean experimental values, while I_f (0.5-10 000 eV)=1268.43 b.

The appreciable increase observed in the Γ_n^0 values for resonances above 24 eV and also the anomalously high $S_0 \approx 1.61 \cdot 10^{-4}$ value obtained from the mean resonance parameters are attributable to not only possible unresolved doublets but also the absence of weak resonances owing to a sharp decline in experimental resolution as the energy increases. Therefore the possible missing resonances were evaluated in the 0-21 eV interval, as in Ref. [3], and the following values obtained:

$$<D> = 0.516 \pm 0.042 \text{ eV} \qquad <\Gamma_n^0> = 0.11187 \text{ meV} \qquad S_0 = (1.15 \pm 0.05) \, 10^{-4}.$$

Using these evaluations instead of the mean values obtained above lowers the $\sigma_f(E)$ curve (see Fig. 2) and thus reduces the resonance fission integral in the 33-10 000 eV region by more than 30%, as a result of which I_f (0.5-10 000 eV) is 1212.03 b. The matter of the I_f value for ^{236}Np remains unresolved. The I_f (0.5-10 000 eV) values from Refs [1 and 5] (1353±86 b and 1040±60 b) can be regarded as the upper and lower interval boundaries of the possible resonance fission integral for the given region. The I_f (0.5-10 000 eV) obtained in this paper, 1212.03 b, lies virtually in the middle of this interval.

Fig. 1. Comparison of the [236]Np experimental fission cross-sections and [236]Np fission cross-sections calculated from two sets of parameters in the 0.01-33 eV energy range. The calculated data in this paper have been renormalized to the experimental data in [1] for ease of comparison.

Fig. 2.   Comparison of the ^{236}Np experimental fission cross-sections and ^{236}Np fission cross-sections calculated from two sets of parameters in the 10-10 000 eV energy range.
    Legend:
1 -   experimental data in [1], renormalized to σ_f^{2200}=2764.74 b;
2 - σ_f(E) calculated from the Table 2 parameters;
3 - σ_f(E), calculated from the mean Table 2 parameters (averaged in the 0-33 eV range);
4 - σ_f(E), calculated from the mean parameters: $<\Gamma_f>$ and $<\Gamma_\gamma>$ from the Table 2 parameters (0-33 eV), $<\Gamma_n^0>$ and $<D>$ from evaluation of the missing resonances.

REFERENCES

1. Danon, Y., Moore, M.S., Koehler, P.E. et al., Nucl. Sci. Eng., 1996, v. 124, p. 482.

2. Morogovskij, G.B., Voprosy atomnoj nauki i tekhniki, Ser.: Yadernye konstanty, 1999, No. 1, p. 19.

3. Morogovskij, G.B, Bakhanovich, L.A., Voprosy atomnoj nauki i tekhniki, Ser.: Yadernye konstanty, 1999, No. 2, p. 91.

4. Japanese Evaluated Data Library, Version 3, JAERI 1319, 1990.

5. Val'skij, G.V., Gromova, E.A., Danichev, V.V. et al., First International Conference on Neutron Physics, Kiev, 1987, v. 3. p. 99.

6. Jaffey, A.H., Lerner, J.L., Report ANL-6600, 1961, p. 124.

7. Lindner, M., Seegmiller, D.W., J., RCA, 1990, v. 49, p. 1.

8. Belyaev, B.N., Gromova, E.A., Kovalenko, S.S. et al., Atomnaya Ehnergia, 1986, v. 60, No. 2, p. 141.

UDC 539.17

EVALUATION OF THE CROSS-SECTIONS OF THRESHOLD REACTIONS LEADING TO THE PRODUCTION OF LONG-LIVED RADIONUCLIDES DURING IRRADIATION OF STEELS BY THERMONUCLEAR SPECTRUM NEUTRONS

A.I. Blokhin, N.N. Buleeva, V.N. Manokhin, M.V. Mikhajlyukova,
S.M. Nasyrova, M.V. Skripova
State Scientific Centre - A.I. Leipunsky Institute for Physics and Power Engineering

EVALUATION OF THE CROSS-SECTIONS OF THRESHOLD REACTIONS LEADING TO LONG-LIVED RADIONUCLIDE PRODUCTION DURING IRRADIATION OF STEELS BY THERMONUCLEAR SPECTRUM NEUTRONS. The present paper analyses and evaluates the cross-sections of threshold reactions leading to the production of long-lived radionuclides during the irradiation, by thermonuclear spectrum neutrons, of steels containing V, Ti, Cr, Fe and Ni. On the basis of empirical systematics. a new evaluation of the (n,2n), (n,p), (n,np), (n,α) and (n,nα) excitation functions is made for all isotopes of V, Ti, Cr, Fe and Ni and for intermediate isotopes produced in the chain from irradiated isotopes up to production of the long-lived radionuclides ^{39}Ar, ^{42}Ar, ^{41}Ca, ^{53}Mn, ^{60}Fe, ^{60}Co, ^{59}Ni and ^{63}Ni. A comparison is made with the experimental and other evaluated data.

Introduction

When steels containing V, Ti, Cr, Fe and Ni are irradiated, the long-lived radionuclides ^{39}Ar, ^{42}Ar, ^{41}Ca, ^{53}Mn, ^{60}Fe, ^{60}Co, ^{59}Ni and ^{63}Ni are produced as a result of (n,2n), (n,p), (n,np), (n,α), (n,nα), (n,d), (n,t) and (n,2p) threshold reactions and radiative capture reactions. The contribution of the individual isotopes and reactions in the production of these radionuclides depends on the incident neutron spectrum. The present paper sets out the reaction chains leading to the production of these radionuclides, and also the contributions of the steel isotope components in their production for thermonuclear spectrum neutrons. All these data are taken from [1].

Analysis of the available experimental and evaluated data reveals significant discrepancies in many cases. For this reason, a new evaluation was performed on the basis of systematics developed earlier [2] which, in our view, yield more reliable conclusions.

Reactions determining the activation of steels

When steels containing the elements V, Ti, Cr, Fe and Ni are irradiated with thermonuclear spectrum neutrons a number of long-lived radionuclides are produced, determining the activation

of the steels that can be used as the first wall of a fusion reactor. A list of such isotopes, and the reactions leading to their production, is given in the following tables which are based on the reaction chains given in [1].

1.   **Vanadium**. Natural vanadium contains two isotopes: $^{50}V(0.25\%)$ and $^{51}V(99.75\%)$. Irradiation of natural vanadium with thermonuclear spectrum neutrons results in the production of the following long-lived radionuclides: ^{39}Ar (269.0 years), ^{42}Ar (33.0 years), ^{41}Ca ($1.0 \cdot 10^5$ years) (Table 1).

As can be seen, activation of vanadium is determined by the ^{51}V isotope.

From [1] it follows that we need to know the cross-sections of five types of threshold reaction in the isotopes of vanadium, titanium, scandium, calcium and argon (Table 2).

2.   **Titanium**. Natural titanium contains five stable isotopes: ^{46}Ti (8.0%), ^{47}Ti (7.3%), ^{48}Ti (73.8%), ^{49}Ti (5.5%) and ^{50}Ti (5.4%).

Irradiation of natural titanium with thermonuclear spectrum neutrons results in the production of the following long-lived radionuclides: ^{39}Ar (269.0 years), ^{42}Ar (33.0 years) and ^{41}Ca ($1.03 \cdot 10^5$ years).

Table 1

Contribution of vanadium isotopes in the production of the long-lived nuclides indicated

Nuclides	Contribution of vanadium isotopes, %	
	^{50}V	^{51}V
^{39}Ar	3.44	95.56
^{42}Ar	0.61	99.38
^{41}Ca	1.08	98.92

Table 2

List of reactions and isotopes leading to the production of ^{39}Ar, ^{42}Ar and ^{41}Ca nuclides during vanadium activation

Reaction	Isotopes
n,2n	^{40}Ar, ^{42}Ca, ^{43}Ca, ^{44}Ca, ^{47}Ti, ^{50}V
n,α	^{45}Sc, ^{42}Ca, ^{45}Ca, ^{46}Ti, ^{47}Ti, ^{48}Ti, ^{49}Ti, ^{50}V, ^{51}V
n,nα	^{46}Sc, ^{43}Ca, ^{44}Ca, ^{46}Ca, ^{51}V
n,d	^{50}V
n,2p	^{47}Ti

Table 3

Contribution of titanium isotopes in the production of ^{39}Ar, ^{42}Ar and ^{41}Ca nuclides

Nuclides	Contribution of titanium isotopes, %				
	^{46}Ti	^{47}Ti	^{48}Ti	^{49}Ti	^{50}Ti
^{39}Ar	97.06	0.86	2.08	$3.35 \cdot 10^{-3}$	$3.54 \cdot 10^{-5}$
^{42}Ar	13.90	0.35	84.65	1.09	$5.41 \cdot 10^{-3}$
^{41}Ca	84.45	0.50	15.04	$1.14 \cdot 10^{-2}$	$4.45 \cdot 10^{-5}$

Table 4

List of reactions and isotopes leading to the production of ^{39}Ar, ^{42}Ar and ^{41}Ca nuclides during titanium activation

Reaction	Isotopes
n,2n	^{40}Ar, ^{42}Ca, ^{43}Ca, ^{44}Ca, ^{48}Ca, ^{47}Ti, ^{49}Ti, ^{50}Ti
n,α	^{45}Sc, ^{42}Ca, ^{43}Ca, ^{45}Ca, ^{46}Ca, ^{46}Ti, ^{47}Ti, ^{48}Ti, ^{49}Ti, ^{50}Ti
n,nα	^{43}Ca, ^{44}Ca, ^{46}Ca
n,d	^{46}Ti
n,2p	^{43}Ca, ^{46}Ti
n,t	^{47}Ti

3. **Chromium.** Natural chromium contains four stable isotopes: ^{50}Cr (4.345%), ^{52}Cr (83.789%), ^{53}Cr (9.501%) and ^{54}Cr (2.365%).

Irradiation of natural chromium with thermonuclear spectrum neutrons results in the production of the following long-lived radionuclides (Tables 5 and 6): ^{39}Ar (269.0 years), ^{42}Ar (33.0 years), ^{41}Ca ($1.03 \cdot 10^5$ years) and ^{53}Mn ($3.697 \cdot 10^6$ years).

4. **Iron**. Natural iron contains four stable isotopes: ^{54}Fe (5.8%), ^{56}Fe (91.72%), ^{57}Fe (2.2%) and ^{58}Fe (0.28%).

Irradiation of natural iron with thermonuclear spectrum neutrons results in the production of the following long-lived radionuclides (Tables 7 and 8): ^{53}Mn ($3.697 \cdot 10^6$ years), ^{60}Fe ($2.998 \cdot 10^5$ years), ^{60}Co (5.268 years), ^{59}Ni ($7.495 \cdot 10^4$ years) and ^{63}Ni (100.03 years).

5. **Nickel**. Natural nickel contains five stable isotopes: ^{58}Ni (68.27%), ^{60}Ni (26.10%), ^{61}Ni (1.13%), ^{62}Ni (3.59%) and ^{64}Ni (0.91%).

Irradiation of natural nickel with thermonuclear spectrum neutrons results in the production of the following long-lived radionuclides (Tables 9 and 10): ^{60}Co (5.268 years), ^{59}Ni (7.495·10^4 years) and ^{63}Ni (100.03 years).

Table 5

Contribution of chromium isotopes in the production of ^{39}Ar, ^{42}Ar, ^{41}Ca and ^{53}Mn nuclides

Nuclides	Contribution of chromium isotopes, %			
	^{50}Cr	^{52}Cr	^{53}Cr	^{54}Cr
^{39}Ar	98.26	1.74	4.09·10^{-3}	1.42·10^{-4}
^{42}Ar	17.50	82.32	0.17	1.37·10^{-3}
^{41}Ca	92.33	7.66	1.05·10^{-2}	5.80·10^{-4}
^{53}Mn	0	3.57·10^{-3}	1.75	98.24

Table 6

List of reactions and isotopes leading to the production of ^{39}Ar, ^{42}Ar, ^{41}Ca and ^{53}Mn nuclides during chromium activation

Reaction	Isotopes
n,2n	^{40}Ar, ^{42}Ca, ^{43}Ca, ^{44}Ca, ^{46}Ca, ^{47}Ti, ^{49}Ti, ^{50}Ti, ^{53}Cr
n,α	^{45}Sc, ^{42}Ca, ^{45}Ca, ^{46}Ca, ^{46}Ti, ^{47}Ti, ^{48}Ti, ^{49}Ti, ^{50}Ti, ^{49}V, ^{51}V, ^{50}Cr, ^{52}Cr, ^{53}Cr, ^{54}Cr
n,nα	^{46}Sc, ^{43}Ca, ^{44}Ca, ^{46}Ca, ^{50}Cr, ^{52}Cr, ^{53}Cr, ^{54}Cr
n,d	^{50}Cr

Table 7

Contribution of iron isotopes in the production of the long-lived ^{53}Mn, ^{60}Fe, ^{60}Co, ^{59}Ni and ^{63}Ni radionuclides

Nuclides	Contribution of iron isotopes. %			
	^{54}Fe	^{56}Fe	^{57}Fe	^{58}Fe
^{53}Mn	99.93	0.07	1.22·10^{-5}	8.08·10^{-6}
^{60}Fe	0.0	0.08	1.83	98.09
^{60}Co	0.0	0.05	1.44	98.50
^{59}Ni	0.0	0.02	0.87	99.11
^{63}Ni	0.0	0.01	0.71	99.28

Table 8

List of reactions and isotopes leading to the production of ^{53}Mn, ^{60}Fe, ^{60}Co, ^{59}Ni and ^{63}Ni nuclides during iron activation

Reactions	Isotopes
n,2n	^{54}Mn,^{55}Mn,^{56}Fe,^{57}Fe,^{59}Fe,^{60}Ni
n,α	^{58}Fe
n,p	^{60}Co
n,d	^{54}Fe,^{56}Fe
n,t	^{57}Fe,^{59}Fe

Table 9

Contribution of nickel isotopes in the production of ^{60}Co, ^{59}Ni and ^{63}Ni nuclides

Nuclides	Contribution of nickel isotopes. %				
	^{58}Ni	^{60}Ni	^{61}Ni	^{62}Ni	^{64}Ni
^{60}Co	10.86	88.60	0.33	0.21	$1.43 \cdot 10^{-4}$
^{59}Ni	61.26	38.72	$1.79 \cdot 10^{-2}$	$3.7 \cdot 10^{-4}$	$6.82 \cdot 10^{-7}$
^{63}Ni	$2.35 \cdot 10^{-6}$	$4.27 \cdot 10^{-3}$	0.11	66.89	33.00

Table 10

List of reactions and isotopes leading to the production of ^{60}Co, ^{59}Ni and ^{63}Ni nuclides during nickel activation

Reaction	Isotopes
n,2n	^{60}Ni, ^{61}Ni, ^{62}Ni, ^{64}Ni
n,α	^{62}Ni, ^{64}Ni, ^{63}Cu
n,nα	^{63}Ni
n,p	^{58}Ni
n,d	^{58}Ni, ^{61}Ni

Method for evaluating the excitation functions

The threshold reaction excitation functions were evaluated on the basis of systematics developed previously at the Nuclear Data Centre and described in detail in [2]. The main data selection and evaluation criteria are set down below:

The recommended excitation functions were evaluated using the systematics developed in [2 and 3]. The main features of these systematics, the procedures and evaluation criteria for the recommended curves are given below.

1. The forms of the (n,2n) reaction excitation function are similar in the incident neutron energy regions ranging from the (n,2n) reaction threshold to the (n,3n) reaction threshold. For $Q_{n2n} < Q_{nnp}$ the maximum (limiting) (n,2n) reaction cross-section is determined by the relationship:

$$\sigma_{top} = 65.4 \, A^{2/3} \, mb, \tag{1}$$

where Q_{n2n}, Q_{nnp} are the energies of the (n,2n) and (n,np) reactions, respectively, and A is the mass number.

For $Q_{n2n} > Q_{nnp}$ the maximum (n,2n) reaction cross-section is determined by the relationship:

$$\sigma_{top} = \sigma_{n,2n} + \sigma_{n,np} \tag{2}$$

The (n,2n) reaction cross-section in the energy region from threshold up to the maximum is calculated on the basis of the universal normalized function [2].

The (n,2n) reaction cross-section above the maximum is calculated by deducting the (n,3n) reaction from the maximum (n,2n) reaction cross-section. In turn, the (n,3n) reaction cross-section from threshold to maximum is calculated using the normalized function and the maximum cross-section, determined from the systematics of the maximum (n,3n) cross-sections as a function of A.

2. The forms of the (n,p) reaction excitation function are similar for isotopes with the same (N-Z). The maximum (n,p) reaction cross-sections at the (lnσ - A) co-ordinates decrease linearly as a function of A for the isotopes of a given element and increase linearly as a function of Z for isotopes with the same (N-Z).

3. The forms of the (n,α) reaction excitation functions are similar for isotopes with the same (N-Z). The maximum (n,p) reaction cross-sections at the (lnσ - A) co-ordinates decrease linearly as a function of A for the isotopes of a given element and increase linearly as a function of Z for isotopes with the same (N-Z).

4. The position of the maxima of the (n,p) reaction is proportional to the difference in the thresholds of the (n,np) and (n,p) reactions.

5. The position of the maxima of the (n,α) reaction is proportional to the difference in the thresholds of the (n,nα) and (n,α) reactions.

The excitation functions of the threshold reactions leading to the production of long-lived radionuclides obtained in this paper are presented as graphs in the Annex (Figs 1-50) compared with existing experimental data and evaluated excitation functions from other evaluated nuclear data libraries.

ANNEX

Graphs of the excitation functions of threshold reactions leading to the production of long-lived radionuclides during the irradiation, with thermonuclear spectrum neutrons, of steels containing V, Ti, Cr, Fe and Ni (Figs 1-50).

The abbreviations for the libraries used for comparison with the evaluations performed in this paper are:

ADL-3   - activation data library (Russia);
BROND-2 - recommended evaluated neutron data library, Version 2 (Russia);
JENDL-3.2 - Japanese evaluated nuclear data library, Version 3.2;
ENDF-B6 - evaluated nuclear data file, Version 6 (USA);
JEF-2   - joint European library, Version 2 (western Europe).
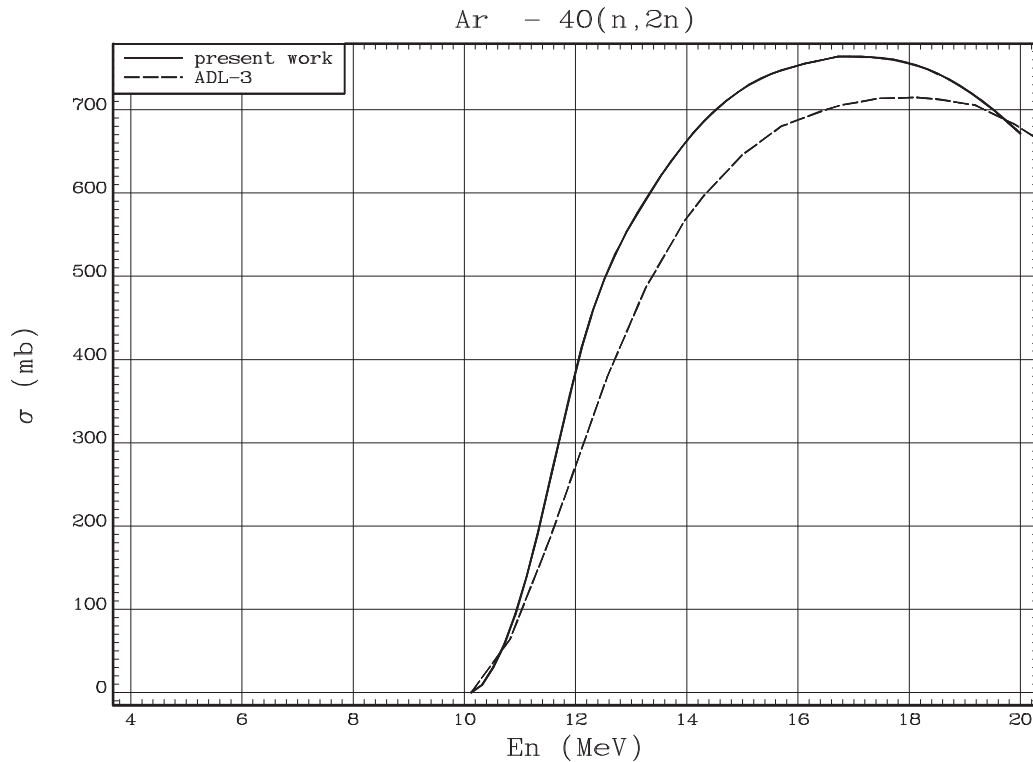
Fig. 1. ^{40}Ar(n,2n)^{39}Ar reaction cross-section

Ca − 42(n,2n)
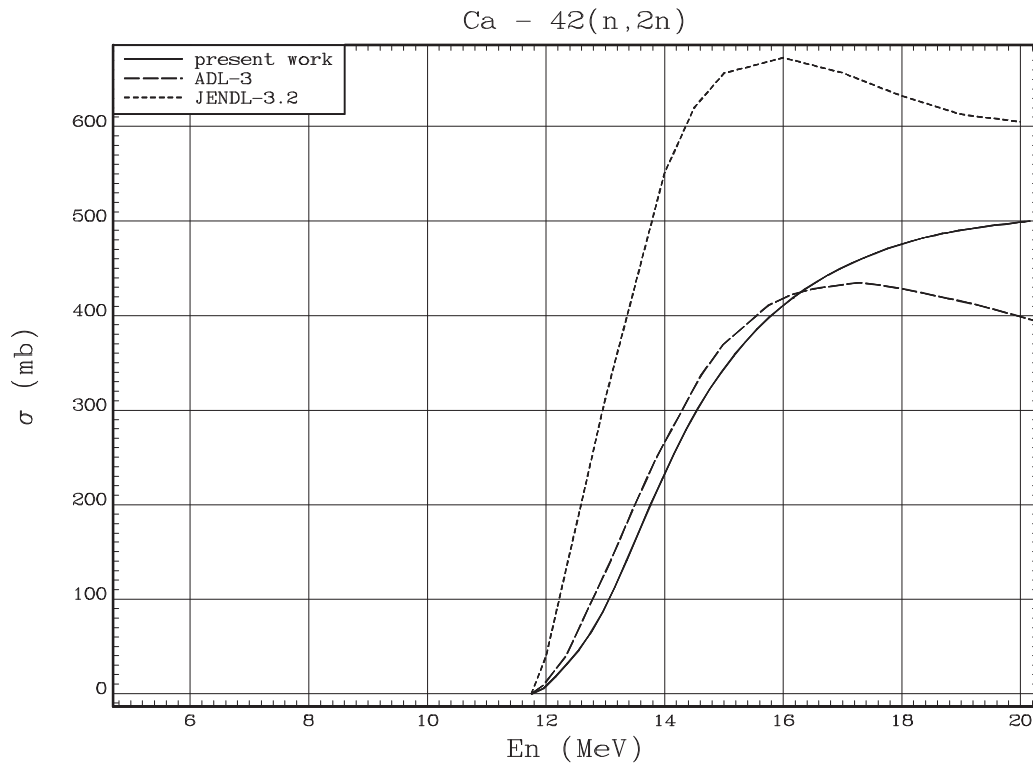
Fig. 2. ^{42}Ca(n,2n)^{41}Ca reaction cross-section

CA −42(n,a)
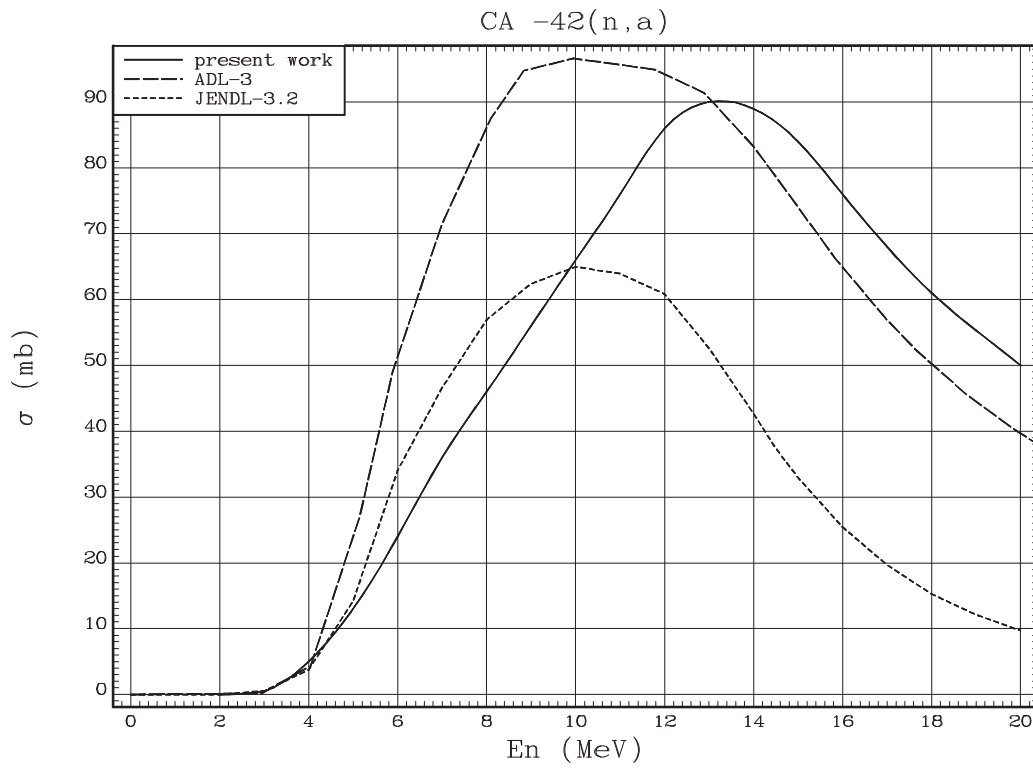
Fig. 3. ^{42}Ca(n,α)^{39}Ar reaction cross-section
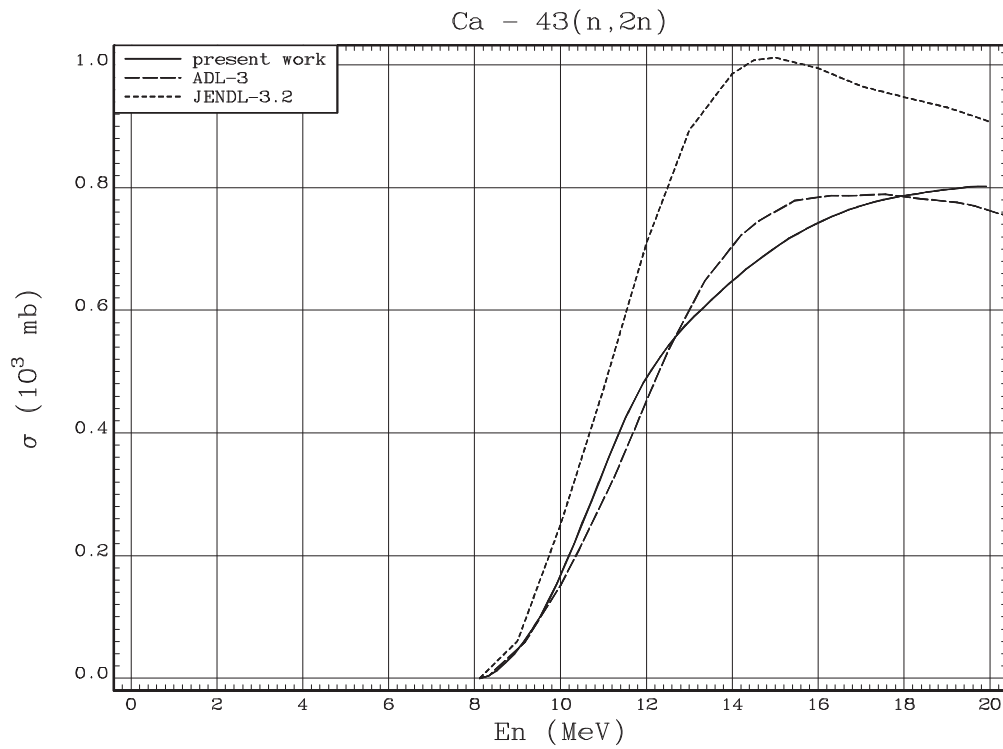
Fig. 4. ^{43}Ca(n,2n)^{42}Ca reaction cross-section
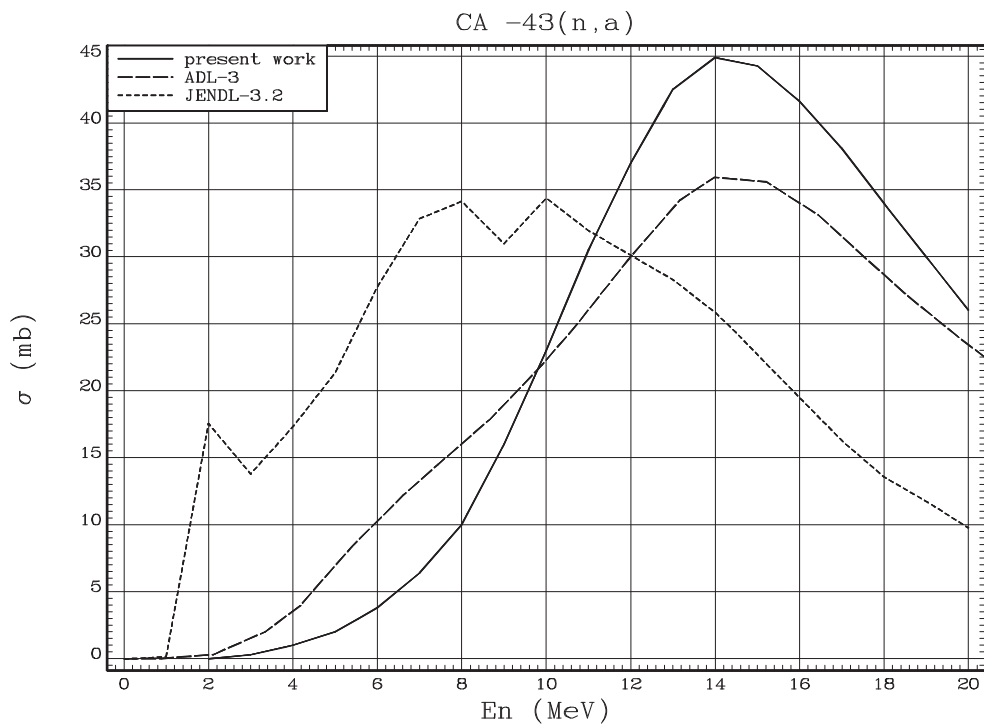
Fig. 5. ^{43}Ca(n,α)^{40}Ar reaction cross-section

CA -43(n,na)
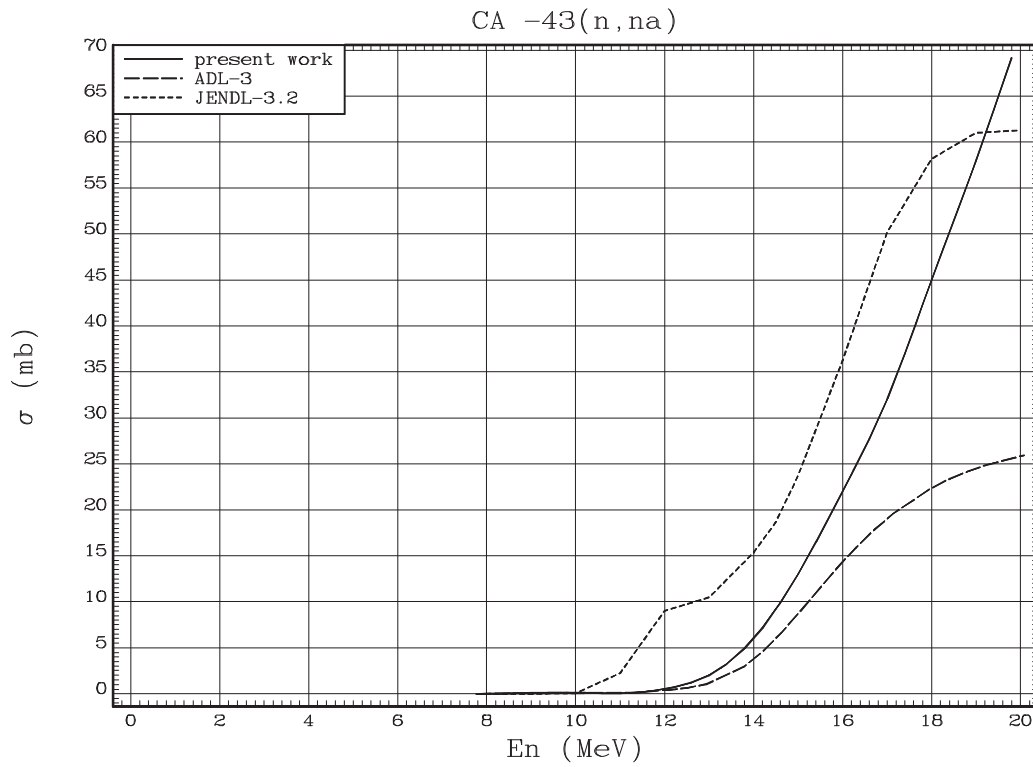
Fig. 6. ^{43}Ca(n,nα)^{39}Ar reaction cross-section

Ca - 44(n,2n)
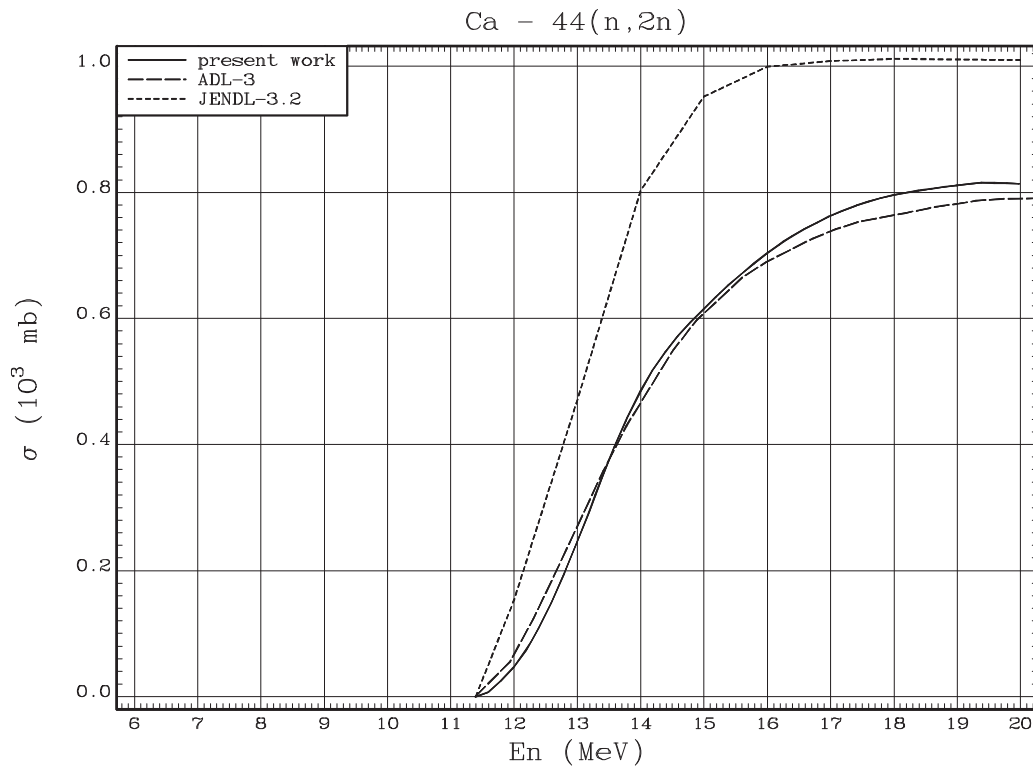
Fig. 7. ^{44}Ca(n,2n)^{43}Ca reaction cross-section

CA -44(n,na)

Fig. 8. ^{44}Ca(n,nα)^{40}Ar reaction cross-section

CA -45(n,a)
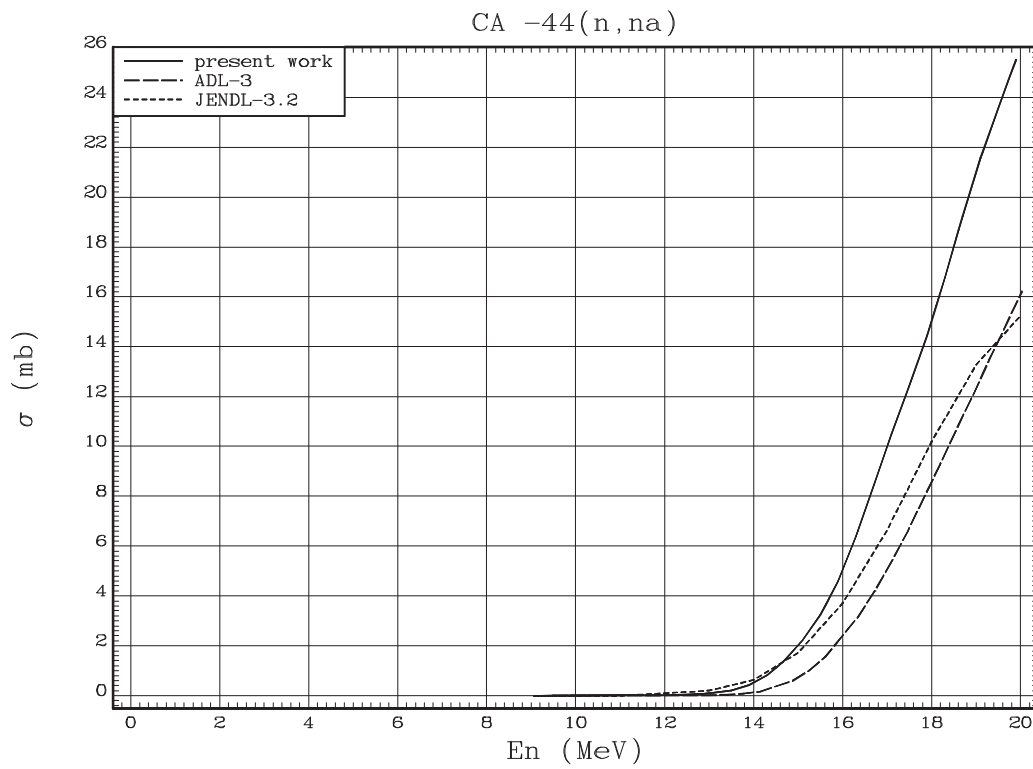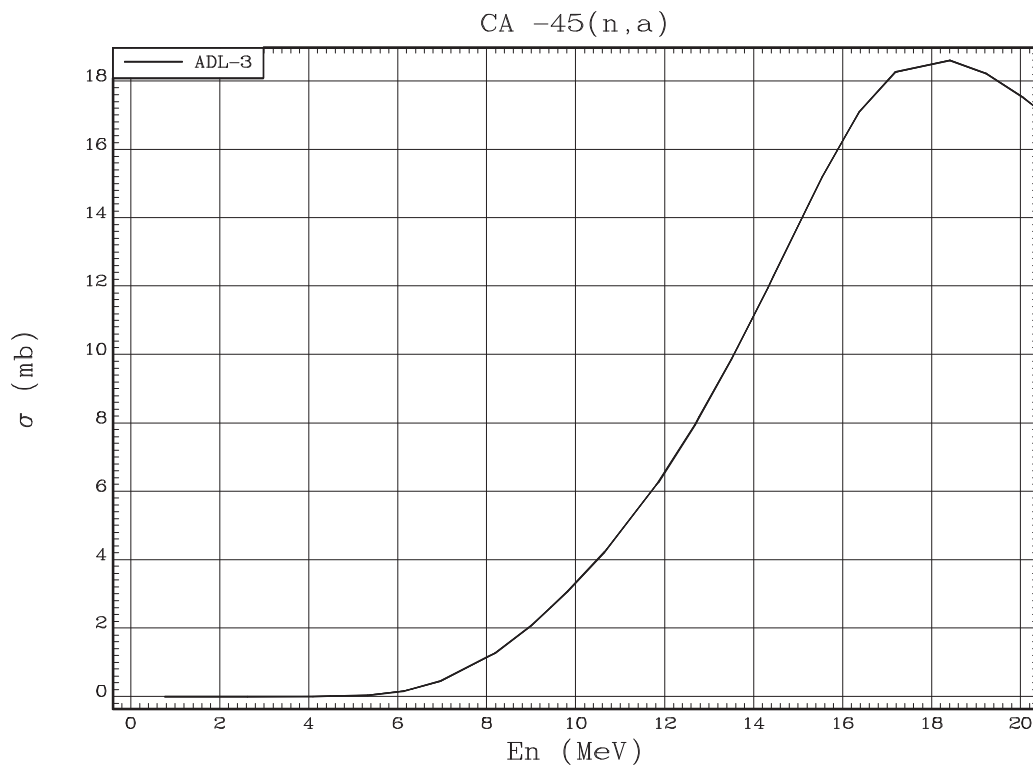
Fig. 9. ^{45}Ca(n,α)^{42}Ar reaction cross-section
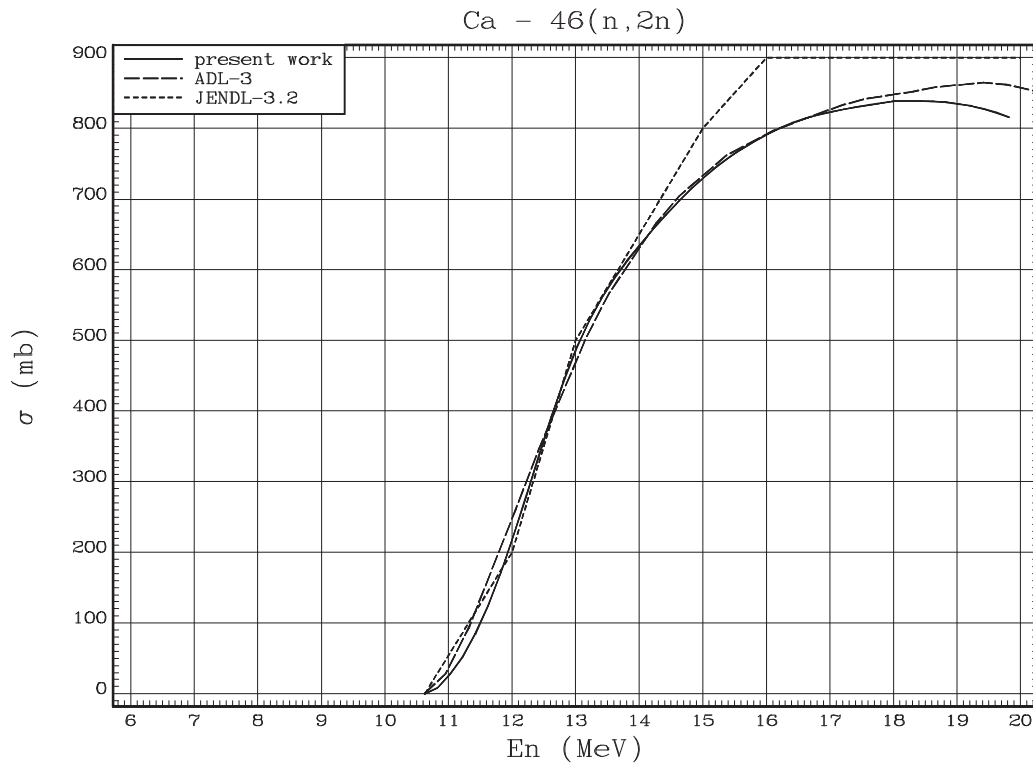
Fig. 10. ^{46}Ca(n,2n)^{43}Ca reaction cross-section
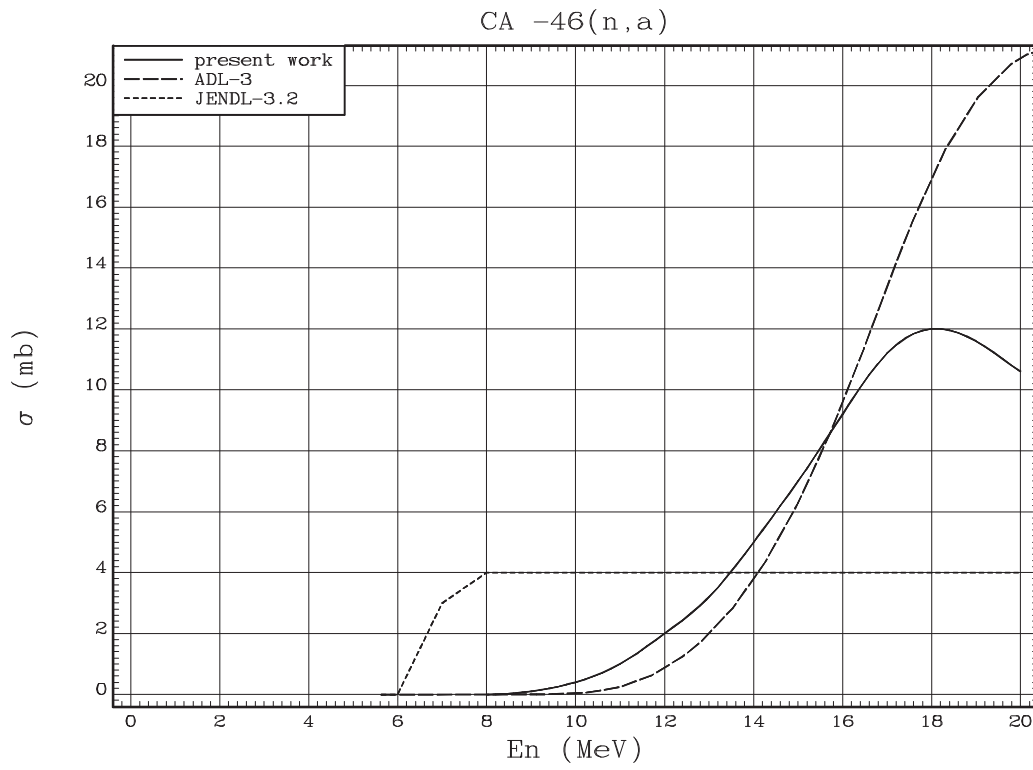
Fig. 11. ^{46}Ca(n,α)^{43}Ar reaction cross-section

CA -46(n,na)
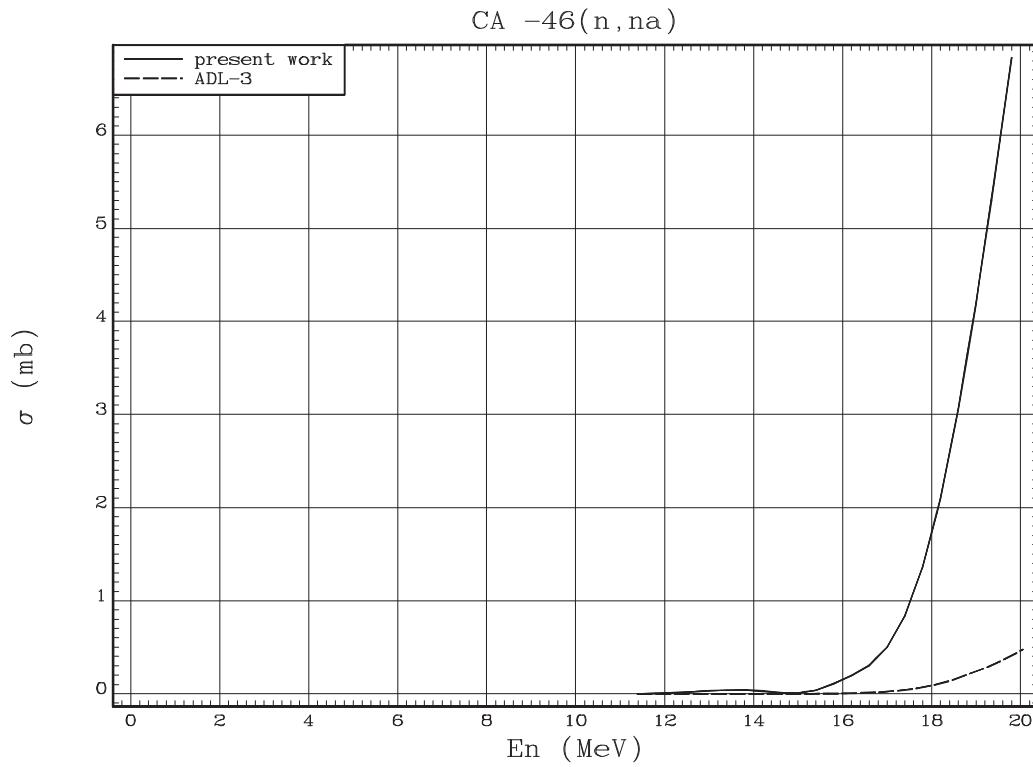
Fig. 12. ^{46}Ca(n,nα)^{42}Ar reaction cross-section

Ca - 48(n,2n)
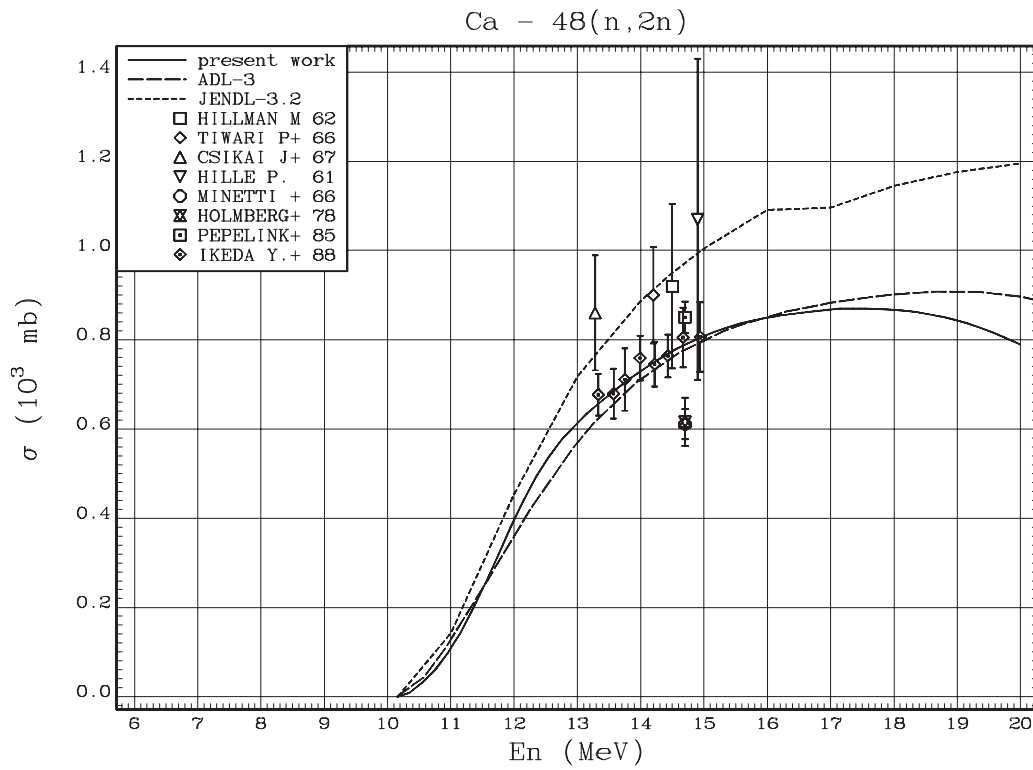
Fig. 13. ^{48}Ca(n,2n)^{43}Ca reaction cross-section
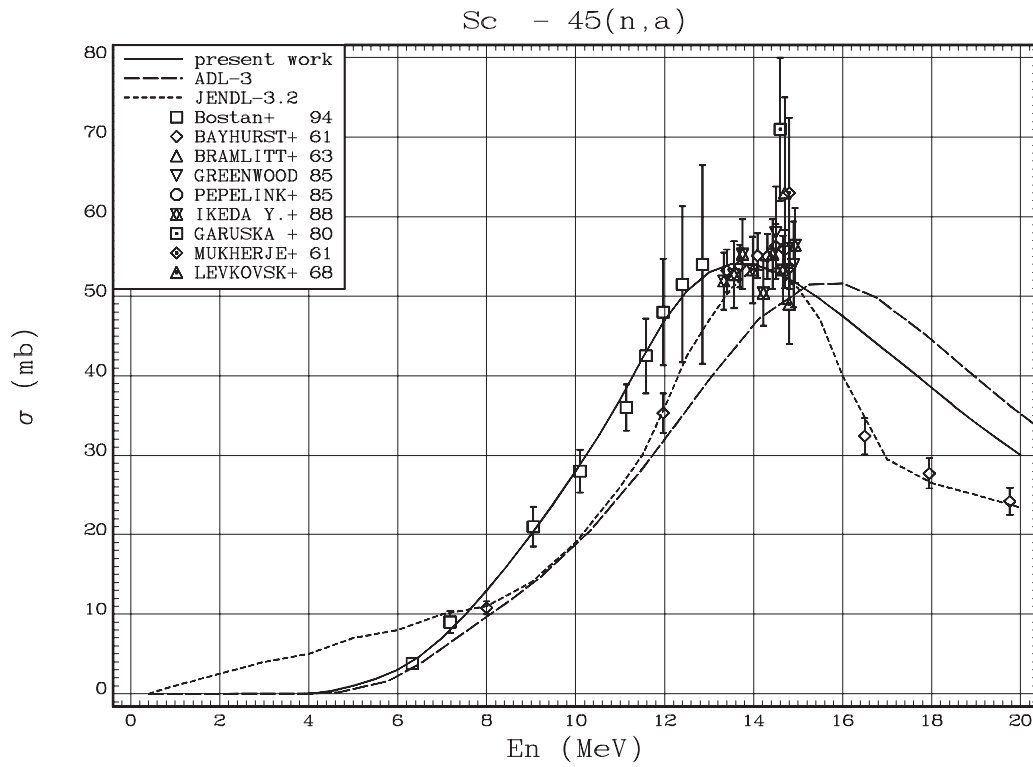
Fig. 14. ^{45}Sc(n,α)^{42}K reaction cross-section
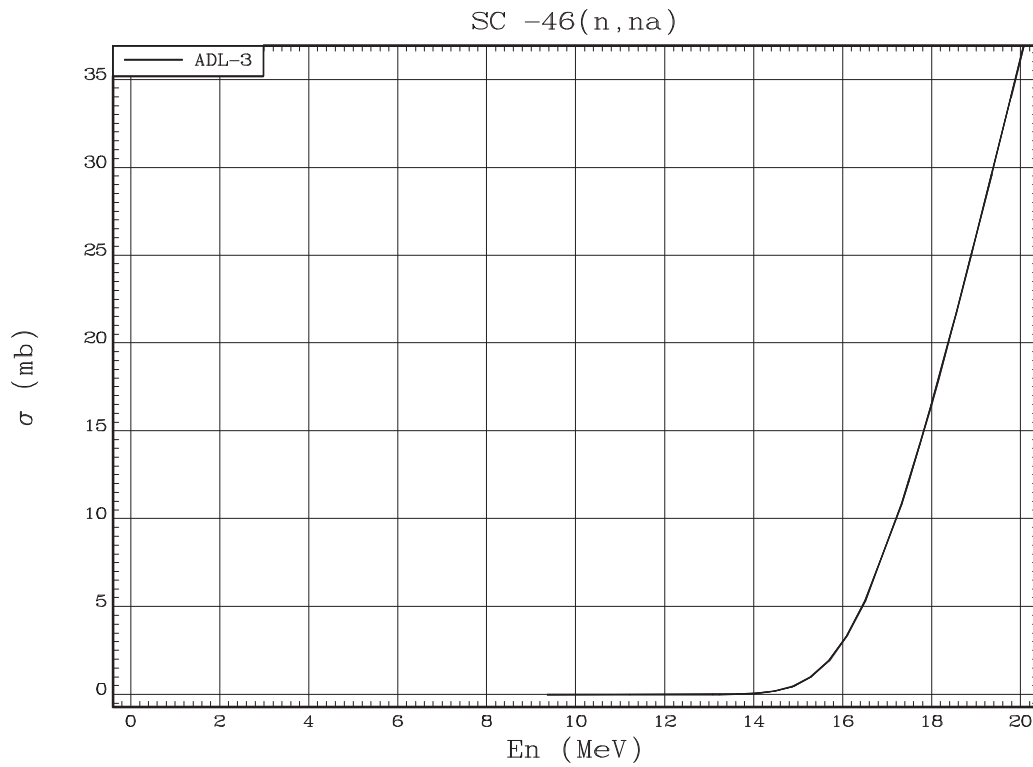
Fig. 15. ^{46}Sc(n,nα)^{42}K reaction cross-section

Ti -46(n,a)
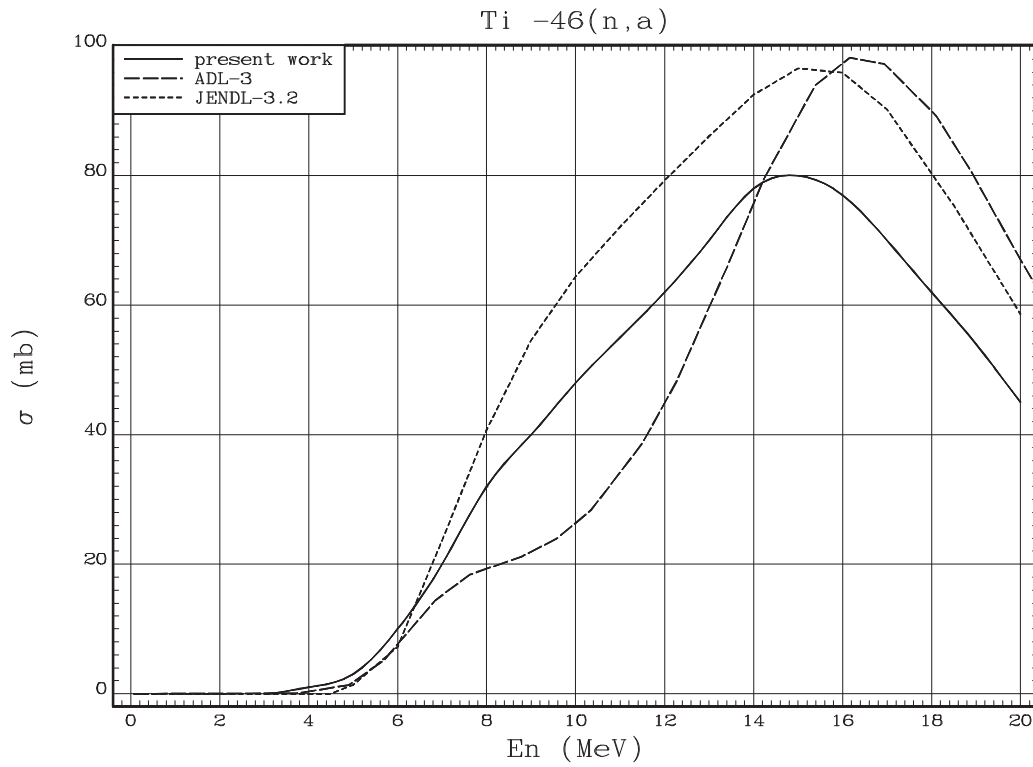
Fig. 16. ^{46}Ti(n,α)^{43}Ca reaction cross-section

Ti - 47(n,2n)
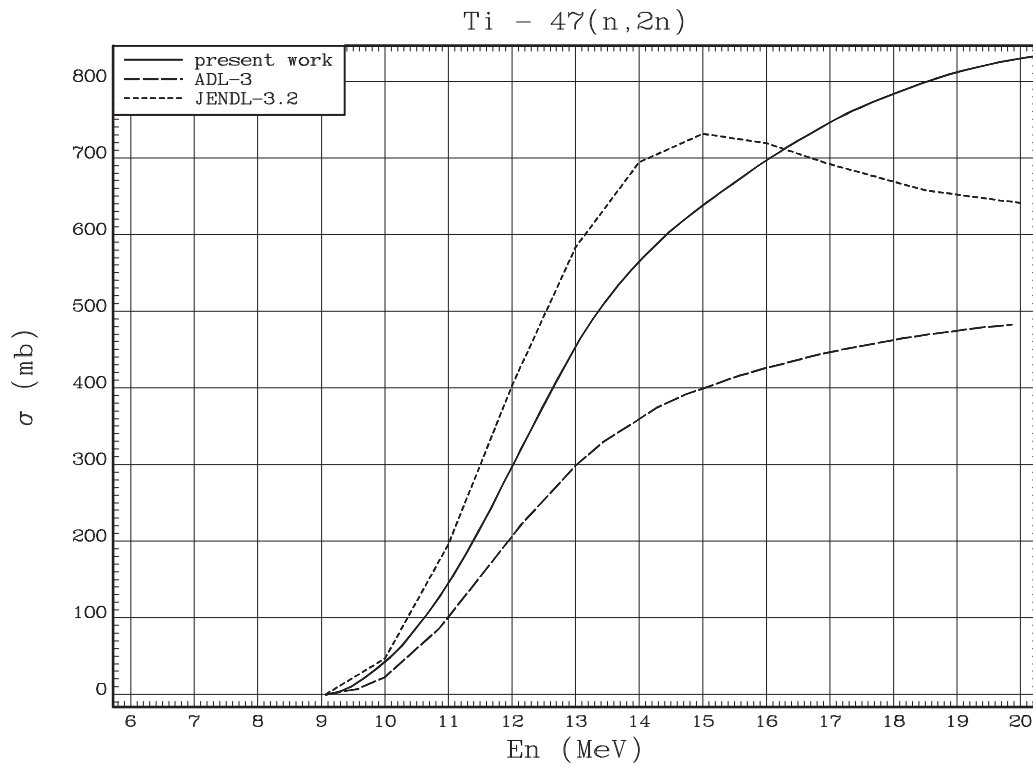
Fig. 17. ^{47}Ti(n,2n)^{46}Ti reaction cross-section

Ti -47(n,a)
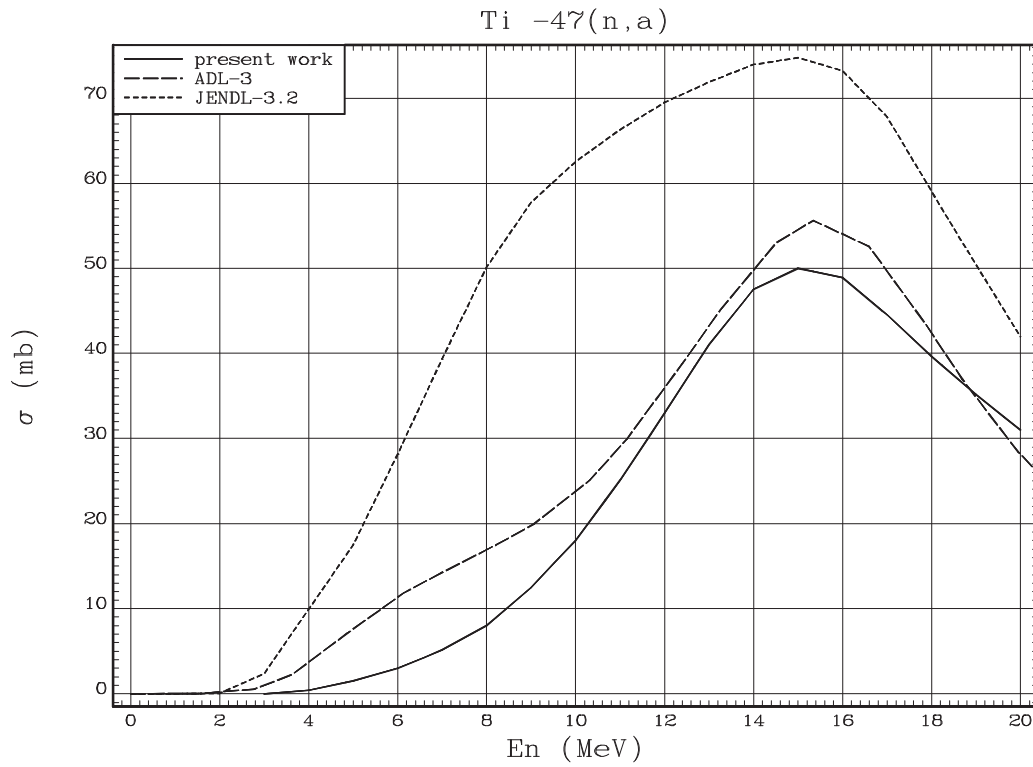
Fig. 18. ^{47}Ti(n,α)^{44}Ca reaction cross-section

Ti-48(n,a)Ca-45
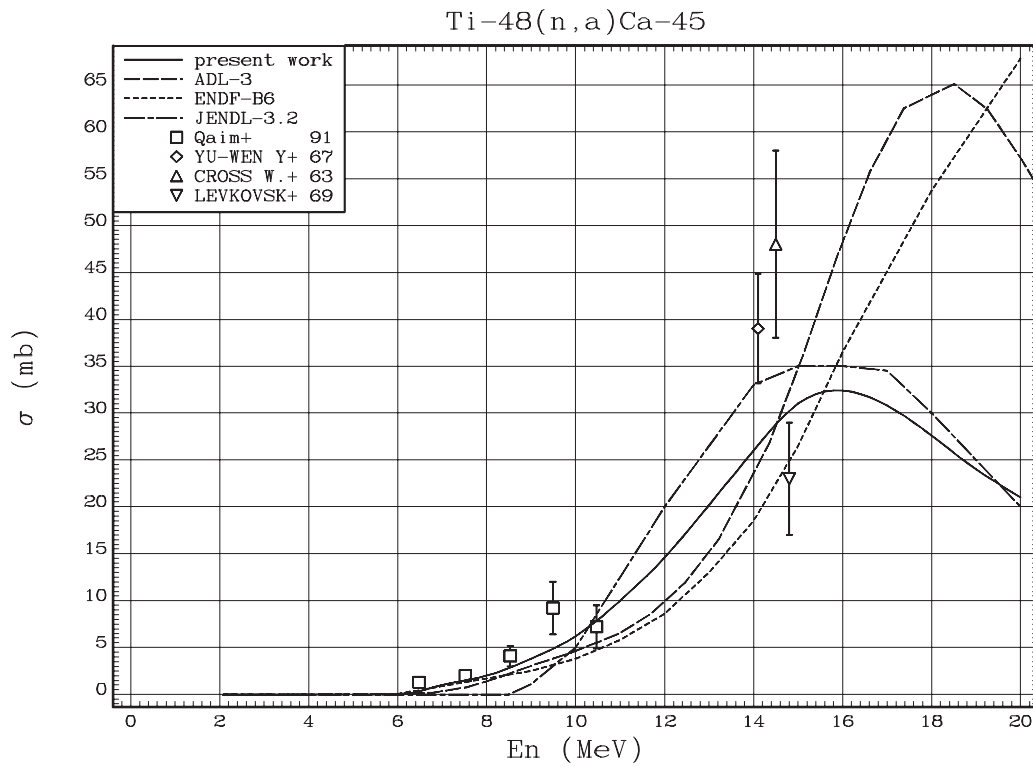
Fig. 19. ^{48}Ti(n,α)^{45}Ca reaction cross-section

Ti - 49(n,2n)
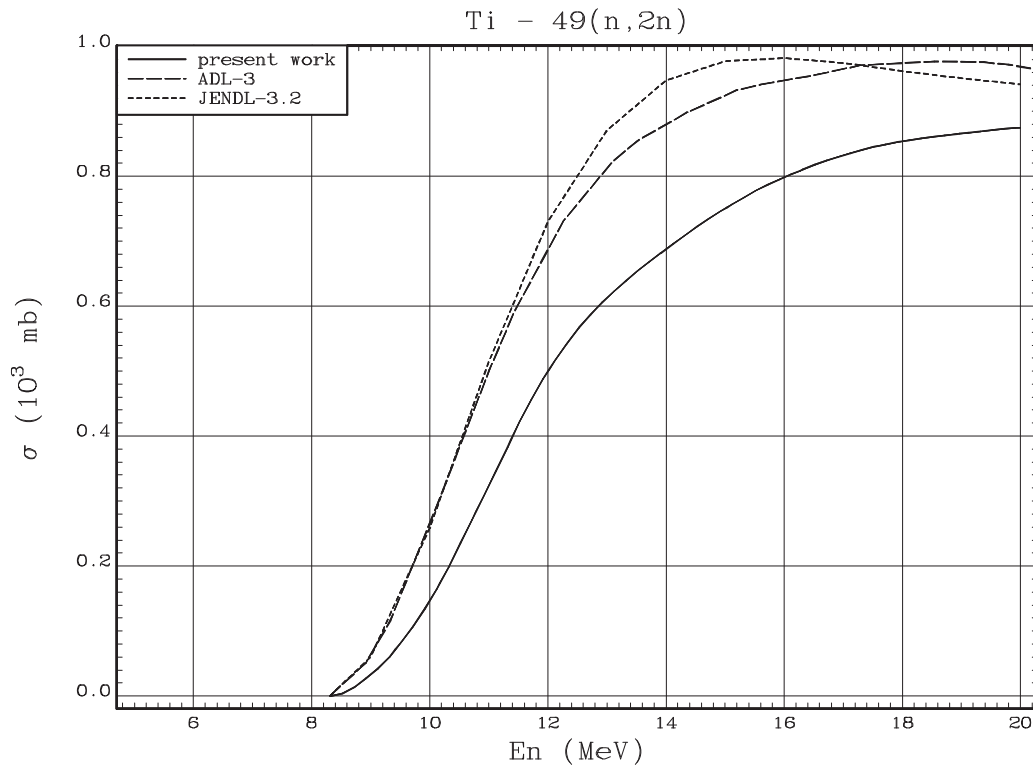
Fig. 20.　^{49}Ti(n,2n)^{48}Ti reaction cross-section

Ti -49(n,a)
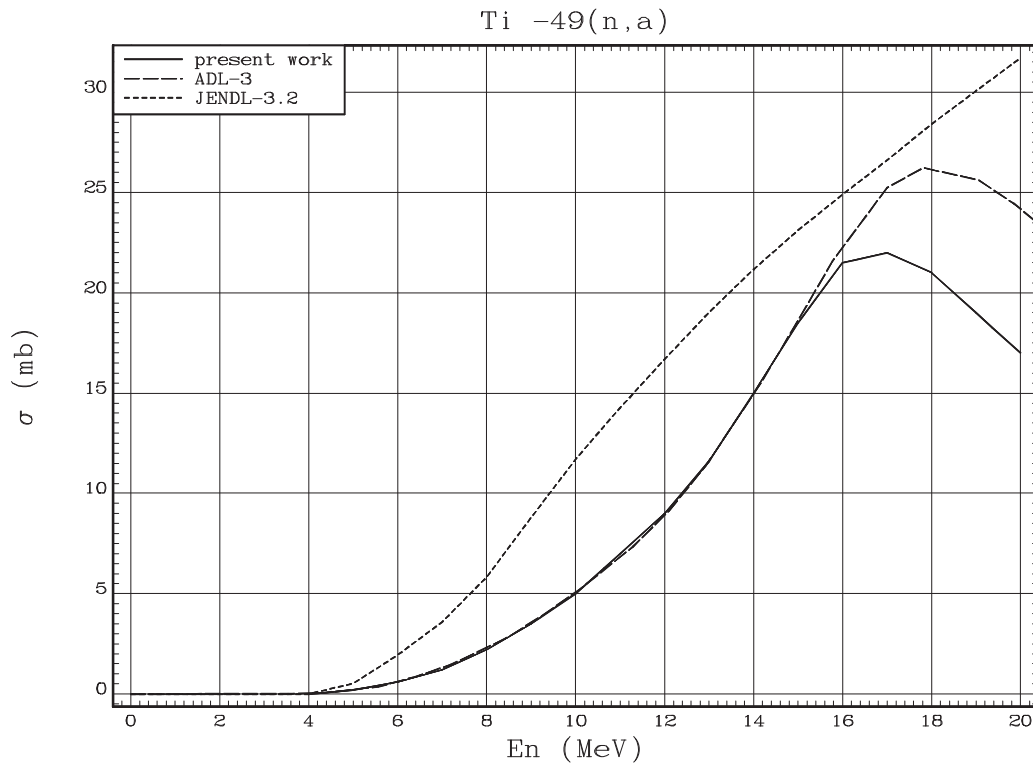
Fig. 21.　^{49}Ti(n,α)^{46}Ca reaction cross-section

Ti – 50(n,2n)
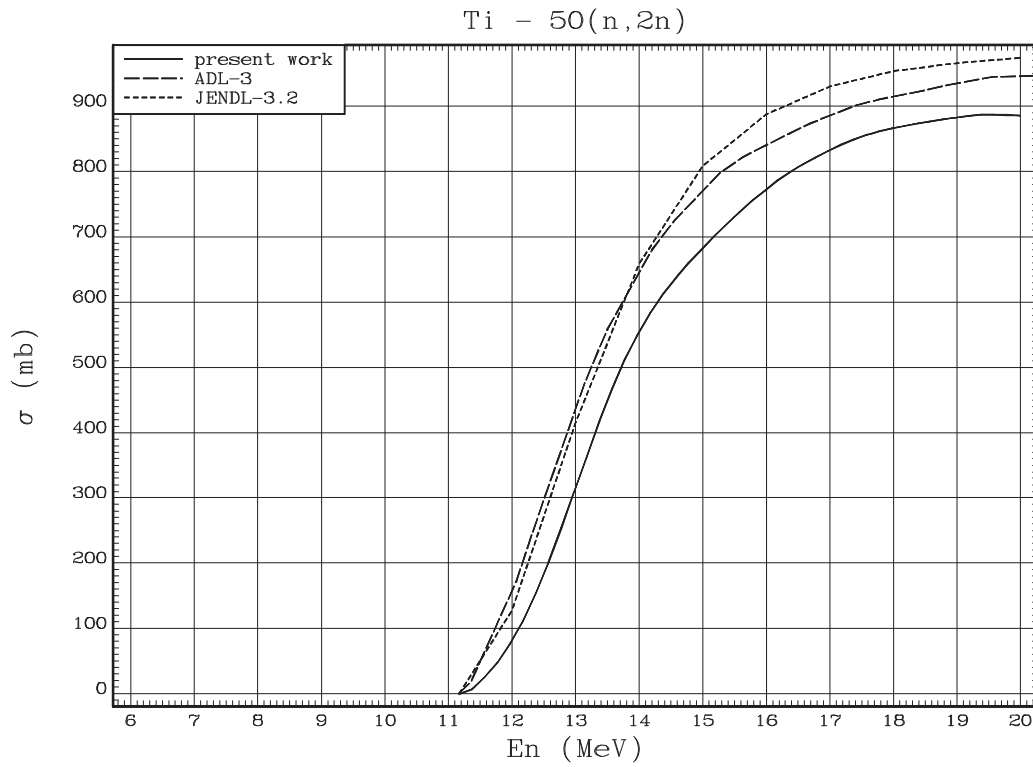
Fig. 22. ^{50}Ti(n,2n)^{49}Ti reaction cross-section

Ti –50(n,a)
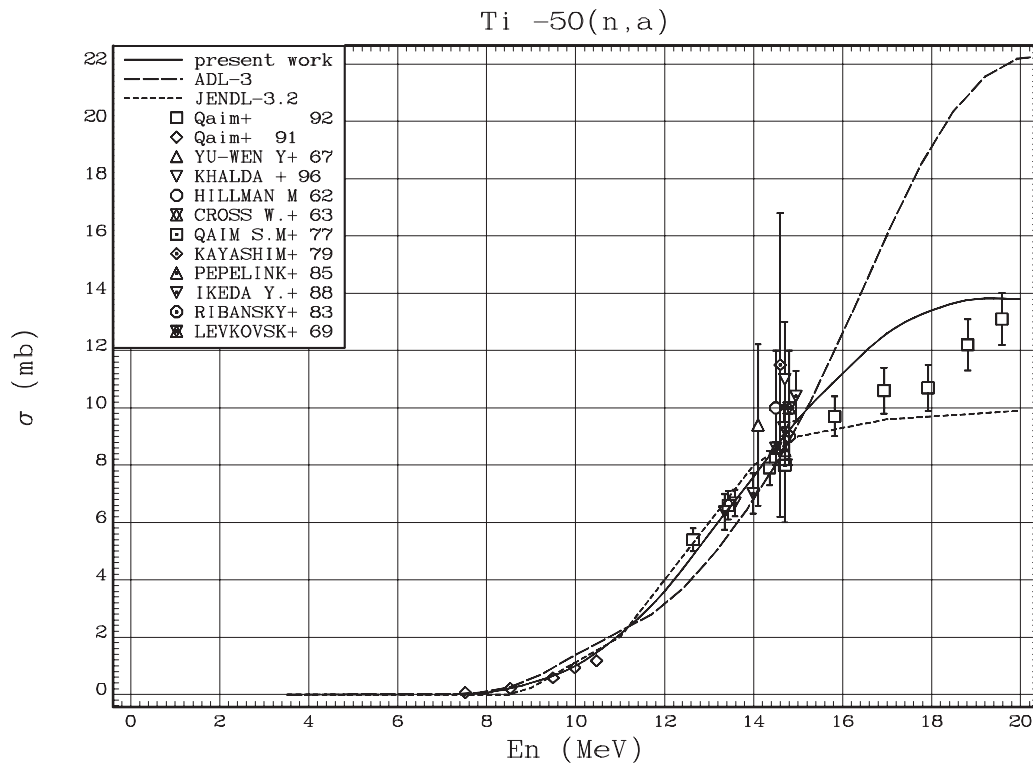
Fig. 23. ^{50}Ti(n,α)^{47}Ca reaction cross-section

V - 49(n,a)
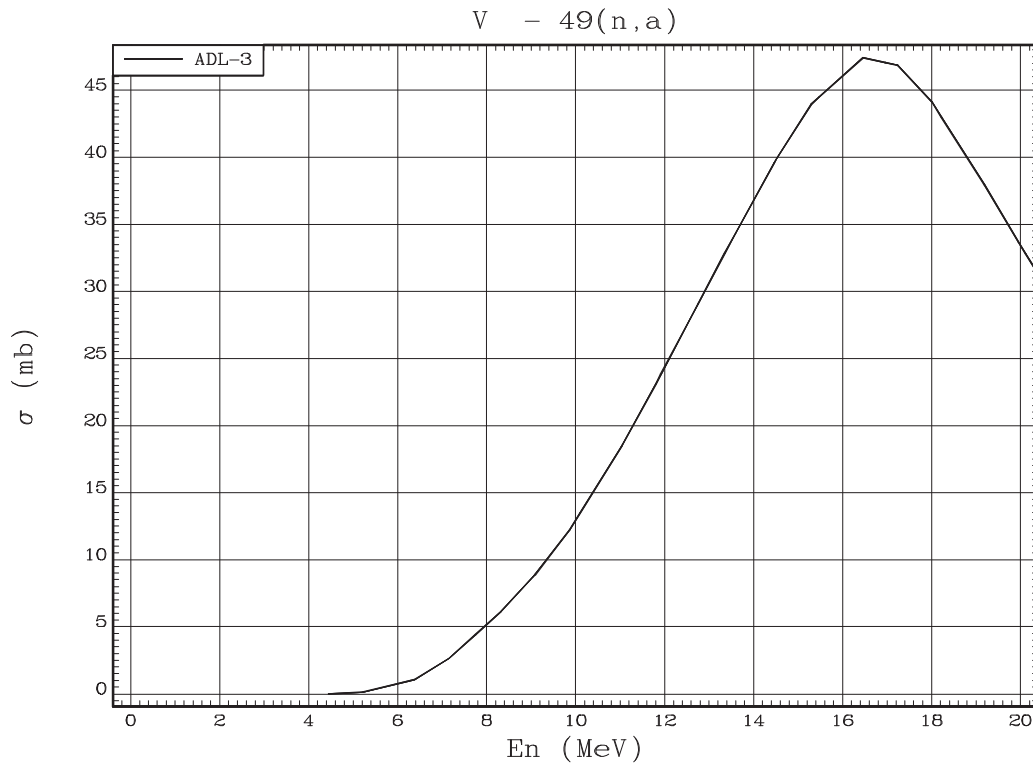
Fig. 24. ^{49}V(n,α)^{46}Sc reaction cross-section

V - 50(n,2n)
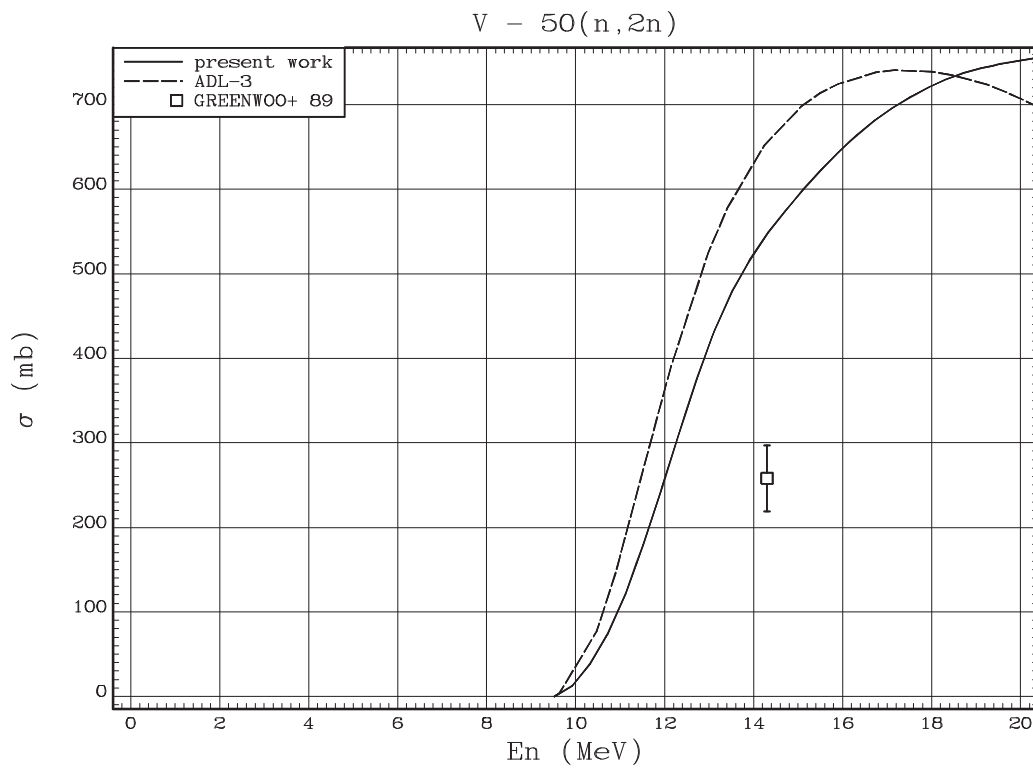
Fig. 25. ^{50}V(n,2n)^{49}V reaction cross-section

V — 50(n,a)

Fig. 26. ^{50}V(n,α)^{47}Sc reaction cross-section

V —51(n,a)
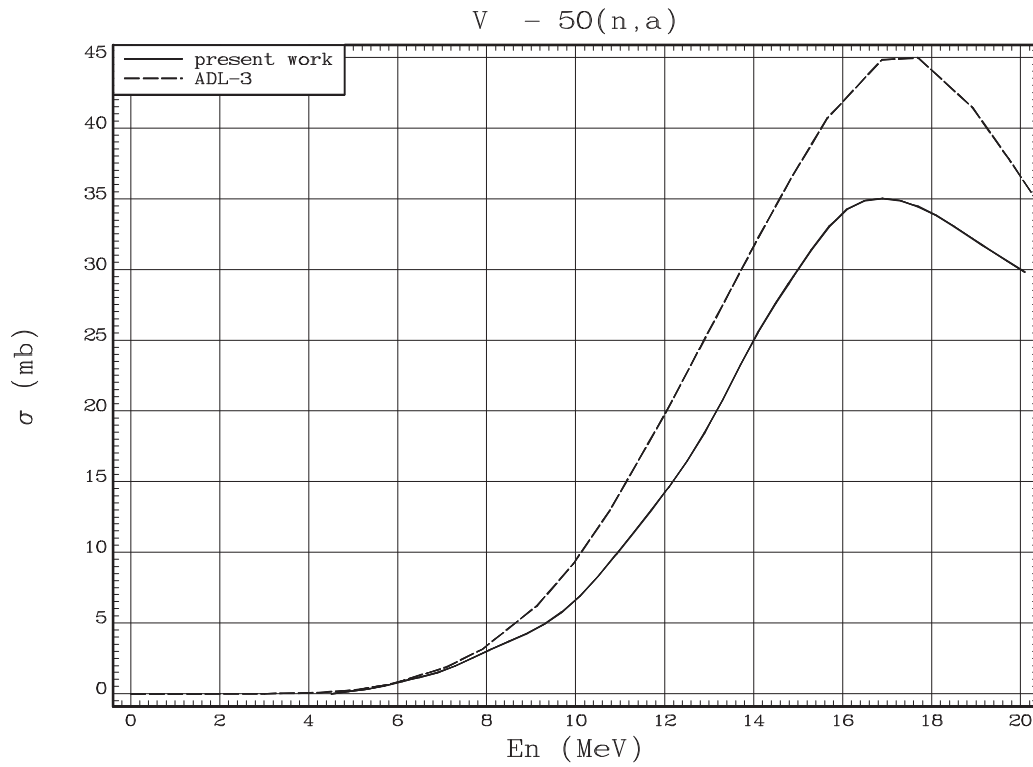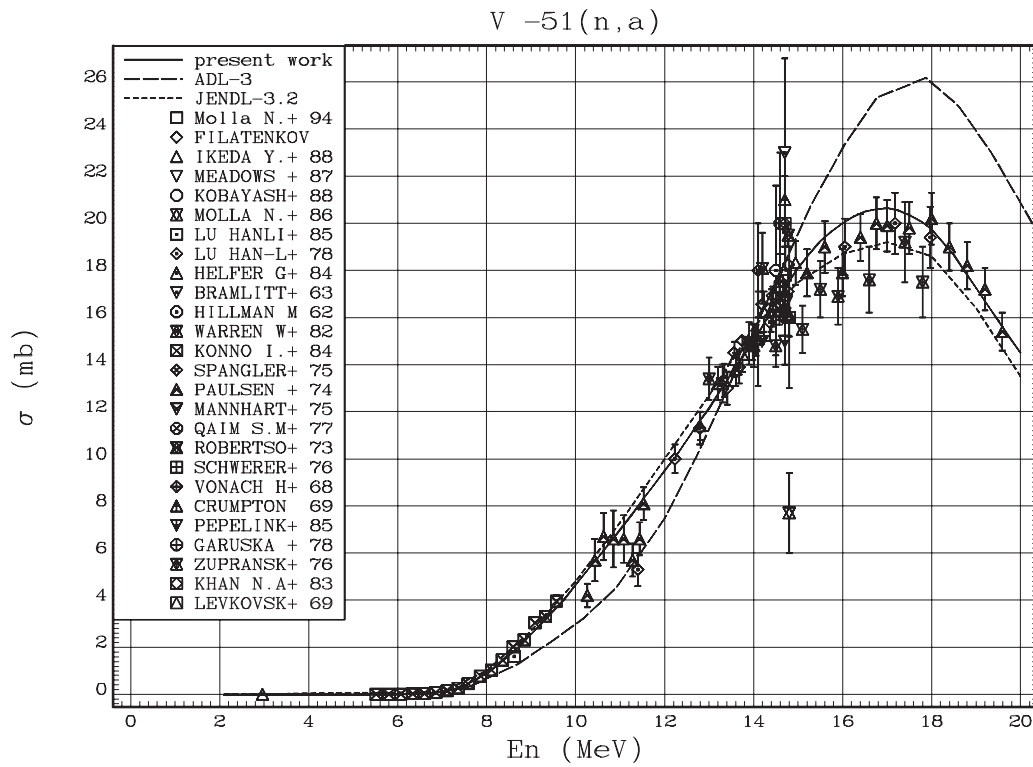
Fig. 27. ^{51}V(n,α)^{48}Sc reaction cross-section

V -51(n,na)
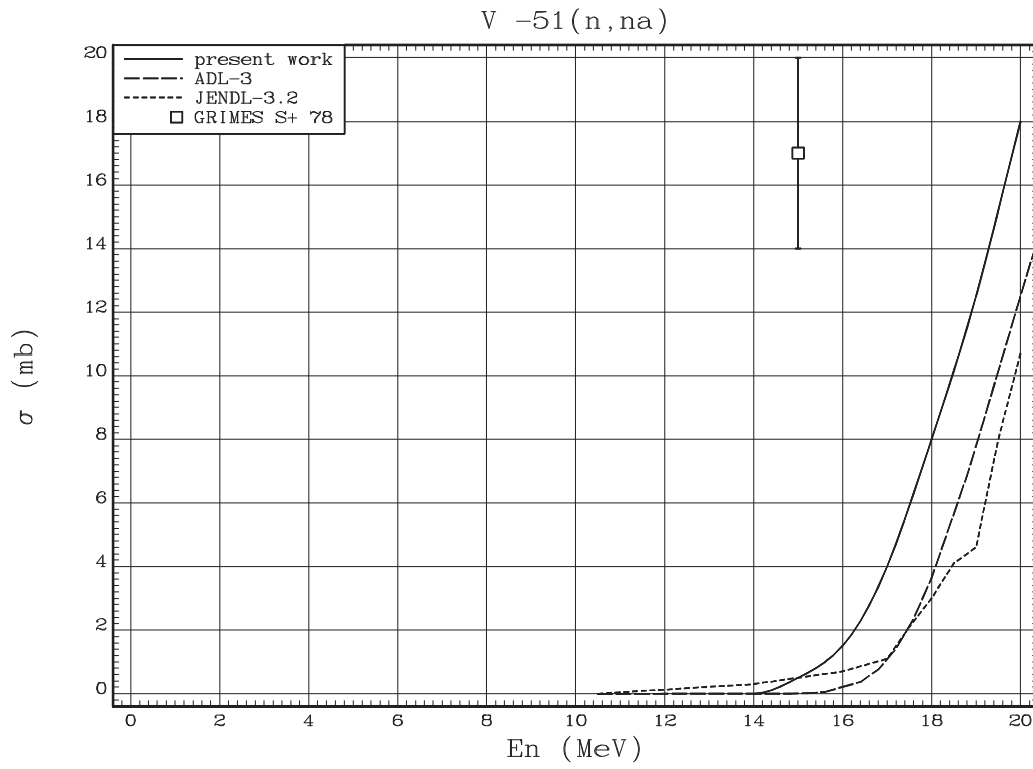
Fig. 28. $^{51}V(n,n\alpha)^{47}Sc$ reaction cross-section

Cr -50(n,a)
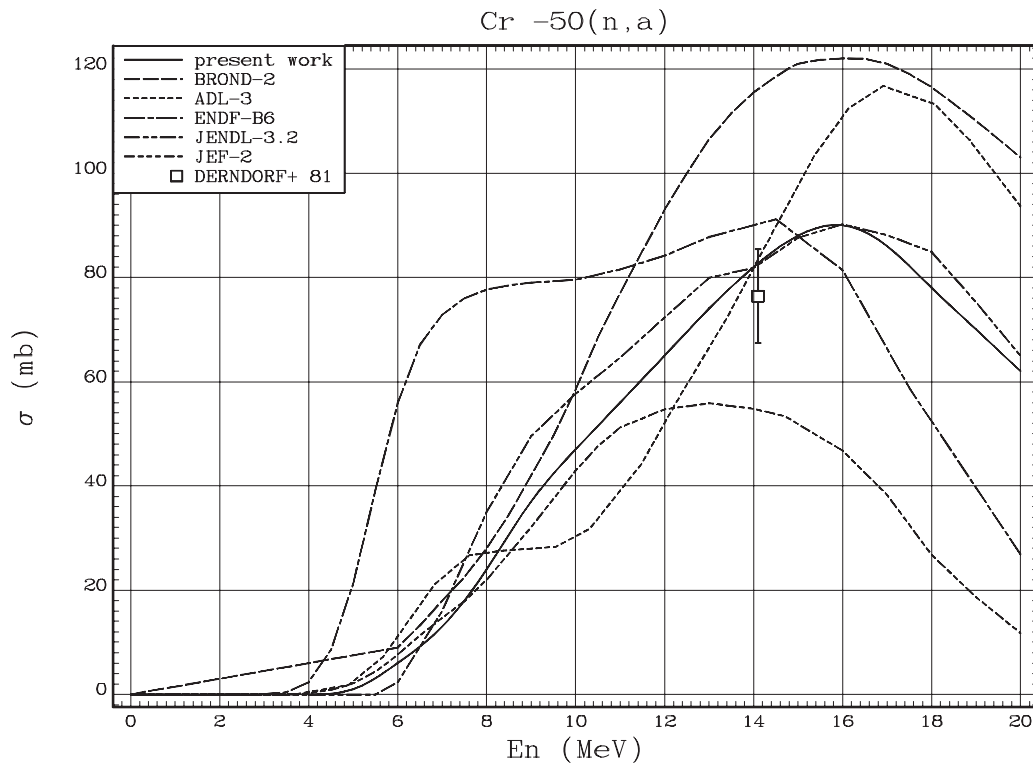
Fig. 29. $^{50}Cr(n,\alpha)^{47}Ti$ reaction cross-section
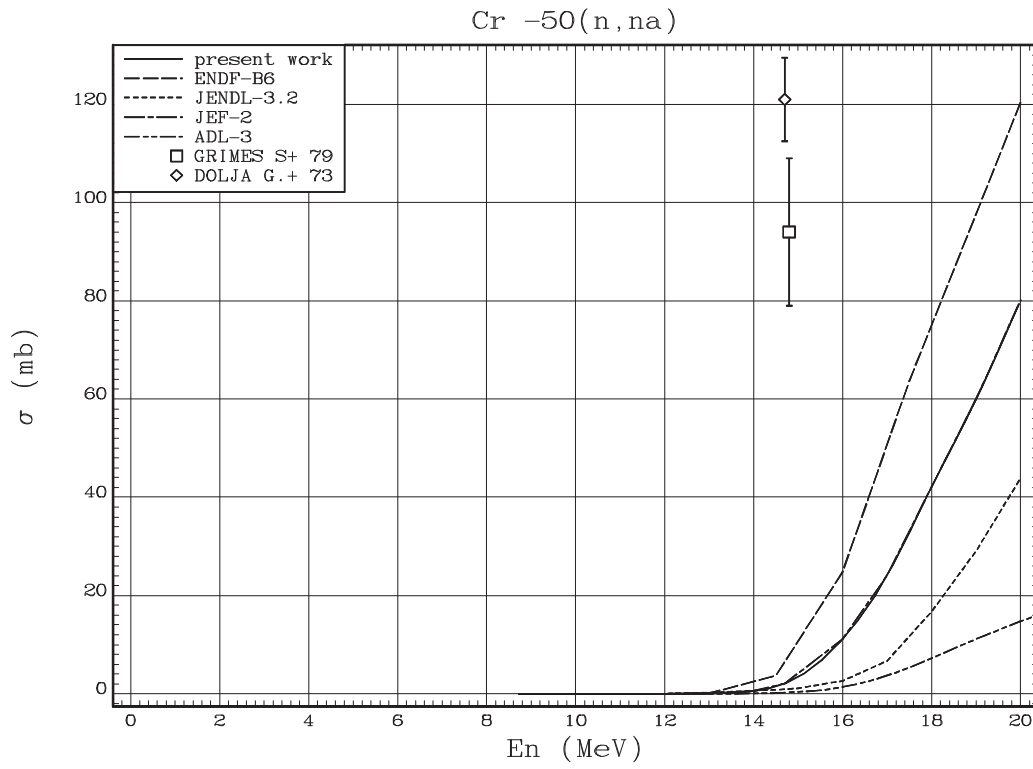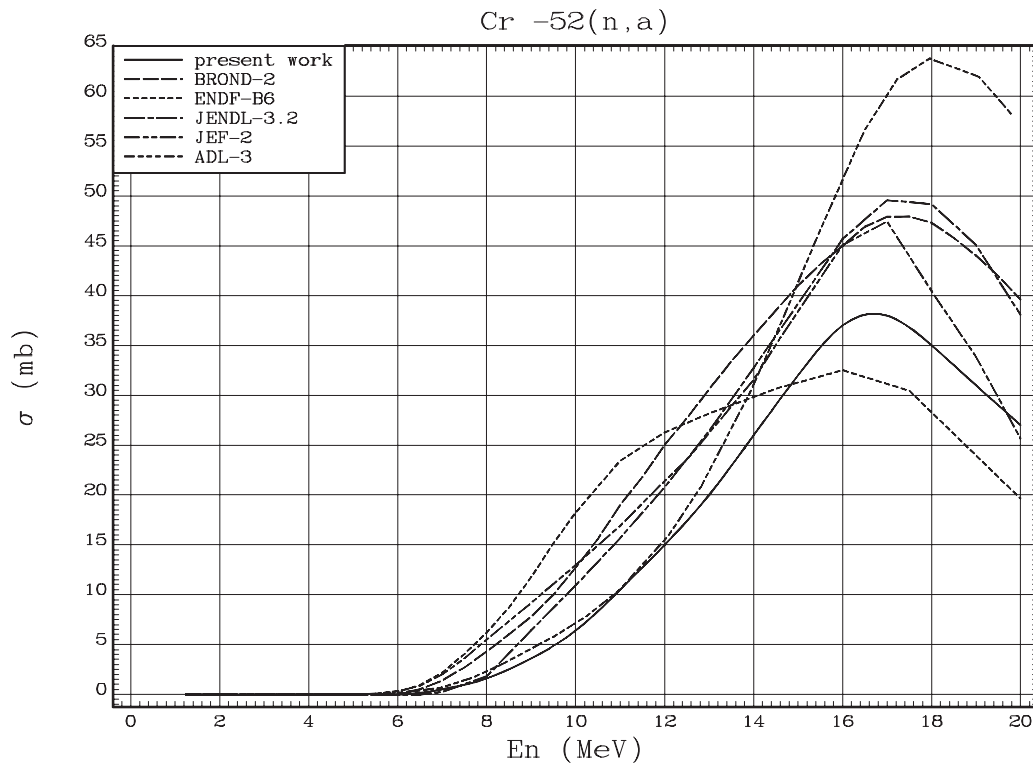
Cr -50(n,na)

Fig. 30. ^{50}Cr(n, nα)^{46}Ti reaction cross-section

Cr -52(n,a)

Fig. 31. ^{52}Cr(n,α)^{49}Ti reaction cross-section

Cr -52(n,na)

Fig. 32. ^{52}Cr(n, nα)^{48}Ti reaction cross-section

Cr -53(n,a)

Fig. 33. ^{53}Cr(n,α)^{50}Ti reaction cross-section

Cr −53(n,na)

Fig. 34. ^{53}Cr(n, nα)^{49}Ti reaction cross-section

Cr −54(n,a)
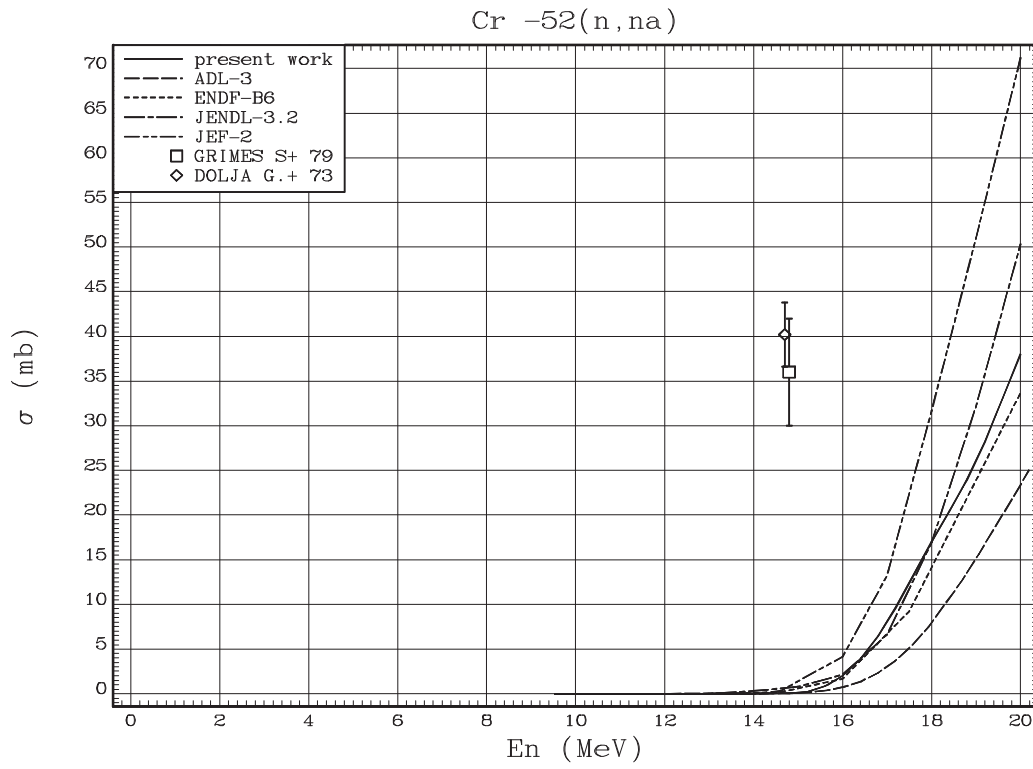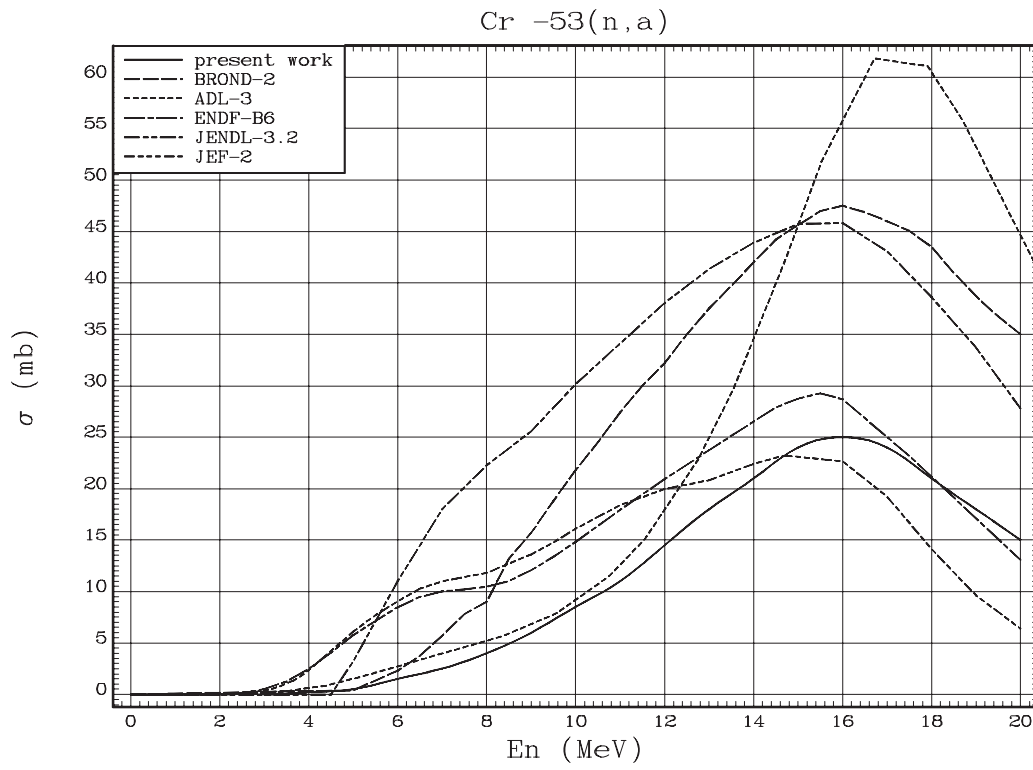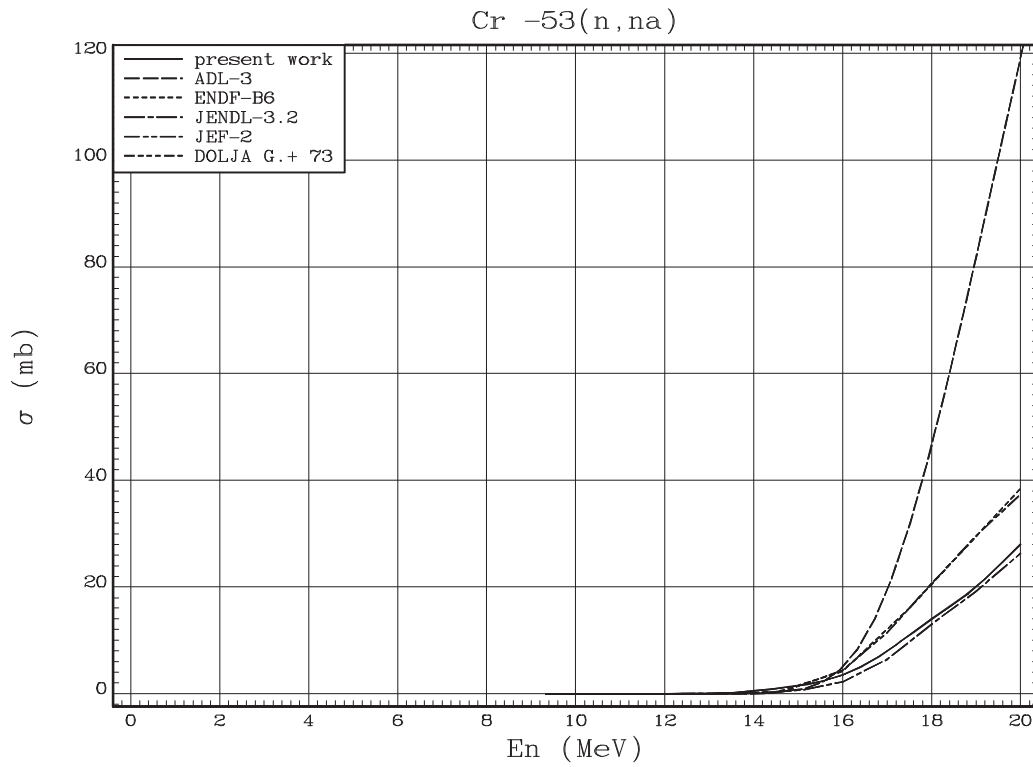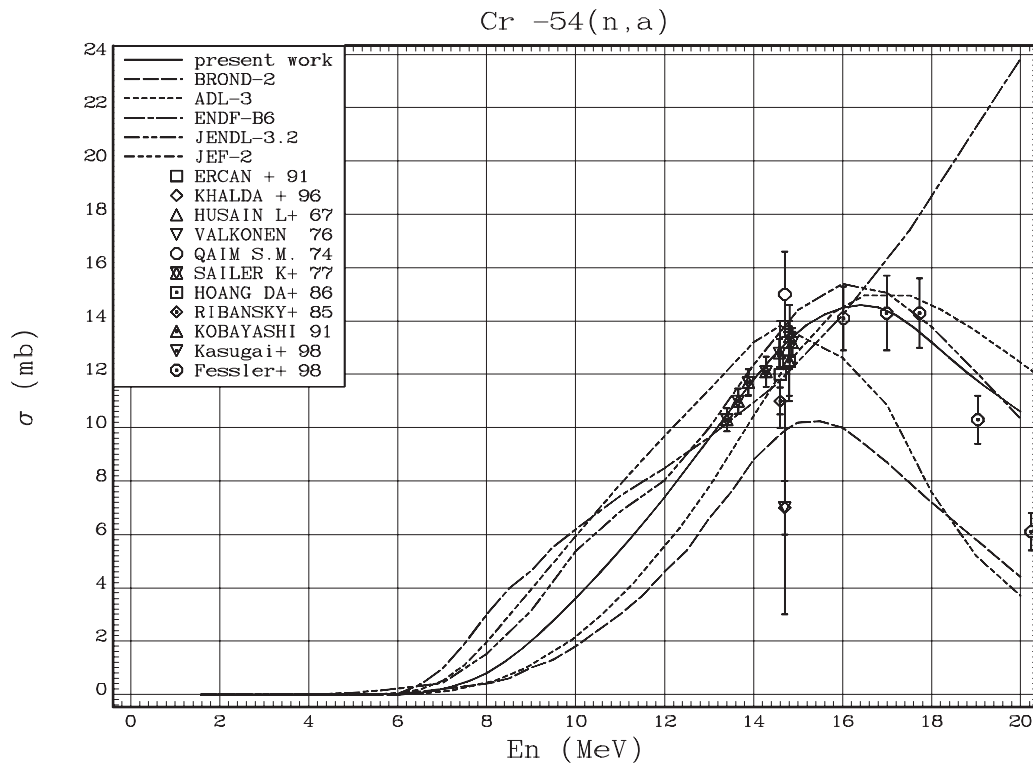
Fig. 35. ^{54}Cr(n,α)^{51}Ti reaction cross-section

Cr -54(n,na)
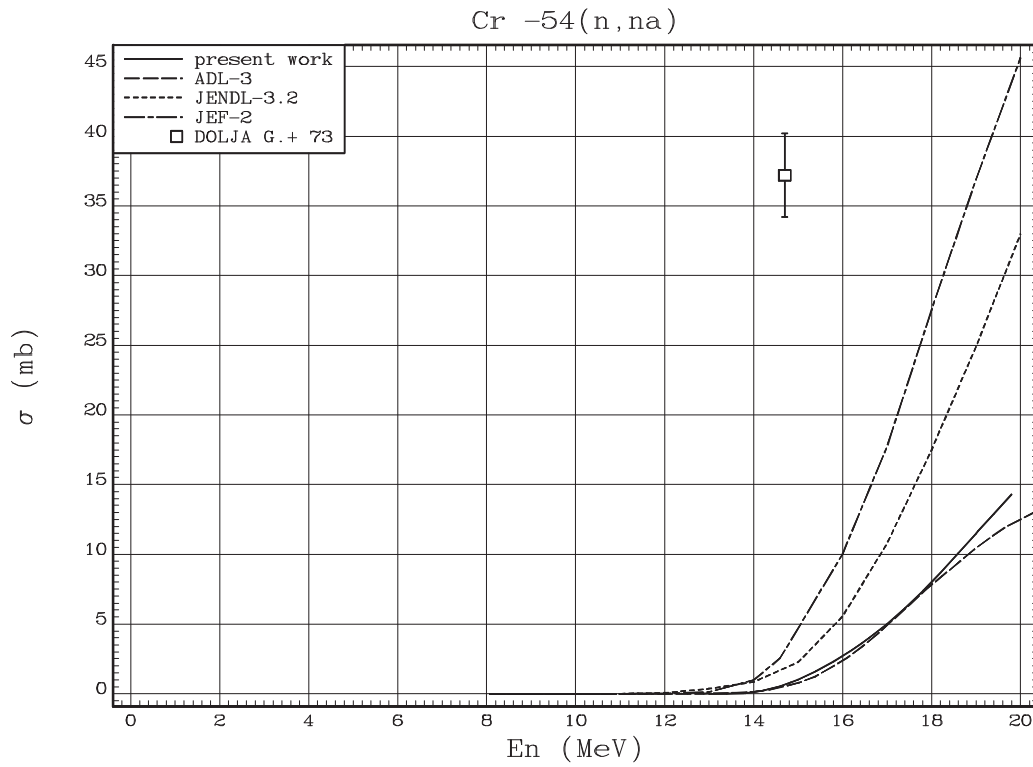
Fig. 36. ^{54}Cr(n, nα)^{50}Ti reaction cross-section

Mn-55(n,2n)
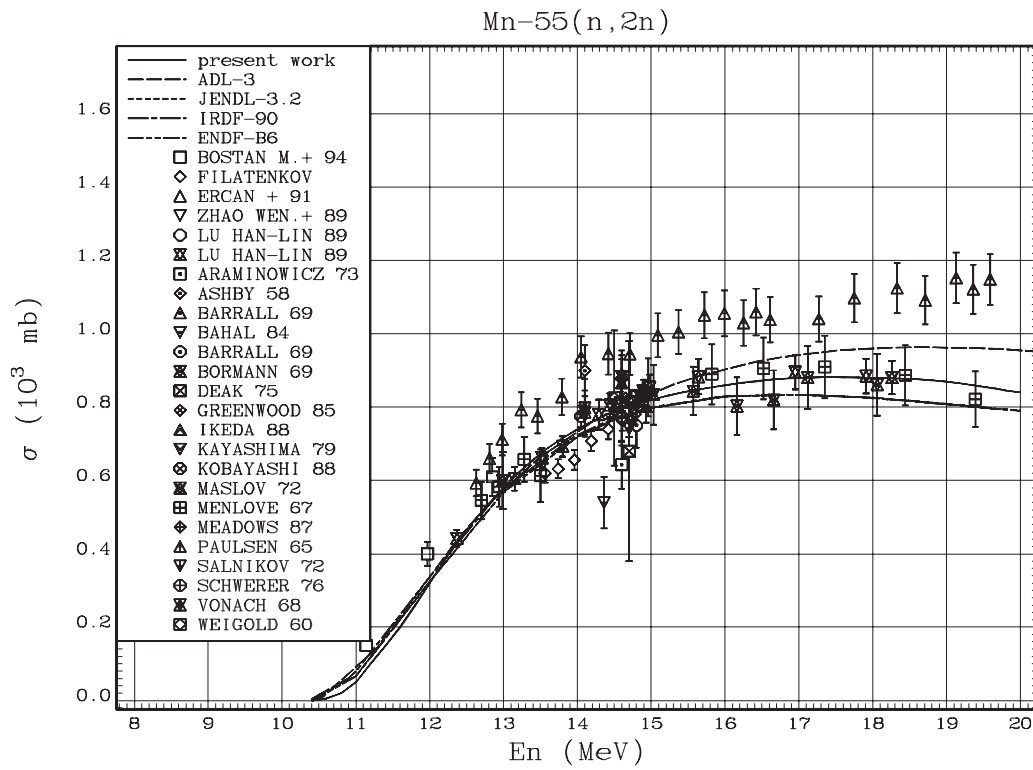

Fig. 37. ^{55}Mn(n,2n)^{54}Mn reaction cross-section
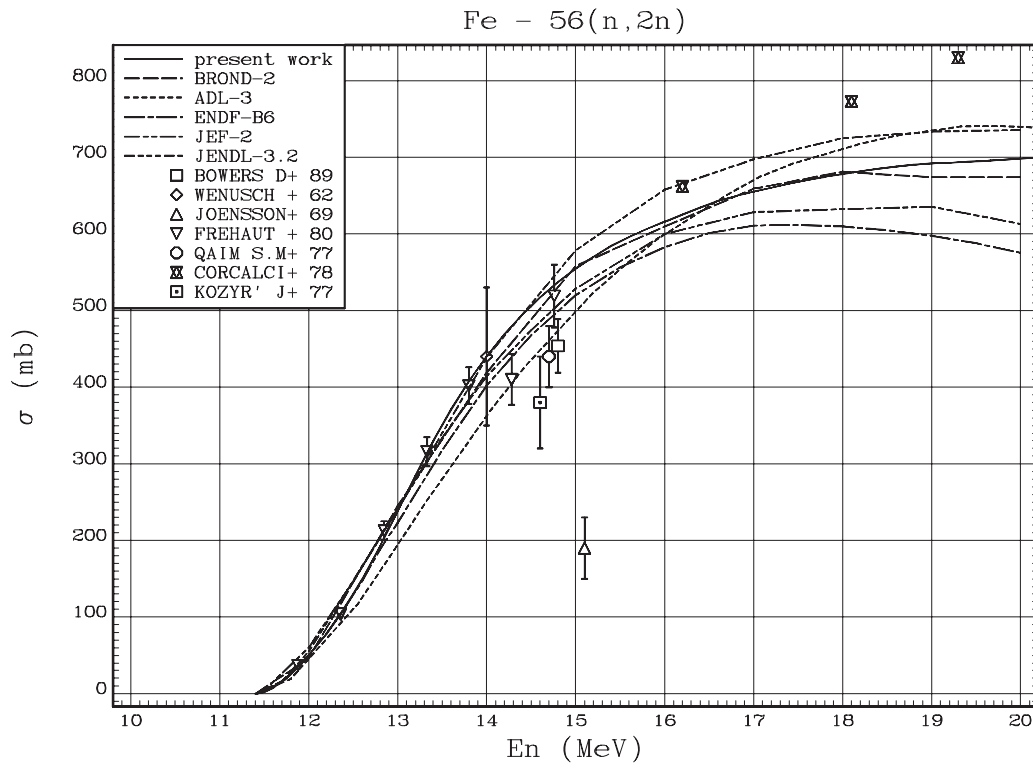
Fig. 38. ^{56}Fe(n,2n)^{55}Fe reaction cross-section
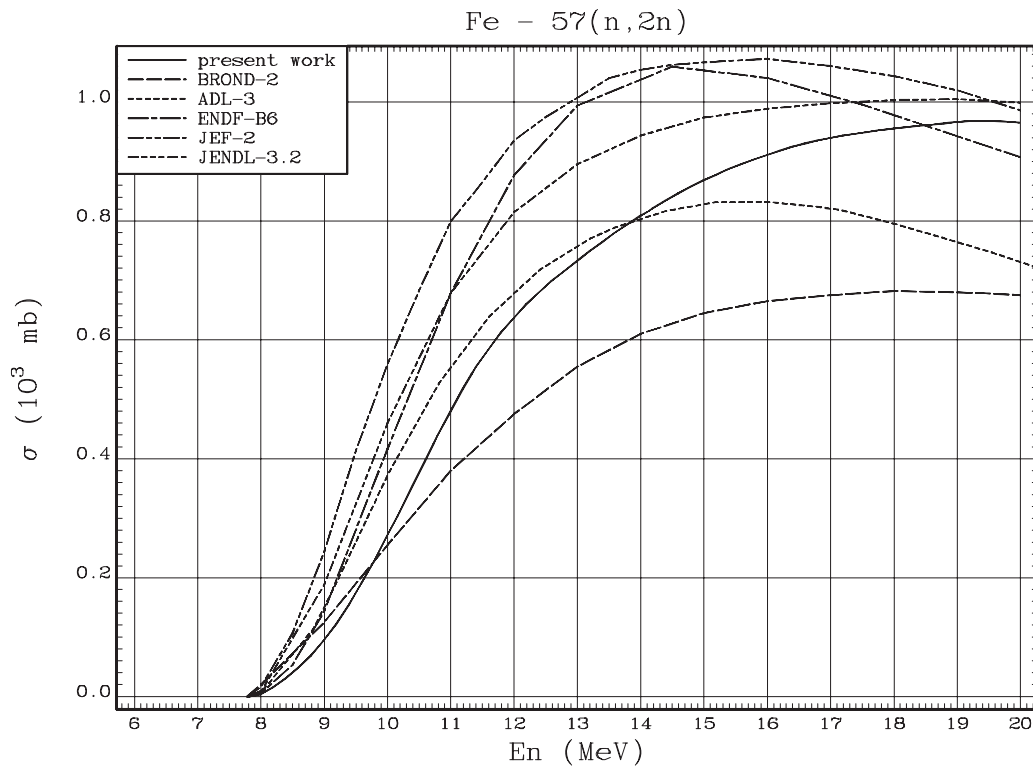
Fig. 39. ^{57}Fe(n,2n)^{56}Fe reaction cross-section
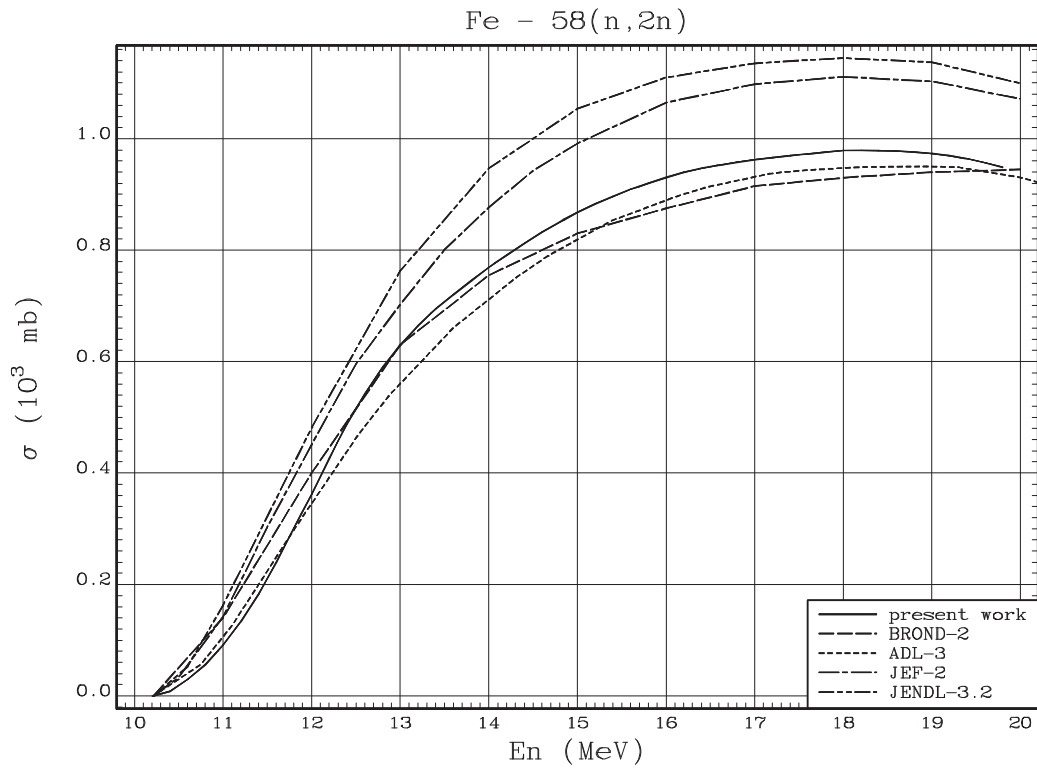
Fig. 40. ^{58}Fe(n,2n)^{57}Fe reaction cross-section
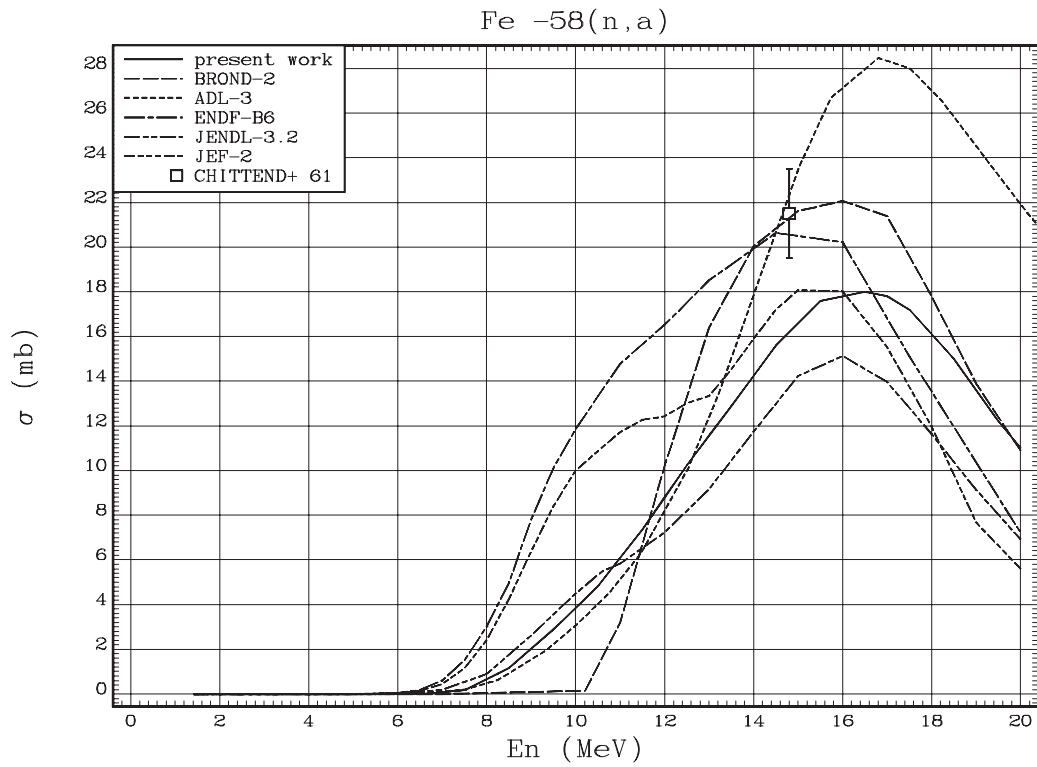
Fig. 41. ^{58}Fe(n,α)^{55}Cr reaction cross-section

Co -59(n,p)
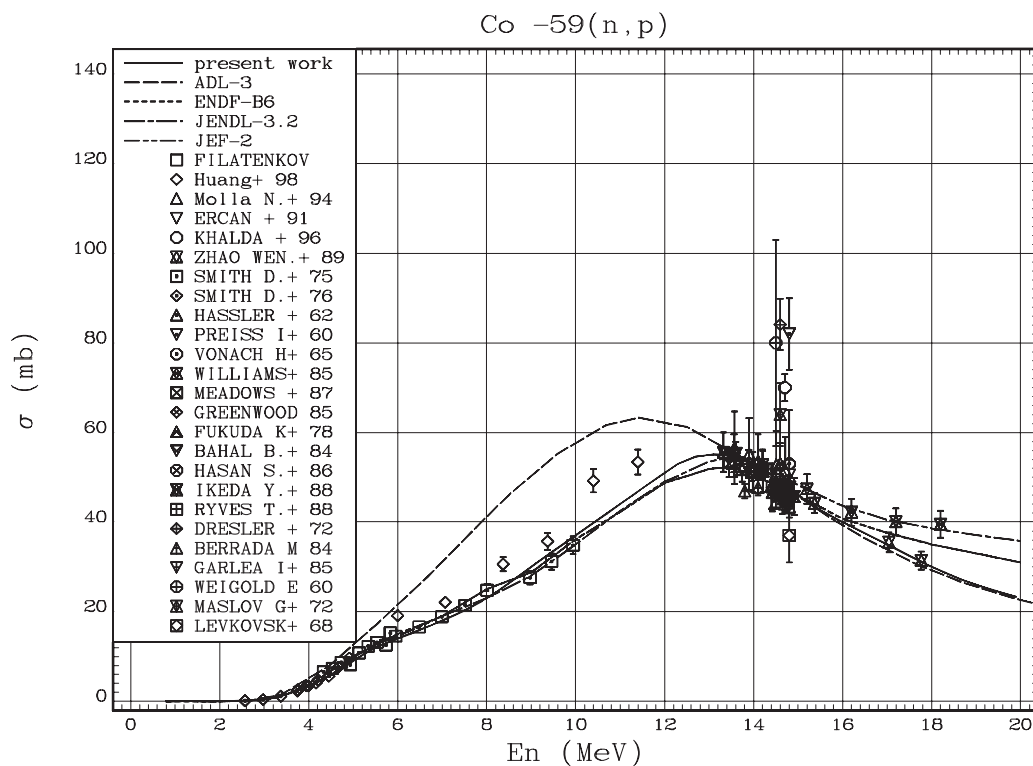
Fig. 42. ^{59}Co(n,p)^{59}Fe reaction cross-section

Ni -58(n,p)
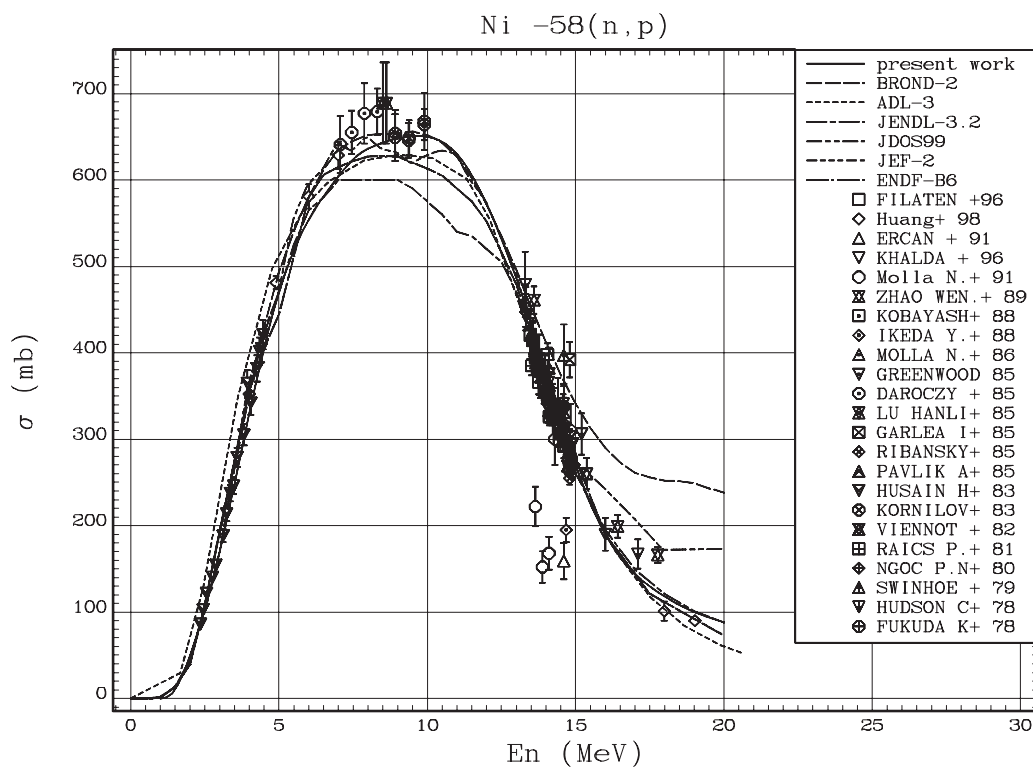
Fig. 43. ^{58}Ni(n,p)^{58}Co reaction cross-section

Ni - 60(n,2n)
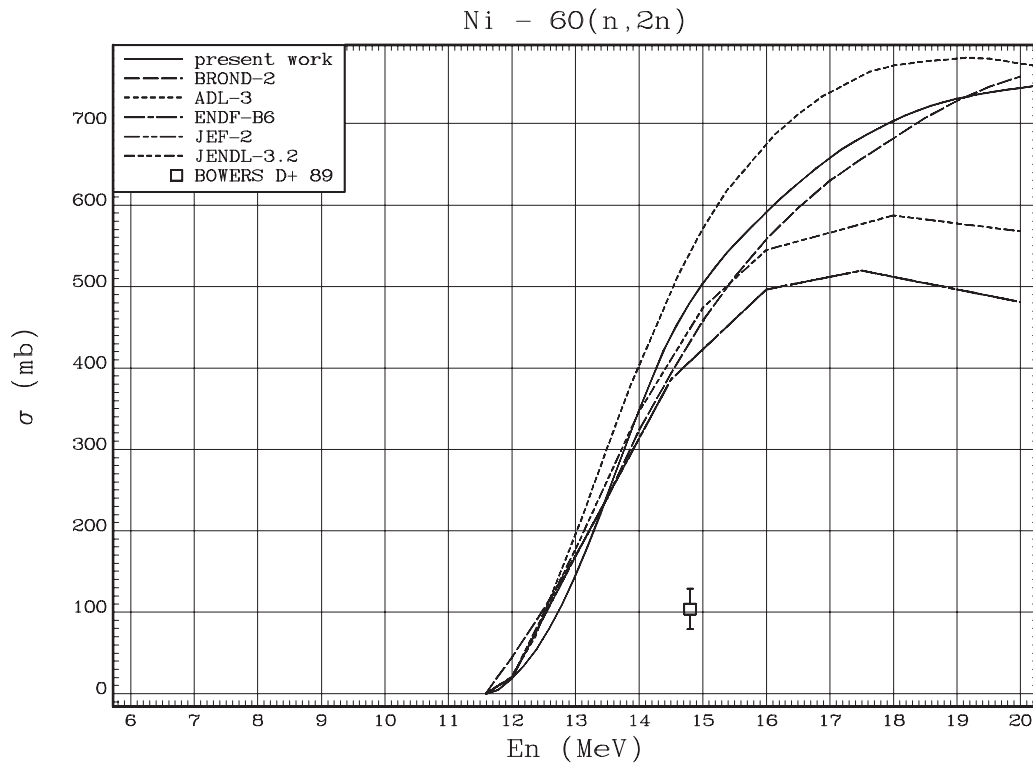
Fig. 44. ^{60}Ni(n,2n)^{59}Ni reaction cross-section

Ni - 61(n,2n)
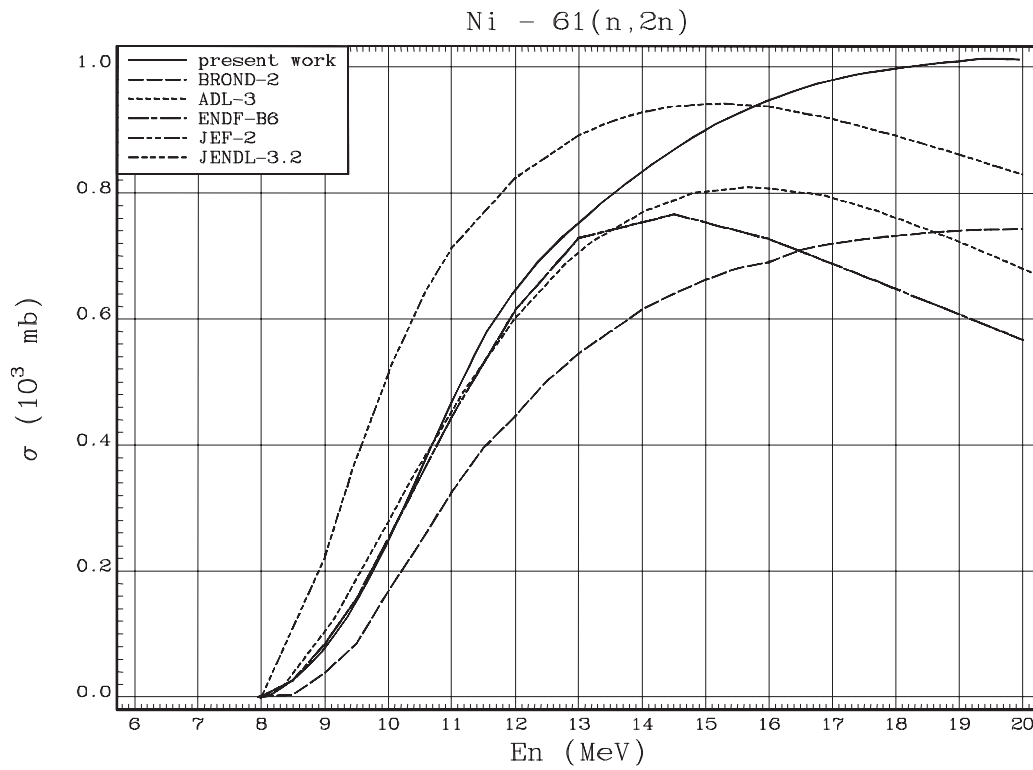
Fig. 45. ^{61}Ni(n,2n)^{60}Ni reaction cross-section

Ni – 62(n,2n)
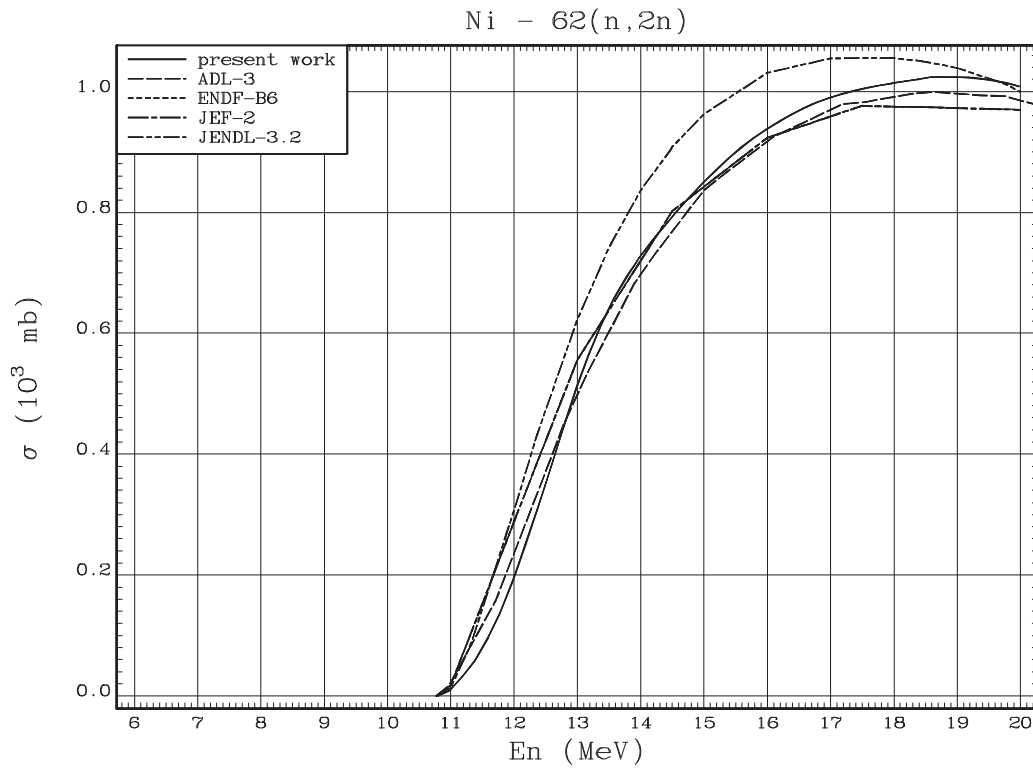
Fig. 46. ^{62}Ni(n,2n)^{61}Ni reaction cross-section

Ni –62(n,a)

Fig. 47. ^{62}Ni(n,α)^{59}Fe reaction cross-section

Ni -63(n,na)
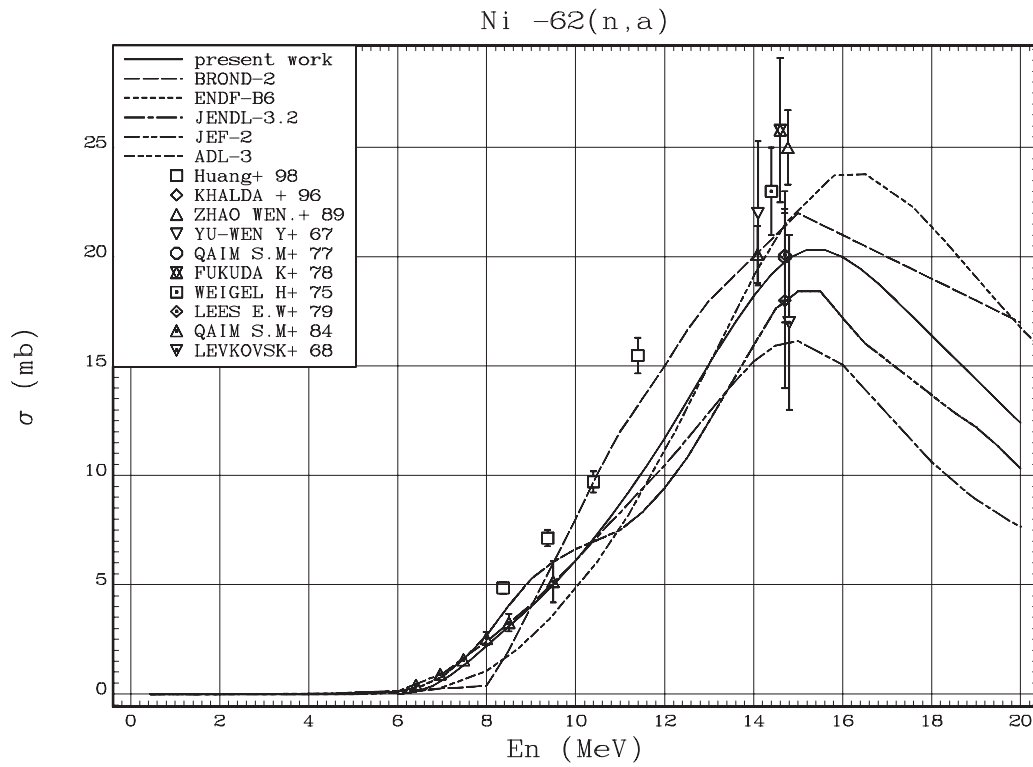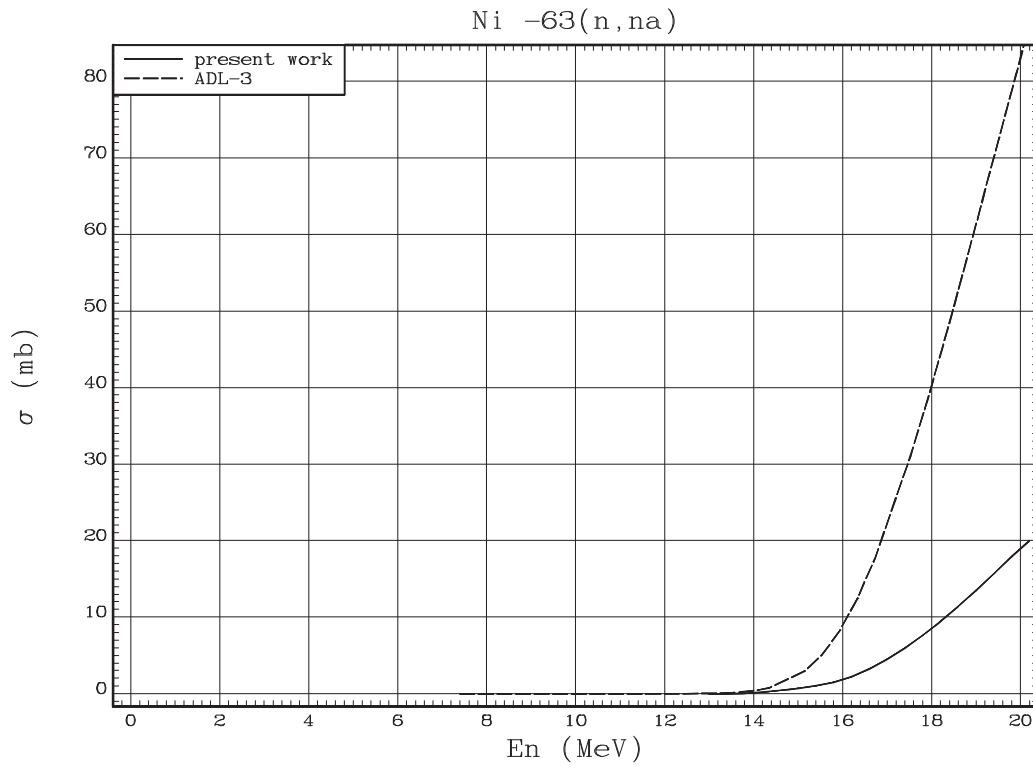
Fig. 48. ^{63}Ni(n,nα)^{58}Fe reaction cross-section

Ni - 64(n,2n)
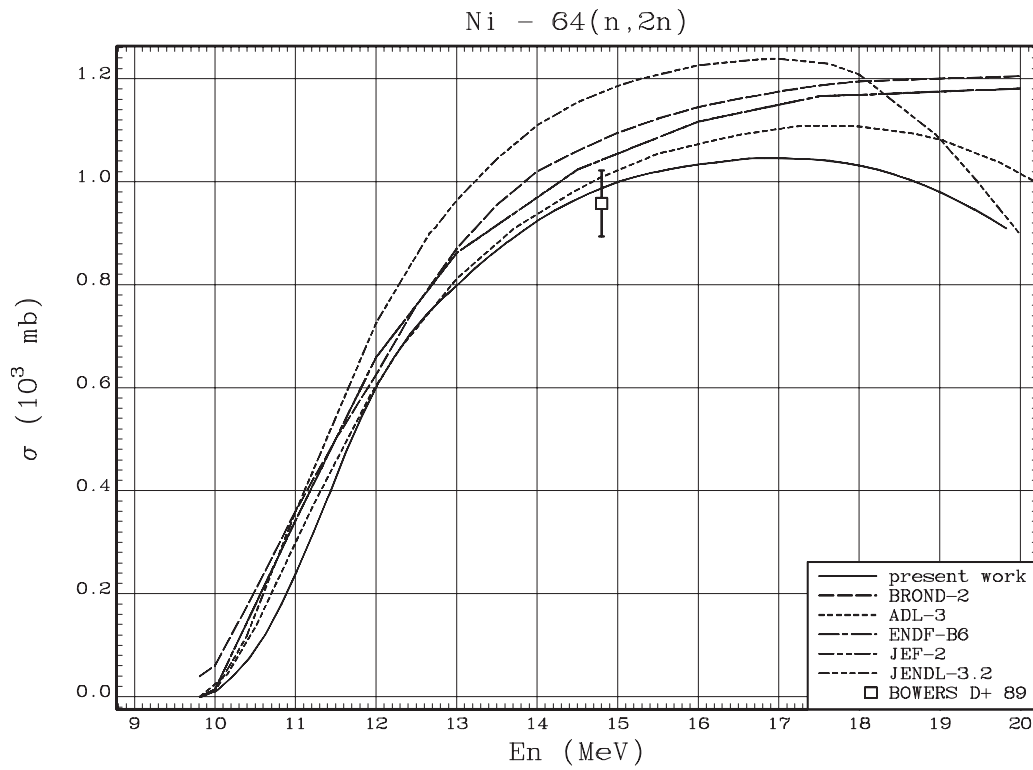
Fig. 49. ^{64}Ni(n,2n)^{63}Ni reaction cross-section
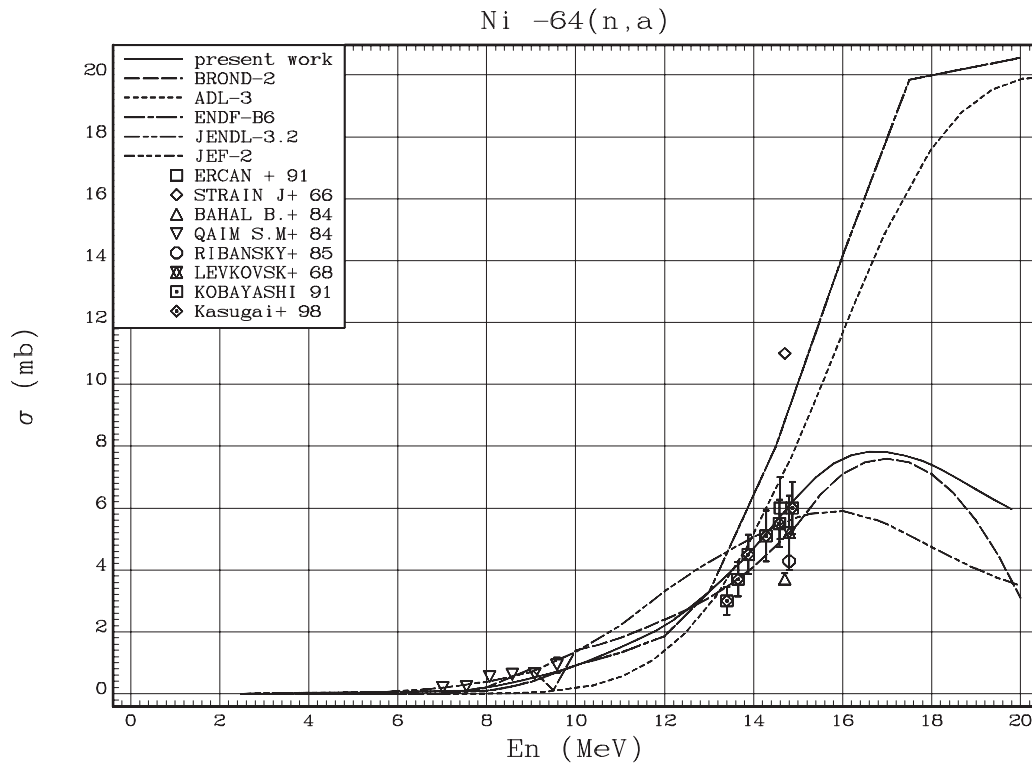
Fig. 50. ^{64}Ni(n,α)^{61}Fe reaction cross-section

REFERENCES

1. Forrest, R.A., Endacott, D.A.J., Activation data for some elements relevant to fusion reactors, Report AERE-R-13402, 1989.

2. Blokhin A.I., Manokhin V.N., Nasyrova S.M., Study of the excitation functions of threshold neutron reactions using the similarity method. Preprint FEhI - 2620 (Institute of Physics and Power Engineering), 1997, Obninsk.

3. Manokhin V.N., Some criteria for selection of evaluated threshold reaction excitation functions. Report INDC(CCP)-397, 1997, Vienna.

01-11405 (132) [005]
<u>Translated from Russian</u>

UDC 539.173.84

8-GROUP RELATIVE DELAYED NEUTRON YIELDS FOR MONOENERGETIC NEUTRON INDUCED FISSION OF [239]Pu

V.M. Piksaikin, L.E. Kazakov, S.G. Isaev, G.G. Korolev,
V.A. Roshchenko, R.G. Tertychnyj

Institute for Physics and Power Engineering, Obninsk, Russia

8-GROUP RELATIVE DELAYED NEUTRON YIELDS FOR MONOENERGETIC NEUTRON INDUCED FISSION OF [239]Pu. The energy dependence of the relative yield of delayed neutrons in an 8-group model representation was obtained for monoenergetic neutron induced fission of [239]Pu. A comparison of this data with the available experimental data by other authors was made in terms of the mean half-life of the delayed neutron precursors

The kinetics of power facilities which operate on a nuclear fission chain reaction basis are in many ways determined by delayed neutron physical characteristics, especially the relative yields, a_i, and half-lives, T_i, of the individual groups of delayed neutrons. There is therefore a need for these data to be accurate. As we know, the accuracy of any evaluated nuclear physics characteristics depends not only on the quality of an individual experiment, but also on the quantity of experiments whose data are used in evaluating and producing recommended data. Different criteria are used to assess the reliability of these data depending on the nuclear constant type. No procedure has yet been developed for averaging the data for the group delayed neutron parameters (a_i, T_i) obtained in various experiments, and the recommended data used are derived from one experiment [1]. On the one hand, this is attributable to the high quality of Keepin's experimental data [1]. On the other, it has been caused by the lack of any procedure for averaging group delayed neutron parameters where there is a strong correlation between the group parameters belonging to one specific delayed neutron group and also to various delayed neutron groups. Even if we disregard the influence of various experimental parameters (the time taken to deliver the sample to the neutron detector or the time taken to record neutron activity decay, background conditions, and so forth) on the degree of correlation between the group delayed neutron parameters, we are still left with uncertainty due to insufficient information about the primary neutron spectrum. Most of the basic information accumulated to date on relative delayed neutron yields and the half-lives of their nuclear precursors relates to thermal neutrons, fast neutrons (the reactor neutron spectra, including the fission neutron spectrum) and the neutron spectrum from the $T(d,n)^4He$ (14 MeV) reaction [2].

As discovered in [3], each compound nucleus undergoing neutron-induced fission has a specific mean life-time value for the delayed neutron nuclear precursors, which is clearly connected with the mean delayed neutron half-life. Figure 1 shows the mean half-life of delayed

neutron nuclear precursors as a function of the nuclear fissility parameter, Z^2/A_c, for fast neutron fission of thorium, uranium, plutonium and americium isotopes.

Thus, the mean half-life of delayed neutron precursors, in addition to the reactivity-asymptotic reactor period, can serve as a reliable criterion for evaluating delayed neutron group parameters [4]. In view of this, the energy dependence of the mean half-life of delayed neutron precursors during monoenergetic neutron-induced fission of heavy nuclei is of considerable interest because analysis of the experimental data specifically in terms of the mean half-life of delayed neutron nuclear precursors can be used to establish and investigate the nature of the delayed neutron group parameter energy dependence.
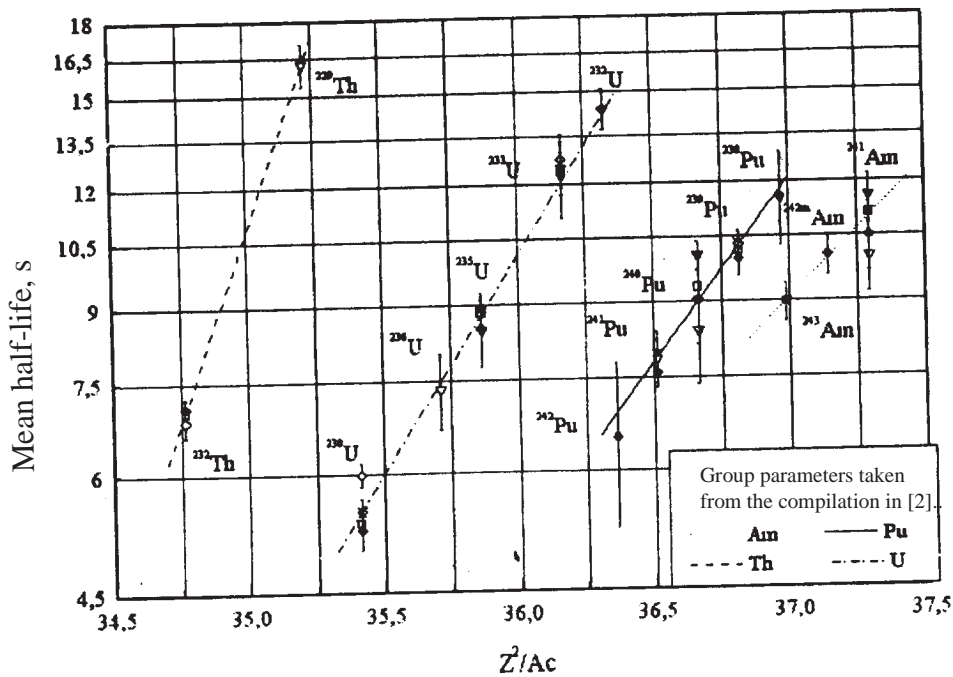
Fig. 1.   Systematics of the mean half-life of delayed neutron nuclear precursors during fast neutron fission of heavy nuclei.

Recently, interest has arisen in an 8-group representation of the time behaviour of delayed neutrons, based on a single set of delayed neutron nuclear precursor decay constants averaged according to groups for different fissile systems. From a reactor physics point of view at any rate, there are several fundamental reasons for the interest in a new 8-group representation of the time behaviour of delayed neutrons based on a single set of delayed neutron nuclear precursor decay constants which are group averaged [5]. The primary reason is simplification of the dynamic model of a complex system consisting of more than one fissioning isotope. Thus, for example, using a 6-group model to describe the total activity of a delayed neutron system comprising 5 fissioning isotopes requires 30 differential equations. This is because each isotope in the system is characterized by its own set of decay constants. If however 8 decay constants are

fixed for all fissioning isotopes, only 8 differential equations are required to describe a system comprising 5 fissioning isotopes.

The second reason for interest in a new representation of the time behaviour of delayed neutrons is indicated in [10] and is connected with obtaining a universal set of delayed neutron spectra for the individual delayed neutron groups. The spectra for the first delayed neutron group, obtained on the basis of the existing 6-group model for ^{235}U and ^{238}U, differ noticeably. In fact, the delayed neutron spectra in the first group should be identical for both isotopes (^{235}U, ^{238}U) as this group corresponds to the dominant delayed neutron nuclear precursor, ^{87}Br. In the new model, the spectra of the first delayed neutron group will be virtually identical for all the fissioning isotopes, as the ^{137}I and ^{87}Br delayed neutron nuclear precursors which have similar decay constants will correspond to different delayed neutron groups. In this case, the additional contribution from the ^{137}I nuclear precursor will not be included in the first group.

An important feature of the 8-group representation of delayed neutron time behaviour is its lack of any correlational dependence between the delayed neutron half-lives and yields, unlike the 6-group representation where this is one of the factors which makes the averaging of data relating to different sets of relative delayed neutron yields and half-lives more difficult.

This paper aims to:

1.   Measure the energy dependence of the relative delayed neutron yields and the half-lives of their nuclear precursors during ^{239}Pu nuclear fission in the 0.37-5 MeV primary neutron energy range;

2.   Establish a procedure for transferring the data measured into an 8-group model representation of delayed neutron time behaviour.

Experimental method and results

T(p,n)^{3}He and D(d,n)^{3}He reactions served as the monoenergetic neutron sources. Tritium and deuterium targets were irradiated with an accelerated proton or deuteron beam in the IPPE KG-2.5 cascade generator. The neutron energy distribution from the accelerator target was recorded using a ^{3}He neutron spectrometer.

The measurement procedure involved cyclic irradiation of a ^{239}Pu sample with subsequent measurement of the time dependence of the delayed neutron activity decay [6]. The sample was transferred from the irradiation position to the neutron detector using a pneumatic device. Sample delivery took 150 ms on average. The delayed neutron activity decay dependence was measured for 720s. The sample irradiation time selected was 300 s.

Initial processing of the experimental data consisted of summing the delayed neutron intensity decay time dependences obtained in the individual measurement cycles. The aggregated delayed neutron activity decay curves were analysed using the iterative least squares method to obtain an evaluation of the delayed neutron group parameters in a 6-group delayed neutron representation [6]. A similar procedure was also used when obtaining data for the 8-group model relative delayed neutron yields. There are however other ways of obtaining data on

the group yields in an 8-group delayed neutron representation. One of these is described in detail in [5].

We used one further method of "converting" the data obtained in the 6-group model into an 8-group delayed neutron representation. This method is based on plotting the delayed neutron activity decay curve with respect to the relative 6-group delayed neutron yields and half-lives. The delayed neutron activity decay curves plotted in this way were then processed using the iterative least squares method. By choosing different time intervals on the decay curve in a six-step procedure, based on successively obtaining the relative yields for each delayed neutron group, it was possible to improve the accuracy of the data obtained substantially.

As noted above, it was discovered in [3] that each fissile nucleus has a specific value of the mean half-life of the delayed neutron nuclear precursors. The mean delayed neutron nuclear precursor half-life is clearly characterized by a specific set of delayed neutron group parameters irrespective of how they are represented, i.e. the number of delayed neutron groups used. Analysis of the mean delayed neutron precursor half-life data for 6 and 8 groups obtained directly from the experimental curves and the data from the "conversion" method showed that, if the statistical accuracy of the experimental data is low (less than $(2-5) \cdot 10^5$ of the total number of counts), the value of the mean delayed neutron nuclear precursor half-life corresponding to the set of 8-group model group parameters obtained directly from the experimental delayed neutron activity decay curve differs from the corresponding 6-group model value by 1-4%. On the other hand, the delayed neutron nuclear precursor mean half-life data corresponding to the set of group parameters obtained in the 8-group model using the "conversion" method agree very accurately with the 6-group model delayed neutron data. In view of this, the final 8-group relative delayed neutron yield data in this paper are those obtained using the method to "convert" the 6-group model into an 8-group model. The 8-group relative delayed neutron yields for monoenergetic neutron induced fission of [239]Pu are given in Table 1.

As the data on delayed neutron time behaviour in a number of previous papers by other authors were obtained in the conventional 6-group representation, they can only be compared with those in this paper, obtained in an 8-group delayed neutron representation, on the basis of the mean delayed neutron nuclear precursor half-life. The mean delayed neutron nuclear precursor half-life data for neutron induced [239]Pu fission are given in Fig. 2.

The data on the mean half-life of the delayed neutron nuclear precursors in this paper (8 groups) agree with the mean half-life values obtained on the basis of the delayed neutron group parameter data of other authors [1, 7, 8]. However, there is a marked discrepancy between the mean half-life data we obtained and the $\langle T \rangle (E_n)$ energy dependence data obtained by Maksyutenko [9]. The mean half-life decay values obtained on the basis of the delayed neutron group parameters in [9] are far higher than the mean half-life values obtained in this paper: according to [9], the values of $\langle T \rangle$ for neutron induced [239]Pu fission with energies of 3.8, 5.5, 6.5, 7, 7.5 and 7.8 MeV are 11.39, 11.47, 10.92, 11.86, 10.2 and 12.87 s, respectively. The primary neutron energy change ranges in our paper and in [9] only partially overlap. However, in view of the good agreement between the mean half-life energy dependence obtained in this paper and the data from [1, 7, 8] it is difficult to explain the considerable increase in $\langle T \rangle$ when the primary neutron energy was increased in [9]. Since, however, the mean delayed neutron

precursor half-life value increases as compound nucleus mass decreases, opening the emissive fission (*n.n'*) channel could give rise to an increase in the mean half-life of delayed neutron precursors starting with a neutron energy of ~ 6 MeV.

Table 1

The 8-group representation of relative delayed neutron yields for monoenergetic neutron-induced fission of ^{239}Pu

$E_n,$ MeV	Group number and half-life (s)								Mean half-life, s	
	1 55.6	2 24.5	3 16.3	4 5.21	5 2.37	6 1.04	7 0.424	8 0.195	8-group	6-group
0.37 ±0.06	0.028 ± 0.001	0.236 ± 0.008	0.078 ± 0.003	0.182 ± 0.007	0.284 ± 0.010	0.097 ± 0.005	0.071 ± 0.004	0.024 ± 0.001	10.37 ±0.21	10.36 ±0.15
0.62 ±0.06	0.030 ± 0.001	0.231 ± 0.008	0.083 ± 0.004	0.184 ± 0.007	0.294 ± 0.010	0.088 ± 0.004	0.068 ± 0.003	0.022 ± 0.001	10.46 ±0.22	10.47 ±0.17
0.86 ±0.06	0.032 ± 0.001	0.212 ± 0.007	0.097 ± 0.004	0.173 ± 0.007	0.300 ± 0.010	0.088 ± 0.004	0.076 ± 0.004	0.022 ± 0.001	10.29 ±0.20	10.27 ±0.13
1.06 ±0.06	0.032 ± 0.001	0.220 ± 0.008	0.089 ± 0.004	0.172 ± 0.007	0.322 ± 0.010	0.061 ± 0.003	0.084 ± 0.004	0.020 ± 0.001	10.38 ±0.22	10.37 ±0.11
3.27 ±0.14	0.036 ± 0.001	0.190 ± 0.007	0.099 ± 0.004	0.167 ± 0.007	0.346 ± 0.011	0.051 ± 0.003	0.093 ± 0.005	0.018 ± 0.001	10.06 ±0.20	10.06 ±0.19
3.81 ±0.11	0.038 ± 0.001	0.173 ± 0.006	0.090 ± 0.004	0.175 ± 0.007	0.339 ± 0.010	0.082 ± 0.004	0.078 ± 0.004	0.025 ± 0.001	9.66 ±0.18	9.68 ±0.11
4.27 ±0.11	0.039 ± 0.001	0.164 ± 0.006	0.097 ± 0.004	0.179 ± 0.007	0.336 ± 0.010	0.080 ± 0.004	0.082 ± 0.004	0.023 ± 0.001	9.62 ±0.18	9.65 ±0.14
4.81 ±0.13	0.042 ± 0.002	0.154 ± 0.006	0.102 ± 0.004	0.172 ± 0.007	0.348 ± 0.011	0.078 ± 0.004	0.083 ± 0.004	0.021 ± 0.001	9.61 ±0.20	9.62 ±0.11
4.97 ±0.13	0.043 ± 0.002	0.138 ± 0.005	0.122 ± 0.004	0.146 ± 0.006	0.399 ± 0.011	0.030 ± 0.002	0.110 ± 0.005	0.012 ± 0.001	9.55 ±0.18	9.59 ±0.16
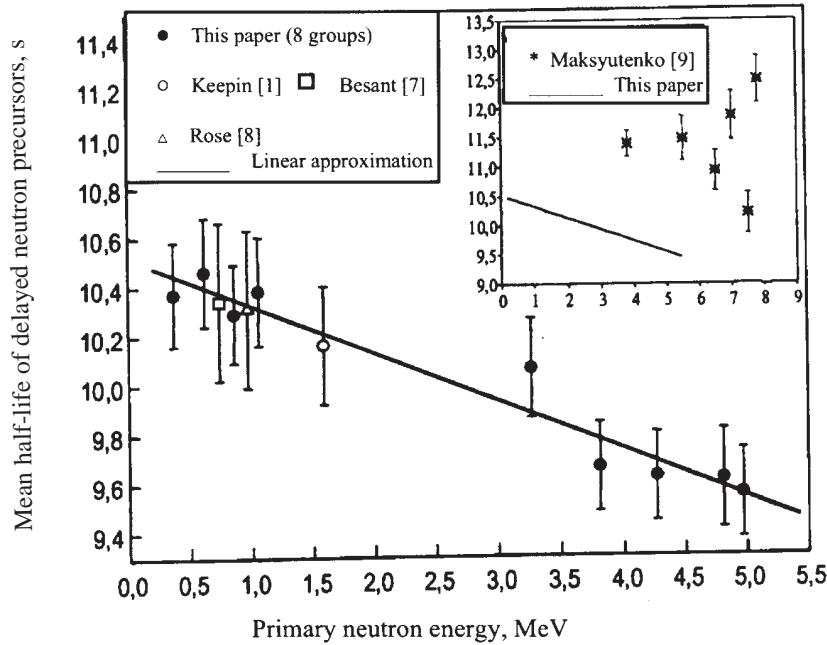
Fig. 2.   The dependence of the mean half-life of delayed neutron nuclear precursors on primary neutron energy for neutron induced [239]Pu fission.

Conclusion

This paper measures values for the delayed neutron group parameters (a_i, T_i) for monoenergetic neutron induced [239]Pu fission in the 0.37-5 MeV energy range. The delayed neutron group parameter energy dependence obtained is compared with data from other authors in terms of the mean delayed neutron nuclear precursor half-life. The approach developed made it possible, for the first time, to show the nature and scale of the change in delayed neutron group parameter values as the excitation energy of the fissile [240]Pu compound nucleus changes.

The delayed neutron energy dependence for neutron induced [239]Pu fission discovered in this paper is reflected as a ≈10% reduction in the mean delayed neutron nuclear precursor half-life in the 2.85 eV-5 MeV primary neutron energy range. It is abundantly clear that this change in the delayed neutron group parameter values must be taken into account in reactor calculations because. as we have established. the relative change in the mean delayed neutron precursor half-life $\Delta{<}T{>}/{<}T{>}$ causes a relative change in reactivity $\Delta\rho/\rho$ (provided that the same sets of delayed neutron group parameters are used in both cases).

The delayed neutron intensity decay data measured in this paper were used to obtain sets of delayed neutron group constants corresponding to the 8-group delayed neutron model currently being developed which is based on a universal set of delayed neutron precursor decay constants for various fissile systems [5]. Data on the energy dependence of the relative delayed neutron

yields have been obtained for the first time in an 8-group representation. The delayed neutron nuclear precursor half-life values obtained on the basis of the 8-group delayed neutron time behaviour data (the result of "conversion") agree, within the uncertainty limits indicated, with the corresponding values obtained on the basis of the original 6-group model (before "conversion").

The results obtained here should undoubtedly be taken into account when producing recommended data on delayed neutron group parameters for reactors with an intermediate neutron spectrum, which differs from both the thermal and the "fast" (fission neutron spectrum).

REFERENCES

1. Keepin G.R., Wimett T.F., et al., J. Nuclear Energy, 1957, v.6, p. 1.

2. Spriggs G.D., Campbell J.M., Report LA-UR-98-918, LANL, March 6, 1998.

3. Piksaikin V.M., Isaev S.G., Correlation properties of delayed neutrons from fast neutron induced fission, Report INDC(CCP)-415, October 1998, p. 1, IAEA, Vienna, Austria.

4. Spriggs G.D., Nucl. Sci. Eng. 1993, v.114, p. 342.

5. Spriggs G.D., Campbell J.M., Piksaikin V.M., Report LA-UR-98-1619, LANL, March 28, 1999.

6. Piksaikin V.M., Balakshev Yu.F., Isaev S.G., Korolev G.G., Semenova N.N., Sergachev A.I., Tarasko M.Z., Voprosy atomnoj nauki i tekhniki. Series: Yadernye konstanty 1-2, 1997, p. 18.

7. Besant C.B., Challen P.J., McTaggart M.H., Tavoularidis P., Williams J.G., J. Br. Nucl. Energy Soc., 1977, v.16, p. 161.

8. Rose H. and Smith R.D., J. Nuclear Energy, 1957, v.4, p. 133.

9. Maksyutenko B.P., et al., Yadernaya Fizika, 1974, v.19, No. 4, p. 748.

10. Spriggs G.D., Campbell J.M., Report LA-UR-99-2988, LANL, June 6, 1999.

01-11405 (130)   [006]

<u>Translated from Russian</u>

UDC 539.173.84

8-GROUP RELATIVE DELAYED NEUTRON YIELDS FOR EPITHERMAL NEUTRON INDUCED FISSION OF ^{235}U AND ^{239}Pu

V.M. Piksaikin, L.E. Kazakov, S.G. Isaev, G.G. Korolev,
V.A. Roshchenko, R.G. Tertychnyj

Institute for Physics and Power Engineering, Obninsk, Russia

8-GROUP RELATIVE DELAYED NEUTRON YIELDS FOR EPITHERMAL NEUTRON INDUCED FISSION OF ^{235}U AND ^{239}Pu. An 8-group representation of relative delayed neutron yields was obtained for epithermal neutron induced fission of ^{235}U and ^{239}Pu. These data were compared with ENDF/B-VI data in terms of the average half-life of the delayed neutron precursors and on the basis of the dependence of reactivity on the asymptotic period.

Present-day nuclear power development programmes give considerable importance to the development of new nuclear reactor designs with a harder neutron energy spectrum, complex nuclear fuel composition, and which can be used for transmutation of nuclear waste. The need for these reactors to operate safely and effectively has placed more stringent requirements on the entire set of nuclear physics constants which are used in practical reactor work, including delayed neutron databases. However, in spite of significant efforts to study the delayed neutron emission process ever since their discovery, much uncertainty still exists in the nuclear physics data for delayed neutrons, even for the main fuel isotopes ^{238}U and ^{239}Pu.

To date individual sets of delayed neutron group parameters (relative yield of the *i*-th group of delayed neutrons, a_i, half-life of nuclear precursors relating to the *i*-th group of delayed neutrons, T_i) have mainly been checked by comparing the reactivity dependence on the asymptotic reactor period, obtained on the basis of these data, with the corresponding experimental data. Using this approach, Ref. [1] shows that the delayed neutron group parameters for ^{235}U obtained by Keepin [2] satisfactorily describe the dynamic behaviour of the reactor on which the experiments were carried out. In particular, the author of [1] had shown that Keepin's data for ^{235}U [2] can predict the reactivity of the system to within 3%. On the other hand, it was shown that the delayed neutron group parameters for ^{235}U from the ENDF/B-VI data library, obtained using the microscopic approach [3], underestimate the reactivity by 2-47% when it changes in the range from +0.80 to –0.80$.

It was shown in [4] that a set of relative yields and half-lives of individual delayed neutron groups for a particular fissioning system can be presented in the form of a reactor physics magnitude - the mean lifetime of the delayed neutron nuclear precursors. It was discovered that for each compound nucleus undergoing neutron-induced fission there is a specific mean lifetime value of the delayed neutron nuclear precursors. The application of a systematic approach to the mean half-life of delayed neutron nuclear precursors [4], based on the delayed neutron properties indicated above, has revealed a significant difference between the (a_i, T_i) group parameters for a large set of fissioning systems presented in the ENDF/B-IV library of evaluated data and the corresponding experimental data. A particularly large discrepancy was discovered in the fission of plutonium and americium isotopes [5].

There is now increased interest in the new 8-group representation of the time behaviour of delayed neutrons, which is based on a single set of delayed neutron group half-lives [6], with a view to simplifying the dynamic model of a complex system comprising more than one fissile isotope, and obtaining a more universal set of delayed neutron spectra.

This paper aims to measure the relative yields of delayed neutrons and the half-lives of their nuclear precursors for epithermal neutron induced fission of ^{235}U and ^{239}Pu using a single experimental method, and to carry out a comparative analysis of the data obtained with the recommended data of other authors. Experimental data for delayed neutron time behaviour in a 6-group representation were used to obtain the relative delayed neutron yields in an 8-group representation, based on a universal set of group half-lives for delayed neutron precursors [6].

Experiment

The relative delayed neutron yields and half-lives of their nuclear precursors for epithermal neutron induced fission of ^{235}U and ^{239}Pu were measured on a facility based on the KG-2.5 electrostatic accelerator at the Institute for Physics and Power Engineering. The measurement method and procedure are described in [7]. The difference here was that the samples under investigation were irradiated in a polyethylene cube by a neutron beam, produced by the T(p,n)^{3}He reaction, incident on one face. The cube's dimensions were identical to those of the polyethylene block in [2]. However, the energy distribution of the primary neutron beams in the present study differed from that in [2]. The present paper used a quasi-monoenergetic neutron beam, whereas [2] used a fission neutron spectrum. Figure 1 shows the position of the sample under investigation relative to the neutron target of the accelerator. Figure 2 shows the primary neutron spectrum after moderation in the polyethylene cube, averaged over the sample volume. Primary neutron spectrum data were obtained using a neutron source program on the basis of T(p,n)^{3}He, D(d,n)^{3}He and T(d,n)^{4}He charged particle reactions [8]. Account was taken of all the known effects which influence the energy distribution form of the neutrons emitted from the neutron target of the accelerator, as well as all the possible interaction processes of these neutrons with the nuclei of structural materials and the sample itself. We can see from Fig. 2 that, after moderation in the polyethylene cube, the neutron spectrum is not strictly speaking thermal. The average neutron energy in the sample in this experiment was ~2.85 eV.

After irradiation in the neutron flux, the sample was moved using a pneumatic transfer system to a neutron detector, consisting of an assembly of 30 SNM-11 boron counters in the form

of three concentric circles in the polyethylene block. Sample transfer took 150 ms on average. The irradiation time was 15 and 300 s. The time for recording the delayed neutron intensity was 720 s, enabling accurate evaluation of the background component in the neutron activity decay curve.
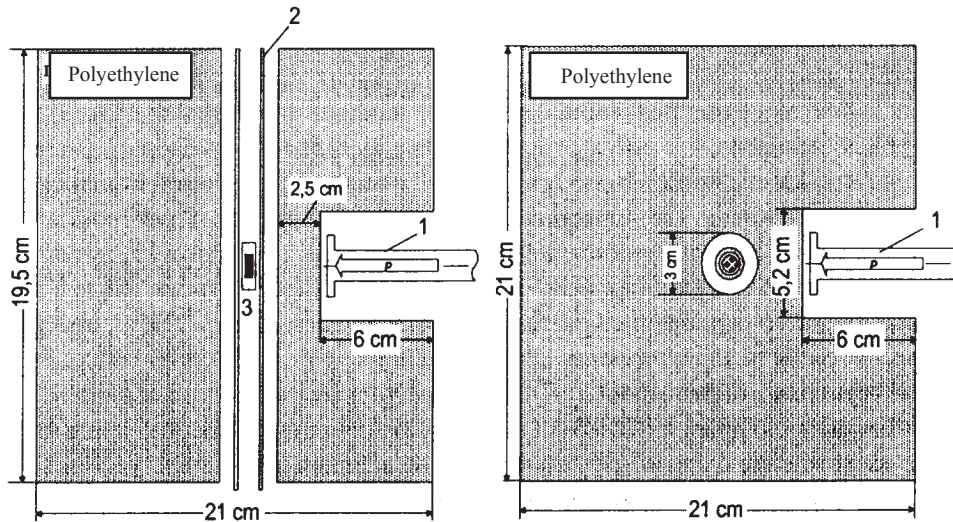

Fig. 1. Diagram of target array for measuring delayed neutron group parameters from epithermal neutron induced fission of heavy element isotopes. 1 – target holder, 2 - channel of sample transfer system, 3 – fissile sample.
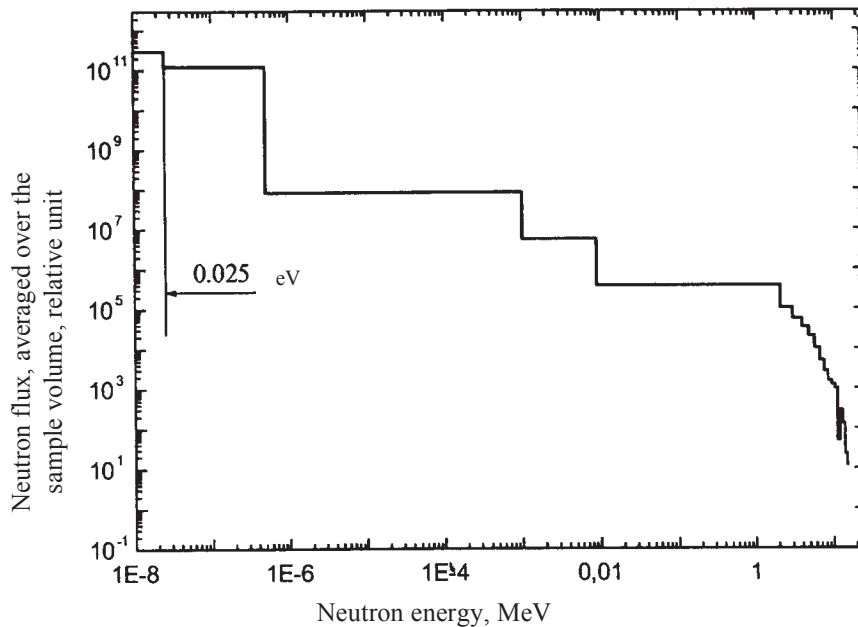

Fig. 2. Neutron energy distribution, averaged over the volume of an irradiated ^{235}U sample positioned in the centre of a polyethylene cube.

Processing of experimental data and results

The number of counts registred in each measurement cycle was aggregated in one delayed neutron activity decay curve. Delayed neutron group parameters were evaluated using the iterative least squares method described in [9] in the conventional 6-group representation. Processing one series of measurements resulted in a set of relative delayed neutron yield values, a_i half-lives of their nuclear precursors, T_i, and a correlation matrix of the group parameters. To average the delayed neutron group parameters obtained in the individual measurement series a procedure was devised which takes account of the correlations of the relative yields and the delayed neutron half-lives.

In matrix notation the vector $\bar{a}$ of average values for a set of delayed neutron group parameters measured in N independent measurements series can be written as

$$\bar{a} = \overline{\Sigma} \cdot (\Sigma_1^{-1} \cdot \bar{a}_1 + \Sigma_2^{-1} \cdot \bar{a}_2 + ... + \Sigma_i^{-1} \cdot \bar{a}_i + ... + \Sigma_N^{-1} \cdot \bar{a}_N),$$

where $\overline{\Sigma}$ is the covariance matrix of the average values for the set of group parameters

$$\overline{\Sigma} = (\Sigma_1^{-1} + \Sigma_2^{-1} + ... + \Sigma_i^{-1} + ... + \Sigma_N^{-1})^{-1},$$

$\bar{a}_i = \left(a_i^1 T_i^1, ..., a_i^6 T_i^6\right)^T$ is the vector of the group parameters (relative yields and delayed neutron half-lives) obtained in the i-th measurement series, and Σ_i is the covariance matrix of the group parameters obtained in the i-th measurement series.

Values for the squares of the uncertainties of the averaged delayed neutron group parameters are diagonal elements of the covariance matrix of the $\overline{\Sigma}$ average values for the delayed neutron group parameter set.

The data for relative delayed neutron yields in an 8-group representation were obtained by "converting" the 6-group model data into an 8-group representation. This method is based on plotting a delayed neutron activity decay curve for the 6-group relative delayed neutron yields and half-lives obtained in this paper. These delayed neutron activity decay curves were then processed using the iterative least squares method.

The mean half-life of the delayed neutron precursors was derived from the evaluated delayed neutron relative yields and the known half-lives of their precursors using the equation

$$<T> = \sum_{j=1}^{8} T_j \cdot a_j$$

Table 1 gives the final data on 8-group relative delayed neutron yields for epithermal neutron induced fission of ^{235}U and ^{239}Pu.

It was not our aim to carry out a complete analysis of all the existing data for the nuclei under investigation. Two sets of recommended data were chosen for comparison: the experimental data in [2] from the ENDF/B-V library and the data in [10] obtained by taking a microscopic approach to ENDF/B-VI.

Comparison of the relative delayed neutron values and the half-lives of their nuclear precursors thus obtained with Keepin's analogous recommended experimental data [2] in terms of the mean half-life of the delayed neutron nuclear precursors showed a 1% difference in the data. However, our experimental data on the delayed neutron group parameters have fewer uncertainties than [2]. There were substantially fewer uncertainties in the delayed neutron group parameters for ^{239}Pu fission in comparison with the data in [2]. This result is attributable to optimization of the facility's parameters and also the more accurate procedure for averaging the delayed neutron group parameters, taking account of their correlations.

The aforementioned comparison relates to the data obtained from analysis of the delayed neutron intensity decay curves measured after neutron irradiation of the samples under investigation. In addition to experimental data, recommended data are also now available for the delayed neutron group parameters obtained by means of the so-called "microscopic approach" (see, for example, [3]). In this approach the delayed neutron group parameters are calculated by summing the contributions of the delayed neutrons corresponding to the individual delayed neutron nuclear precursors. This is precisely the type of delayed neutron data which has been included in the ENDF/B-VI evaluated data library [10]. Comparison of the mean half-life values of the delayed neutron precursors for epithermal neutron induced fission of ^{235}U and ^{239}Pu obtained in this paper with analogous data from ENDF/B-VI reveals a substantial difference between them, which reaches 13% for fission of ^{235}U nuclei.

Comparing sets of delayed neutron group parameters on the basis of the reactivity dependence on the asymptotic period of a critical system

As already noted above, different sets of delayed neutron group parameters can be compared on the basis of the reactivity dependence on the asymptotic period of a critical system, obtained using the inhour equation

$$\rho = \frac{\Lambda}{T} + \sum_{i=1}^{n} \frac{(\beta_i)_{eff}}{1 + \lambda_i \cdot T},$$

where Λ is the prompt fission neutron production, T is the asymptotic period of the system, λ_i is the decay constant of the i-th group of delayed neutrons, and $(\beta_i)_{eff}$ is the effective fraction of the i-th group of delayed neutrons. Neglecting the prompt fission neutron term and considering that $(\beta_i)_{eff}$ can be approximated by the expression $\beta_{eff} a_i$ [11], then the reactivity of the system can be presented in the form

$$\rho = \beta_{eff} \cdot \sum_{i=1}^{n} \frac{a_i}{1 + \lambda_i \cdot T},$$

where β_{eff} is the effective fraction of the delayed neutrons and a_i is the relative yield of the i-th group of delayed neutrons.

Figures 3 and 4 show reactivity as a function of the period for data from the present paper (continuous line) and from ENDF/B-VI [10] (dotted line) in relation to the corresponding $\rho_{Keepin}(T)$ dependence in [2]. We can see from Figs 3 and 4 that the difference in the mean half-

life of the present paper and [2] leads to a discrepancy in reactivity values that is within 1% for the nuclei examined over the entire given range of change in the period T (positive values of the period are examined). At the same time, the reactivity values obtained on the basis of the ENDF/B-VI (a_i, T_i) data [10] diverge significantly from corresponding data calculated on the basis of the delayed neutron group parameters in [2]. For ^{235}U and ^{239}Pu fission, the reactivity values vary by 12% and 10%, respectively. It should be noted, in particular, that this difference coincides with the difference in the mean half-life values of the nuclear precursors for the fissile nuclei indicated (see Table 1). This shows that the mean half-life $<T>$ of the nuclear precursors can be viewed as an additional quality criteria for a specific set of delayed neutron group parameters.

Table 1

Relative delayed neutron yields in an 8-group representation for epithermal neutron induced fission of ^{235}U and ^{239}Pu

Isotope	Group number and half-life (s)								Mean half-life, s	
	1 55.6	2 24.5	3 16.3	4 5.21	5 2.37	6 1.04	7 0.424	8 0.195	8-group	6-group
^{235}U	0.034 ±0.001	0.153 ±0.006	0.086 ±0.004	0.212 ±0.007	0.298 ±0.009	0.105 ±0.005	0.073 ±0.004	0.039 ±0.002	9.00 ±0.18	8.98 ±0.11
									9.02±0.34 [2] 7.90 [10]	
^{239}Pu	0.029 ±0.001	0.240 ±0.008	0.083 ±0.004	0.188 ±0.007	0.289 ±0.010	0.089 ±0.004	0.059 ±0.003	0.023 ±0.001	10.63 ±0.22	10.59 ±0.17
									10.69±1.11 [2] 9.66 [10]	

Fig. 3. Reactivity - asymptotic period dependence derived from delayed neutron group parameter data for neutron induced ^{235}U fission from the present paper and ENDF/B-VI [10] relative to the corresponding dependence obtained using data in [2].
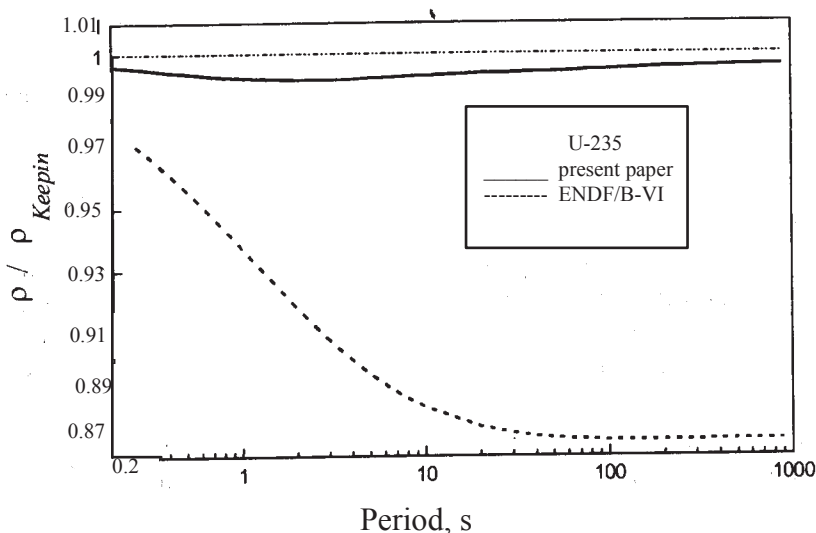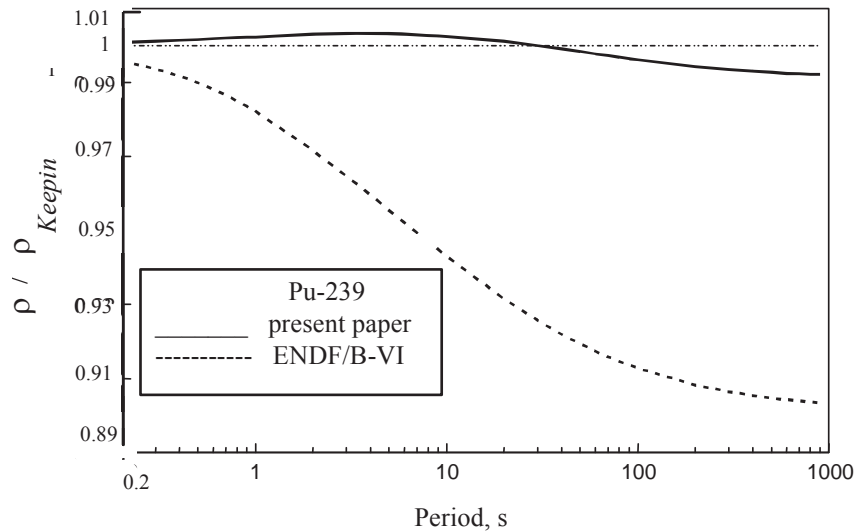
Fig. 4.   Reactivity - asymptotic period dependence derived from delayed neutron group parameter data for neutron induced [239]P fission from the present paper and ENDF/B-VI [10] relative to the corresponding dependence obtained using data in [2].

Conclusion

In the present paper relative delayed neutron yields in an 8-group representation were obtained for epithermal neutron induced fission of [235]U and [239]Pu. The paper sets out a procedure for averaging the delayed neutron group parameters obtained in various series of measurements which takes account of the delayed neutron group parameter correlation. A comparative analysis was made of the data in this paper and in [2] and [10]. The comparison was made in terms of the mean half-life of the delayed neutron nuclear precursors, and also using the reactivity - reactor asymptotic period dependence.

It was shown that the data in the present paper on the mean half-life of the delayed neutron precursors for epithermal neutron induced fission of [235]U and [239]Pu agree - within the limits of uncertainty - with Keepin's recommended experimental data [2]. However, there is substantial divergence between the data obtained using the microscopic approach [10] for the ENDF/B-VI delayed neutron library and the data in the present paper.

In the present paper correlation and covariance matrixes of the delayed neutron group parameters were obtained for each of the nuclei under investigation. An essential attribute of contemporary nuclear physics data evaluation methods, they can be used when generating recommended data for delayed neutron group parameters. The method applied in this paper for comparing the delayed neutron group parameters obtained in different experiments, which is based on the mean half-life of the delayed neutron nuclear precursors, can be used in conjunction with the period-reactivity dependence as an effective instrument for quantitative evaluation of experimental data quality in similar investigations of other fissile nuclei.

REFERENCES

1. Spriggs, G.D., Nucl. Sci. Eng., (1993), v.114, p. 342.

2. Keepin, G.R., Wimett, T.F., et al., J. Nuclear Energy, (1957), v.6, p. 1.

3. Brady, M.C., England, T.R., Nucl. Sci. Eng., (1989), v.103, p. 129.

4. Piksaikin, V.M., Isaev, S.G., Correlation properties of delayed neutrons from fast neutron induced fission, Report INDC(CCP)-415, October (1998), IAEA, Vienna, Austria, p. 1.

5. Isaev, S.G., Piksaikin, V.M., Kazakov, L.E., Goverdovski, A.A., Proc. of 8th International Seminar on Interaction of Neutrons with Nuclei, Dubna, May 17-20 (2000), p. 306.

6. Spriggs, G.D., Campbell, J.M., Piksaikin, V.M., Report LA-UR-98-1619, LANL, March 28, (1999).

7. Piksaikin, V.M., Balakshev, Yu.F., Isaev, S.G., et al., Measurements of the energy dependence of relative delayed neutron yields and the half-lives of their precursor for fast neutron fission ^{237}Np, Atomnaya energiya, 1998, v.85, No.1, p. 51.

8. Piksaikin, V.M., Shorin, V.S., Tertytchnyi, R.G., Report INDC(CCP)-422, IAEA, Vienna, August, 1999.

9. Piksaikin, V.M., Balakshev, Yu.F., Isaev, S.G., Korolev, G.G., Semenova, N.N., Sergachev, A.I., Tarasko, M.Z., Voprosy atomnoj nauki i tekhniki, Ser.: Yadernye konstanty No. 1-2, 1997, p. 18.

10. ENDF-102, Data Formats and Procedures for the Evaluated Nuclear Data File ENDF-6, (1991), edited by: Rose, P.F. and Dunford, C.L.

11. Stevenson, J.M., Delayed neutron parameter requirements for reactor physics purposes, Proceedings of the Specialists' Meeting on Delayed Neutron Properties, University of Birmingham, England, (ed. Weaver, D.R.), September 15-19, 1986, p. 1-20.

UDC 539.173.84

DELAYED NEUTRON YIELD FROM FAST NEUTRON INDUCED FISSION OF ^{238}U

V.M. Piksaikin, L.E. Kazakov, S.G. Isaev, V.A. Roshchenko,
A.A. Goverdovski, R.G. Tertytchnyi

State Scientific Center of the Russian Federation
Institute for Physics and Power Engineering
Bondarenko sq.1, Obninsk, Kaluga region, Russia, 249020

piksa@ippe.obninsk.ru

The measurements of the total delayed neutron yield from fast neutron induced fission of ^{238}U were made. The experimental method based on the periodic irradiation of the fissionable sample by neutrons from a suitable nuclear reaction had been employed. The preliminary results on the energy dependence of the total delayed neutron yield from fission of ^{238}U are obtained. According to the comparison of experimental data with our prediction based on correlation properties of delayed neutron characteristics, it is concluded that the value of the total delayed neutron yield near the threshold of (n,f) reaction is not a constant.

Introduction

The fundamental role of delayed neutrons in the safety operation and time-dependant behavior of nuclear reactors has been well known and is now a matter of practical experience in hundreds of nuclear installations around the world. A satisfactory evaluation of the macroscopic effects of the delayed neutrons following fission in a nuclear reactor requires, among other data, an accurate knowledge of the delayed neutron (DN) data. Those data that of great importance to the kinetics and safety operations of nuclear reactors (including the Accelerator Driven Systems) are the absolute yield of DN, relative abundances of DN, half-lives of their precursors, and energy spectra of DN. In spite of great efforts devoted to the investigation of delayed neutron physics, these fundamental delayed neutron characteristics of even the most common fissionable isotopes – ^{235}U, ^{238}U, ^{239}Pu - encountered in reactor systems are still poorly known and are now under investigation. For example, the experiments conducted at IPPE accelerators have shown that the relative abundances and half-lives of DN incorporated into ENDF/B-VI library and obtained on the basis of the summation techniques systematically deviate from appropriate experimental data [1]. Reactor experiments have shown that ENDF/B-VI group parameters for ^{235}U underestimate the reactivity by 2 to 47% in the range from +0.80 to –0.80\$ [2]. Especially large discrepancies are found for plutonium and americium isotopes. Such results point out on the need for careful checking and improvement of the summation method used as an alternative to the experimental approach for deriving the DN group parameters and DN energy spectra. In the case of fast neutron induced fission of ^{238}U the discrepancy in total DN data is more than 10%. This value was obtained from the comparison of two estimations made by Tuttle [3] in 1979 on the basis of direct measurements – 0.0439 (2.3%) neutrons/fission and by Blashoot et al. [4] in 1990 – (0.043-0.047) neutrons/fission with results of the last evaluation made by Fort at all [5] in 1999 on the basis of statistical analysis of the integral experiments results – 0.04855±0.00112 neutrons/fission. Moreover the ^{238}U data showed are in a significant disagreement with data obtained in "microscopic approach" and used as a basis for recommended data presentation in ENDF/B data library.

Thus the summation method based on the fission product yields and neutron emission probabilities from individual precursors cannot be considered at present time as a reliable tool for generation of the DN data base for MA. The experimental studies of the total delayed neutron yields from neutron induced fission of ^{237}Np made at IPPE show the prominent energy dependence of this value in the energy range of primary neutrons below the threshold of the (n, n'f) reaction [6]. This feature gives the definite indication that the constant value of the total DN yield accepted for the energy range from thermal to 4 MeV in the ENDF/B-VI data base for all elements must be carefully tested.

The purpose of the present work is to investigate the total delayed neutron yields from neutron induced fission of ^{238}U in the energy range 1,01 – 4,94 MeV.

Experimental method

The experimental method employed in the measurements is based on periodic irradiation of fissionable samples by neutrons from suitable nuclear reaction at the accelerator target and following measurements of the delayed neutron activity. The method for the measurements of absolute total delayed neutron yield includes two type of experiments. The first one consists of the measurements of periods and abundances for certain groups of delayed neu-

trons. The measurements with different irradiation and delayed neutron counting time intervals are foreseen to emphasize a certain delayed neutron groups. In the second type of experiment the irradiation time is long as compared with the longest delayed neutron group. The experimental set-up for the measurements of the total delayed neutron yields from neutron induced fission of ^{238}U is shown in Fig.1. The pneumatic transfer system is used for transportation of a sample from irradiation position to the neutron detector. The minimal sample delivery time was about 150 msec.
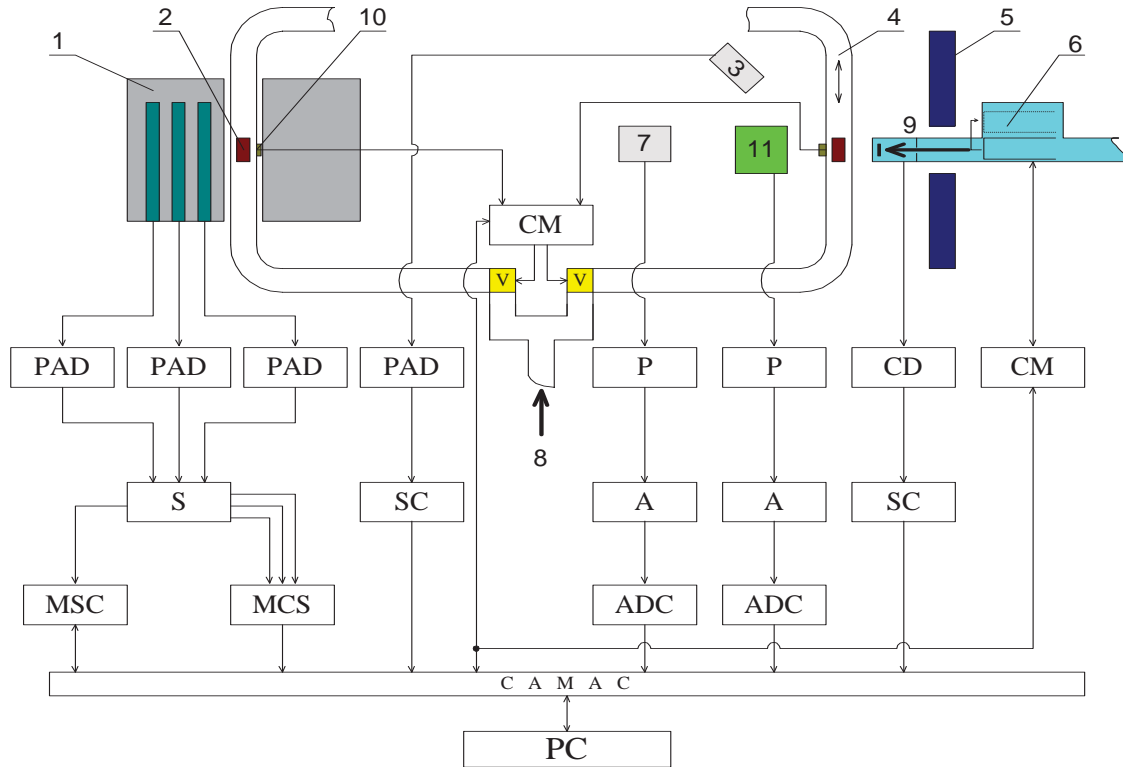

Fig. 1. Experimental set-up

D- discriminator, S- summation module, P- preamplifier, V- electromagnetic valve, CM- control module, CD- charge digitizer, ADC- analog digital converter, SC- scaler, A-amplifier, PC- personal computer, MSC – multiscaler, MCS- multichannel scaler, 1- neutron detector, 2- sample, 3- BF$_3$ neutron flux monitor, 4- pneumatic transfer system, 5- shielding, 6- Faraday cup, 7- ^{3}He spectrometer, 8- gas pressure, 9- ion beam, 10- sample position detector, 11- fission chamber.

Neutron detector is an assembly of 30 boron counters distributed in polyethylene moderator along three concentric circles with diameters of 106, 160 and 220 mm. The outer diameter of moderator is 400 mm, its length is 300 mm. In the center of the detector there is a through hole with diameter of 36 mm to install the sample flight tube. The detector is shielded against the neutron background by borated polyethylene, boron carbide powder and cadmium sheets. The delayed neutron detector used in the present experiment is shown in Fig. 2. Absolute measurements of the total delayed neutron yields from neutron induced fission reactions require the knowledge of the energy dependent absolute efficiency of the neutron detector used for delayed neutron registration. The absolute efficiency of the 4π neutron detector was determined by two different methods. The first one was the activation method based on the ^{51}V(p,n)^{51}Cr reaction.

The second method was based on the measurements of the average number of prompt neutrons from spontaneous fission of ^{252}Cf source coupled with a surface barrier detector. The Monte Carlo calculations were used to determine the energy dependence of the relative efficiency of neutron detector. The absolute energy dependent efficiency of the neutron detector is presented in Fig. 3.
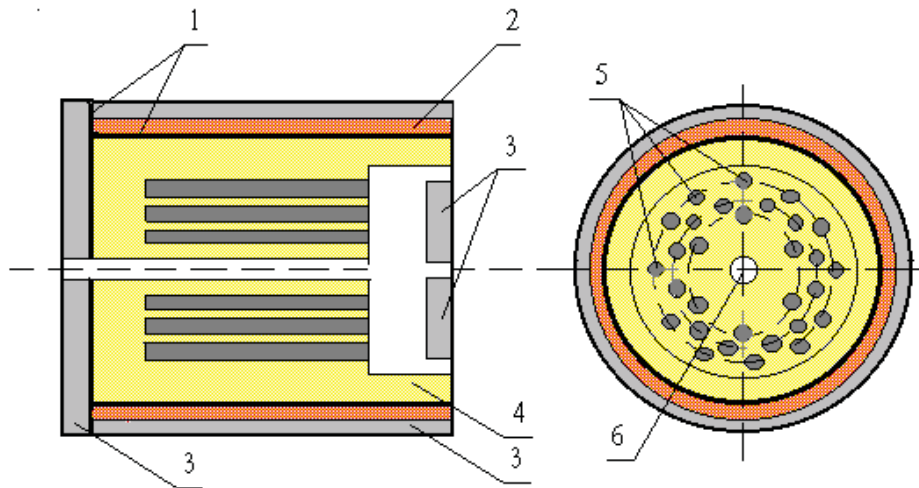
Fig. 2 Delayed neutron detector
1 - cadmium sheet, 2 - boron carbide powder, 3 - boron plastic,
4 - polyethylene, 5 - boron counters (SNM-11), 6 - sample transportation hole.
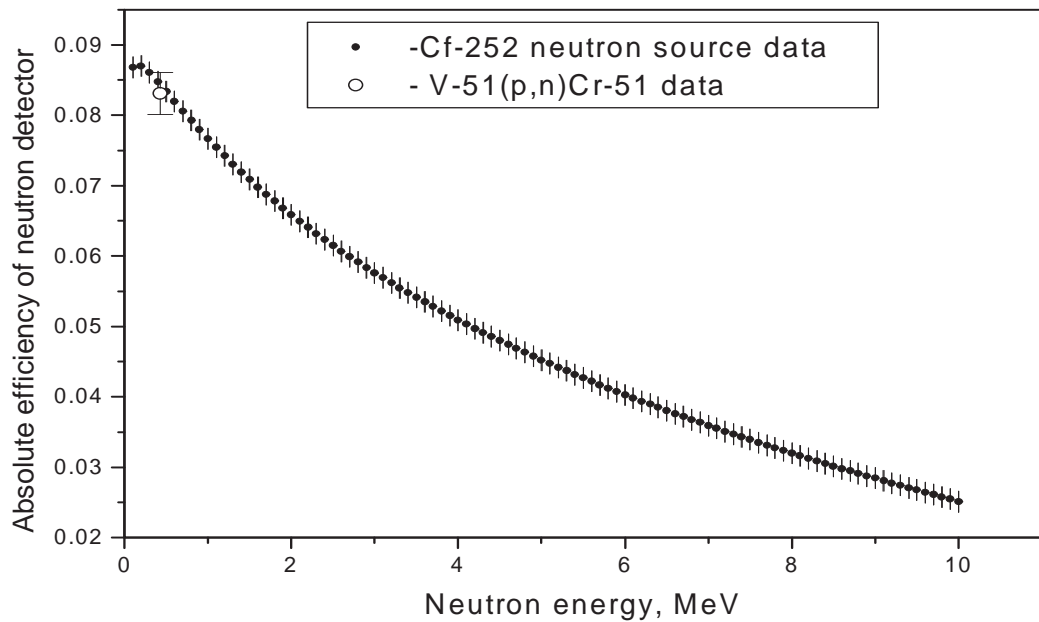
Fig. 3. Absolute efficiency of neutron detector

The fission rate in the fissile samples was determined on the basis of fission rates in parallel plate fission chamber with known number of ^{237}Np atoms and installed behind the sample: Fig. 4. The angle and energy dependence of the neutrons from T(p,n) neutron source as well as neutron multiplscattering effects in construction materials was taken into account.

Data acquisition and processing system makes it possible to measure the following parameters: pulse height distributions from two fission chambers, time dependencies of the neutron flux from the target and ion current on the target of accelerator, time dependence of delayed neutron activity from irradiated samples. The PC computer serves as a central processor controlling the irradiation and counting time, the number and width of the time channels for the delayed neutron activity measurements.
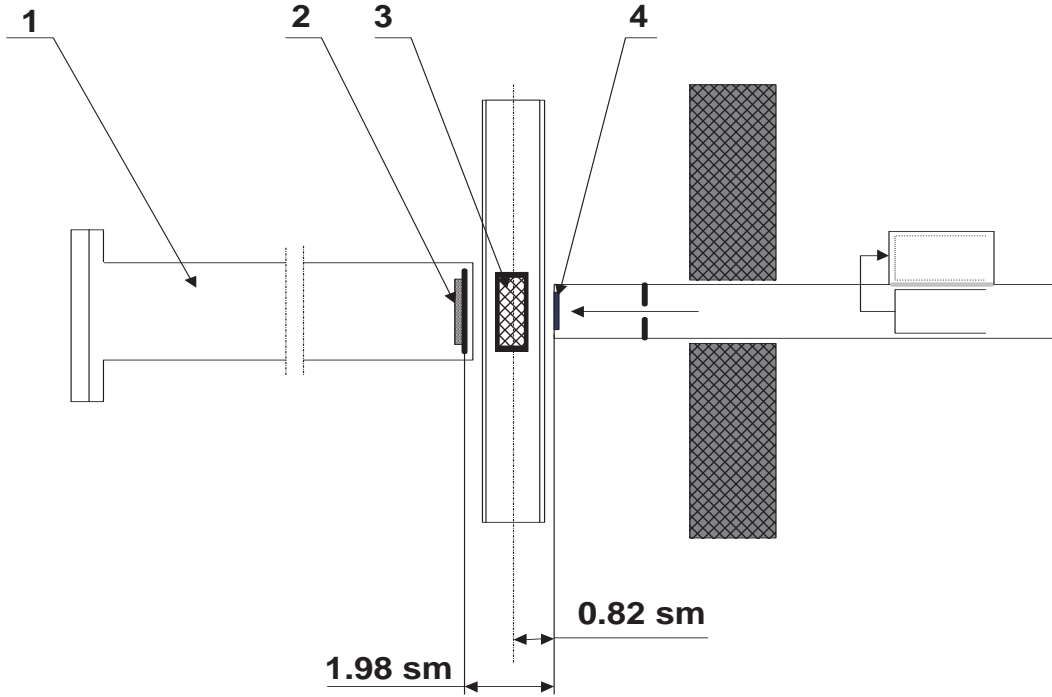
Fig. 4. Geometry configuration used in measurements of the total delayed neutron yields
1 - fission chamber; 2 – ^{237}Np fissile layer; 3 – ^{238}U sample; 4 – neutron target.

Data processing

Absolute delayed neutron yield ν_d was obtained on the basis of the following formula

$$N_d = \sum_{t1}^{t2} N(t) = \langle\varepsilon\rangle \cdot F_s \cdot \nu_d \cdot \sum_i T_i \cdot \frac{a_i}{\lambda_i} \cdot (e^{-\lambda_i t_1} - e^{-\lambda_i t_2}) + B(t_2 - t_1)$$

$$T_i = (1 - e^{-\lambda_i t_i})(\frac{N}{1 - e^{-\lambda_i T}} - e^{-\lambda_i T} \cdot \frac{1 - e^{-N\lambda_i T}}{(1 - e^{-\lambda_i T})^2})$$

where $N(t)$ - delayed neutron emission rate at time t after irradiation,

λ_i and α_i - decay constant and relative yield of the i-th group of delayed neutrons,

t_1 and t_2 - the time of the beginning and the end of delayed neutron counting,

N - number of cycles,

T - duration of one cycle, which includes the irradiation and delayed neutron counting time,

t_i - irradiation time,

F_s - fission rate in the sample under investigation,

$\langle\varepsilon\rangle$ - efficiency of neutron detector averaged over delayed neutron spectrum,

B - neutron background.

Delayed neutron energy spectrum for determining the average value of absolute efficiency of neutron detector was calculated on the basis of approach described in the separate paper [7]. The delayed neutron production rate from a number of repetitive cycles can be considered as the production rate from a single cycle in the infinitely long sequence. In such case the fission rate F_s is the total number of counts in the sample divided by the time of one irradiation cycle t_i. The fission rate in the sample F_s can be represented by the following expression:

$$F_s = \frac{N_s}{t_i} \iint \phi(E_n, \theta, \varphi) \cdot \sigma(E_n) dE_n dV_s,$$

where N_s - number of atoms in the ^{238}U sample,

dV_s - elemental volume of the ^{238}U sample,

$\phi(E_n, \theta, \varphi)$ - absolute neutron flux from the target.

The fission rate F_s was calculated by the Monte Carlo method on the basis of the approach described in [8]. In this approach the relative neutron flux ϕ_r related to absolute neutron flux according to expression $\phi = k \bullet \phi_r$ was used in calculation. The absolute value of the neutron flux was obtained on the basis of the number of counts in the fission chamber N_c registered during irradiation period of the each cycle and appropriate Monte Carlo calculations

$$N_c = N_f \iint k \cdot \phi_r(E_n,\theta,\varphi) \cdot \sigma(E_n) dE_n dV_f$$

where N_f - number of ^{237}Np atoms in the fission chamber deposit,

dV_f - elemental volume of the fission chamber deposit.

The final expression for the fission rate in the sample can be written in the following form

$$F_s = \frac{N_c \cdot N_s \iint \phi_r(E_n,\theta,\varphi)\sigma(E_n)dE_n dV_s}{N_f \cdot t_i \iint \phi_r(E_n,\theta,\varphi)\sigma(E_n)dE_n dV_f}$$

Results

Obtained results on the energy dependence of the total delayed neutron yields from fission of ^{238}U are shown on the Fig. 5 by solid circles. Solid line is drown through these points for easier comparison with appropriate data of other authors. The energy dependence of the total delayed neutron yields was measured before the present work only by Krick [9] (opened circles) and by Cox (open squares – [10] and solid squares – [11]). The second type data obtained by Cox [11] and data obtained by Krick [9] were used as a basis for recommended data presentation in ENDF/B data library. The first type data obtained by Cox [10] were not taken in consideration. Data by Maksyutenko are presented at two points (by crosses) [12]. All other data were obtained mainly in reactor experiments. The average energy of primary neutrons in these experiments was around 3 MeV. It is seen from Fig. 5 that the present results on the total delayed neutron yields show the strong energy dependence below neutron energy of 3 MeV.

It is worth to note that the presented experimental results below 4 MeV are in a good agreement with the appropriate results obtained on the basis of delayed neutron systematics developed in the IPPE [1,13,14]:

$$\nu_d(E_n) = a \cdot \left[\overline{T}(E_n)\right]^b,$$

where: $\overline{T}$ - average half-life of delayed neutron precursors;

a, b – being constant for definite Z of the fissioning system.

These data are shown on Fig. 6 by solid triangles connected by dash-dotted line. For comparison, in this figure the following data are shown: solid line – ENDF/B-VI data; dash line – JEF 2.2 data; dot line – data obtained on the basis of Lendel's model [15].

Thus the obtained results show that the energy dependence of the total delayed neutron yields for fission of ^{238}U below 3 MeV is not a constant as it is assumed in the ENDF/B-VI and JEF 2.2 data libraries. This result is of great importance for reactor practice. Therefore a further investigation of the effect should be studied including consideration of theory background.
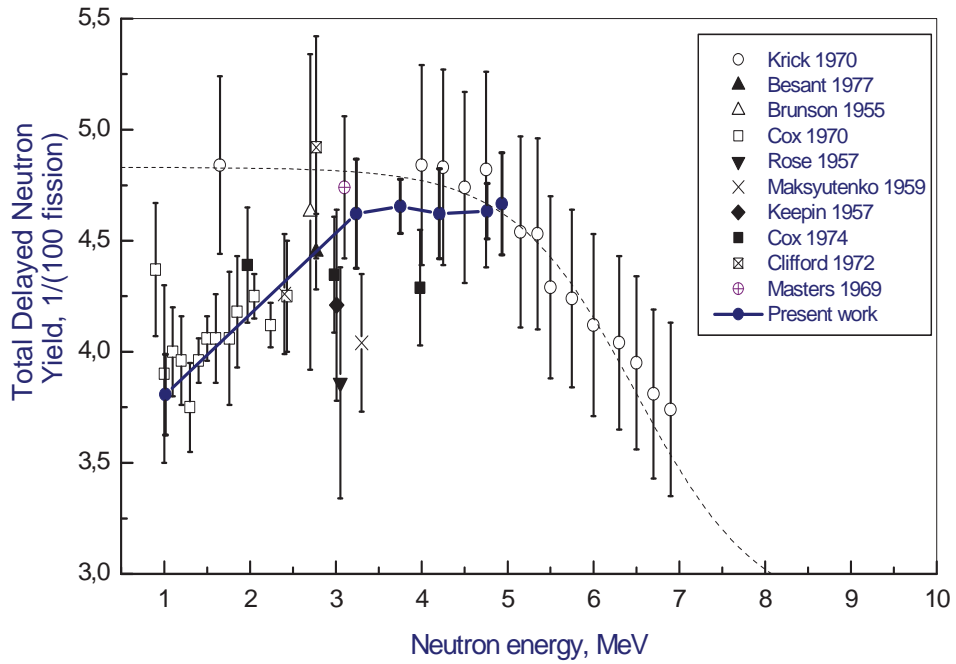
Fig. 5. Energy dependence of the total delayed neutron yields. Comparison with other available data
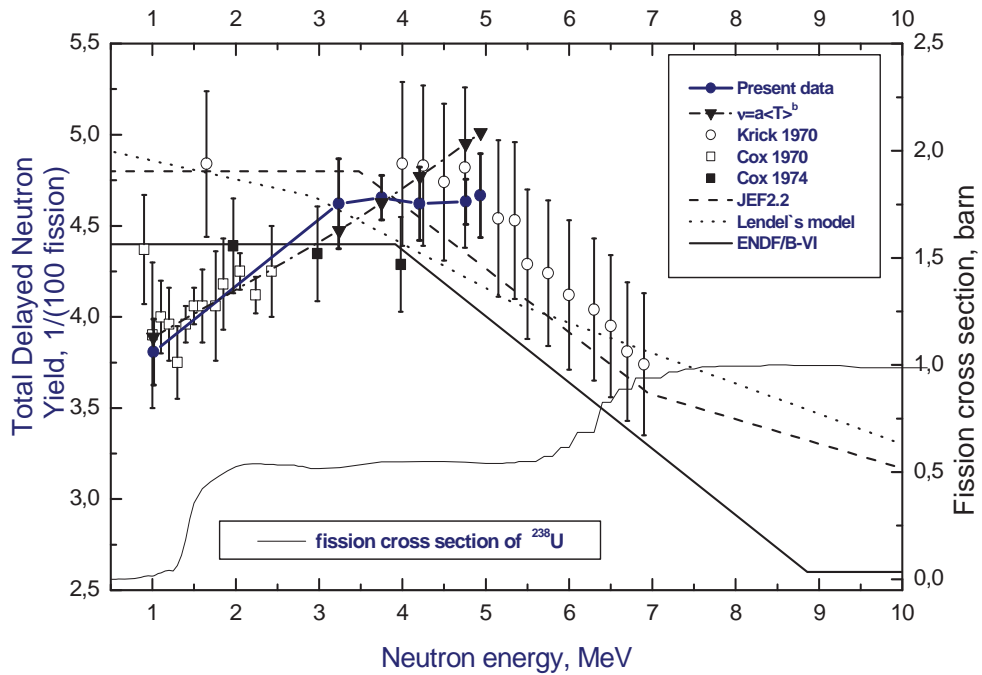

Fig. 6. Energy dependence of the total delayed neutron yield.
Comparison with data from nuclear data libraries.

References

1. Isaev S.G., Piksaikin V.M., Kazakov L.E., Goverdovski A.A. "Systematics of the delayed neutron characteristics and validation of the delayed neutron data base obtained in the microscopic approach." // Proceedings of the 8-th International Seminar on Interaction of Neutrons with Nuclei, JINR, Dubna, 2000, p.306.
2. Spriggs G.D.// Nucl.Sci.Eng., v.114, p.342., 1993.
3. Tuttle R.J. Report INDC(NDS) – 107/G // Proceedings of the Consultants' meeting on Delayed Neutron Properties, Vienna, IAEA, 1979, p.29
4. Blachot J., Brady M.C., Filip A., Mills R.W. and Weaver D.R. "Status of Delayed Neutron Data – 1990", Report NEACRP-L-323 NEANDC-299"U", Committee on Reactor Physics and Nuclear data Committee, Nuclear Energy Agency, Organization for Economic Cooperation and Development, 1990.
5. Fort E., Zammit-Averlant V., Salvatores M., Filip A., "Recommended values of the delayed neutron yield for U-235, U-238, and Pu-239"// Status report of the WPEC Subgroup 6 (SG6) activities (editor A. D'Angelo), OECD, NEA/NSC, 2000.
6. Piksaikin, V.M., Balakshev, Yu.F., Isaev, S.G. et al., Measurements of the energy dependence of the relative yields of delayed neutrons and the half-lives of their precursors during ^{237}Np fast neutron fission, Atomnaya ehnergiya, 1998, v. 85, No. 1, p. 51.
7. Piksaikin V.M., Isaev S.G., at al., "Absolute calibration of neutron detector with ^{252}Cf neutron source, Monte Carlo calculations and activation technique" // Proc. of Int. Conf. on Nuclear Data for Science and Technology, Triest (19-24 May, 1997), p.646.
8. Piksaikin V.M., Shorin V.S., Tertytchnyi R.G., "Fission rate determination in delayed neutron emission measurements with T(p,n) and D(d,n) neutrons" // Proc. of XIV-th Int. Workshop on Nuclear Fission Physics, 12-15 October, 1998, pp.265-275.
9. Krick M.S. and Evans A.E. // Nucl. Sci. Eng., v.47, p.311, 1972.
10. Cox, S.A., Whiting, D.E.E., Report ANL-7610, 1970, p.45, data included in Tuttle, R.J., Nuclear Science and Engineering, 1975, v. 56, p. 37.
11. Cox S.A., "Delayed neutron data – review and evaluation", ANL/NDM-5, Argonne National Laboratory, 1974, data taken from Tuttle, R.J., "Delayed neutron yields in nuclear fission" // Proc. of the Consultants' Meeting on Delayed neutron Properties, p.29, Vienna, 26-30 March 1979.
12. Maksyutenko, B.P., Atomnaya ehnergiya, 1959, v. 7, p. 474.
13. Piksaikin V.M., Isaev S.G. "Correlation properties of delayed neutrons from fast neutron induced fission" // Report INDC(CCP)-415, October 1998, IAEA, Vienna, Austrian, P.1
14. Isaev S.G., Piksaikin V.M., Kazakov L.E., Tarasko M.Z., "Energy dependence of average half-life of delayed neutron precursors in fast neutron induced fission of ^{235}U and ^{236}U" // Proc. of XIV-th Int. Workshop on Nuclear Fission Physics, 12-15 October, 1998, pp. 257-264.
15. Lendel, A.I., Marinets, T.I., Sikora, D.I., Charnovich, E.I., Determination of delayed neutron yields using polyempirical formulas, Atomnaya ehnergiya,1986, v. 61, No. 3.
16. Rose H., Smith R.D., - J. Nucl. Energy, v.1, p.133, 1957.
17. Brunson G.S., Petit E.N., and McCurdy, "Measurement of delayed neutron yields in plutonium, uranium-233, uranium-238, and thorium relative to yield in uranium-235", ANL – 5480, Argonne National Laboratory, 1955.
18. Besant S.B. at al. // J. Br. Nucl. Energy, v.16, p.161, 1977.
19. Keepin G.R. at al. // J. Nucl. Energy, v.6, p.1, 1957; also, Phys. Rev., v.107, p.1044, 1957.
20. Clifford, D.A., PhD thesis, Imperial College, London, 1972, data taken from Tuttle, R.J., Delayed neutron yields in nuclear fission, Proc. of the Consultants' Meeting on Delayed Neutron Properties, Vienna, 26-30 March 1979, p. 29.
21. Masters C.F. at al. // Nucl. Sci. Eng., v.36, p.202, 1969.

UDC 539.173.84

DELAYED NEUTRONS AS A PROBE OF NUCLEAR CHARGE DISTRIBUTION IN FISSION OF HEAVY NUCLEI BY NEUTRONS

S.G. Isaev, V.M. Piksaikin, L.E. Kazakov, V.A. Roshchenko

Institute of Physics and Power Engineering, Obninsk, Russia

A method of the determination of cumulative yields of delayed neutron precursors is developed. This method is based on the iterative least-square procedure applied to delayed neutron decay curves measured after irradiation of ^{235}U sample by thermal neutrons. Obtained cumulative yields in turns were used for deriving the values of the most probable charge in low-energy fission of the above-mentioned nucleus.

Introduction

Individual delayed neutron precursors were identified in numerous investigations. Improvements in the experimental techniques allow obtaining quite a large data base of such precursors characteristics as the delayed neutron emission probabilities and their half-lives. Although this data base are far from complete there are sufficient data available to expand delayed neutron measurement technique for obtaining more information on distribution of fission fragments in fission of heavy nuclei by neutrons. The primary purpose of the present work was to make measurements of the delayed neutron activities in thermal neutron induced fission of ^{235}U and to use this information for obtaining cumulative yields of bromine and iodine precursors. Obtained cumulative yields in turns were used for deriving the values of the most probable charge in low-energy fission of the above mentioned nuclei.

Experimental method

The experimental method employed in the measurements is based on periodic irradiation of the fissionable samples by neutrons generated in the T(p,n) reaction at the accelerator target and measurements of the composite decay of the gross neutron activity [1]. In the present experiment the irradiation time of 300.06 s and counting time 724.5 s were used. Sample delivery time of 150 ms was used in the measurements.

The decay curve analysis was executed within the framework of a 12 delayed neutron group model. Two sequences of decay constants were derived on the basis of known half-lives of delayed neutron precursors. The group periods were chosen so that to proper allocate the appropriate delayed neutrons precursors. In the framework of such approach the effective periods of composite groups were obtained by averaging procedure with the values of relative DN yield as a weight

$$T = \frac{\sum_{i=1}^{N}(T_{1/2} \cdot a)_i}{\sum_{i=1}^{N} a_i},$$ (1)

where $T_{1/2}$ – precursor half-life, a_i – relative abundance, corresponding to *i-th* delayed neutrons precursor, N – number of precursors including in group.

Thus the final results of the precursor half-lives were obtained for 4 individual precursors and 8 groups of combined precursors. These data were used in further processing of the experimental composite DN decay curves. In the present work 17 delayed neutron precursors were considered. The considered precursors are responsible for about 70% of the total DN yield from the neutron induced fission of ^{235}U. The 12 delayed neutron group models are presented in the Table 1.

The analysis of delayed neutron decay curves was carried out by iterative least square procedure. Data processing procedure included six steps. On the first step of analysis the appriore relative abundances data for all 12 groups were obtained. On the other five steps the relative abundances were obtained using the data from first step. In this case the relative abundances obtained in the previous step were fixed in the current step. Such procedure was chosen with the purpose to enhance the resolution of the used method. The data processing procedure is presented in Table 2.

Table 1

12 group models

12 (iodine) model		Precursor	Half-life, s	12 (bromine) model	
Group number	Group period, s			Group number	Group period, s
1	55.69	^{87}Br	55.69	1	55.69
2	24.50	^{137}I	24.50	2	24.50
3	16.30	^{88}Br	16.30	3	16.30
4	6.46	^{138}I	6.46	4	6.37
5	4.67	^{93}Rb	5.93		
		^{89}Br	4.38	5	4.38
6	2.76	^{94}Rb	2.76	6	2.76
7	2.30	^{139}I	2.30	7	2.09
8	2.056	^{85}As	2.08		
		^{98m}Y	2.00		
9	1.119	^{93}Kr	1.289	8	1.289
		^{144}Cs	1.002	9	0.942
10	0.860	^{140}I	0.860		
11	0.443	^{91}Br	0.542	10	0.542
		^{95}Rb	0.384	11	0.384
12	0.195	^{96}Rb	0.203	12	0.195
		^{97}Rb	0.170		

Table 2

Data processing procedure

№ Step / analysis start (c.)						Group	Bromine model		Iodine model	
1	2	3	4	5	6		Precursor	Period	Precursor	Period
Tf	8.5	6.0	1.5	0.75	Tf					
		fixed	fixed	fixed	fixed	1	^{87}Br	55.69	^{87}Br	55.69
		fixed	fixed	fixed	fixed	2	^{137}I	24.50	^{137}I	24.50
			fixed	fixed	fixed	3	^{88}Br	16.30	^{88}Br	16.30
				fixed	fixed	4	^{138}I, ^{93}Rb	6.37	^{138}I	6.46
				fixed	fixed	5	^{89}Br	4.38	^{93}Rb, ^{89}Br	4.67
					fixed	6	^{94}Rb	2.76	^{94}Rb	2.76
					fixed	7	^{139}I, ^{85}As, ^{98m}Y	2.09	^{139}I	2.30
						8	^{93}Kr	1.289	^{85}As, ^{98m}Y	2.056
						9	^{144}Cs, ^{140}I	0.942	^{93}Kr, ^{144}Cs	1.119
						10	^{91}Br	0.542	^{140}I	0.860
						11	^{95}Rb	0.384	^{91}Br, ^{95}Rb	0.443
						12	^{96}Rb, ^{97}Rb	0.195	^{96}Rb, ^{97}Rb	0.195

(First column, vertical label: *Apriori relative abundances data obtained*)

So the relative abundances of delayed neutrons, related to ^{87}Br, ^{88}Br, ^{89}Br, ^{91}Br, ^{137}I, ^{138}I, ^{139}I and ^{140}I, from thermal neutron induced fission of ^{233}U, ^{235}U and ^{239}Pu were obtained. The cumulative yields values can be given by

$$CY = \frac{Y}{Pn} \cdot \nu_d,$$

(2)

where Y – relative abundance of delayed neutrons, Pn – delayed neutron emission probability, ν_d - total delayed neutrons yield.

The total DN yields values from thermal neutron induced fission of ^{235}U is 1.642±0.018 [2].

The values of the delayed neutron emission probability are presented in the Table 3 [3].

The bromine and iodine cumulative yields from thermal neutron induced fission of ^{235}U are presented in the Table 4. and on the Fig. 1.

Table 3.

**Probability of delayed neutron emission
from bromine and iodine**

Precursor	Emission probability [2]
^{87}Br	2.52 ± 0.07
^{88}Br	6.58 ± 0.18
^{89}Br	13.8 ± 0.4
^{91}Br	20.0 ± 3.0
^{137}I	7.14±0.23
^{138}I	5.46±0.18
^{139}I	10.0±0.3
^{140}I	9.3±0.1

Table 4

The bromine and iodine cumulative yields from thermal neutron induced fission of ^{235}U

Precursor	Cumulative yield				
	Present	[7]	[8]	[9]	[2]
^{87}Br	2.180±0.076	2.0180	2.11±0.32	2.19±0.12	2.03±0.26 IS 2.08±0.10 MS
^{88}Br	2.504±0.088	2.0344	2.19±0.35	1.32±0.07	1.53±0.11 MS
^{89}Br	1.284±0.066	1.3190	1.11±0.17	0.90±0.08	0.88±0.15 IS 1.137±0.08 MS
^{91}Br	0.310±0.049	0.2458	----------	0.34±0.09	0.34±0.09 IS
^{137}I	3.352±0.130	3.2222	3.10±0.47	2.45±0.21	2.78±0.36 IS 3.48±0.10 MS 3.30±0.50 RC
^{138}I	1.619±0.090	1.5927	1.24±0.28	0.69±0.16	1.52±0.11 MS
^{139}I	1.235±0.071	0.9814	0.89±0.19	0.67±0.13	0.67±0.13 IS 0.54±0.20 MS
^{140}I	0.253±0.013	0.2178	----------	0.15±0.03	0.145±0.032 IS

Type of measurement: IS – Isotope-Separator-on-Line System
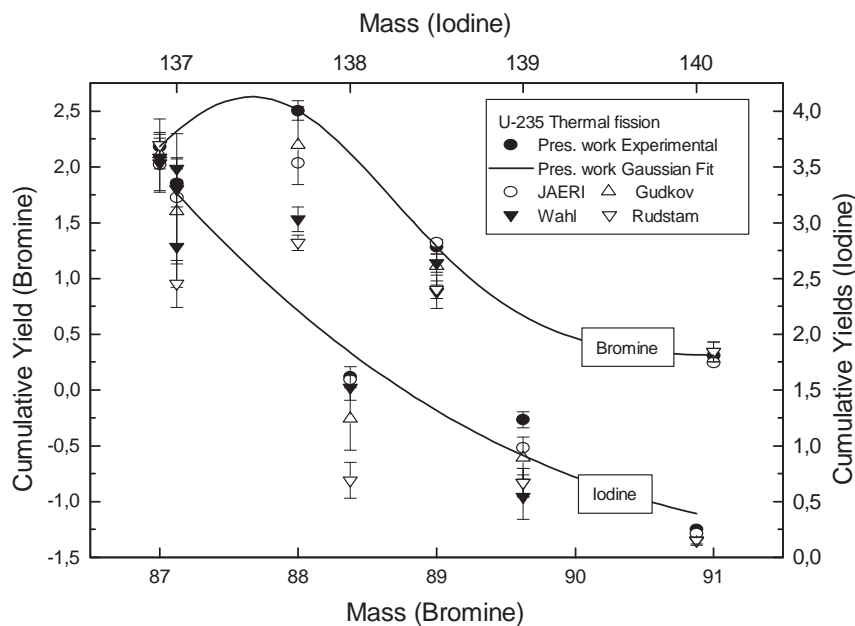MS – Mass spectrometer
RC – Radiochemistry

Fig. 1. Cumulative yields from thermal neutron induced fission of ^{235}U

The most probable charge of fission products *Zp* estimation

Charge distribution is usually discussed in terms of charge dispersion among the fission products with definite mass number and variation with mass number of the most probable charge *Zp* for a given mass number. The fractional independent yield is represented by Gaussian curve [4]

$$IY = \frac{1}{\sqrt{2 \cdot \pi \cdot \sigma^2}} \cdot \exp\left[-\frac{1}{2 \cdot \sigma^2} \cdot (Z - Zp)^2 \right] \tag{3}$$

As it was shown by Wahl et al. [5] the charge dispersion in low energy fission of actinides is approximately independent of the isobaric mass chain. On the basis of comprehensive analysis of the experimental data [2] it was found that the average value of σ in the region outside of $Zp=50$ for thermal fission of ^{235}U is 0.531. Cumulative form of the above Gaussian distribution gives the cumulative yield of the fission product with charge Z

$$Ym \cdot \sum_{0}^{Z} (IY)_n = \frac{Ym}{\sigma \cdot \sqrt{2 \cdot \pi}} \cdot \int_{-\infty}^{(Z+1/2)} \exp\left[\frac{-(n - Zp)^2}{2 \cdot \sigma^2} \right] dn = \frac{1}{2} + \frac{1}{2} \cdot f\left[(Z - Zp + \frac{1}{2}) \Big/ \sigma \right], \tag{4}$$

$$f[X] = \frac{1}{\sqrt{2 \cdot \pi}} \cdot \int_{-X}^{X} \exp\left[\frac{-\alpha^2}{2} \right] d\alpha .$$

In the present work the equation (4) was used for obtaining the most probable charge *Zp* for given isobaric chains on the basis of cumulative yields derived from delayed neutron decay curves and average values of charge dispersion σ from Wahl's evaluation [2].

The obtained data on the most probable charge *Zp* for isobaric chains with *A*=81-91 and *A*=137-140 are shown on Fig. 2 for thermal neutron induced fission ^{235}U (the data are plotted versus mass number of the product after neutron evaporation). In addition to the above isobaric chains the appropriate data for complementary fission products were calculated on the basis of the conservation of the charge

$$Z_c = Z_{pL} + Z_{pH} , \tag{5}$$

where Z_c – a charge of compound nucleus, Z_{pL} – a charge of the light fission product, Z_{pH} – a charge of the heavy fission product.

The mass number of complementary fission product was obtained on the basis of equation

$$A_c = A_L + A_H + \nu_p , \tag{6}$$

where A_c – mass number of compound nucleus, A_L and A_H - mass numbers of light and heavy fission product respectively, ν_p - the average number of prompt neutrons emitted (both fragments) in the fission.
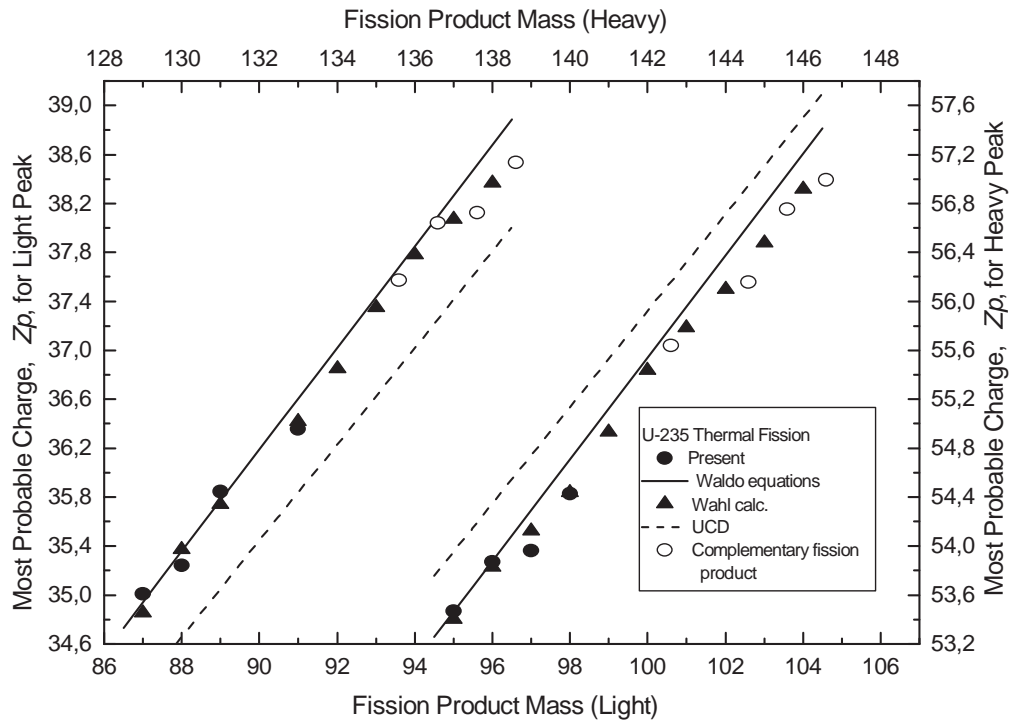

Fig. 2. The most probable charge of fission fragments Z_p from thermal neutron induced fission of ^{235}U

In the present the average number of prompt neutrons emitted (both fragments) in the thermal fission of ^{235}U was equal 2.4 [2].

Comparison of the obtained results was made with empirical Z_p values calculated by Wahl [2] in frame of Z_p-model. In the paper by Waldo et al.[6] the most probable charge of fission products Z_p from thermal neutron induced fission of ^{235}U was parameterized by the following equation

$$Z_p(A) = 0.4153 \cdot A - 1.19, \qquad A < 116 \qquad (7)$$

and

$$Z_p(A) = 0.4153 \cdot A - 3.43, \qquad A > 116 \qquad (8)$$

The dash lines in Figure is the Zp function for unchanged charge distribution (UCD), calculated on the assumption that each fission fragment, on the average, evaporates half the average number ν_p of neutrons emitted in fission. The second postulate, UCD, proposes that the compound nucleus fissions rapidly in such way that the fragments both have the same neutron-to-proton ratio as the compound nucleus. In this case the Zp values are calculated using the following equation

$$Z_p(A) = \frac{Z_c}{A_c - \nu_p} \cdot A, \qquad (9)$$

where ν_p – the average number of prompt neutrons emitted (both fragments) in the fission.

The most probable charge of fission products from thermal neutron induced fission of ^{235}U are presented in the Table 5.

For a more careful analysis of the Z_p data it is useful to present data as a deviation from the Z_p(UCD) as a function of complementary light and heavy primary fragments A', before neutron evaporation

$$A'_L = A_L + \nu_{pL}$$
$$A'_H = A_H + \nu_{pH} \qquad (10)$$
$$\Delta Z(A') = Z_p - A' \cdot \frac{Z_c}{A_c}$$

On the Fig. 3 the difference between the most probable charge Z_p and unchanged charge distribution values is presented.

Table 5.

The most probable charge of fission products from thermal neutron induced fission of ^{235}U

| Mass | Most probable charge Z_p | | | | |
	Present work	[2] calculations	[2] experimental	[6]	[UCD]**)
87	35.010±0.059	34.852	34.920	34.941	34.263
88	35.244±0.036	35.370	35.398	35.356	34.657
89	35.846±0.022	35.740	35.798	35.771	35.051
91	36.358±0.041	36.416	36.437	36.602	35.839
93.6*)	37.573	----------	----------	37.682	36.863
94.6*)	38.040	----------	----------	38.097	37.257
95.6*)	38.128	----------	----------	38.513	37.651
96.6*)	38.534	----------	----------	38.928	38.045
137	53.466±0.027	53.399	53.434	53.466	53.955
138	53.872±0.023	53.824	53.835	53.881	54.349
139	53.960±0.022	54.121	54.125	54.296	54.743
140	54.427±0.013	54.433	54.381	54.919	55.136
142.6*)	55.642	----------	----------	55.792	56.161
144.6*)	56.154	----------	----------	56.622	56.949
145.6*)	56.756	----------	----------	57.038	57.342
146.6*)	56.990	----------	----------	57.453	57.736

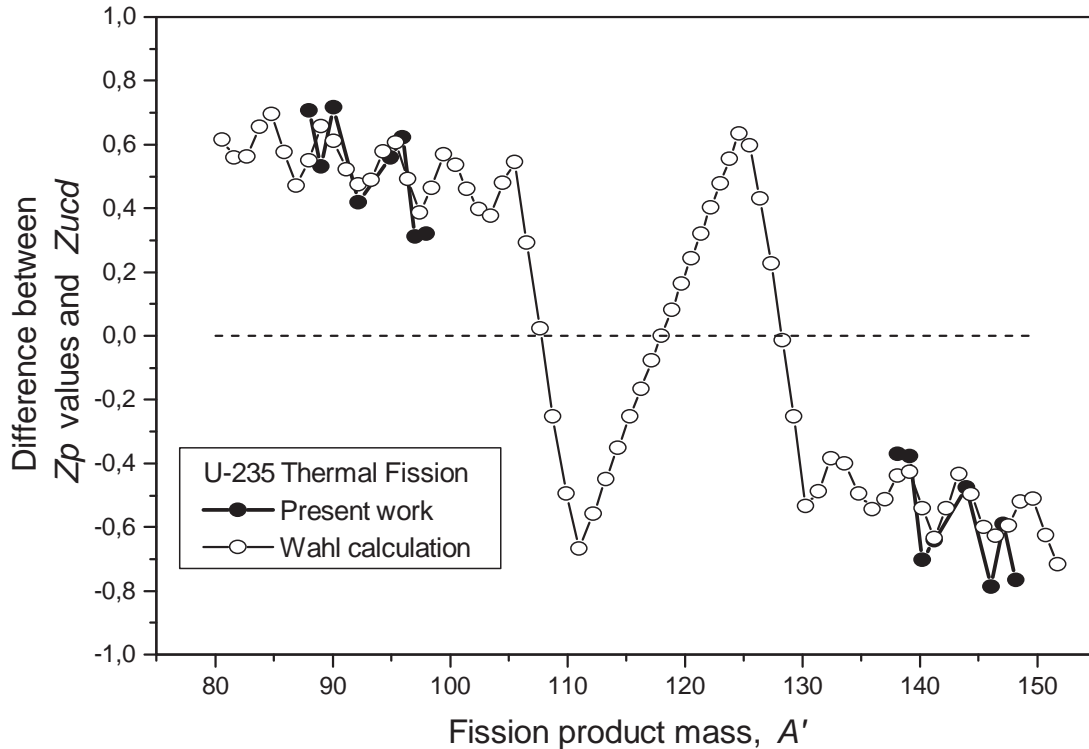*) – complementary fission products,
**) – after prompt neutron emission.

Fig. 3. Difference between the most probable charge Zp value and value of unchanged charge division from thermal neutron induced fission of ^{235}U

Conclusion

A method of the determination of cumulative yields of delayed neutron precursors is developed. This method is based on the iterative least-square procedure applied to delayed neutron decay curves measured after irradiation of ^{235}U sample by thermal neutrons. As compared with the analogous method developed by Gudkov et al. [8] in the present work the different model of precursors and method of decay curves analysis [1] were applied.

The cumulative yields of bromine and iodine precursors obtained in the most studied thermal neutron induced fission of ^{235}U in general are in a good agreement with corresponding data obtained by other authors.

On the basis of the cumulative yields the most probable charge of isobaric chains with mass numbers (87-89, 91), (137-140) and their complements was calculated. These data show good agreement with appropriate data by Wahl [2] obtained in frame of Zp-model.

Fission product yield measurements usually are made using expensive mass separator facilities, complicated time of flight methods and by fast radiochemistry. As a rule the energy range of primary neutrons is quite restricted. Obtained in the present work results open the possibilities to expand present investigations to the systematic studies of cumulative yields and the most probable charges (at least for bromine and iodine precursors) in fission of nuclei with different excitation energies using the electrostatic accelerators.

References

1. S.G. Isaev, V.M. Piksaikin, L.E. Kazakov, M.Z. Tarasko. Energy dependence of average half-life of delayed neutron precursors in fast neutron induced fission of ^{235}U and ^{236}U// Proc. of the XIV International Workshop on Nuclear Fission Physics, Obninsk, October 12-15, 1998, p.257-264.
2. A.C. Wahl, Atomic Data and Nuclear Data Tables, 12, 1988, p.1-156
3. G. Rudstam, K. Aleklett, L. Sihver. Delayed-neutron branching ratios of precursors in the fission product region // Atomic Data and Nuclear Data Tables, Vol.53, No.1, January1993, p.1-22.
4. H. Farrar, R.H. Tomlinson // Nucl. Phys. 34, 1962, p.367.
5. A.C. Wahl, R.L. Ferguson et al. // Phys. Rev., Vol.126, No.3, p.1112.
6. R.W. Waldo, R.A. Karam, R.A. Meyer. Delayed neutron yields: Time dependent measurements and a predictive model // Phys. Rev. C, Vol.23, No.3, March 1981, p.1113-1127.
7. (Ed.) Hitoshi Ihara, Tables And Figures from JNDC Nuclear Data Library of Fission Products, Version 2, JAERI-M 89-204.

8. A.N. Gudkov, S.V. Krivasheyev, A.B. Koldobski, V.V. Kovalenko, E.Yu. Bodkov, V.M. Givun, "Yields of Delayed Neutron Precursors in the Fission of Actinides", Radiochimica Acta, 57, 1992, p.69-75.

9. G. Rudstam, P. Aagaard, B. Ekstrom, E. Lund, H. Gokturk, H.U. Zwicky. Yields of Products from Thermal Neutron-Induced Fission of ^{235}U // Radiochimica Acta, 49, 1990, p.155-191.

UDC 539.173.84

THE ENERGY SPECTRUM OF DELAYED NEUTRONS FROM THERMAL NEUTRON INDUCED FISSION OF ^{235}U AND ITS ANALYTICAL APPROXIMATION

A.Yu. Doroshenko, V.M. Piksaikin, M.Z. Tarasko

State Scientific Center of the Russian Federation Institute for Physics and Power Engineering, Obninsk, Russia
piksa@ippe.rssi.ru

The energy spectrum of the delayed neutrons is the poorest known of all input data required in the calculation of the effective delayed neutron fractions. In addition to delayed neutron spectra based on the aggregate spectrum measurements there are two different approaches for deriving the delayed neutron energy spectra. Both of them are based on the data related to the delayed neutron spectra from individual precursors of delayed neutrons. In present work these two different data sets were compared with the help of an approximation by gamma-function. The choice of this approximation function instead of the Maxwellian or evaporation type of distribution is substantiated.

Introduction

The energy spectrum of delayed neutrons from fission of heavy nuclei is the poorest known of all input data in reactor calculations (i.e. in the calculation of effective delayed neutron fractions). At present there are two sources of information on the delayed neutron spectrum – experimental data on the aggregate delayed neutron spectrum and experimental data on delayed neutron spectra from individual precursors. In frame of so-called "microscopic approach" pure experimental data on the delayed neutron spectra from individual precursors are used for calculating the group and composite spectra by summing the contributions from individual precursors [1]. There is another approach in deriving the group and composite energy spectra of delayed neutrons in frame of microscopic approach. It was concluded by the authors [2] that some of the delayed neutron spectra are not adequate in the measured energy range and therefore these data should be supplemented by nuclear model calculations. Namely this approach was put at the basis of the ENDF/B-VI delayed neutron data base.

In the present work these two representative spectra ([1] and [2]) were analyzed with the help of the analytical approximation taken in the form of the gamma-function. Advantage of this approximation is that the gamma-function depending on the values of its parameters can approximate both the Maxwell and evaporation type of energy distribution.

Rudstam's method

This method is based on the available experimental data of spectra for individual delayed neutron precursors used by Rudstam [1] in his evaluation of delayed neutron spectra for the thermal neutron induced fission of ^{235}U. There were 67 precursors with known half-lives and delayed neutron branching ratios (Pn values) among the fission products. For about half of them with few exceptions including all the important cases there were also known the shape of the delayed neutron energy spectrum.

With the additional information on fission yields the time distribution of the delayed neutrons including the time variation of the resulting energy spectrum can be evaluated for any nuclear fuel and irradiation history. Since all precursors are short-lived saturation is rapidly attained. This means that the time distribution of the composite decay curve of the delayed neutrons will be given by the expression

$$D(t) = \sum a_i \exp(-\lambda_i t) , \tag{1}$$

where the sum is to be taken over all precursors of decay constants λ_i. The values of a_i equal to

$$a_i = nN\sigma_k Y_{ki} P_{ni} , \tag{2}$$

where n - neutron flux, N - number of fissile nuclei, σ_k - fission cross section, Y_{ki} - cumulative fission yield.

This expression refers to a given fissile nuclide. Also the resulting delayed neutron energy spectrum $\Psi(E,t)dE$ and its time dependence can be written as

$$\Psi(E,t)dE = \sum_i a_i \exp(-\lambda_i t)\varphi_i(E)dE. \tag{3}$$

The energy spectra of the individual precursors normalized to unity are here given by $\varphi_i(E)$. The half-life limits are chosen to be 55.6 s, 10 to 30 s, 4 to 10 s, 1.4 to 4 s, 0.4 to 1.4 s, and <0.4 s for groups 1 through 6, respectively. There were a certain number of precursors with the half-lives such that they can be just as well placed in any of two adjacent groups.

Brady's method

This method [2] is quite similar to the Rudstam's approach. But in this case the experimental data were supplemented with model spectra and model values were added for probable unmeasured precursors.

Based on energetics 271 fission products should be delayed neutron precursors. The primary advantage of this approach is that a single set of precursor data (delayed neutron emission probabilities and energy spectra) can be used to predict delayed neutron production for any fissioning system, provided fission product yields are available. The fission product yields are as important as the emission probabilities Pn and lead to the largest uncertainty in calculations. The total equilibrium delayed neutron emission rate per fission ν_d for example is simply a sum of YC_iPn over all precursors, where YC_i is the cumulative fission yield along a mass chain for precursor i [2].

Spectra for 34 precursors have been measured. According to the authors' opinion [2] thirty of these were found to be inadequate in the measured energy range and had to be supplemented by nuclear models. Two models were used. The BETA code was used to extend 30 measured spectra. For the remaining 237 precursors they used a modified evaporation model. The largest effort in the evaluation was directed at model estimates of unmeasured spectra and the expansion of the incomplete measured spectra [2].

It is assumed that a delayed neutron precursor contributes to either or both of the adjacent temporal groups as determined by the decay constants as in

$$\lambda_i < \lambda_k < \lambda_{i+1} \tag{4}$$

Therefore, the decay rates may be represented by the following approximation:

$$\lambda_k \exp(-\lambda_k t) \cong f_{k,i}\lambda_i \exp(-\lambda_i t) + f_{k,i+1}\lambda_{i+1} \exp(-\lambda_{i+1}t), \tag{5}$$

Recalling that the index k represents the precursor nuclide, and i and $i+1$ the adjacent temporal groups defined by Eq. (4).

It is also required that

$$f_{k,i} + f_{k,i+1} = 1 \tag{6}$$

These fractions $f_{k,i}$ were determined by requiring the least-squares error,

$$\int_0^\infty \{\lambda_k \exp(-\lambda_k t) - [f_{k,i}\lambda_i \exp(-\lambda_i t) + (1 - f_{k,i})\lambda_{i+1} \exp(-\lambda_{i+1}t)]\} \tag{7}$$

to be minimal.

The equilibrium group spectra were then found as

$$\Phi_i(E) = \sum_k f_{k,i}Y_k Pn_k \phi_k(E), \tag{8}$$

where $\phi_k(E)$ is the normalized delayed neutron spectrum of precursor k, and for the equilibrium case Y_k represents the cumulative yield from fission for precursor k.

Approximation

The main purpose of this work is to compare the above types of delayed neutron spectra with the help of an analytical function approximation. The developed method on one hand gives convenient analytical expression for representation of the delayed neutron spectrum; on the other hand it gives the opportunity to make some conclusion on the overall shape of the delayed neutron spectrum. Additional advantage of the proposed approach is possibility to obtain the data near the limits of the delayed neutron spectrum (100 keV > E_n > 1.5 MeV) where experimental data are scarce or not available.

The analytical expression was taken in the form of the gamma-distribution

$$f(E) = \frac{\beta}{\Gamma(\alpha)}(\beta \cdot E)^{\alpha-1} \exp(-\beta \cdot E), \tag{9}$$

where α and β - parameters of the distribution

$$\Gamma(\alpha) = \int_0^\infty x^{\alpha-1} e^{-x} dx \text{ - gamma function.} \tag{10}$$

The average energy and dispersion of the gamma-distribution can be represented by α and β parameters

$$<E> = \frac{\alpha}{\beta}, \ D = \frac{\alpha}{\beta}. \tag{11}$$

If one defines the temperature parameter T as $1/\beta$ then $\alpha = <E>/T$ and the gamma distribution (9) can be rewritten in the form

$$f(E) = \frac{C_0}{T \cdot \Gamma(\alpha)} (\frac{E}{T})^{\alpha-1} \exp(-\frac{E}{T}), \tag{12}$$

where C_0 – normalization factor. It is easy to check that distribution $f(E)$ transforms into the Maxwell distribution in case of $\alpha=3/2$ and the evaporation distribution in case of $\alpha=2$.

The developed approach was used for approximation of the group spectra and aggregate spectrum of delayed neutrons for fission of [235]U taken from [1] and ENDF/B-VI data base based on the approach described in [2]. The group parameters (relative abundances of DN) for the determination of the aggregate spectrum of [235]U where used as a weight function

$$\Phi(E_n)dE_n = \sum a_i \varphi_i(E_n) dE_n, \tag{13}$$

where $\Phi(E_n)$ – the composite delayed neutron spectrum, $\varphi_i(E_n)$ – delayed neutron spectrum of i-th delayed neutron group of [235]U (thermal fission) and a_i – relative abundance of i-th group of delayed neutrons were taken from [1] and [2].

Results

The results on separate groups and aggregate spectra for the thermal neutron induced fission of [235]U are presented in Figs. 1-7. In Table 1 the results on the average neutron energy of separate groups and aggregate spectra are given.

The comparison of the aggregate spectra from fission of [235]U corresponding to delayed neutron group spectra and relative abundances from Rudstam's data [1] and the ENDF/B-VI data along with the appropriate calculated delayed neutron energy spectra based on the analytical approximation by gamma-function are shown in Fig. 1. The average energy of aggregate delayed neutron energy spectrum calculated on the basis of analytical approximation of Rudstam's data [1] and ENDF/B-VI data are 420.6 and 504.4 keV respectively.

The comparison of the Rudstam's data and the ENDF/B-VI data for each of the 6 delayed neutron groups are made in Fig. 2 through Fig. 7 along with the appropriate calculated delayed neutron energy spectra based on the analytical approximation by gamma-function. It is seen also from Fig. 2 (this is delayed neutron spectrum of the first group which is mainly consist of [87]Br precursor neutrons) that there is a large difference between ENDF/B-VI data based on both the experimental data and model calculations and the appropriate data from [1] based on the experimental spectra from individual precursors only. The ENDF/B-VI data shows more high energy delayed neutrons.

Table 1.

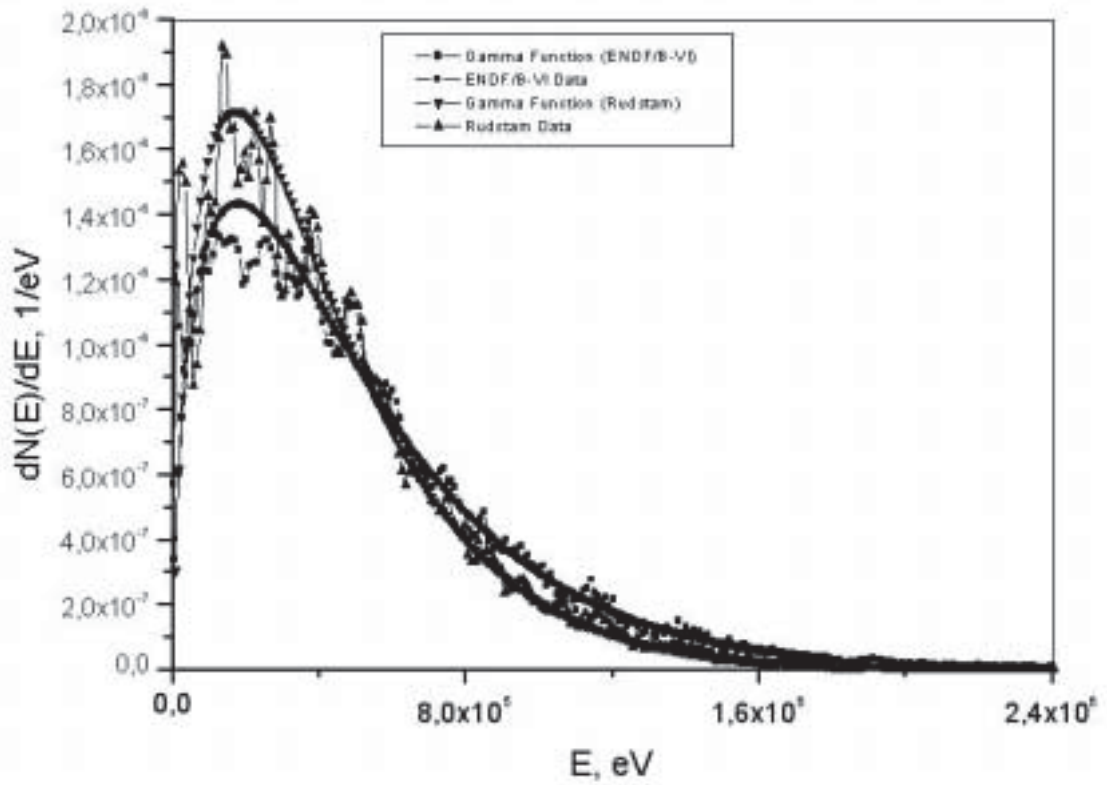| Group number	Brady's data		Rudstam's data	
	α	$<E>$	α	$<E>$
1	1.54	400.3	1.63	200.8
2	1.99	466.5	2.01	422.4
3	1.86	437.6	2.26	406.4
4	1.64	552.4	1.65	470.0
5	1.3	513.2	1.33	339.2
6	1.16	535.2	1.52	403.0
Aggregate	1.55	504.4	1.68	420.6

Gamma-function approximation parameters

Fig. 1. Aggregate delayed neutron spectra and their approximation

Fig. 2. The 1st group delayed neutron spectra and their approximation

Fig. 3. The 2nd group delayed neutron spectra and their approximation

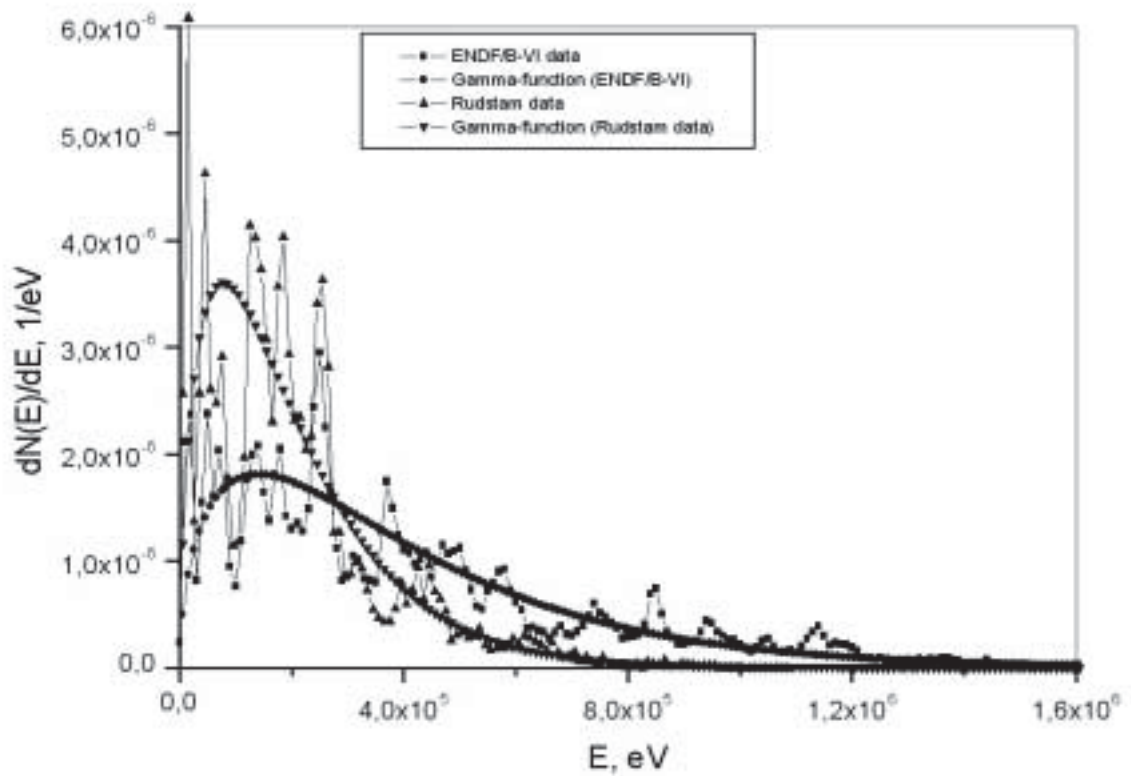Fig. 4. The 3^{d} group delayed neutron spectra and their approximation
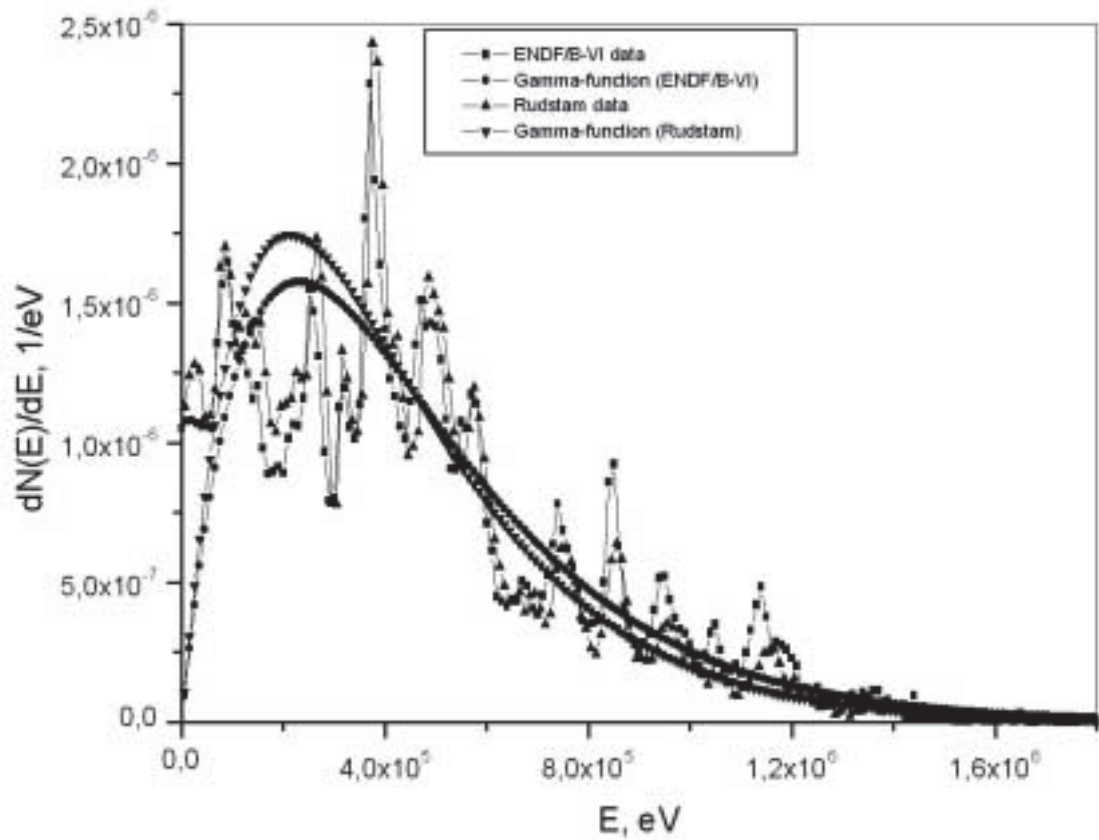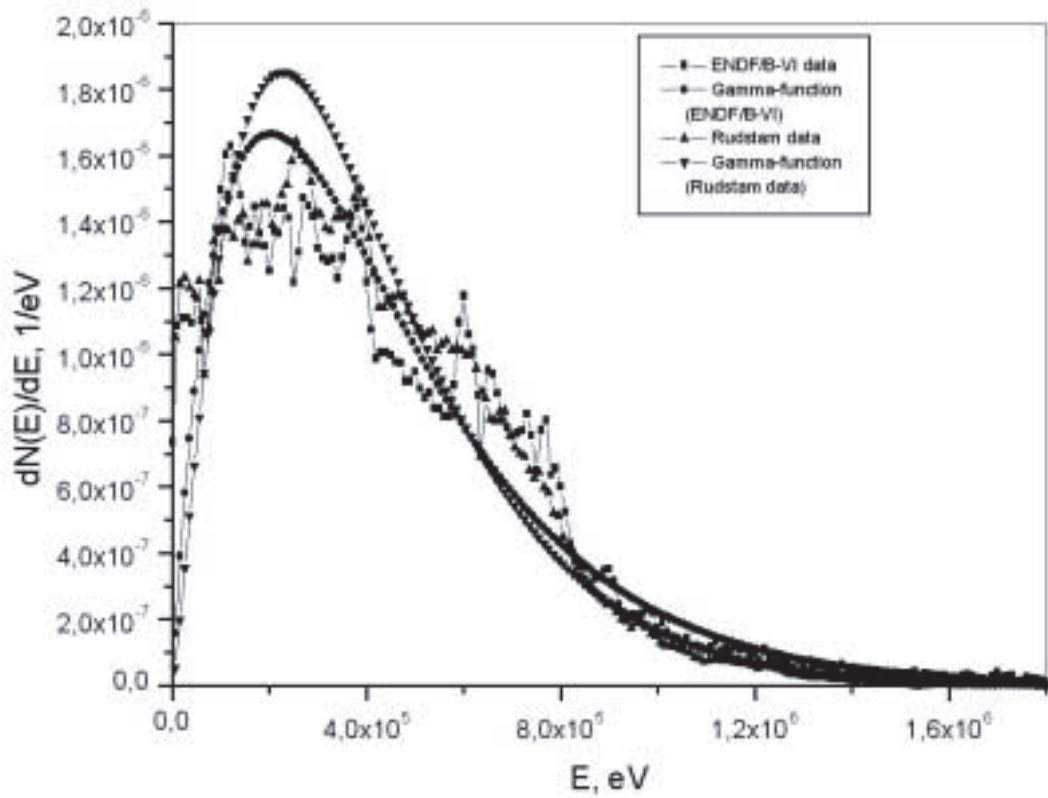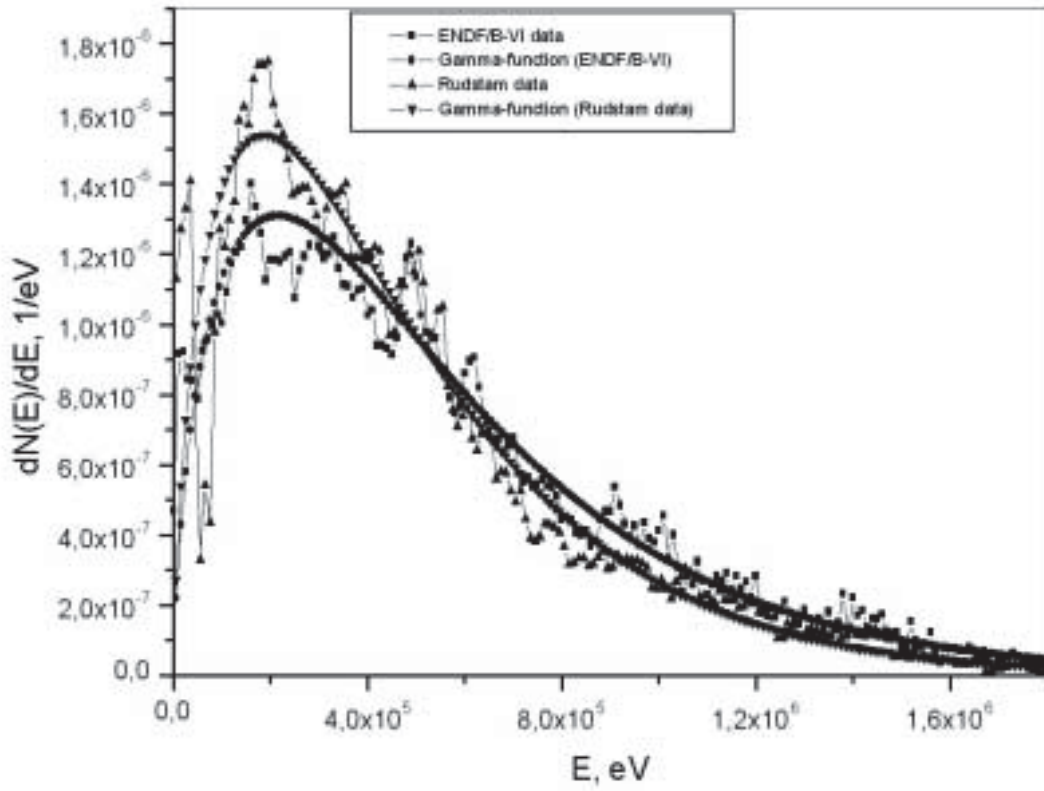
Fig. 5. The 4th group delayed neutron spectra and their approximation
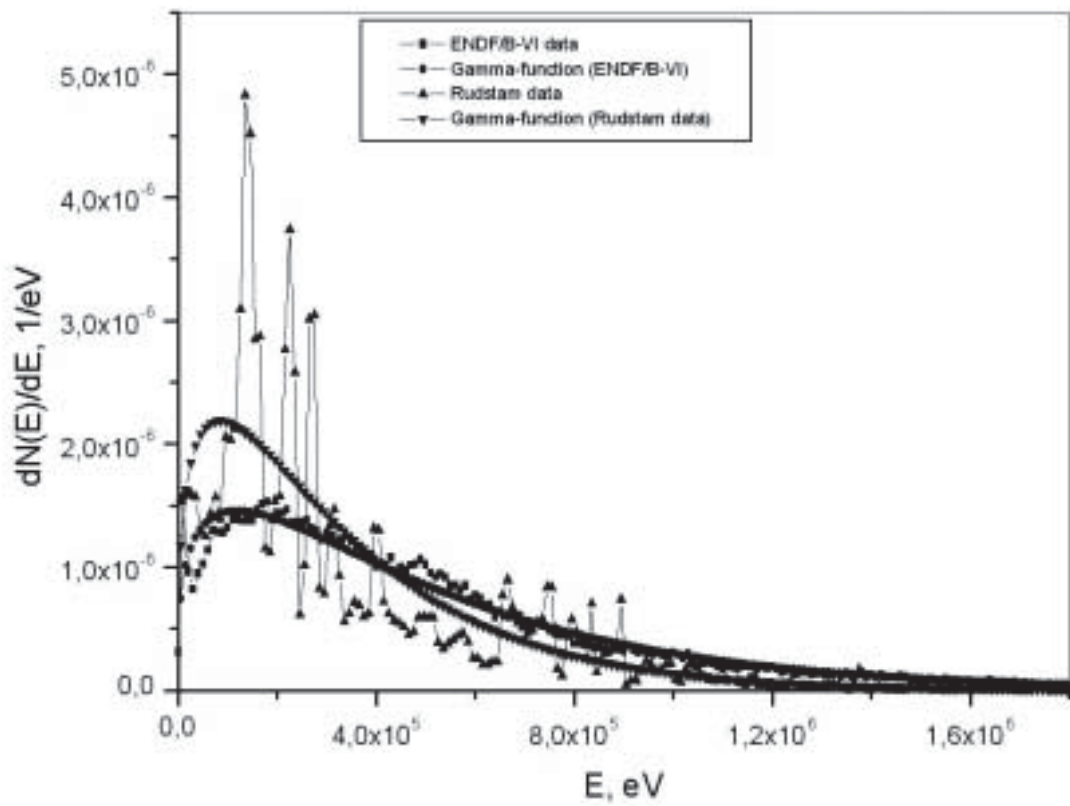

Fig. 6. The 5th group delayed neutron spectra and their approximation
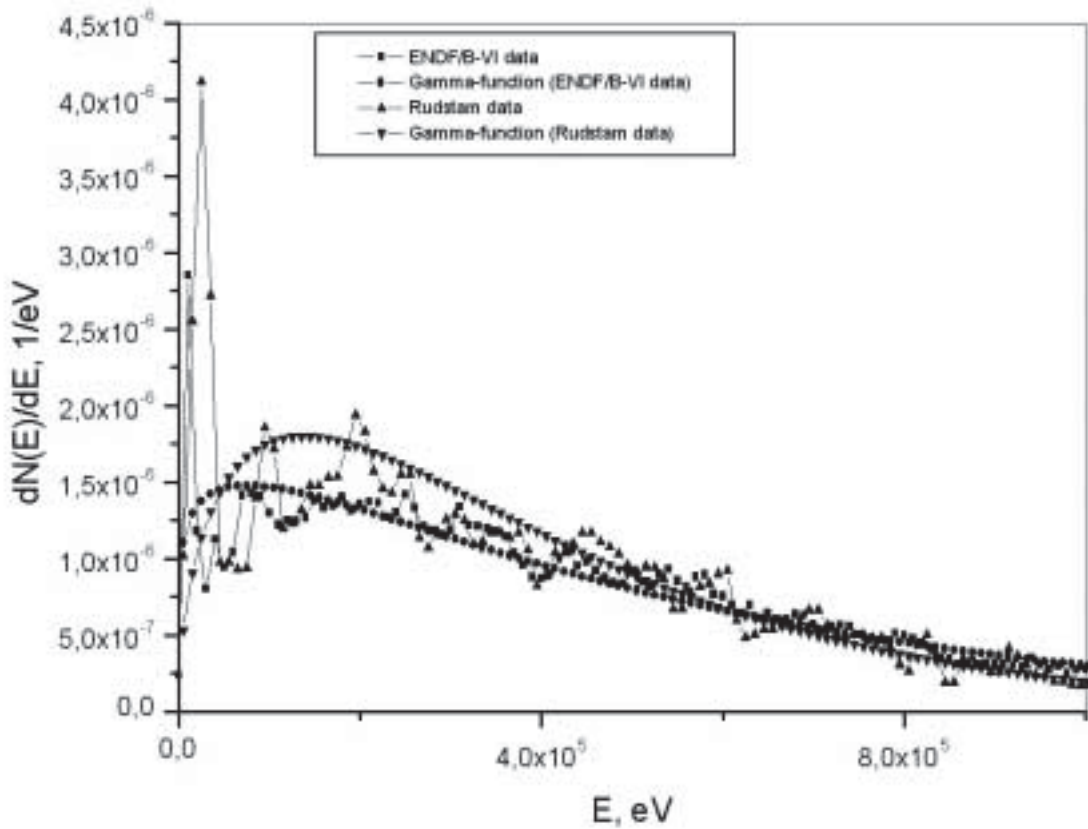
Fig. 7. The 6th group delayed neutron spectra and their approximation

Conclusion

The approximation of delayed neutron spectra by gamma-function is an effective tool for comparison of data obtained by different methods. The main result of present analyses is rather large difference in the average energy of the composite delayed neutron spectra obtained on the basis of experimental data only [1] and experimental data supplemented by model calculations [2]. Especially large difference is observed in case of the first group of delayed neutrons which consist of mainly one precursor – ^{87}Br. It was found that overall form of the delayed neutron spectra related to separate groups can not be represented by distribution that is pure Maxwell or evaporation type.

References

1. G. Rudstam // Nucl. Sci. and Engineering, 1982, v.80, p.238.
2. M.C. Brady, T.R. England // Nucl. Sci. Eng., 1989, v.103, p.129.

01-11405 (137)   [10]
<u>Translated from Russian</u>

UDC 539.172

NEW POSSIBILITIES FOR IMPROVING THE ACCURACY OF PARAMETER CALCULATIONS FOR CASCADE GAMMA-RAY DECAY OF HEAVY NUCLEI

A.M. Sukhovoj, V.A. Khitrov
Joint Institute for Nuclear Research, Dubna

E.P. Grigor'ev
Physics Institute, University of St. Petersburg, St. Petersburg

NEW POSSIBILITIES FOR IMPROVING THE ACCURACY OF PARAMETER CALCULATIONS FOR CASCADE GAMMA-RAY DECAY OF HEAVY NUCLEI. The level density and radiative strength functions which accurately reproduce the experimental intensity of two-step cascades after thermal neutron capture and the total radiative widths of the compound states were applied to calculate the total γ-ray spectra from the (n,γ) reaction. In some cases, analysis showed far better agreement with experiment and gave insight into possible ways in which these parameters need to be corrected for further improvement of calculation accuracy for the cascade γ-decay of heavy nuclei.

Introduction

Practical demands for nuclear data require the development of models for the properties of nuclear matter in order to facilitate calculations of nuclear reaction parameters not determined experimentally and to maximize the accuracy of experimental data evaluation. In turn, the dynamics of developing model representations of nuclei can be useful in interpreting experimental data and conducting new experiments.

Current models of nuclei all take into account the co-existence and interaction of two different types of excitation: quasiparticles and phonons - the Quasiparticle Phonon Model (QPM) [1]; fermions and bosons - different versions of the IBM [2]; phase transition from a superfluid state to a normal one - the generalized superfluid model of the nucleus [3]. Naturally, the reproduction accuracy of the given nuclei parameters in any of these approaches is determined in the first place by the experimental database used to develop the relevant model. In the second place, it is determined by the approximations used. There is also no doubt that extrapolation of any model representations to a nuclear excitation region for which there are no experimental data is bound to have an unknown and, possibly, significant error. For this reason, one should not only treat with caution any predictions derived from the above models for excitation energies between ~1-2 MeV and ~B_n for odd and even-even deformed nuclei, for example, but also look for different ways of obtaining reliable experimental information.

The (n,γ) reaction could be suitable for this purpose. It owes its uniqueness inter alia to the fact that the range of levels which are simultaneously excited in it corresponds to the area of maximum change in the structure of their wave function: here, the simplest low-lying small component states are transformed into extremely complex Bohr compound states (containing multiparticle and multibackground wave function components). And although there have been more nuclear physics studies of this reaction than any other, it is still not known how this change occurs.

In other words, to date there is no information as to which wave function components mainly determine the properties of the given levels which are excited, for example, by cascade γ-transitions to different energies. It is clear that this type of detailed information cannot be obtained directly from an experiment or a theoretical study. This conclusion follows from the form of the matrix element of any transition during disintegration of a highly-excited state (see, for example, [1]); its value is determined by the sum of a large number of terms which include a different number of quasiparticles and phonons. If one also considers the results of the theoretical description [4] of the process of fragmentation of states with a different number of quasiparticles and phonons on levels with a different excitation energy, then one should also take into account the possibility of significant dependence of the process of γ-ray decay of neutron resonances on neutron energy, for example.

This is why in order to understand the main features of the processes occurring in the nucleus when its excitation energy changes and to calculate accurately the nuclear reaction parameters of practical importance, it is necessary to have a model of the process of cascade γ-decay of a compound state (of a neutron resonance) which is sufficiently simple for interpretation and accurate for calculation. It should depict the most important parameters of the process under investigation with greater accuracy and reliability than is possible with current representations of the nucleus.

In practice, the first step in developing such a model is experimental determination of the level density, as well as the average widths of transitions which excite and discharge these levels throughout the whole range of excitation energies below the neutron binding energy B_n. Such work has to be carried out, first and foremost, in heavy nuclei for which very few experimental data are available. With theoretically interpreted values of the level density and the average widths of gamma transitions it is possible to calculate and compare with experiment those functions of the cascade γ-ray decay process which can be determined by existing techniques and methods of experimental data analysis. Naturally, no model of the process can be fully adequate, even in principle. The discrepancy between experiment and model calculations is a natural indicator of the need both to improve the understanding of nucleus properties at different excitation energies and to continue accumulating new experimental data specifically for those mass and excitation energy regions where the greater discrepancy is observed.

2. Calculation of parameters for γ-ray decay of a compound state

2.1. *Current situation*

To date, the level densities and radiative strength functions required for calculations have been repeatedly determined, both theoretically and experimentally, but not for all nuclei or all energies. Thorough analysis of the situation with accurate reproduction in calculations of the γ -ray decay parameters of the neutron resonance of a deformed nucleus, for example, shows that, first and foremost, new experiments to determine level density, and radiative strength functions are required in order to understand how the complexity of the structure of nuclear levels increases. The methods used to determine these values have to be very different from the existing methods and ensure greater reliability of the information obtained.

Reference [5] which studied two-quantum cascades of slow neutron radiative capture satisfies the above requirements. Analysis of the results of these experiments has yielded two rather important conclusions:

a) the density of the excited states and the strength functions of the cascade transitions observed differ most from the model predictions usually used in such calculations in the $E_{excit} \approx 0.5B_n$ region;

b) the very considerable influence of the structure of the three states, linked by such a cascade, on its intensity can be observed in a number of cases [5] .

The greatest achievement in the analysis of experiments carried out in the past has been the development [6] of a new independent method for simultaneous determination of the range of possible values for level density and the strength functions of E1 and M1 dipole transitions, which makes virtually no use of model representations.

This is rather significant since the level density has hitherto been derived from the spectra of nuclear reactions always using model representations for the emission probability of a reaction product which leads to the excitation of the given energy level. In addition, the method described in [6] has maximum response at the minimum level density. In conventional methods of determining the level density, maximum response of the experiment (maximum intensity of the reaction products in the measured spectra) corresponds to the maximum level density. However, the greatest discrepancy between nucleus models and reality should be anticipated in the region of the minimum level density.

The same is to all interests and purposes true of determination [7] of the radiative strength functions from γ-radiation spectra in the region of γ-transitions which cannot be detected by modern spectrometers. So the results of the known methods for determining level density and radiative strength functions in a region with high level density always have some systematic error which is almost impossible to eliminate using available methods of analysis.

2.2. *New possibilities for calculating cascade γ-ray decay parameters*

Unfortunately, the method given in [6] for simultaneous determination of level density and strength functions on the basis of the intensity distributions of two-quantum cascades between the neutron resonance and the given low-lying levels also produces results with some systematic error. Its sources are:

a)   a systematic error in the known [8] intensities of high-energy primary γ-transitions of radiative capture of thermal neutrons (used for normalization of the experiment in [5]);

b)   inaccuracy in determination [9] of the dependence of cascade intensity on the energy of the primary transition only;

c)   the fact that in [6] the assumption has to be made that the energy dependence of the strength functions of primary and secondary cascade transitions of a given type and multipolarity is identical;

d)   the use of several model representations of the anticipated dependence of level density on the spin.

It is essential to emphasize here that the influence of a) on the final results is, most probably, negligible in comparison with the other sources of systematic error.

The error due to uncertainty in determination of γ-cascade intensity dependence on the primary transition energy can be easily evaluated [10]. For this, any extrapolation to the registration threshold of the experimentally observed random fluctuations of the intensity of the resolved cascade peak pairs from their mean energy can be used. The error is reduced as statistics of the accumulated γ-γ coincidences increase.

The influence of all four sources of systematic error on the level density and strength functions being determined is bound to decrease when modern HPGe-detectors are used and cascades in neutron resonances with different spin are examined.

The analysis results in [6] differ significantly from the generally accepted notions about the dynamics of change in nucleus properties below B_n in that they cannot be explained without the introduction of a hypothesis about radical change in the structure of the wave function of nucleus levels in this excitation region. For this reason, it is now quite urgent to prove that the level density and radiative strength functions obtained in [6] reflect at least the most important features of these parameters of cascade γ-ray decay, despite the systematic errors listed above.

The most significant physical result in [6] is that the level density of a deformed (in the first place) nucleus in the $\sim 0.5B_n$ region is a lot lower than predicted by non-interacting Fermi gas models. In other words, the dependence of level density on excitation energy undergoes a "sharp change". This also contradicts the level density representations of the latest model - the generalized superfluid nucleus model, in its current version [3].

The existence of the level density feature mentioned above is clearly determined by the number of known low-lying levels, the average distance between the neutron resonances, and the existing considerable overshoot of the observed cascade intensity over calculations which use the Fermi gas level density. Since reducing the model density increases the calculated cascade intensity, the existence of a "sharp change" is the only explanation for the experiment. It is essential to note that modern [11] analysis of cross-sections of the interaction between neutrons and actinides also requires taking into account the non-monotonous ("stepwise") dependence of level density on the excitation energy of the nucleus. Maslov is quite justified in linking this to the effect of the splitting of paired nucleons.

It is necessary to emphasize that the contradiction between the representations in [3] and the results in [6] can be easily eliminated, at least qualitatively. The most important parameter of the generalized superfluid nucleus model - the temperature of the phase transition T_c - is linked to the correlation function δ of two nucleons by the known BCS (Bardeen, Cooper, Schrieffer)-theory correlation [12]:

$$T_c = 0.567\delta \tag{1}$$

However, this condition corresponds to the superliquid-normal state phase transition in an infinite, homogeneous medium. It is also known that the temperature of the phase transition to a superconducting state differs considerably from metal to metal. Also the temperature of this transition in a liquid helium isotope mixture decreases significantly in comparison with pure ^{4}He so there is no reason to suppose that $T_c = 0.567\delta$ is the only possible temperature for phase transition in nuclei.

If one takes into account the inevitable presence of quasiparticles (fermions) in the nucleus, then by analogy with the liquid helium isotope mixture, it can be anticipated that a reduction of T_c by a factor of 1.4-1.5 compared with (1) would lead to a twofold reduction in the phase transition energy

$$U_c = aT_c^2 \tag{2}$$

.

This is quite sufficient [13] for the energy dependence of the level density in generalized superfluid nucleus model representations to acquire the "sharp change" observed in [6] in the 3-4 MeV energy excitation region, without changing any other parameters in this model. But it is also necessary to develop new model representations for the dependence of nucleus entropy and temperature on excitation energy below T_c. By contrast, if the phase transition temperature is lower than (1), the model [3] predicts an increase in the temperature of the nucleus when its excitation energy is reduced. The above should not be taken as a criticism of model [3]. It is obvious that in the absence of the required experimental information, the authors had to make some kind of assumptions to extrapolate their representations to a region not studied previously.

The above shows that there is no reason to consider the results obtained in [6] as clearly incorrect solely on the basis of their divergence from the generally accepted representations of the [3, 19] type. Nevertheless, additional independent verification of these results is required.

2.3. γ-radiation spectra and level population

Deriving level density and radiative strength functions from the spectra of double quantum cascade intensities is determined by the specific form of their dependence on the density of the excited states: cascade intensity is approximately inversely proportional to level density. As shown in [6], this fact plus the known values of the total radiative widths of neutron resonances [14] allow a range of such values of level density and strength functions to be chosen for any excitation energy which simultaneously reproduce both the cascade intensity and the total radiative widths. It is very important that the width of this range is small enough for the results [6] to permit a definite conclusion both about the correlation of the model and the experimental level densities as well as the radiative strength functions, and about the way in which the relevant models need to be modified, despite the fact that the method described in [6] cannot give a single value for the parameters listed even for zero error of the experimental data.

Unfortunately, information about the double quantum cascade intensities is obtained only when the energy E_f of their final level does not exceed ~1 MeV. At higher E_f the double quantum cascade intensity quickly decreases while the background increases and isolating them in γ-γ correlation spectra becomes virtually impossible for Ge-detectors of low efficiency. This limitation means that extrapolation of the results [6] to the whole cascade γ-decay process can lead to erroneous conclusions, for example, about the strength function of the secondary transitions of compound state disintegration when they link levels with excitation energy above 1 MeV. At the same time, there are no barriers in principle to studying double quantum cascades on final levels with an energy of E_f >1 MeV, although this would require a more up-to-date spectroscopic technology than that used by the authors of [5].

Nevertheless, it is possible to verify to what extent the data in [6] on γ-ray decay parameters can be extrapolated to the entire nuclear excitation region below B_n despite the approximations of this analysis. This is done below in two ways:

a) by comparing the calculated and experimental population of known levels of nuclei up to an excitation energy of 3-4 MeV;

b) by comparing the calculated (with level density and strength functions [6]) and experimental γ-radiation spectra of the radiative capture of thermal [15] and fast [16] neutrons.

2.3.1. Level population

The cascade intensity i_γ which excites an intermediate level with energy E_i can be expressed through the known intensities of the primary i_1 and secondary i_2 transitions and also the sum of the latter Σi_2 in the following way:

$$i_{\gamma\gamma} = \frac{i_1 \times i_2}{\sum i_2}$$

(3)

In practice, the i_1 and i_2 intensities can be taken from the γ-ray spectra of slow neutron radiative capture [8] only if there is a well-established decay scheme for the nucleus in question to an excitation energy no lower than 2-3 MeV and if it is proven that these transitions are in fact linked to excitation of the level E_i. To date this has been done only for the compound nuclei ^{156}Gd and ^{168}Er [17].

As a result, the experimental sum Σi_2, which is the sum of the intensities of primary transition to level E_i and all possible cascades which end with it, can be determined from Eq. (3). Calculation using any model approximations or level densities and strength functions [6] does not present difficulties. The calculated and experimental population of a series of levels for the two nuclei indicated are shown in Figs 1 and 2. It should be pointed out that the primary transitions to these levels were excluded from the analysis in order to reduce the influence of the anticipated Porter-Thomas fluctuations [18] in their intensities.

It can be seen that using the level density from [6] and the corresponding strength functions reduces the discrepancy between experiment and calculation as compared, for example, with the values calculated on the basis of a model using the representations in [19-21]. Consequently, the level densities and radiative strength functions obtained in [6] do not contradict the real parameters of cascade γ-ray decay even for the part of the process not observed in the experiment [5]. This is at least true for the two deformed nuclei indicated.

2.3.2. Total gamma radiation spectrum

All the information about the cascade γ-ray decay of a compound state of any nucleus is contained in the total γ-radiation spectrum. This spectrum can be reproduced within the experimental error range by an infinite number of possible level densities and strength functions. However, for arbitrary excitation energy and the γ-transition energy these parameters can also be found within the limited range of their values. This follows directly from the values listed in [6] of possible variations in the indicated parameters of the process in question and the infinite number of possible level density and strength function values which can be used to reproduce the spectrum of the primary transitions. Thus, even full agreement between an experimental γ-spectrum and one calculated on the basis of a model does not prove that the model values used in the calculation correspond to the experimental ones. However, discrepancy between these spectra indicates indisputably that a specific combination of model representations for level density and radiative strength functions does not correspond to experiment. Moreover, it can be assumed that a smaller discrepancy between calculation and experiment points, at least in

principle, to a possible approach to modification of the model representations for level density and radiative strength functions in order to achieve agreement within experimental accuracy limits.

The total γ-radiation spectra of thermal neutron radiative capture have been measured in [15, 16] for the nuclei which we have examined. They are given below in the form of the product of γ-quanta intensity in a certain range δE and their energy in order to monitor the accuracy of the experimental and the calculated data and also to have a more clear comparison, especially in the high-energy region of the spectrum.

Comparison of the experimental spectrum and the spectrum calculated with the parameters from [6] shows (Figs 3-18) varying degrees of improvement (including virtual agreement) for the compound nuclei [114]Cd, [128]I, [158]Gd, [166]Ho [16], [168]Er, [182]Ta, [196]Pt, [198]Au and [200]Hg and overshoot of the calculated intensity over the experimental intensity for [140]La, [150]Sm, [156]Gd, [160]Tb [16], [164]Dy [16], [176]Lu [16] and ^{192}Ir at a gamma-ray energy of 3-4 MeV and more when using only the data in [6].

As shown below, this discrepancy decreases when the strength functions for the secondary transitions with weaker energy dependence than in [6] are used in the calculation. At the same time, calculation with the data from [6] may diverge less from experiment than when the models in [19-21] are used.

Possible qualitative interpretation of the causes of this discrepancy does not present difficulties - all the information about properties of levels with excitation energy ranging from 1-2 to 3-4 MeV, obtained during the study with cascades, points [14] to the dominating role of vibration excitations in the structure of their wave functions. Also the fast growth (maximum for deformed nuclei) of the strength functions observed in [6], occurring when the energy of the γ -transition increases, can be attributed to the well-known collective improvement of the probability of a γ-transition for a level with large vibration components in the wave functions. Naturally, this hypothesis has to be proven or refuted through theoretical analysis. However, at present and unless and until this - or any other similar - hypothesis is put forward, it is impossible to interpret the results of a comparison between experiment and calculations.

If the proposed explanation proves correct, the increase in the strength functions observed in [6] is linked to level structure at a specific excitation energy and not to the characteristics of the strength function itself. Consequently, the assumption made in [6] about the identical energy dependence of the strength functions of primary and secondary transitions (but not their absolute values) cannot reproduce the of γ-ray decay process for well-deformed nuclei with absolute accuracy. Any re-distribution of the values of the secondary transition strength functions, for example, is enough to improve agreement, as long as this distribution does not distort the relative intensity of these transitions to levels with energy $E_f < (0.5-1)$ MeV.

The experimental spectra in [15, 16] are compared with the results of two types of calculation to check this possibility:

a)   the spectrum calculated only with the parameters in [6];

b)   the level density and strength functions of the primary transitions of compound state decay from [6], and the strength functions of the secondary transitions defined according to the models in [20, 21].

The results of the calculations and of the experimental spectra are given in Figs 3-18. It can be seen that neither the first nor the second calculation can accurately reproduce the experimental spectra of thermal neutron radiative capture in all the well-deformed nuclei. Regions of discrepancy and the fluctuation direction are in some sense alternating. However, for transitional nuclei with A>180 it is precisely the level density obtained in [6] which ensures good correlation between calculation and experiment in the high-energy part of the spectrum. Models similar to [19] i.e. [22, 23] cannot.

Comparison of the data in Figs 1-18, taking into account the existing links between level density and partial radiative widths, shows that:

a)   in a number of cases, the experimental level density may be even smaller than that indicated in [6];

b)   the strength functions of secondary transitions to final levels with energy E_f~1-4 MeV can be increased in comparison with the results in [6];

c)   as suggested earlier in [5], it is possible that (as minimum) two or more systems of excited levels with identical quantum numbers J^π but very different wave function structures co-exist and interact inside the nucleus. As a result, they are selectively excited, at least during disintegration of the low-energy neutron resonances. It cannot be ruled out that these systems might dominate at various excitation energies. This possibility is indicated by the results of the calculation of the total spectra for the mass A~150 region where the discrepancy between the experimental spectra and the spectra calculated on the basis of the data in [6] is greatest. In this last scenario, the nucleus parameters obtained in [6] should be attributed to the system which is excited the most during thermal neutron radiative capture. This has to be verified experimentally.

Conclusion

Comparison of the calculated and experimental population of low-lying levels and total cascade γ-ray decay spectra (also using, for example, the known results in [22, 23]) shows that in a number of cases the values for level density and radiative strength functions obtained in [6] significantly improve the accuracy of description of this process compared with the models in [19-21].

Of course, owing to experimental errors and analysis approximations, the data in [6] contain both random and systematic errors. However, whatever their values they cannot affect the main conclusions of this paper in a significant manner.

The results of the analysis performed show that the cascade γ-ray decay parameters determined experimentally [6] possibly reflect the most characteristic features of the process and have specific features which must be incorporated into the existing models [19-21] in order to improve the accuracy of nuclear parameter calculations.
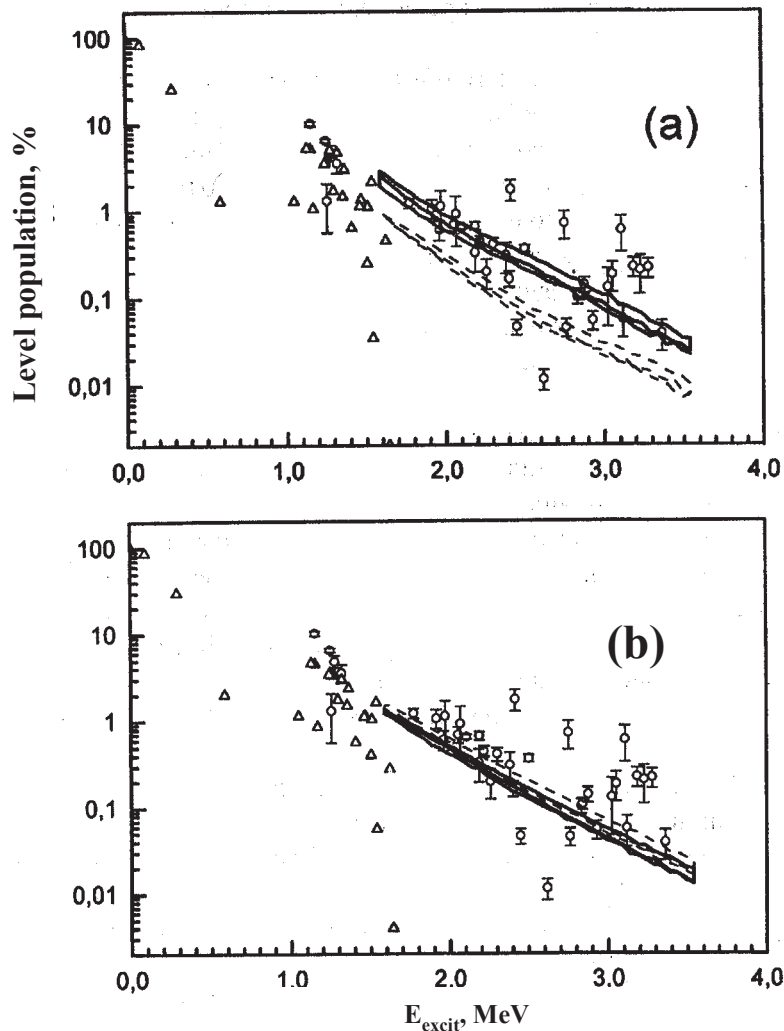
Fig. 1.:   Experimental population of low-lying ^{156}Gd levels (circles with errors). Lines - calculated population of levels excited by primary E1 and M1 transitions. Triangles - calculated population of discrete levels. Calculation versions: (a) - for parameters from [6], (b) - from models [19-21].
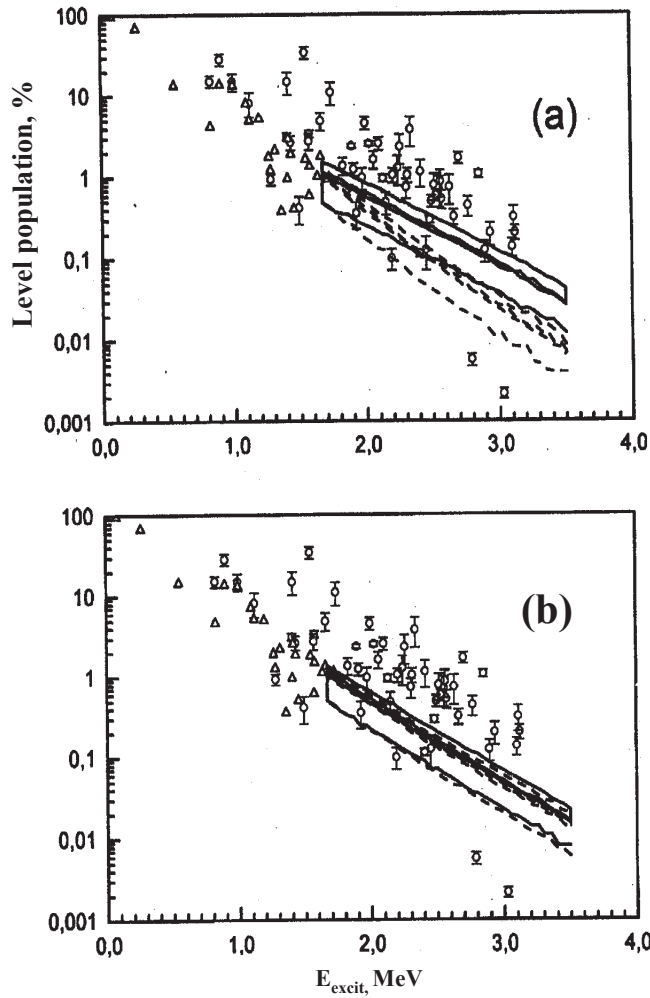
Fig. 2.: As for Fig. 1, for [138]Er.
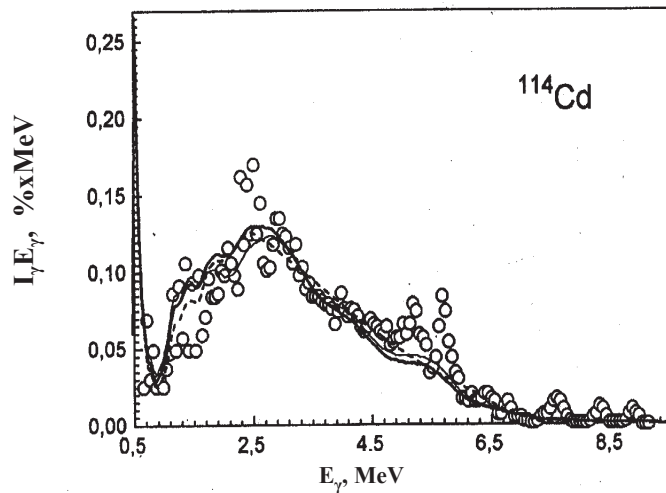
Fig. 3.: Total experimental (circles) and calculated spectra of γ-radiation following neutron capture for the compound nucleus of [114]Cd. Dotted line - parameters from [19-21], thin line - [6], bold line - level density and strength functions of primary transitions from [6], secondary - according to [20, 21].

Fig. 4.: As for Fig. 3, for ^{128}I.

Fig. 5.: As for Fig. 3, for ^{140}La.

Fig. 6.: As for Fig. 3, for ^{150}Sm.
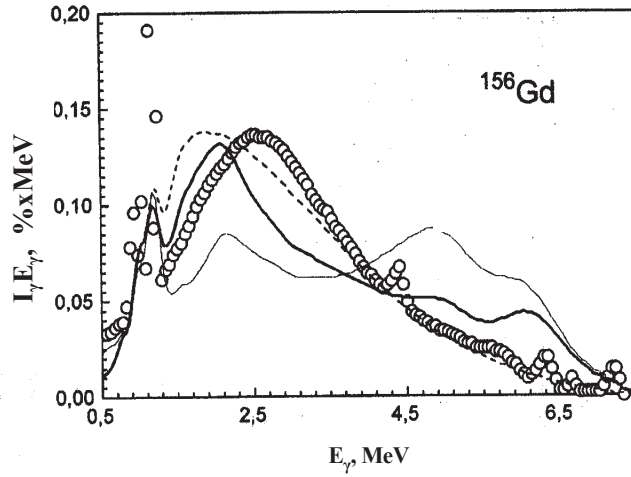
Fig. 7.: As for Fig. 3, for ^{156}Gd.

Fig. 8.: As for Fig. 3, for ^{158}Gd.

Fig. 9.: As for Fig. 3, for ^{160}Tb.

Fig. 10.: As for Fig. 3, for ^{164}Dy.

Fig. 11.: As for Fig. 3, for ^{166}Ho.

Fig. 12.: As for Fig. 3, for ^{168}Er.

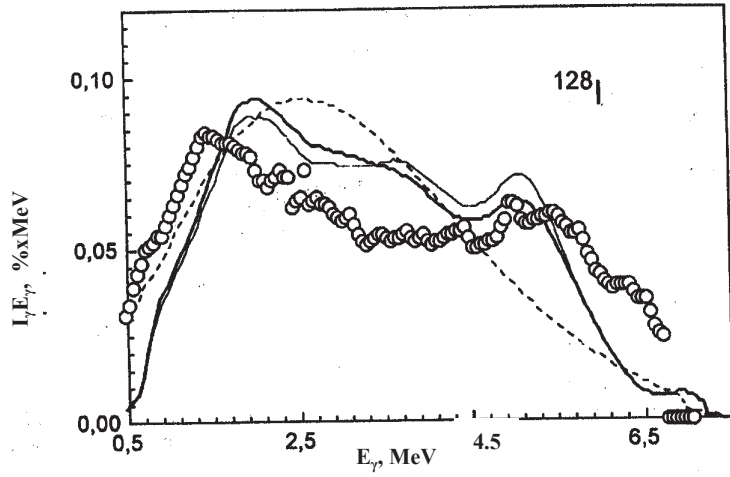Fig. 13.: As for Fig. 3, for ^{176}Lu.
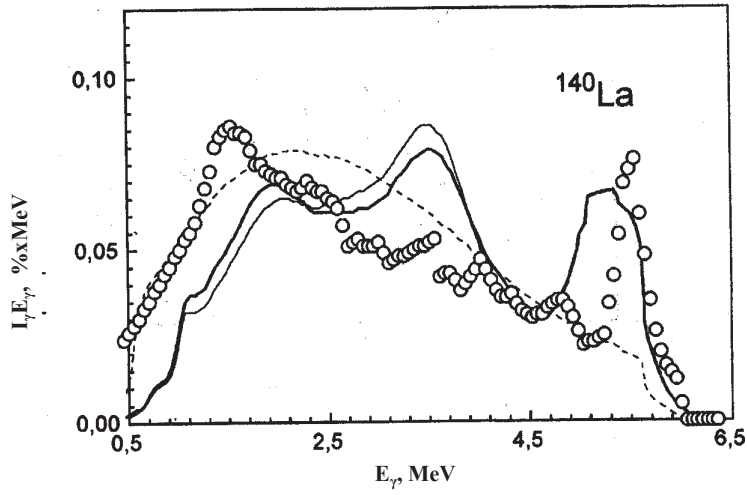

Fig. 14.: As for Fig. 3, for ^{182}Ta.

Fig. 15.: As for Fig. 3, for ^{192}Ir.

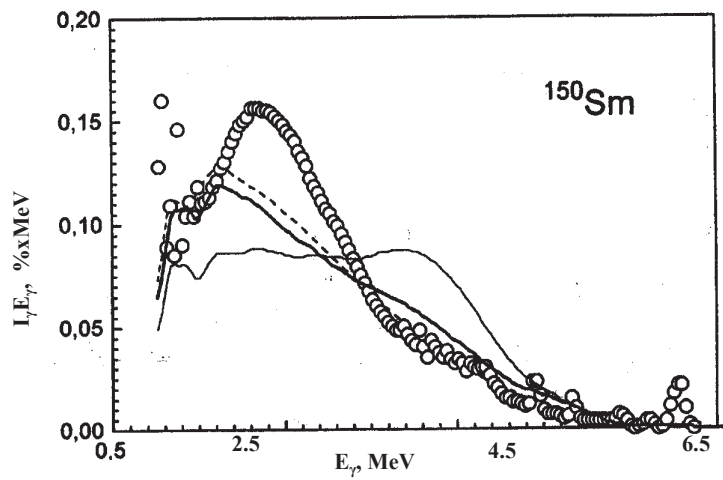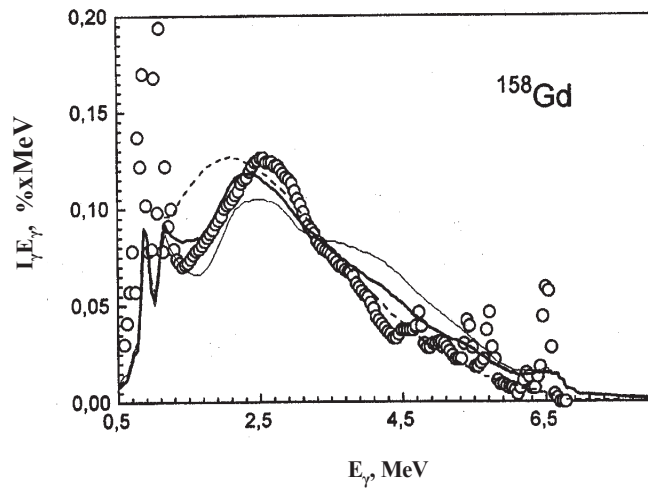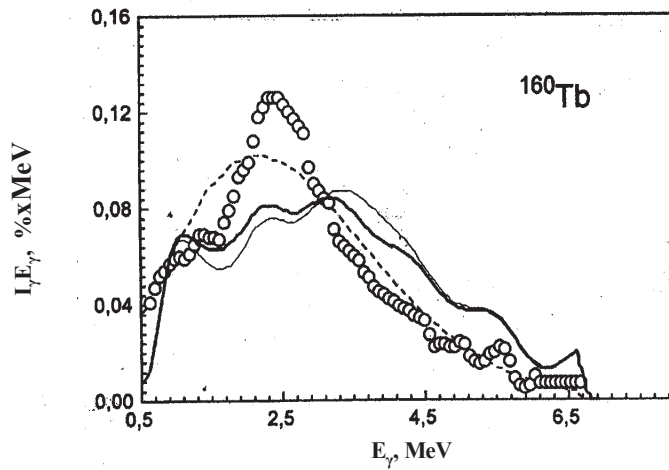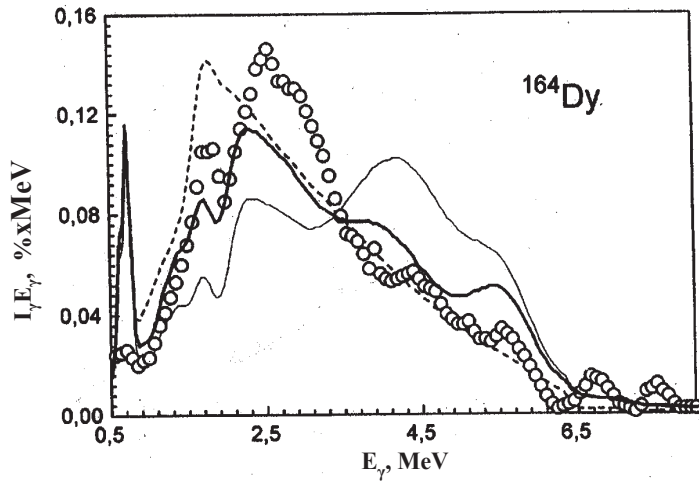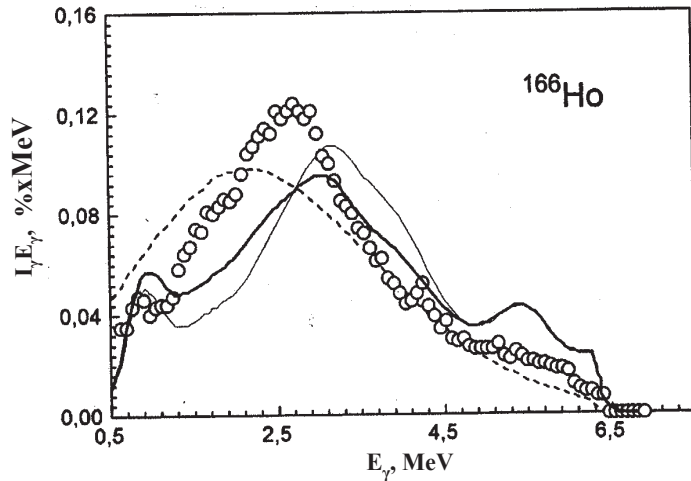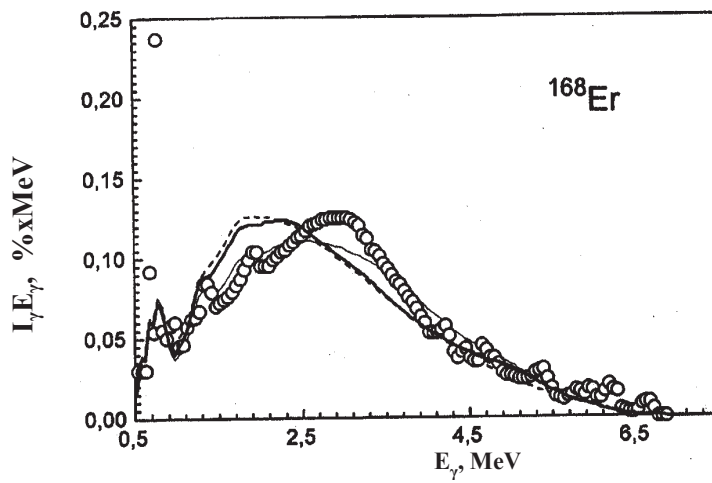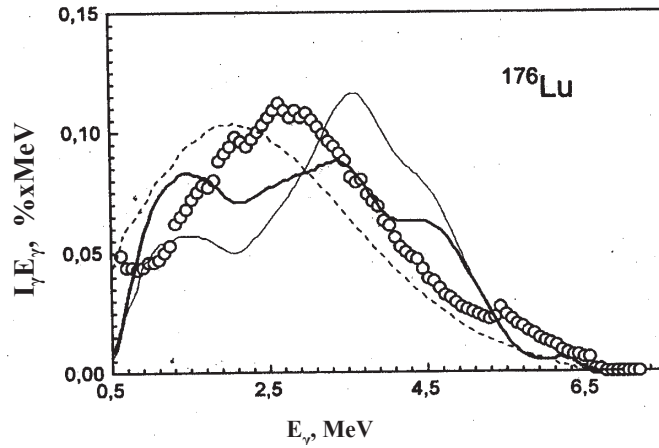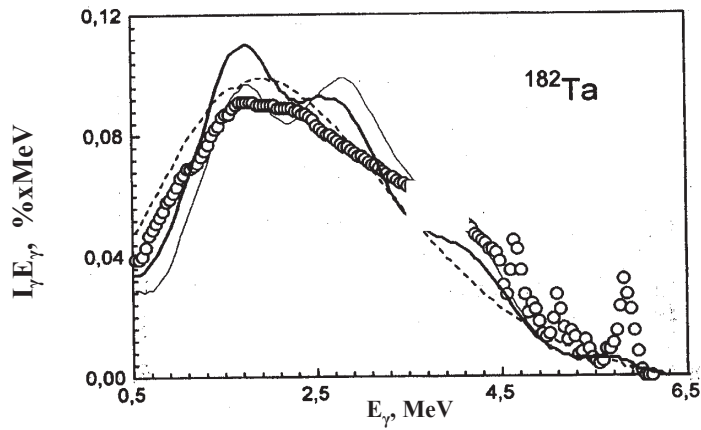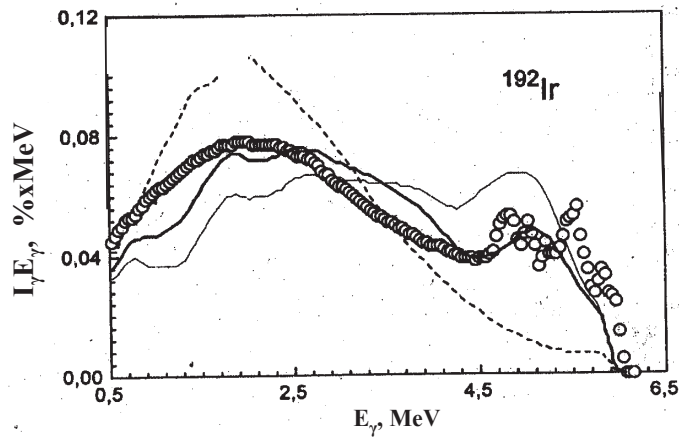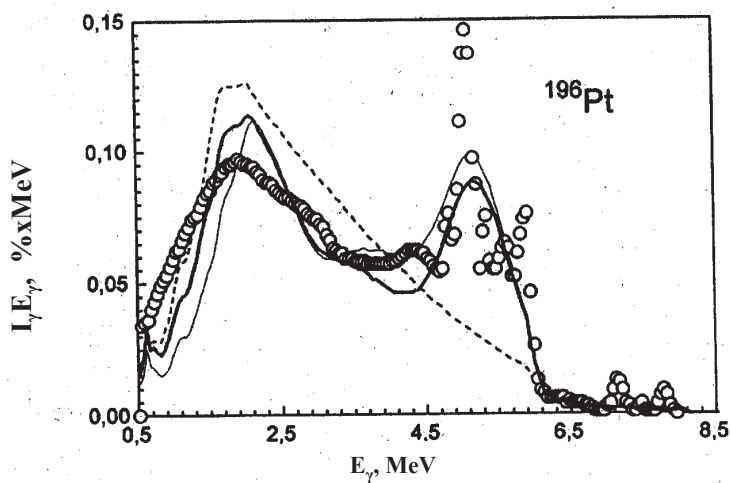Fig. 16.: As for Fig. 3, for ^{196}Pt.
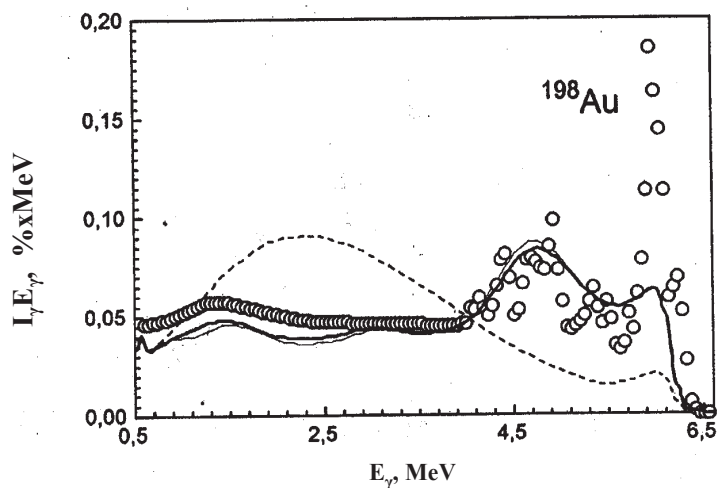
Fig. 17.: As for Fig. 3, for ^{198}Au.
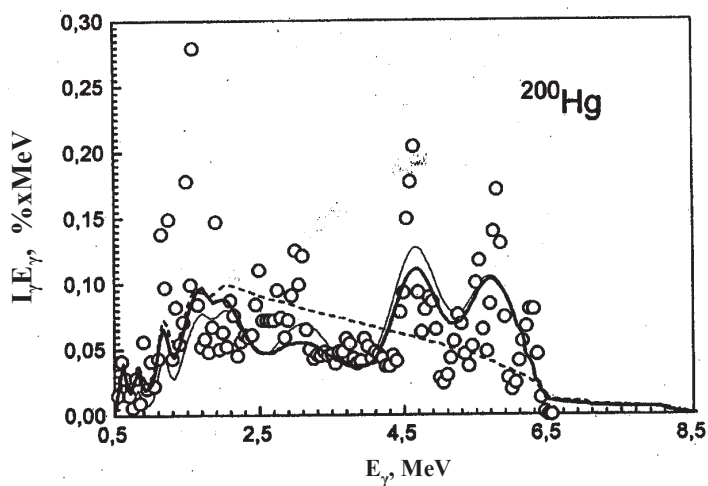
Fig. 18.: As for Fig. 3, for ^{200}Hg.

REFERENCES

1. Solov'ev V.G., Theory of heavy nuclei, Moscow, Nauka, 1971 [in Russian].

2. Iachello F. and Arima A., The Interacting Boson Model, Cambridge University Press, Cambridge, 1987.

3. Rastopchin E.M., Svirin M.I., Smirenkin G.N., Testirovanie osnovnykh fenomenologicheskikh modelej plotnosti urovnej, Nuclear Physics, v. 52, (1990), p. 1258.

4. Malov L.A., Solov'ev V.G., Obshchie zakonomernosti fragmentatsii odnochastichnykh sostoyanij v deformirovannykh yadrakh, Nuclear Physics, v. 26(4), 1977, p. 729.

5. Boneva S.T., Vasil'eva Eh.V., Popov Yu.P., Sukhovoj A.M., Khitrov V.A., Dvukhkvantovye kaskady radiatsionnogo zakhvata nejtronov 1. Spektroskopiya vozbuzhdennykh sostoyanij slozhnykh yader v diapazone ehnergii svyazi nejtrona, Problemy fiziki ehlementarnykh chastits i atomnogo yadra, v. 22(2), 1991, p. 479.

    Osnovnye parametry i osobennosti gamma-raspada kompaund-sostoyanij slozhnykh yader, Problemy fiziki ehlementarnykh chastits i atomnogo yadra, 22(6), 1991, p. 1433.

    Boneva S.T., Vasil'eva Eh.V., Simonova L.I., Bondarenko V.A., Sukhovoj A.M., Khitrov V.A., Reaktsiya (n,γ) v tyazhelom yadre. Nablyudaemye ehffekty proyavleniya ego struktrury pri vozbuzhdeniyakh $E < B_n$, Yadernaya Fizika, v. 62(5). 1999, p. 892.

6. Vasil'eva Eh.V., Sukhovoj A.M., Khitrov V.A., Level density, radiative strength functions and main properties of heavy nuclei below neutron binding energy, Proc. Russian Academy of Sciences, Ser. Fiz., 65(5), 2000, p. 718 [in Russian].

7. Bartholomew G.A., Earle E.D., Ferguson A.J., Knowles J.W., Lone M.A., Gamma-Ray Strength Functions, Advances in nuclear physics, 7 (1973) p. 229.

8. Lone M.A., Leavitt R.A., Harrison D.A., Prompt Gamma Rays from Thermal - Neutron Capture// Nuclear Data Tables, 26, 1971, p. 511.

9. Boneva S.T., Khitrov V.A., Sukhovoj A.M., Vojnov A.V., Excitation study of high-lying states of differently shaped heavy nuclei by the method of two-step cascades// Nucl. Phys., A589, 1995, p. 293.

10. Sukhovoj A.M., Khitrov V.A., Ehksperimental'naya otsenka plotnosti urovnej tyazhelogo yadra, real'no vozbuzhdaemykh v reaktsii (n,γ) pri $E_{BO3} < 3\text{-}4$ MeV, Yadernaya Fizika, 62(2), 1999, p. 24.

11. Maslov V.M., Phys. of Atomic Nuclei, 63(2), (2000) p. 161.

12. Bardin J., Cooper L., Schriffer J., Theory of Superconductivity, Phys. Rev., 108, (1957) p. 1175.

13. Sukhovoj A.M., Khitrov V.A., Cascade gamma decay of the compound state of a heavy nucleus: experimental picture, Proc. Russian Academy of Sciences, Ser. Fiz., 61(11), 1997, p. 2068 [in Russian].

    Khitrov V.A., Sukhovoj A.M., States of heavy nuclei strongly excited in the (n,γ) reaction: possible dominant component at E_{ex}<3-5 MeV, Proc. International Conference on Nuclear Data for Science and Technology, May 19-24, 1997, Trieste, Italy. Ed. Reffo G., Ventura A., Grandi G., Bologna, Italy: Italian Physical Society, 1997, p. 750.

    Boneva S.T. et al., On improving the accuracy of describing the parameters of neutron resonance cascade gamma-decay using the idea of nuclear phase transition, Proc. International Conference on Nuclear Data for Science and Technology, May 19-24, 1997, Trieste, Italy, Ed. Reffo G., Ventura A., Grandi G., Bologna, Italy: Italian Physical Society, 1997, p. 799.

14. Mughabghab S.F., Neutron Cross Sections, Part B, NY: Academic Press 1984.

15. Groshev L.V et al., Atlas of the γ-ray spectra of radiative capture of thermal nuclei, Moscow, 1958 [in Russian].

16. Voignier J., Joly S., Greinier G., Capture Cross Sections and Gamma-ray Spectra from Interaction of 0.5 to 3 MeV Neutron with Nuclei in the Mass Range A=63 to 209, Nucl. Sci. Eng., 93, 1986, p. 43.

    Igashira M., Kitazawa H., Shimizu M. et al., Systematics of the Pygmy Resonance in keV Neutron Capture Gamma-Ray Spectra of Nuclei with N=82-126, Nucl. Phys. A457, 1986, p. 301.

17. Grigoriev E.P., Khitrov V.A., Sukhovoj A.M., Vasilieva E.V., A search for the γ-decay of the ^{168}Er compound in the (n,2γ) reaction, Fizika B (Zagreb), 9(4), 2000, p. 147.

18. Porter C.F., Thomas R.G., Fluctuations of nuclear reaction widths, Phys. Rev., 104(2) (1956) p. 483.

19. Dilg W., Schantl W., Vonach H., Uhl M., Level Density Parameters for the Back-Shifted Fermi Gas Model in the Mass Range 40<A<250, Nucl. Phys., A217, 1973, p. 269.

20. Axel P., Electric Dipole Ground Transitions Width Strength Function and 7 MeV Photon Interactions, Phys. Rev., 126(2) (1962) p. 671.

21. Blatt J.M., Weisskopf V.F., Theoretical Nuclear Physics, New York (1952).

22. Lomachenkov I.A., Furman V.I., Theoretical description of γ-ray spectra of thermal neutron capture, JINR R4-85-466, Dubna, 1985 [in Russian].

23. Grudzevich O.T., Strukture of γ-ray spectra during radiative neutron capture, Voprosy atomnoj nauki i tekhniki, Ser.: Yadernye konstanty, 3-4, 1997, p. 94.

THE CONSTANTS AND PARAMETERS OF
NUCLEAR STRUCTURE AND NUCLEAR REACTIONS

01-11405 (133) [011]
<u>Translated from Russian</u>

UDC 539.163

HALF-LIVES OF RADIONUCLIDES USED IN NUCLEAR
GEOCHRONOLOGY AND COSMOCHRONOLOGY
(EVALUATED DATA)

V.P. Chechev
V.G. Khlopin Radium Institute, St. Petersburg

HALF-LIVES OF RADIONUCLIDES USED IN NUCLEAR GEOCHRONOLOGY AND COSMOCHRONOLOGY (EVALUATED DATA). Evaluated half-life values are given for the radionuclides ^{26}Al, ^{40}K, ^{53}Mn, ^{60}Fe, ^{87}Rb, ^{93}Zr, ^{98}Tc, ^{107}Pd, ^{129}I, ^{135}Cs, ^{146}Sm, ^{176}Lu, ^{182}Hf, ^{187}Re, ^{205}Pb, ^{232}Th, ^{235}U, ^{238}U, ^{244}Pu and ^{247}Cm. These were obtained from an analysis of published information up to 2001. These half-lives are used in geochronology and cosmochronology to determine different radiometric ages in the history of the earth, solar system and galaxy.

1. General remarks

As we know, nuclear geochronology can determine the age of objects containing radionuclides using the constancy of the laws of radioactive decay and, in particular, the fact that the decay rate is not dependent on external conditions. When studying rock from the earth, the moon or meteorites, its measurable age is the time which has passed since the mineral crystallized (solidified) because a solid crystalline substance acts as a trap retaining the atoms of daughter products. By measuring the parent radionuclide content in a mineral $N(A) = N_0(A)\exp(-\lambda\theta_M)$ and its stable decay product content $N(B)$, we can determine the age of the mineral θ_M, i.e. the time which has passed since it solidified, if the initial quantity of the daughter isotope B can be evaluated. This can be done if the content of any other stable isotope of the daughter product of nonradiogenic origin is known, since the relative isotopic composition is usually well known and is a constant.

It would appear that only errors in the measurement of $N(A)$, $N(B)$ affect the accuracy of geochronological values obtained in this way, since the nuclear constants $\lambda \equiv \ln2/T_{1/2}$ ($T_{1/2}$ is the half-life of the radionuclide) are relatively more accurately known. However, as isotope concentration RATIOS are generally used in geochronology, in recent years it has become clear that the accuracy of nuclear constants is vital in estimating the age of minerals [1]. The reason here is the divergence in some of the experimental data on radionuclide half-lives. The authors

of Ref [1] state that the accuracy of radiometric ages is currently restricted by the accuracy of radioactive decay constants.

As reliable information on the accuracy of nuclear constants can only be obtained by evaluating all the published data i.e. by determining an evaluated value and its uncertainty, one of the aims of this paper is to obtain evaluated half-life values for "geochronological" radionuclides such as ^{40}K, ^{87}Rb, ^{176}Lu, ^{187}Re, ^{232}Th, ^{235}U and ^{238}U.

The second aim of this paper relates to the interest which has arisen in the half-lives of radionuclides used as long-lived and short-lived cosmochronometers [2, 3]. While nuclear geochronology determines the age of minerals containing radionuclides, nuclear cosmochronology determines the age of the actual radionuclides produced by various galactic nuclear fusion processes (nucleosynthesis).

In contrast to geochronology, astrophysical models of galactic nucleosynthesis are crucial in this instance. Here, the accuracy of the nuclear constants takes precedence over the accuracy of the model parameters. Therefore it is mainly a matter of examining the widest possible range of radionuclides which can be used to verify and refine galactic nucleosynthesis models. In recent years, the number of such radionuclides has increased significantly as regards relatively short-lived cosmochronometers ($T_{1/2} \equiv 10^8$ years). The long familiar long-lived cosmochronometers ^{187}Re, ^{232}Th, ^{235}U, and ^{238}U, and the short-lived cosmochronometers ^{129}I and ^{244}Pu have been joined by ^{26}Al, ^{53}Mn, ^{60}Fe, ^{93}Zr, ^{107}Pd, ^{135}Cs, ^{146}Sm, ^{182}Hf, ^{205}Pb and ^{247}Cm which have been discovered (or are assumed) to have existed in the early history of the solar system [4].

While long-lived radionuclides are used to determine the mean age of elements and the duration of nucleosynthesis in the galaxy before the solar system was formed, short-lived cosmochronometers can be used to obtain detailed information on nucleosynthesis during the early history of the solar system and, in particular, the period when planetary and meteorite material was solidifying [3, 4].

We shall conclude this brief review by mentioning one of the most important branches of nuclear astrophysics where evaluated half-life uncertainties are acquiring major significance for cosmological findings. We refer to research into possible change in fundamental constants over cosmological time [5]. Such change must, in one way or another, affect the basic premise of nuclear geochronology that radioactive decay constants remain invariable over time, causing discrepancies in the determination of different radiometric ages, which means that (on the basis of observational and experimental data) limits can be introduced for the possible change in constants over time. The most direct method of determining the limits on half-life change over time is to compare $T_{1/2}$ evaluated in two ways:

1) In laboratory experiments based on the measured specific activity;
2) From an isotopic analysis of the minerals based on the accumulated daughter products.

By determining evaluated $T_{1/2}$ values separately for both these methods and comparing the results, limits can be obtained for the possible change in fundamental constants over time. This is done for [187]Re decay in this paper.

The evaluated half-life values for 20 radionuclides used in nuclear geochronology and cosmochronology are examined below.

Our evaluated $T_{1/2}$ values are compared with those in the ENSDF file [6], and with Holden's evaluations [7]. The evaluation technique we have adopted and verified over the past few years [8, 9] is based on an analysis of the results of data processing using a number of statistical procedures. It is performed using the EV1NEW computer program [10]. This program selects different statistical data processing options depending on the χ^2 value. In some cases we also use the LWEIGHT computer program described in Ref. [11]. Like EV1NEW, this uses the limitation of relative statistical weight method using a value of 0.05 (LRSW method, see Refs [20, 21]). However, where there are discrepancies in the data, the total uncertainty of the evaluated value can be increased to include the most accurate experimental result (see Ref. [11]).

2.   [26]Al

It has now been established that [26]Al was not only present in the early solar system (from the abundance of its daughter product [26]Mg in meteorites) but is also present in galactic objects where nucleosynthesis is currently occurring (from intensive gamma radiation with an energy of 1809 keV) [4].

We obtained the evaluated half-life value $T_{1/2}(^{26}Al)=7.17(24)\cdot10^5$ years as the weighted mean of the following 4 measurement results: 7.16(12) [12], 7.05(24) [13], 7.02(56) [14] and 7.8(5) [15] (in units of 10^5 years). (Here and below, the uncertainty is given in round brackets after the figure in units of the last significant figure of the value at the 1σ level (confidence level P=0.68)). The lowest uncertainty given by the persons conducting the experiment was taken as the uncertainty of the evaluated value of $T_{1/2}$ (^{26}Al) [8,9].

Since, in this case, the same evaluation technique and the same set of experimental data [12-15] were used in ENSDF [6] (2000 evaluation), the results of both evaluations coincide and agree well with Holden's evaluation of $7.1(2)\cdot10^5$ years [7].

3.   [40]K

The well known, natural long-lived radionuclide [40]K is transformed into stable [40]Ca by β-decay (89.14% of the total number of decays) and stable [40]Ar by electron capture (10.86% of the total number of decays). There are many measurements in the literature of both the total half-life of [40]K ($T_{1/2}$) and the partial half-lives $T_{1/2}\beta$ and $T_{1/2}\varepsilon$. All these measurement results (from 34 papers) are given in Ref. [7]. To avoid this paper becoming unwieldy, we shall not give them here but just use their reference numbers from Ref. [7]. Holden recommended a non-weighted mean of the results from 14 studies (Refs 64, 67, 69, 71-80, 83 in Ref. [7]) as the evaluated [40]K half-life value. He does not explain this choice of data in his paper.

For our evaluation, we used all existing experimental results for which the authors give uncertainties (Refs 51-57, 59-83 in [7]) (Table 1).

Table 1

Measurement results for the partial half-lives of ^{40}K scaled to the total half-life $T_{1/2}$, using the accepted branching ratios in ^{40}K decay - β^- 89.14(13)% and ε 10.86(13)%

Primary author	Year	$T_{1/2}$ / (10^9 years)	Ref. No. in Ref. [7] and measurement type(β^-,ε or total $T_{1/2}$)	Remarks
Gleditsch	1947	1.2 (2)	51 (ε)	
Ahrens	1948	1.26 (22)	52 (ε)	
Graf	1948	1.32 (6)	53 (β^-)	
Stout	1949	1.15 (7)	54 (β^-)	
Floud	1949	1.5 (4)	55 (total $T_{1/2}$)	Excluded from evaluation
Sawyer	1950	1.3 (1)	56 (ε)	
Graf	1950	1.3 (2)	57 (ε)	
Faust	1950	1.14 (10)	59 (total $T_{1/2}$)	
Sawyer	1950	1.27 (5)	60 (total $T_{1/2}$)	
Houtermans	1950	1.31 (7)	61 (total $T_{1/2}$)	
Smaller	1950	1.57 (5)	62 (β^-)	Excluded from evaluation
Delaney	1951	1.11 (1)	63 (β^-)	Excluded from evaluation
Good	1951	1.30 (3)	64 (β-)	
Burch	1953	1.27 (5)	65 (ε)	
Suttle	1955	1.20 (3) 1.46 (2)	66 (β^-) 66* (ε)	Excluded from evaluation
Kono	1955	1.21 (5)	67 (ε)	
Backenstoss	1955	1.23 (5)	68 (ε)	
McNair	1956	1.28 (1)	69 (β^-)	
Wetherill	1956	1.32 (7)	70 (ε)	
Wetherill	1957	1.27 (4)	71 (β^-)	
Kelly	1959	1.30 (3)	72 (β^-)	
Saha	1960	1.34 (7) 1.22(4)	73 (ε) 73* (β^-)	
Fleishman	1962	1.3 (4)	75 (β^-)	
Glendenin	1961	1.248 (13)	74 (β^-)	
Brinkman	1965	1.21 (2)	76 (β^-)	
Leutz	1965	1.32 (3) 1.248 (2)	77 (ε) 77* (β^-)	Uncertainty increased to 0.0054 using LRSW method [4]
Feuerhake	1966	1.26 (2)	78 (β-)	
DeRuytter	1966	1.32 (2)	79 (ε)	
Egelkraut	1966	1.28 (5)	80 (ε) 80* (β^-)	
Venkataramaiah	1971	1.17 (5)	81 (β^-)	
Gopal	1972	1.01 (5)	82 (β^-)	Excluded from evaluation
Cesana	1977	1.34 (4)	83 (ε)	

The statistical processing of the set of 36 experimental results, scaled to the total half-life of ^{40}K, was done using the LWEIGHT computer program [11]. The program turned up 5 statistical outliers (Refs 55, 62, 63, 66* and 82 in Ref. [7]). Having excluded these, the program increased the uncertainty of the most accurate measurement result of 1.248(2) (Ref. 77* in Ref. [7]) to 0.0054 and proposed a weighted mean of 1.258(10) as the evaluation, with an increase in the total uncertainty to include the most precise measurement (all values are in 10^9 years).

Thus, our evaluated half-life value for ^{40}K, based on 31 experimental results, is $T_{1/2}(^{40}$K$)= 1.258(10) \cdot 10^9$ years. This can be compared with Helmer's 2000 evaluation in ENSDF [6, 16] by converting the old evaluation of $1.277(8) \cdot 10^9$ years [17] using better nuclear constants. This conversion yielded a value of $1.265(13) \cdot 10^9$ years.

4. ^{53}Mn

Traces of ^{53}Mn have recently been discovered in meteorites using the ^{53}Cr/^{52}Cr isotope anomaly (see Ref. [4] and its references). The half-life of ^{53}Mn, which decays to stable ^{53}Cr by electron capture, has been measured in 7 studies (Refs 84-90 in Ref. [7]). For our evaluation using the EV1NEW program, we excluded the 3 early measurement results (Refs 84-86 in Ref. [7]) and used the 4 experimental values revised by Holden [7] (Table 2).

Our evaluated value of $T_{1/2}$ (^{53}Mn$)=3.7(2) \cdot 10^6$ years coincides with Holden's evaluation [7], which only used the last 3 values from Table 2. It can also be compared with the 1999 ENSDF evaluation [6], where one of the best experimental results, $3.74(4) \cdot 10^6$ years [18], is taken as the evaluated value without revision.

Table 2

Measurement results for the half-life of ^{53}Mn

Primary author	Year	$T_{1/2}$ / (10^6 years)	Ref. No. in Ref. [7]	Remarks
Sheline	1957	2	84	Excluded from evaluation
Kaye	1965	1.9 (5)	85	Excluded from evaluation
Hohlfelder	1969	10.8 (45)	86	Excluded from evaluation
Matsuda	1971	2.9 (12)	87	
Hondo	1971	3.7 (2)	88	Value revised by Holden [7]
Woeldle	1972	3.8 (6)	89	Value revised by Holden [7]
Heimann	1974	3.7 (4)	90	Value revised by Holden [7]

5. ^{60}Fe

This short-lived chronometer of the early history of the solar system has been thoroughly studied in a number of recent papers containing analyses of the linear correlation of the relative abundances of ^{60}Ni/^{58}Ni in meteorites (see Ref. [4] and its references). The half-life of ^{60}Fe, which decays into ^{60}Co^m and then into stable ^{60}Ni, has been measured with an uncertainty only in one study [19], by analysing the time dependence of ^{60}Co^m gamma radiation intensity (10.5 min): $T_{1/2}$ (^{60}Fe) = 1.5(3)$\cdot$10^6 years.

6. ^{87}Rb

^{87}Rb is widely used in nuclear geochronology, as it is assumed that ^{87}Rb and its daughter product ^{87}Sr, and ^{86}Sr, were formed simultaneously during nucleosynthesis [3]. This means that the development of the ^{87}Rb/^{86}Sr and ^{87}Sr/^{86}Sr ratios must be represented as a straight (isochronous) line, which in turn means that the ages of the minerals containing these nuclides can be determined reliably if the half-life of ^{87}Rb is known.

Since 1931 there have been 27 measurements of the half-life of ^{87}Rb [7]. However, Neumann and Huster (Ref. 113 in Ref. [7]) demonstrated that the early measurement results have major systematic errors and we have therefore used the experimental values obtained since 1964 for our evaluation (Table 3).

Table 3

Measurement results for the half-life of ^{87}Rb

Primary author	Year	$T_{1/2}$ / (10^{10} years)	Ref. No. in Ref. [7]	Remarks
Kovach	1964	4.77 (10)	110	
Thode	1965	4.60 (6)	111	
Brinkman	1965	5.22 (15)	76	
McMullen	1966	4.72 (4)	112	Excluded from evaluation
Neumann	1974	4.88 (8)	113	
Davis	1977	4.89 (4)	114	Revised result for McMullen's measurement
Akatsu	1981	5.560 (25)	115	Excluded from evaluation

During statistical processing, the EV1NEW program excluded Akatsu's measurement result (Ref. 115 in Ref. [7]) as a statistical outlier. A modified Bayerian procedure [20, 21] was selected when obtaining the evaluated value for the set of the 5 remaining measurement results. Our evaluated value of $T_{1/2}$ (^{87}Rb)=4.82(8)$\cdot$10^{10} years can be compared with the 1991 ENSDF evaluation of 4.77(4)$\cdot$10^{10} years [6], which was obtained as the weighted mean of McMullen's and Neumann's measurement results (Refs 112 and 113 in Ref. [7]) not taking into account the

revision of McMullen's result, and with Holden's evaluation of $4.88(5) \cdot 10^{10}$ years [7], also used the non-weighted mean of Neumann's and Davis' results (Refs 113 and 114 in Ref. [7]).

7. ^{93}Zr

No traces of this short-lived chronometer of the early history of the solar system have yet been found in meteorites, but it is assumed that it is formed in s-process nucleosynthesis and may be injected into the protosolar nebula from asymptotic-branch red giants [22].

The half-life of ^{93}Zr, which decays into stable ^{93}Nb, is measured with an uncertainty in only one paper: $T_{1/2}$ (^{93}Zr)$=1.53(10) \cdot 10^6$ years [23].

8. ^{98}Tc

The discovery of technetium lines in the spectra of stars, technetium having no stable isotopes, is important evidence of ongoing nucleosynthesis [3]. ^{98}Tc is the technetium isotope with the longest half-life. In line with ENSDF (1998 evaluation) [6], we adopt the measurement result of $T_{1/2}$ (^{98}Tc)$=4.2(3) \cdot 10^6$ years from Ref. [24] as the evaluated value, as the other measurements are much less accurate and their results are given without uncertainties (see Ref. [6]).

9. ^{107}Pd

The presence of this radionuclide in the early solar system is confirmed by convincing data on the correlation of the ^{107}Ag/^{109}Ag concentration ratio with the relative ^{108}Pd/^{109}Ag content in meteorites [25]. The half-life of ^{107}Pd, which decays into stable ^{107}Ag, is measured in Ref. [26]: $T_{1/2}$ (^{107}Pd)$=6.5(3) \cdot 10^6$ years.

10. ^{129}I

^{129}I is one of the primary short-lived chronometers indicating the possibility of a burst of nucleosynthesis immediately before the solar system was formed [3, 4].

To evaluate the half-life of ^{129}I formed in r-process nucleosynthesis [3] and decaying into stable ^{129}Xe, we used all 4 existing experimental values (Table 4).

Table 4

Measurement results for the half-life of ^{129}I

Primary author	Year	$T_{1/2}$ / (10^7 years)	Ref. No. in Ref. 7	Remarks
Katcoff	1951	1.72 (9)	117	
Russel	1957	1.56 (6)	118	
Emery	1972	1.57 (4)	119	Uncertainty increased to 0.047
Kuhry	1973	1.97 (14)	120	

During the statistical processing of the set of 4 results studied, the EV1NEW program - using the LRSW method [20, 21] - increased the uncertainty of the 1972 measurement (Ref. 119 in Ref. [7]) to 0.047 and selected as the evaluated value the following weighted mean with an external error: $T_{1/2}$ (^{129}I)=1.61(7)$\cdot$10^7 years. This value can be compared with the 1996 ENSDF evaluation of 1.57(4)$\cdot$10^7 years [6] adopted on the basis of the 1972 measurement result (Table 4, Ref. 119 in Ref. [7]), and with Holden's evaluation of 1.7(1)$\cdot$10^7 years [7] obtained as the non-weighted mean of the 4 results shown in Table 4.

11. ^{135}Cs

It is assumed that ^{135}Cs, like ^{60}Fe, ^{83}Zr and ^{107}Pd, is formed in the s-process at the helium-burning stage in asymptotic-branch red giant stars [22].

As in Ref. [6] (1998 evaluation), we obtained the evaluated half-life value for ^{135}Cs by weighting the three existing measurement results, 2.1(7)$\cdot$10^6 years [27], 2.95(30)$\cdot$10^6 years [28] and 2.0(2)$\cdot$10^6 years [29]: $T_{1/2}$ (^{135}Cs)=2.4(4)$\cdot$10^6 years.

The difference between this evaluated value and the ENSDF evaluation of 2.3(3)$\cdot$10^6 years is due to our statistical procedure's use of the limitation of relative statistical weight method (LRSW) [20, 21] which increases the uncertainty from Ref. [29] to 0.276$\cdot$10^6 years, and to the use of the Student coefficient to increase the uncertainty of the evaluated value when the number of measurements is small [8, 9].

12. ^{146}Sm

^{146}Sm is transformed into stable ^{142}Nd by alpha decay. The existing data on the radiogenic ^{142}Nd content in meteorites diverge significantly, but they do indicate the presence of ^{146}Sm in the early solar system. The half-life of ^{146}Sm is measured in 5 studies (Table 5).

Table 5

Measurement results for the half-life of ^{146}Sm

Primary author	Year	$T_{1/2}$ / (10^7 years)	Reference	Remarks
Dunlavey	1953	5	[30]	Excluded from evaluation
Friedman	1963	8.5 (12)	[31]	
Nurmia	1964	7.4 (15)	[32]	
Friedman	1966	10.26 (48)	[33]	
Meissner	1987	10.31 (45)	[34]	

We used the 4 values with an uncertainty from Table 5 [31-34] and obtained an evaluated value $T_{1/2}$(^{146}Sm)=1.00(5)$\cdot$10^8 years, which may be compared with the 1997 ENSDF evaluation of 1.03(5)$\cdot$10^8 years [6] obtained as the weighted mean of the last two measurement results from Refs [33, 34].

13. ^{176}Lu

This long-lived radionuclide plays an important role in s-process cosmochronology, since the other long-lived chronometers ^{187}Re, ^{232}Th, ^{235}U and ^{238}U are formed in r-process nucleosynthesis. ^{176}Lu is shielded from the r-process by the stable ytterbium isotope ^{176}Yb and appears to be formed only in the s-process as the p-process contribution to its formation is estimated at < 5 % [2, 3].

Since 1938 there have been 21 measurement results for the half-life of ^{176}Lu [6, 7, 47]. Based on the analysis in Ref. [35], which indicates significant systematic errors in a number of studies where sources of natural Lu_2O_3 were measured, 8 measurement results since 1965 can be included in the evaluation (Table 6).

The EV1NEW program proposed using a modified MBAYS procedure (see Refs 20, 21]) to obtain the evaluated value. The evaluated value of $T_{1/2}$ (^{176}Lu)=3.77(5)$\cdot 10^{10}$ years was obtained as the weighted mean of 8 measurement results with an uncertainty using MBAYS. In the 1998 ENSDF evaluation [6], 7 measurement results from 1965-1992 were used and the evaluated value of 4.00(22)$\cdot 10^{10}$ years was obtained as a non-weighted mean, increasing the total uncertainty to include the most precise value of 3.78(2)$\cdot 10^{10}$ years. As a result, the uncertainty of the evaluated value does not correspond to the accuracy level of the majority of published studies, levelling the results obtained in them. Our evaluation agrees better with Holden's of 3.8(1)$\cdot 10^{10}$ years [7] which, however, used a different set of data for the evaluation (Refs 158-162 in Ref. [7]).

Table 6

Measurement results for the half-life of ^{176}Lu

Primary author	Year	$T_{1/2}$ / (10^{10} years)	Ref. No. in Ref. [7]	Remarks
Brinkman	1965	3.59 (5)	76	
Sakamoto	1967	5.0 (3)	155	
Komura	1972	3.79 (3)	158	
Norman	1980	4.08 (24)	159	
Sato	1983	3.78 (2)	162	
Gehrke	1990	4.05 (9)	-	[35]
Dalmasso	1992	3.73 (5)	-	[36]
Nir-El	1998	3. 68(2)	-	[47]

The criticism in Ref. [48] of the measurement result in Ref. [47] should be noted. M.M. Be [48] indicates that the uncertainty of this measurement is low owing to insufficiently accurate detector calibration in the 200-300 keV gamma radiation energy region. We nevertheless used the result given by the authors in Ref. [47] for the evaluation, to avoid introducing a subjective element in the statistical processing.

14. ^{182}Hf

Neither traces of ^{182}Hf nor of ^{93}Zr have yet been found in meteorites, but it is assumed that it must have been present in the early solar system owing to the ejection of s-process elements from asymptotic-branch red giant stars [22].

The evaluated half-life value of ^{182}Hf, which decays into ^{182}Ta and then into stable ^{182}W, was obtained using the LRSW method [20, 21] as a weighted mean of the two measurement results with uncertainties: 8.0(5)·10^6 years [37] and 9(2)·10^6 years [38]. The third measurement result (8.5·10^6 years, see Ref. [6]), is given without an uncertainty. The evaluated value of $T_{1/2}$ (^{182}Hf)=8.5(14)·10^6 years can be compared with the 1995 ENSDF value of 9(2)·10^6 years [6] - this value is taken from Ref. [38].

15. ^{182}Re

^{187}Re is of considerable significance in nuclear cosmochronology; one of the methods for evaluating the age of the galaxy and the length of r-process nucleosynthesis is based on its half-life [2, 3].

The half-life of ^{187}Re has been measured in many studies since 1948 [7]. It was thought that measuring $T_{1/2}$(^{187}Re) by determining the specific activity using a proportional counter yielded values which were systematically too high (~6·10^{10} years) because of unobservable decay to ^{187}Os bound states. However, Ref. [40] recently demonstrated that more thorough measurements using a proportional counter agree, within the margins of error, with mass spectrometry measurements yielding a decay branch to bound states of (3±6)%.

We used 8 experimental values to obtain the evaluated value for the half-life of ^{187}Re (Table 7).

Table 7

Measurement results for the half-life of ^{187}Re

Primary author	Year	$T_{1/2}$ / (10^{10} years)	Ref. No. in Ref. [7]	Remarks
Herr	1958	6.2(7)	179	Excluded from evaluation
Hirt	1962	4.3(5)	182	[41]
Brodzinski	1965	6.6(13)	183	Excluded from evaluation
Payne	1965	4.7(5)	-	See Ref. [6] in Ref. [40]
Luck	1980	4.28(21)	-	-
Luck	1983	4.56(12)	185	Revised by Holden [7]
Naldrett	1984	3.5(4)	8	
Lindner	1989	4.23(13)	186	Revised value [39]
Ashktorab	1993	4.5(3)	-	[40]
Galeazzi	2001	4.12(11)	-	[42]

The value of $4.23(13) \cdot 10^{10}$ years given in Lindner et al. (Ref. 186 in Ref. [7]) is a correction by the authors of their 1986 measurement ($4.35(13) \cdot 10^{10}$ years) [39] based on mass spectrometry observation of ^{187}Os growth. The latter value was adopted in ENSDF [6] as the evaluated value (1991 evaluation).

Our evaluation takes into account the results of new $T_{1/2}$ (^{187}Re) measurements performed in the laboratory using a high temperature quartz proportional counter [40] and a cryogenic microcalorimeter [42]. The evaluated value obtained as a weighted mean with an uncertainty which is the lowest from the available experimental data: $T_{1/2}$ (^{187}Re)=$4.29(11) \cdot 10^{10}$ years.

We also performed a separate evaluation of the half-life of ^{187}Re for 2 sets consisting, respectively, of 3 measurements performed using isotope analysis of molybdenum ores and meteorites, and 5 results from laboratory measurements using a proportional counter, a liquid scintillator and a cryogenic microcalorimeter, and mass spectrometry analysis of ^{187}Os growth. The first set comprises the values 4.3(5), 4.28(21) and 4.5(2) (Refs 182, 185 and 186 in Ref. [7] and Ref. [41]). The second set comprises the values 4.7(5), 3.5(4), 4.5(3), 4.12(11) and 4.23(13) (see Ref. [40] and its references, and also Ref. [42] and Ref. 186 in Ref. [7]). (All values are in 10^{10} years).

The evaluated values obtained for the two sets are $4.42(13) \cdot 10^{10}$ years and $4.18(11) \cdot 10^{10}$ years respectively. Comparing these data, $\Delta T_{1/2} = 0.24(18) \cdot 10^{10}$ years. Thus we may conclude that the decay rate of ^{187}Re did not change by more than 10% in $4 \cdot 10^9$ years (the age of the ores and meteorites), i.e. $|d\lambda/\lambda dt| \leq 2 \cdot 10^{-11}$ a^{-1}. If the change in λ was caused by a change over time in the fine structure constant α (see Ref. [2]), the upper limit for the rate of change in α is $|d\alpha/\alpha dt| \leq 10^{-15}$ a^{-1}. If this change is related to a change over time in the weak interaction constant g_w, the upper limit is $|dg_w/g_w dt| \leq 10^{-11}$ a^{-1}.

16. ^{205}Pb

Several attempts have been made in various years to find evidence of the presence of ^{205}Pb in meteorite matter during its solidification. These have resulted in the establishment of an upper limit for the relative ^{205}Pb/^{204}Pb concentration at the point of meteorite solidification [2]. As ^{205}Pb is formed in s-process nucleosynthesis, its discovery in the early solar system is of great significance in evaluating how the time interval between the solidification of matter in the solar system and the last s-process nucleosynthesis events.

^{205}Pb decays into the stable thallium isotope ^{205}Tl by electron capture. The decay energy is low (55 keV) and only LX- and MX-radiation are observed in ^{205}Pb decay. Only the partial half-life of ^{205}Pb has been measured experimentally for L-capture: $T_{1/2}$ (ε_L)=$2.5(1) \cdot 10^7$ years [43].

In this paper, we have not made a new evaluation of the total half-life of ^{205}Pb, because no newer experimental data have been published than that on which the 1993 ENSDF evaluation is based [6]. The calculation of the total half-life of ^{205}Pb in Ref. [6], which is based on the theoretical value $\varepsilon_{MNO/\varepsilon_L} = 0.639$, yields a value of $T_{1/2}$ (^{205}Pb)=$1.53(7) \cdot 10^7$ years.

17. ^{232}Th, ^{235}U, ^{238}U

The long-lived radionuclides ^{232}Th, ^{235}U and ^{238}U are formed in r-process nucleosynthesis and can be used to determine its duration in the Galaxy.

As there have been no new publications on the half-lives of ^{232}Th and ^{238}U, we use our old evaluations from Ref. [44] here: $T_{1/2}$ (^{232}Th)=1.40(1)·10^{10} years, $T_{1/2}$ (^{238}U)=4.468(3)·10^{9} years. The evaluated value for the half-life of ^{235}U and ^{238}U is a rounding of the most accurate measurement result from Ref. [45]: $T_{1/2}$ (^{235}U)=7.038(5)·10^{8} years.

18. ^{244}Pu

Research into ^{244}Pu traces began in 1960 when an abundance of heavy xenon isotopes was found in the Pasamonte achondritic meteorite whose origin was ascribed to spontaneous fission of nuclei which had decayed during the lifetime of the meteorite. It was subsequently demonstrated that the fissile radionuclide was ^{244}Pu [2].

The half-life of ^{244}Pu is determined mainly by its alpha decay into ^{240}U which eventually, through a decay chain, transforms into ^{232}Th. We obtained the evaluated value for the total half-life of ^{244}Pu of $T_{1/2}$ (^{244}Pu)=8.02(11)·10^{7} years in Ref. [46], and it is based on the data from 4 experimental studies. The results of two of these were corrected using up-to-date constant values (see Ref. [46]). Our evaluated value is slightly different from the 1996 ENSDF evaluation of 8.00(9)·10^{7} years [6] studies based on the same measurement results.

19. ^{247}Cm

^{247}Cm is formed in r-process nucleosynthesis and eventually decays into ^{235}U. Therefore the relative ^{235}U content in meteorites may serve as an indication of the presence of ^{247}Cm in the early solar system [2, 4].

We evaluated the half-life of ^{247}Cm as the weighted mean of the results of 2 measurements (see Ref. [46]): $T_{1/2}$(^{247}Cm)=1.56(5)·10^{7} years. This coincides with the 1993 ENSDF evaluation [6].

20.   Conclusion

Table 8 summarizes the evaluated half-life values for the 20 radionuclides, showing the number of experimental results included in the evaluation and their time span.

As can be seen from the table, for the 20 radionuclides studied very few of the evaluated half-life values are based on up-to-date experimental data. Additional measurements are required primarily for the half-lives of ^{60}Fe, ^{93}Zr, ^{98}Tc, ^{107}Pd, ^{135}Cs, ^{182}Hf and ^{205}Pb. The author wishes to thank the following staff at the Radionuclide Data Centre of the Radium Institute for their help with this study: L.M. Bak, T.B. Posternyak, E.S. Chechev.

Table 8

**Evaluated half-life values for 20 radionuclides
used in nuclear geochronology and cosmochronology**

Nuclide	Number of measurement results included in evaluation	Time span of publications	Evaluated half-life value, years
^{26}Al	4	1972-1984	$7.17(24) \cdot 10^5$
^{40}K	31	1947-1977	$1.258(10) \cdot 10^9$
^{53}Mn	4	1971-1974	$3.7(2) \cdot 10^6$
^{60}Fe	1	1964	$1.5(3) \cdot 10^6$
^{87}Rb	5	1964-1977	$4.82(8) \cdot 10^{10}$
^{93}Zr	1	1972	$1.53(10) \cdot 10^6$
^{98}Tc	1	1973	$4.2(3) \cdot 10^6$
^{107}Pd	1	1969	$6.5(3) \cdot 10^6$
^{129}I	4	1951-1973	$1.61(7) \cdot 10^7$
^{135}Cs	3	1949-1955	$2.4(4) \cdot 10^6$
^{146}Sm	4	1963-1987	$1.00(5) \cdot 10^8$
^{176}Lu	8	1965-1998	$3.74(4) \cdot 10^{10}$
^{182}Hf	2	1961	$8.5(14) \cdot 10^6$
^{187}Re	8	1958-2001	$4.29(11) \cdot 10^{10}$
^{205}Pb	1	1958	$1.53(7) \cdot 10^7$
^{232}Th	5	1956-1963	$1.40(1) \cdot 10^{10}$
^{235}U	4	1971-1974	$7.038(5) \cdot 10^8$
^{238}U	8	1949-1971	$4.468(3) \cdot 10^9$
^{244}Pu	4	1956-1969	$8.02(11) \cdot 10^7$
^{247}Cm	2	1971	$1.56(5) \cdot 10^7$

References

1. Begemann F., Ludwig K.R., Lugmair G.W., et al., Call for an improved set of decay constants for geochronical use, Geochimica et Cosmochimica Acta, 2001, accepted for publication; see ICRM Liquid Scintillation Counting Worring Group meeting, Saclay November 20 and 21, 2000.

2. Chechev V.P., Kramarovskij Ya.M., Radioactivity and the evolution of the universe, Moscow, Nauka, 1978, p. 61 [in Russian].

3. Kramarovskij Ya.M., Chechev V.P., Element synthesis in the universe, Moscow, Nauka, 1987, p. 143 [in Russian].

4. V.P. Chechev, Izv.AN, ser. Fiz., 2000, v. 64, No. 5.

5. Dyson F.J., The fundamental constants and their time variation, in: Aspects of quantum theory, Ed. A. Salam and E.P. Wigner, Cambridge Univ. Press, 1972.

6. Evaluated Nuclear Structure Data File (ENSDF), Brookhaven National Laboratory, USA.

7. Holden N.E., Pure and Appl. Chem., 1990.

8. Chechev V.P., Voprosy atomnoj nauki i tekhniki, ser.: Yadernye konstanty, 1996, No. 2, p. 126.

9. Chechev V.P., Izmeritel'naya Tekhnika, 1998, No. 8, p. 47

10. Chechev V.P. and Egorov A.G., Appl. Radiat. Isotop., 2000, v. 52, No. 3, p. 601.

11. Browne E., Limitation of relative statistical weights, a method for evaluating discrepant data, INDC (NDS) - 363, IAEA, Vienna, 1998.

12. Samworth E.A., Warburton E.K., Engelbertink, Phys. Rev. C, 1972, v. 5, p. 138.

13. Norris T.L., Gancarz A.J., Rokop D.J., Thomas K.W., J. Geophys. Res. (supplement), 1983, v. 88B, p. 333.

14. Middleton R., Klein J., Raisbecr G.M., Yiou F., Nucl. Instr. Meth., 1983, v. 218, p. 430.

15. Thomas J.H., Rau R.L., Skelton R.T., Kavanagh R.W., Phys Rev. C, 1984, v. 30, p. 385

16. Be M.M., Duchemin D., Browne E., Chechev V., Helmer R., Schonfeld E., Table de Radionucleides, Comments on evaluations, Comments M.M.Be, Document CEA-ISBN 2 7272 02113, CEA, Saclay, 1999.

17. Endt P.M., Leun C. van der, Nucl Phys. A, 1973, v. 214, p. 1.

18. Hondo M., Imamura M., Phys. Rev. C, 1971, v. 4, p. 1182.

19. Kutschera W., Billquist P.J., Frekers D., Henning W., Jensen K.J., Xiuzeng Ma, Pardo R., Paul M., Rehm K.E., Smither R.K., Yntema J.L., Mausner L.F., Nucl. Instrum. Meth. Phys. Res., 1984, v. B5, p. 430.

20. Rajput M.U., MacMahon T.D., Nucl. Instr. Meth. Phys. Res., 1992, v. A312, Nos 1, 2, p. 289.

21. Kafala S.I., MacMahon T.D. and Gray P.W., Nucl. Instr. Meth. Phys. Res., 1994, v. A339, p. 151.

22. Wasserburg G.J., Busso M., Gallino R., and Raiteri C.M., The Astrophysical Journal, 1994, v. 424, p. 412.

23. Anonymous F., in: REPT MSUCL 71/72 Annual, 1972, p. 50.

24. O'Kelley G.D., Goeking C.F., Collins L.L., Priv. Comm., August 1973.

25. Nuclear Astrophysics, Ed. Barnes, Clayton D., Schramm D., Moscow, Mir, 1986, p. 124 [in Russian].

26. Griffin H.C., Pierson W.R., Phys. Rev., 1969, v. 183, p. 991.

27. Sugarman N., Phys. Rev., 1949, v. 75, p. 1473.

28. Zeldes H., Brosi A.R., Parker G.W., Hebert G.M., Creek G.E., in: ORNL-286, 1950, p. 48.

29. Parker G.W., Martin W.J., Creek G.E., Lantz P.M., in: Proc. UN Intern. Conf. Peaceful Uses At. Energy, Geneva, 1955, v. 14, p. 96.

30. Dunlavey D.C., Seaborg G.T., Phys. Rev., 1953, v. 92, p. 206.

31. Friedman A.M., Milsted J., Harkness A.L., Bull. Am. Phys. Soc., 1963, v. 8(7), p. 525.

32. Nurmia M., Graeffe G., Valli K., Aaltonen J., Ann. Acad. Sci. Fennicae, 1964, Ser. A VI, No. 148.

33. Friedman A.M., Milsted J., Metta D., Henderson D., Lerner J., Harkness A.L., Rokop D.J., Radiochim. Acta., 1966, v. 5, p. 192.

34. Meissner U-G., Kaiser N., Weise W., Nucl. Phys. A, 1987, v. 466, p. 685.

35.   Gehrke R.J., Casey C., Murray R.K., Phys. Rev. C, 1990, v. 41, p. 2878.

36.   Dalmasso J., Barci-Funel G., Ardisson G.J., Appl. Radiat. Isot., 1992, v. 43, p. 69.

37.   Naumann R.A., Michel M.C., J. Inorg. Nucl. Chem., 1961, v. 17, p. 189.

38.   Wing J., Swartz B.A., Huizenga J.R., Phys. Rev., 1961, v. 123, p. 1354.

39.   Lindner M., Leich D.A., Borg R.J., Russ G.P., Bazan J.M., Simons D.S., Date A.R., Nature, 1986, v. 320, p. 246.

40.   Ashktorab K., Janecke J.W., Becchetti F.D., and Roberts D.A., Phys. Rev. C, v. 47, No 6, p. 2954.

41.   Luck J.M., Birck J.L., and Allegre C.J., Nature, 1980, v.283, p. 256.

42.   Galeazzi M., Fontanelli F., Gatti F., and Vitale S., Phys. Rev. C, 2001, v. 63, p. 014302.

43.   Wing J., Stevens C.M., Huizenga J.R., Phys. Rev., 1958, v. 111, p. 590.

44.   Khol'nov Yu.V., Chechev V.P., Kamynov Sh.V., et al., Evaluated values for the nuclear physics characteristics of radionuclides used in the national economy, Moscow, Ehnergoizdat, 1982 [in Russian].

45.   Jaffey A.M., Flynn K.F., Glendenin L.E., Phys. Rev. C, 1971, v. 4, p. 1889.

46.   Chechev V.P., Kuz'menko N.K., Sergeev V.O., Artamonova K.P., Evaluated values for the nuclear physics characteristics of transuranium radionuclides, Moscow, Ehnergoatomizdat, 1988 [in Russian].

47.   Nir-El Y., Lavi N., Appl. Radiat. Isot., 1998, v. 49, p. 1653.

48.   Be M.-M., Half-life of radionuclides used in geochronology, Comments, in: ICRM Liquid Scintillation Counting Worring Group meeting, Saclay November 20 and 21, 2000.

UDC 539.17:621.039

TEST CALCULATIONS OF PHOTONEUTRONS EMISSION FROM SURFACE OF URANIUM SPHERE IRRADIATED BY 28 MeV ELECTRONS

A.I. Blokhin[1], I.I. Degtyarev[2]

[1]Institute of Physics and Power Engineering, 249020 Obninsk, Russia
[2]Institute for High Energy Physics, Protvino, Russia

1. Introduction

In this paper are reported the results of physical verification for the BOFOD [1] photonuclear data files available for the uranium isotopes U^{235}, U^{238}. These results were compared with calculated data by the parameterization driven model of photonuclear reaction and experimental data. Experimental data of photoneutron yields from surface of uranium sphere irradiated by 28 MeV electrons [2] are used for a verification. Both calculations have been carried out with the RTS&T general purpose Monte Carlo code [3] with detailed electron-photon-nucleon transport simulation using the ENDF/B-VI and EPDL evaluated data libraries.

2. RTS&T Photonuclear Reaction Models

A current version of the RTS&T general-purpose Monte Carlo transport code included the two different models to simulate of photonuclear interactions: high-precision method to make use of evaluated data libraries in ENDF-6 format and fast inclusive method to generate of neutron emission channels.

2.1. Data-Driven Model

In practice of data driven transport simulating, the files of evaluated nuclear data contains the original constant information, however, they are used not directly but after processing to multi-group constant systems. In this approach the systematic errors supplemented by treatment cannot be estimated *in principle*, since it is indivisible from the systematic errors of the evaluated data file. Modelling of transport and discrete nuclear interactions of nucleons (photons) in the energy range from thermal energy up to 150 MeV in the RTS&T code is based on the *direct* (without the interim libraries compilation) uses of ENDF/B-VI evaluated data library to detailed description of low-energy interactions. Universal data reading and preparation procedure allows to use another continuous-energy database recorded in ENDF-6 format (for example JENDL, FENDL, CENDL, JEF, BROND, ENDF-HE, LA150, IAEA Photonuclear Library [4] etc.). Llinearization (fastest method of cross sections interpolation between adjacent data points), restoration of the resolved resonances, temperature dependent Doppler broadening of the neutron cross sections and checking/correcting of angular distributions and Legendre coefficients for negative values are produced automatically with a help of standard *ENDF pre-processing codes* [5] **LINEAR**, **RECENT** (or **RECEN-DD** for Reich-Moore parameters for several elements of JENDL data library only), **SIGMA1** and **LEGEND**. As in the ENDF-6 format, recommended interpolation schemes are used to minimise the amount of data. To correct of upper energy bound problem for evaluated libraries the following extrapolation method is used: if a projectile particle energy is higher than the last energy point of the cross section tabulated in the data file, and the cross section is decreasing , then it will be linearly extrapolated to zero value, otherwise its bound value is used for higher energies. For data storage in memory and their further use the dynamically allocated tree of objects is organized. Basic objects correspond to the standard types of ENDF-6 records. All types of reactions provided by ENDF format are taken into account due to the particle interaction modelling: elastic scattering, radiative capture and reactions with production of one neutron in the exit channel, absorption with production of other type particles (and excitation of states in the residual nuclei), the fission with separate yields of prompt and delayed neutrons and residual nucleus simulation based on MF=8 data, etc. The energies and angles of emitted particles are simulated according to the distributions from 4, 5, 6, 12, 13, 14 and 15 files. For example, the following representations of outgoing energy-angle distributions for secondary particles can be used: tabular energy distributions, angular distributions via equally-probable cosine bins, Kalbach-Mann systematics for continuum energy-angle distributions (ENDF law=44), discrete two-body scattering, N-body phase-space energy distributions. The properties of residual nucleus are defined too.

2.2. Parameterization-driven model

Total cross sections of (γ, in)-channels in GDR region is calculated from the formula: $\sigma(\gamma, in) = \sigma_{abs} \cdot P(E, i)$, where σ_{abs}, P are the absorption cross section and probability of i-neutrons equilibrium emission given by

Jackson's analytical expression [6]: $P(E,i) = I(\Delta_i, 2i-3) - I(\Delta_{i+1}, 2i-1)$, where $I(z,n) = (1/n!)\int_0^z y^n \exp(-y)dy$ is incomplete gamma-function, and $\Delta_k = [(E - \sum_{k=1}^{i} B_k) - E_{thr}^f]/T$. Here, E, B_k, E_{thr}^f and $T = [1 + (1+4aU)^{1/2}]/2a$ are the excitation energy, the binding energy of i−th neutron, threshold energy of photofission reaction, and nuclear temperature, determined from the back-shifted Fermi gas model [7], respectively. $U = E - \Delta$, where Δ is a pairing correction. Level density parameter a is taken from RIPL-recommended systematics as proposed in [8]. The photoabsorption cross section is to calculate as a sum of three components: $\sigma_{abs} = \sum_{i=1}^{3} \sigma_i$. Components of i=1 to 3 correspond to the GDR, QD and baryon resonance production processes. The GDR term is given by a Lorentzian shape. RIPL-recommended compilations of giant resonance parameters are used. The QD component of total photoabsorption cross section calculated from [9]: $\sigma_{QD} = L(NZ/A)\sigma_d(E_\gamma)f_{Pauli}(E_\gamma)$, where $L = 6.5$ is the Levinger parameter, NZ is the number of neutron-proton pairs in the nucleus, σ_d is the free deuteron photodisintegration cross section, f_{Pauli} is the Pauli-blocking function:

$$f_{Pauli} = \begin{cases} a_0 + \sum_{i=1}^{4} a_i E_\gamma^i, & 20 \le E_\gamma \le 140 \ MeV \\ \exp(-D_p/E_\gamma), & otherwise \end{cases}$$

Constant factor $D_p = 73.3$ if $E_\gamma < 20$ MeV and $D_P = 24.2$ for $E_\gamma > 140$ MeV, a_i are the coefficients of polynomial approximations: $a_0 = 8.3714 \cdot 10^{-2}$, $a_1 = -9.8343 \cdot 10^{-3}$, $a_2 = 4.1222 \cdot 10^{-4}$, $a_3 = -3.4762 \cdot 10^{-6}$, $a_4 = 9.3537 \cdot 10^{-9}$. In the energy range of Δ-resonance $[P_{33}(1232)]$ the cross section can be represented by the following Gaussian function:

$$\sigma_\Delta/A = \sigma_0 + C/w\sqrt{\pi/2}\exp[-2(E_\gamma - E_c)^2/w^2],$$

there σ_0, C, E_c and w are the constant parameters obtained by the least squares fitting as listed in Table 1.

Table 1

Numerical values of the parameters for approximation of σ_Δ in the Δ - region

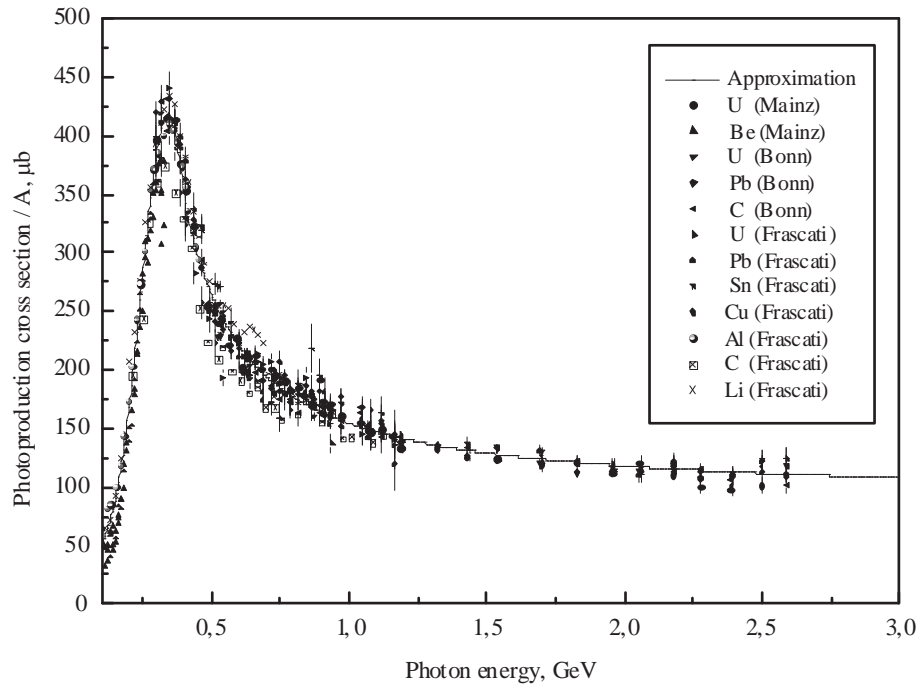| σ_0	C	E_c	w
28.20001± 3.06707	92.87255± 2.13427	0.34388± 0.0013	0.19358± 0.00309

Fig. 1. Total photoabsorption cross section

In the energy range of the higher baryon resonances $P_{11}(1440)$, $D_{13}(1520)$, $S_{11}(1535)$, $F_{15}(1680)$, shadowing threshold and shadowing regions of the total photoabsorption cross section was parameterized in form: $\sigma_\Delta / A = \sigma_0 \exp(\lambda / E_\gamma)$ (μb) where $\sigma_0 = 90.0457$ and $\lambda = 0.5378$ are the constant parameters. Figure 1 shows the parameterization of total photoabsorption cross section in comparison with Frascati, Bonn and Mainz [10-14] experimental data.

Photofission cross section in GDR region is parameterized by a sum of two Lorentzian shapes with a parameters derived from analysis of the experimental data using international nuclear data library EXFOR and original publications. Selected evaluated cross sections are also used. Above the GDR energy region (in QD and isobar production regions) it is given as follows, using the isotope fissility D_f: $\sigma_f = D_f \sigma_{abs}$. The total fission probability is expressed by the following relation [15]: $D_f^{QD} = F_2 / F_1$, where

$$F_i = \begin{cases} f_{Pauli}, & i = 1 \\ \exp(-[D - \Gamma] / E_\gamma)\{1 - \exp(-[D + \Gamma] / E_\gamma)\}, & i = 2 \end{cases}.$$

The A-dependence of the fitting parameter D is [16]: $D = 18A^{0.22} / [1 + \exp(-0.06A)]$. The energy-dependent phenomenological function Γ is quadric in $\sqrt{E_\gamma}$: $\Gamma(E_\gamma) = p_1 + p_2\sqrt{E_\gamma} + p_3 E_\gamma$, where

$$p_i = \begin{cases} p_0 + C / w\sqrt{\pi/2} \exp[-2(A - A_c)^2 / w^2], & i = 1,3 \\ aA^2 + bA + c, & i = 2 \end{cases}$$

In Table 2 the numerical values for p_i parameters are presented. The statistical accuracy is about 10 %.

Table 2

Numerical values of the p_i parameters

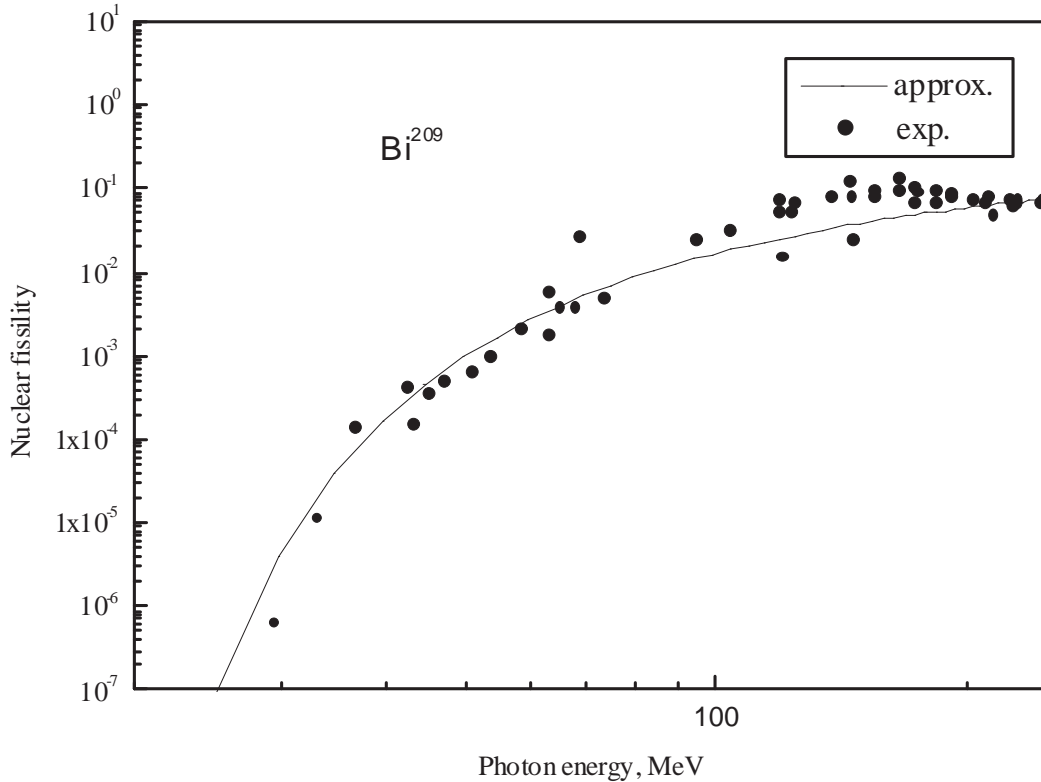| i	p_0	A_c	w	C	a	b	c
1	45.96196	234.39532	21.71405	4599.96159			
3	0.36863	234.62359	21.94853	76.18157			
2					0.0694	-32.0536	3658.581

Fig. 2. Nuclear fissility of Bi^{209}

Fig. 2 plots the experimental data of photofission probability for Bi^{209} at different photon energies from 29 to 280 MeV compared to the parameterization.

Photoneutrons are emitted isotropically with a Maxwellian energy distribution. For neutrons from (γ, f) - channel energy is sampled from fission spectrum which is taken in form proposed in [17] :

$$f(E_\gamma) = \frac{1}{2}\exp[-f_1(E_\gamma)/a]\{\exp[f_2(E_\gamma)] - \exp[-f_2(E_\gamma)]\},$$

where f_1 and f_2 are the functions of incident photon energy and the threshold energy of photofission channel, $a \approx 0.965$ is normalized factor. Average multiplicity of fission neutrons is given by the following expression: $\overline{v}_n = \alpha + \beta \ln E_\gamma$, $\alpha = 2.569$, $\beta = 0.559$.

3. Electromagnetic interactions

In current version (RTS&T 2000) of the RTS&T code following photonic processes are simulated: photoelectric effect from K, L_{I-III} atomic shells (fluorescence x-ray yield and tracking is simulated too), Rayleigh scattering, Compton scattering, pair production by photons, interactions of photons with nuclei. The EPDL [18] evaluated data of total cross sections for photon-interactions, coherent and incoherent scattering form-factors are used in the photon transport simulation for the energy range of about 10 eV to 100 GeV. To simulate the ionization processes induced by the charged particles two different models are provided: continuous energy losses model with delta-ray generation and continuous energy loss model without delta-ray production and full fluctuations below delta-ray production threshold. For calculation the mean or restricted energy loss of electrons and positrons formulae [19] are used. The density effect and shell correction terms in the stopping power formulas are included. The basic procedure used to calculate the density effect correction is described in [20]. Modified [21] set of the parameters is used. Recently, ICRU recommended data for collision stopping power for charged leptons in composite materials was included in the RTS&T 2000 code version. Multiple scattering of charged particles is simulated in modified Moliere approximation. Particle path correction due to multiple Coulomb scattering is included in the calculations as well. The discrete bremsstrahlung photon energy is sampled from a Seltzer and Berger [22] differential cross section for electron kinetic energy below 10 GeV and Bethe-Heitler cross section above this threshold. The angular distribution of emitted photon is sampled according to approximation of double differential cross section. The differences between the radiative stopping power of positrons and electrons is take into account. At very high energies the Landau-Pomeranchuk-Migdal effect is take into account too.

4. Benchmark problem

The benchmark problem was formulated as follows. The target consisted of a 7.62 cm – diameter sphere of depleted uranium (0.22 wt % of U^{235}) plated with 0.0254 cm of copper and 0.0127 cm of nickel and surrounded by a layer of water 0.20 ± 0.03 cm thickness and a type 304 stainless steel jacket, 0.07 cm thickness. A reentrant hole, 2.54 cm in diameter, admitted the 28 MeV electron beam to within 0.85 cm of the sphere. This hole is also lined with a water jacket.
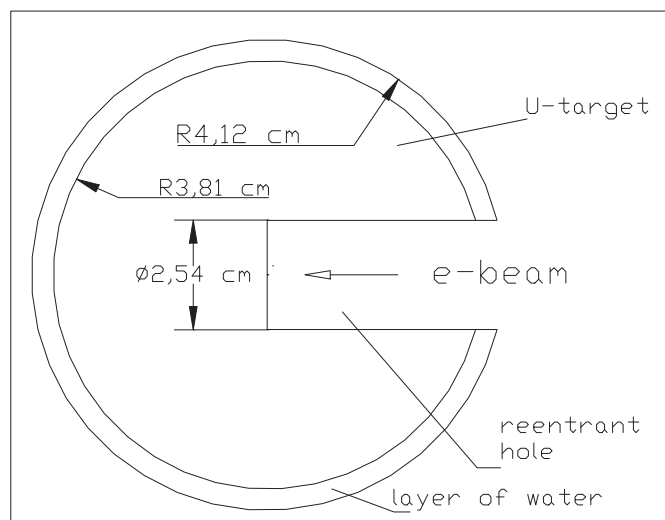

Fig. 3. Schematic target layout

5. Monte Carlo results by RTS&T code

Monte Carlo calculations were performed using RTS&T general purpose code [3]. More details on the code used on can find in the Ref. [23].
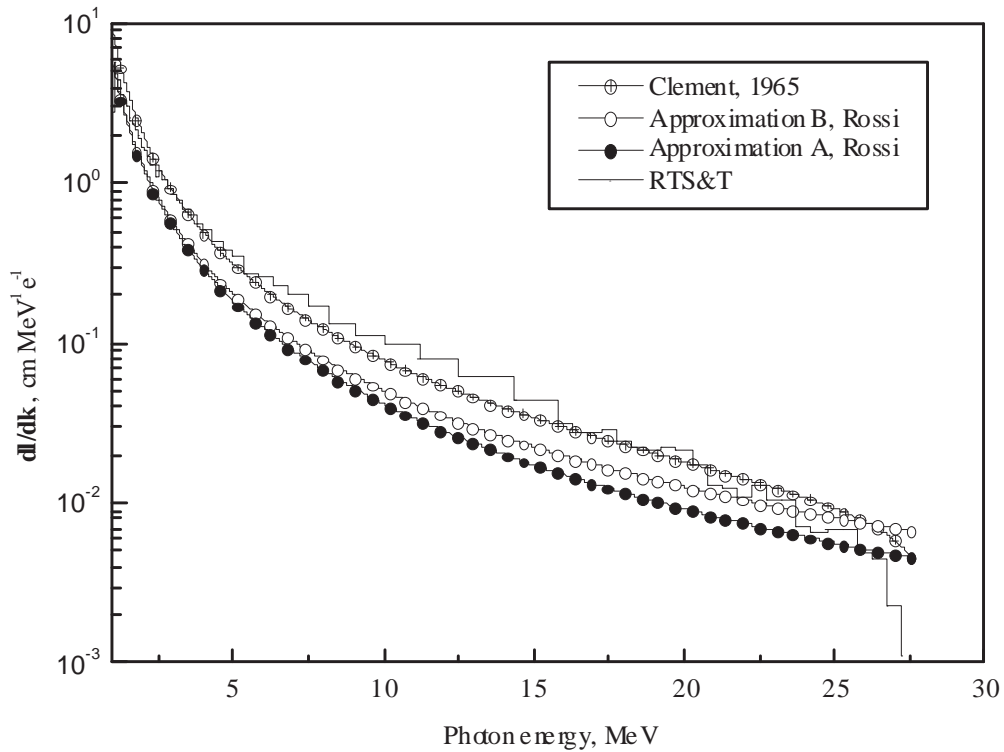

Fig. 4. Differential photon track-length distribution produced in uranium target struck by 28 MeV electrons

Fig. 4 plots the differential track length dl/dk distribution produced in uranium target struck by 28 MeV electrons calculated by RTS&T code in comparison with a three analytical estimating methods are based on Approximations A and B (Rossi , 1952) of electromagnetic shower theory and Clement formula [24], more accurate for photon energies close to that of the primary. Fig. 5 shows the energy distribution of bremsstrahlung photons
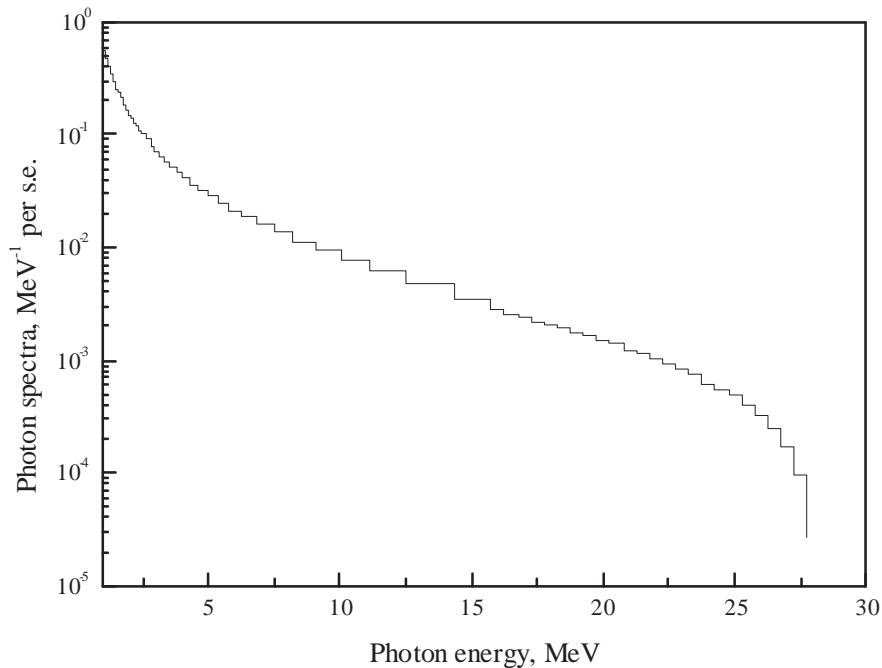

Fig. 5. Bremsstrahlung spectra induced by 28 MeV electrons in uranium target

produced by primary electron inside the target. Fig. 6 displays the hemisphere-integrated leakage spectra, measured by the time-of-flight method [2] compared with RTS&T calculations included a two different photon-nucleus interaction models: data driven model based on the BOFOD data file (DDM) and RTS&T parameterization driven model (PDM) in combination with a general data-driven procedure to simulate of low-energy nucleon (photon) transport.
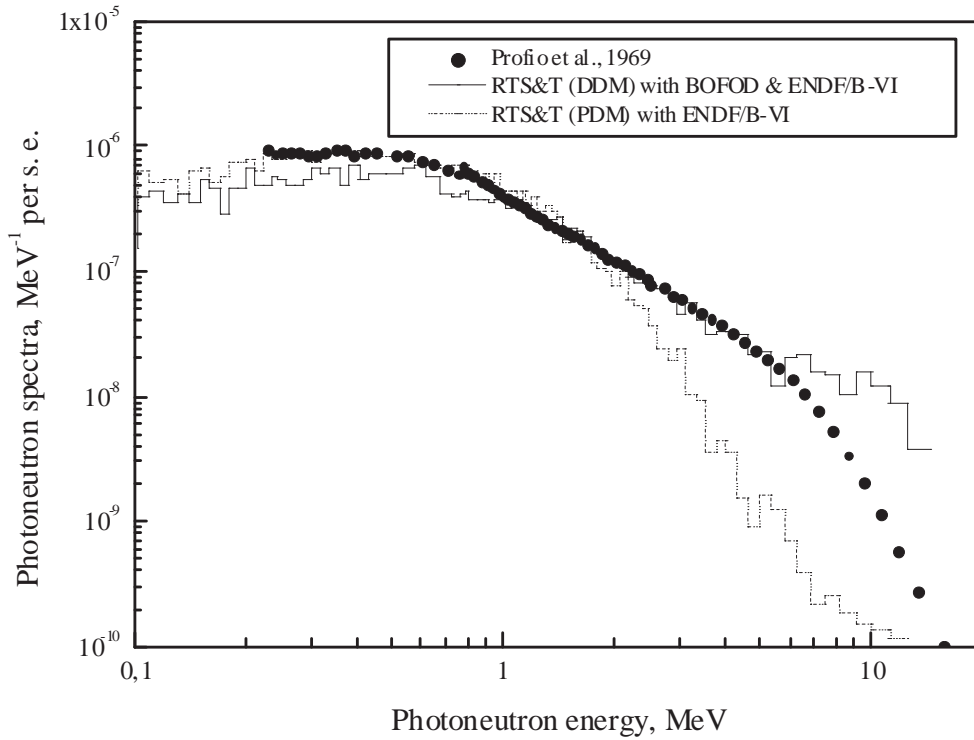

Fig. 6. Comparisons of experimental photoneutron leakage spectrum with calculations using RTS&T code
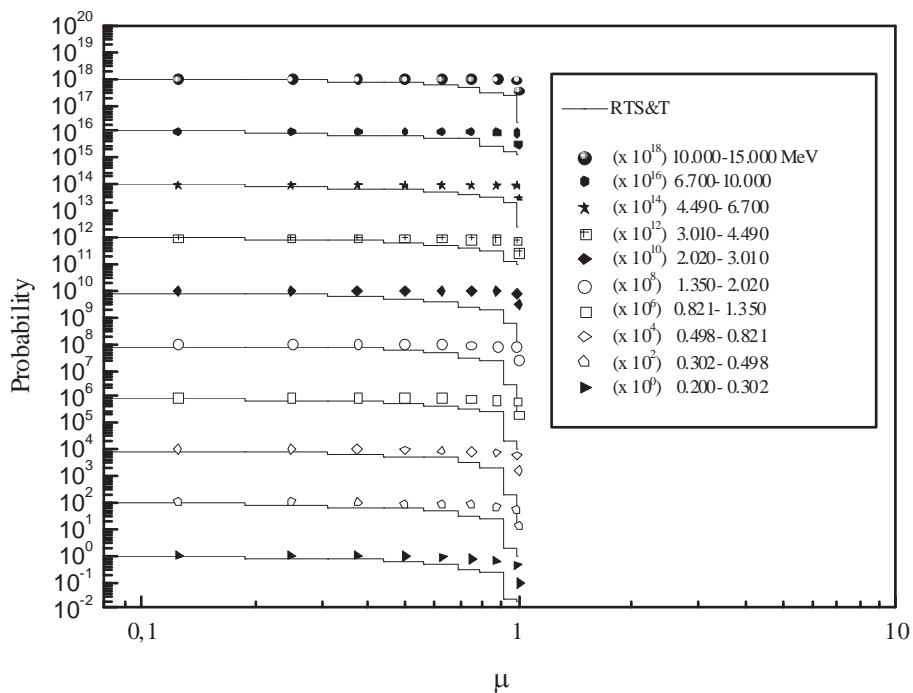

Fig. 7. Cumulative probability for photoneutrons emitted from surface of uranium target

The angular distribution of photoneutrons at the target surface is given in Fig. 7 as cumulative probability versus the cosine of the angle between the radius vector and the direction of the neutron. Numerical data are given by 10 energy groups: 0.200-0.302 , 0.302-0.498, 0.498-0.821, 0.821-1.350, 1.350-2.020, 2.020-3.010, 3.010-4.490, 4.490-6.700, 6.700-10.000, 10.000-15.000 MeV.

References

1. A.I. Blokhin et al., BOFOD-99: Present Status of the Evaluated Photonuclear Data File, IAEA Report INDC(CCP)-426, p. 119.
2. A.E. Profio, H.M. Antunez, and D.L. Huffman // Nuclear Science and Engineering, 35 (1969), p.91-103.
3. A.I. Blokhin, I.I. Degtyarev, A.E. Lokhovitskii, M.A. Maslov and I.A. Yazynin, RTS&T Monte Carlo Code (Facilities and Computation Methods), in Proceedings of the SARE-3 Workshop, KEK, Tsukuba, Japan, May 1997.
4. Handbook on Photonuclear Data for Applications (cross sections and spectra), IAEA-TECDOC-1178, Vienna, October 2000.
5. D.E. Cullen, IAEA-NDS-39, Rev. 9 (1996).
6. J.D. Jackson // Canad. J. Phys. 34 (1956), p.767.
7. W. Dilg et al. // Nucl. Phys., A217 (1973), p.269.
8. Reference Input Parameter Library (Handbook for calculations of nuclear reaction data), IAEA-TECDOC-1034, Vienna, August 1998.
9. M.B. Chadwick, P. Oblozinsky, P.E. Hodson, and G. Reffo // Phys. Rev. C44 (1991), p.814.
10. N. Bianchi et al., Phys. Lett. B299 (1993), p.219.
11. J. Ahrens et al., Phys. Lett. B98 (1981), p.423; B146 (1984), p.303.
12. U. Knessl, Proc. of Second Intern. Conf. on Dynamical Aspects of Nuclear Fission, Dubna, 1994, p. 28.
13. Th. Frommhold et al., Phys. Lett. B295 (1992), p.28.
14. V. Muccifora et al., LANL archives: nucl-ex/9810015 23 Oct. 1998.
15. P.P. Delsanto, A. Fubini, F. Mirgia and P. Quarati, Z. Phys. A342 (1992), p.291-298.
16. V. di Napoli, J. Phys. G15 (1989), L97.
17. H.C. Fesefeldt, Technical Report PITHA 85-02, III Physikalisches Institut, RWTH Aachen Physikzentrum, 5100 Aachen, Germany, September 1985.
18. D.E. Cullen et al., UCRL-50 vol. 6, 1989.
19. S.M. Seltzer and M.J. Berger, NASA Publ. SP-3012.
20. R. M. Sternheimer et al., At. Data Nucl. Data Tables v.30 (1984), p.261.
21. H. Hirayama, KEK Internal Report 95-17.
22. S.M. Seltzer and M.J. Berger // Nucl. Instr. Meth. B12 (1985), p.95-134.
23. I. I. Degtyarev, A.I. Blokhin et al., IAEA Report INDC(CCP)-426, pp. 161-188.
24. G. Clement, C.R. Acad. Sci., 257 (1963) 2971; Thesis 3e Cycle Univ. of Paris, 1964; G. Clement et al., Nuovo Cimento 37 (1965), p.876.

UDC 621.039:539.141

CALCULATIONAL ESTIMATIONS OF NEUTRON YIELD FROM ADS TARGET

I.I. Degtyarev, O.A. Liashenko, I.A.Yazynin
Institute for High Energy Physics, 142284 Protvino, Russia

V.I. Belyakov-Bodin
Institute of Theoretical and Experimental Physics, 117259 Moscow, Russia

A.I. Blokhin
Institute of Physics and Power Engineering, 249020 Obninsk, Russia

Results of computational studies of high power spallation thick ADS (Accelerator-Driven System) targets with 0.8-1.2 GeV proton beams are given. Comparisons of experiments and calculations of double differential and integral n/p yield are also described.

1 PARTICLE PRODUCTION MODELS
1.1 Intermediate energy region

1.1.1. Theory driven model

The intra-nuclear cascade-exciton model is one of the most popular to simulate of the secondary particle parameters for the $h(\gamma)A$-inelastic scattering in the intermediate region and traditionally applied to reaction above ~100 MeV. It allows one to reproduce the experimental observations up to energies ~10-20 GeV. We have developed a new model version (CEM-RTS&T) and included it as event generator to the RTS&T code [1]. In the CEM-RTS&T model the $h(\gamma)$-induced nuclear reaction is assumed to be three-step process: intra-nuclear cascade stage (INC), pre-equilibrium decay of residual nucleus and the compound nucleus decay process (evaporation/fission competition). In the INC model nuclear structure is treated as a two-component degenerated Fermi-gas of nucleons in the spherical type of nuclear density The phenomenological potential for nucleons is described as sum of the nuclear and Coulomb terms: $V^N(r) = V_N^N(r) + V_c(r)$, here $V_N^N(r) = T^F(r) + B(A,Z)$, where Fermi-energy depends on the local density of the nucleus $\rho(r)$: $T^F(r) = \frac{\hbar}{2m}\left[3\pi^2\rho(r)\right]^{1/3}$. The nucleon distribution density is of fundamental parameter of INC model. The most popular Woods-Saxon form does not satisfy the two physical requirements, namely, the asymptotic behavior and the behavior near the center of the nucleus. The semi-phenomenological nucleon density distribution proposed by Gambhir and Patil [2] in the form:

$$\rho_i(r) = \rho_{oi}^N\left\{1 + \left[\frac{1}{2} + \frac{1}{2}\left(\frac{r}{R}\right)^2\right]^{\alpha_i}\left[e^{\frac{r-R}{a_i}} + e^{-\frac{r+R}{a_i}}\right]\right\}^{-1},$$

where R is a measured size of nucleus and a_i and α_i are given in terms of the separation energy S_i of the last nucleon through: $a_i = \frac{\hbar}{2\sqrt{2mS_i}}$; $\alpha_i = \frac{q}{\hbar}\sqrt{\frac{m}{2S_i}} + 1$. Here m is the nucleon rest mass, $q=0$ *(i=n)* and $q=Z-1(i=p)$. This algebraic form designed has been tested in detail by comparing with the experiment the form factors for the electron scattering. The Coulomb potential (only for protons) $V_c(r) = (Ze^2/2R_c)[3 - (r/R_c)^2]$ $(r \le R_c)$ and $V_c(r) = Ze^2/r$ $(r > R_c)$, where R_C is the Coulomb radius. The $\pi(K)A$-interaction potential is taken as $V^{\pi(K)}(r) = -V_0^{\pi(K)}\Theta(r)$, where $V_0^\pi = 25\,\text{MeV}$, $V_0^K = 30\,\text{MeV}$, $\Theta(r)$ – is the unit step function. The center-mass correlations are taken into account as proposed in [3]. One-particle nuclear density $\tilde{\rho}(\vec{r})$ taken from the equation:

$$\rho(\vec{r}) = \int\left[\prod_{i=1}^{A}\tilde{\rho}(\vec{r}_i)\right]\delta\left(\sum_{i=1}^{A}\frac{\vec{r}_i}{A}\right)\prod_{i=2}^{A}d^3\vec{r}_i$$

where $\vec{r}_i$-is the coordinates of i-th nucleon. The Pauli blocking is incorporated in the cascade simulation procedure. The effects of particle refraction by nuclear potential and the decrease of nucleon density during intra-nuclear cascade (co-called *trailing* effect) are taken into account also. The integral hh and γh cross sections taken from the

Particle Data Group compilation. Assuming the charge symmetry the following channel cross sections are taken identical:

$$nn = pp, \ \pi^- p = \pi^+ n, \ \pi^- n = \pi^+ p, \ K^0 p = K^+ n; \ K^0 n = K^+ p.$$

The isobar production channels covered by the INC model are presented in Table 1. The strange channels like $\gamma p \to \Sigma K^+ (\Lambda K^+, \Lambda K^0 \pi^+)$ and non-strange pseudo-scalar and vector meson photoproduction channels $\gamma N \to (\rho / \omega / \eta) N$ are included also. For multi-particle final states we adopt the CERN library GENBOD (W515) routine.

Table 1

Baryon resonance production channels

Entrance channel	Exit channel
pp	$p\Delta^+, n\Delta^{++}, \Delta^+\Delta^+, \Delta^0\Delta^{++}$
pn	$n\Delta^+, p\Delta^0, \Delta^0\Delta^+, \Delta^-\Delta^{++}$
γp	$\Delta^{++}\pi^-, \Delta^{++}\pi^0, \Delta^0\pi^+$
γn	$\Delta^+\pi^-, \Delta^0\pi^0, \Delta^-\pi^+$

The *pre-equilibrium* stage of nuclear reaction simulation is based on the exciton model. The initial exciton configuration for pre-equilibrium decay formed in cascade stage of reaction or postulated in general input (2p1h configuration for incoming particle or 1p0h for incoming photon). The equilibrium stage of reaction (evaporation/fission processes) is performed according to the Weisskopf-Ewing statistical theory of particle emission and Bohr and Wheeler theory of fission. Double-humped fission barrier parameters for Z > 90 taken from the data set obtained in Obninsk and recommended by IAEA Reference Input Parameter Library (RIPL). Experimental single-humped fission barrier heights are incorporated in the RTS&T as proposed in, or according to any theoretical models. The ratio of neutron emission to fission widths taken in form proposed by Kupriyanov et al.:

$$\Gamma_n / \Gamma_f = (\tilde{\Gamma}_n / \tilde{\Gamma}_f) e^{-\frac{\delta W_g^{N-1}}{\tilde{T}_n} e^{-\lambda U_n} + \frac{\delta W_f}{\tilde{T}_f} e^{-\lambda U_f}},$$

where $\tilde{\Gamma}_n / \tilde{\Gamma}_f$ is Vandenbosch and Huizenga form of Fermi-gas model (asymptotic value occurring at high energies), δW is the shell correction term, $\lambda = 0.05$ MeV. The post-fission parameters of the fragments taken from systematics by Adeev (Z_i, A_i) and Zhao et al. (T_{kin}). The inverse reaction cross section is calculated in form $\sigma_{inv}(T) = \sigma_{geom} T_b(T)$ with $\sigma_{geom} = \pi[R + R_b + \tilde{\lambda}]^2$ where $\sigma_{geom}, R, R_b, \tilde{\lambda}$ and $T_b(T)$ are the geometric cross section, radii of the potential residual nucleus and particle, the non-relativistic reduced channel wavelength and the non-relativistic s-wave Coulomb barrier transmission probability, respectively. The s-wave transmission factor is given by expression $T_b(\rho, \eta) = [F_0(\rho, \eta)^2 + G_0(\rho, \eta)^2]^{-2}$, where F_0, G_0 are the non-relativistic zero-order regular and irregular Coulomb wave-functions of variables $\rho = \hbar^{-1}(R_1 + R_2)(2\mu T_{cms})^{1/2}$, $\eta = \hbar^{-1} Z_1 Z_2 e^2 (\mu / 2T_{cms})^{1/2}$ and Z_1, Z_2, R_1, R_2 are the charge and radii of two particles, respectively, μ is the reduced mass of the two particle system, T_{cms} is the kinetic energy in center of mass system. In the current version of RTS&T code the Fermi breakup model for disintegrating of light nuclei has replaced the evaporation model for nuclei with a mass number between 2 to 16. The evaporation of fragments with a mass number A > 4 does not included in current version RTS&T. The RIPL recommended Audi and Wapstra experimental compilation of atomic masses and binding energies is used in the RTS&T model. Level density parameter values are chosen according to the RIPL-systematics for any level density models: Gilbert-Cameron, backed-shifted Fermi-gas model, Ignatyuk form of Fermi-gas model, generalized superfluid model (GSM), microscopic GSM, shell depended model proposed by Kataria and Ramamurthy, Mughabghab and Dunford systematic determined from the neutron resonance data. To estimate of the averaged squared matrix element two different models can be used: estimation in approximation of quasi-free scattering of a nucleon above the Fermi level on a nucleon of the target nucleus [4] or by using a set of semi-empirical parametrizations. CEM-RTS&T has three different models to simulate the gamma-ray emission in pre-equilibrium and equilibrium stages: the Weisskopf single-particle model, the Brink-Axel GDR model, and the Kopecky-Uhl generalized Lorentzian model. To calculate the partial level densities for pre-equilibrium emission simulation the Avrigeanu systematic is used. Composite formulas include the advanced pairing and shell correction

in addition to the Pauli blocking effect, and average energy-dependent single-particle level densities for the excited particles and holes.

1.1.2 Parametrization driven model

The existing rigorous theoretical approaches and models allow to estimate of various characteristics of secondary particle emission due to nuclear inelastic interactions, but they have uncertainly in choice of free parameters and the calculations are time-consuming. In addition, analytical representation of double differential cross sections is important to local estimation of particle fluxes in the transport simulation algorithm. On the basis of EXFOR data sets of experimental data we obtained the improved parameters of Sychev's D2N2 systematic. They represent a better statistical average, as they are based on more experimental data. The intra-nuclear cascade-exciton model is employed to calculate the cross sections which are not measured. For the spallation reaction, the PDM model is applied in a form of summation of the double differential cross sections for secondary particle emission expressed in the laboratory frame by

$$\left(\frac{d^2\sigma}{dTd\Omega}\right)_{ij} = \sum_{k=1}^{7}\left(\frac{d^2\sigma}{dTd\Omega}\right)_k,$$ where i,j are the indexes of incident (γ, N, $\pi^{\pm}$, $K^{\pm}$, K^0, $\overline{N}$, ions) and secondary (γ, N, $\pi^{\pm}$,

$K^{\pm}$, K^0, $\overline{N}$, ions, Δ, ρ, ω) particles. Components of k=1 to 7 correspond to the quasi-elastic and charge-exchange scattering, lider particle emission, production of cascade particles, the pre-equilibrium/equilibrium relaxation, the fragmentation, the binary fission, and parametrized in functional form:

$$\left(\frac{d^2\sigma}{dTd\Omega}\right)_k = \sigma_{in}n_{ij}\frac{dN}{dT}f(T,\theta),$$ where σ_{in}, n_{ij}, $f(T,\theta)$ are inelastic cross section, average multiplicity of secondary

particles of j-th type, energy-angle correlation function, respectively.

1.2. High-energy hadronic interactions

Simulation of hA - inelastic collisions at E $\geq$ 5-10 GeV is based on a set of the inclusive semi-empirical formulas for one-particle production in *pp*-interactions, coupled with the additive quark model of $hA-$ interactions for fast- and phenomenological model for slow particles. To correct simulation of the correlations in inelastic hh- and hA-interactions modified [5] FRITIOF code can be used.

1.3. Low-energy n (γ)A-interactions

Transport and modelling of interactions of nucleons in the energy range from *thermal* energy up to 150 MeV in the RTS&T code is based on the direct uses of ENDF/B-VI evaluated data library for detailed description of low-energy interactions. Universal data reading and preparation procedure allows to use another database written in ENDF format (JENDL, FENDL, CENDL, JEF, BROND, LA150, IAEA Photonuclear Data Library etc.). Linearization, restoration of the resolved resonances, temperature dependent Doppler broadening of the neutron cross sections and checking/correcting of angular distributions and Legendre coefficients for negative values are produced automatically with a help of Cullen's ENDF pre-processing codes LINEAR, RECENT (RECEN-DD for Reich-Moore parameters of several isotopes of JENDL library only), SIGMA1 and LEGEND [6]. Recommended interpolation schemes are used to minimize the amount of data. For data storage in memory and their further use the dynamically allocated tree of objects is organized. All types of reactions provided by ENDF-6 format are taken into account due to the nucleon transport modelling: elastic scattering, radiative capture and production of one neutron in the exit channel, absorption with production of other type particles (with excitation of states in the residual nuclei), the fission with separate yields of prompt and delayed neutrons and residual nucleus simulation based on MF=8 data, etc. The energies and angles of emitted particles are simulated according to the distributions from MF=4, 5, 6, 12, 13, 14 and 15 files. For example, the following representations of outgoing energy-angle distributions for secondary particle can be used: tabular energy distributions, angular distributions via equally-probable cosine bins, Kalbach-Mann systematics for continuum energy-angle distributions (ENDF law=44), discrete two-body scattering, N-body phase-space energy distributions.

2 EXPERIMENTAL DATA ANALYSIS

The experimental results (NESSI, SATURNE) are compared with calculations performed with the RTS&T general-purpose transport code. Comparison of total neutron yield from cylindrical lead-target (d=20 cm, L=60 cm) as a function of incident proton energy is presented in Fig. 1. Fig. 2 displays the total neutron yield from Hg-, Pb-, and W-cylindrical targets (d=15 cm) irradiated by 1.2 and 2.5 GeV proton beam. The double differential cross sections of neutron production measured at Ep=0.8 GeV on 2 cm thick Pb cylindrical target presented on Fig. 3. Experimental data were obtained at the SATURNE accelerator at close angles (0, 25, 130, and 160 deg.).
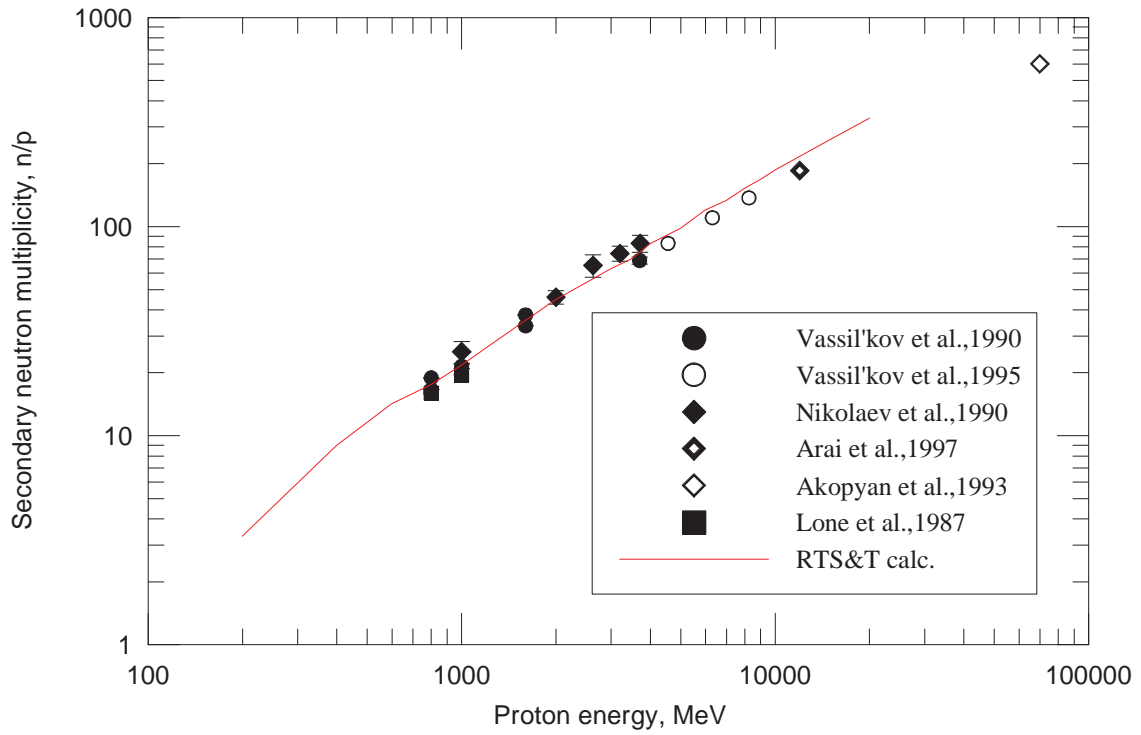
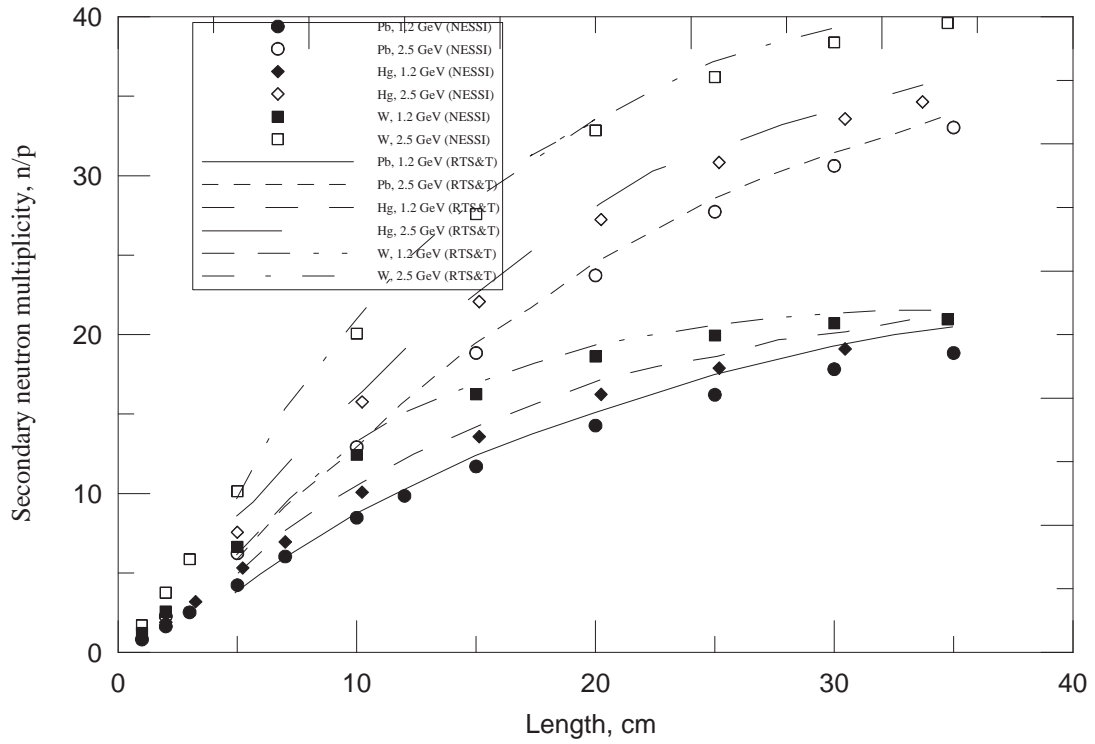Fig. 1. Total neutron yield as a function of incident proton energy

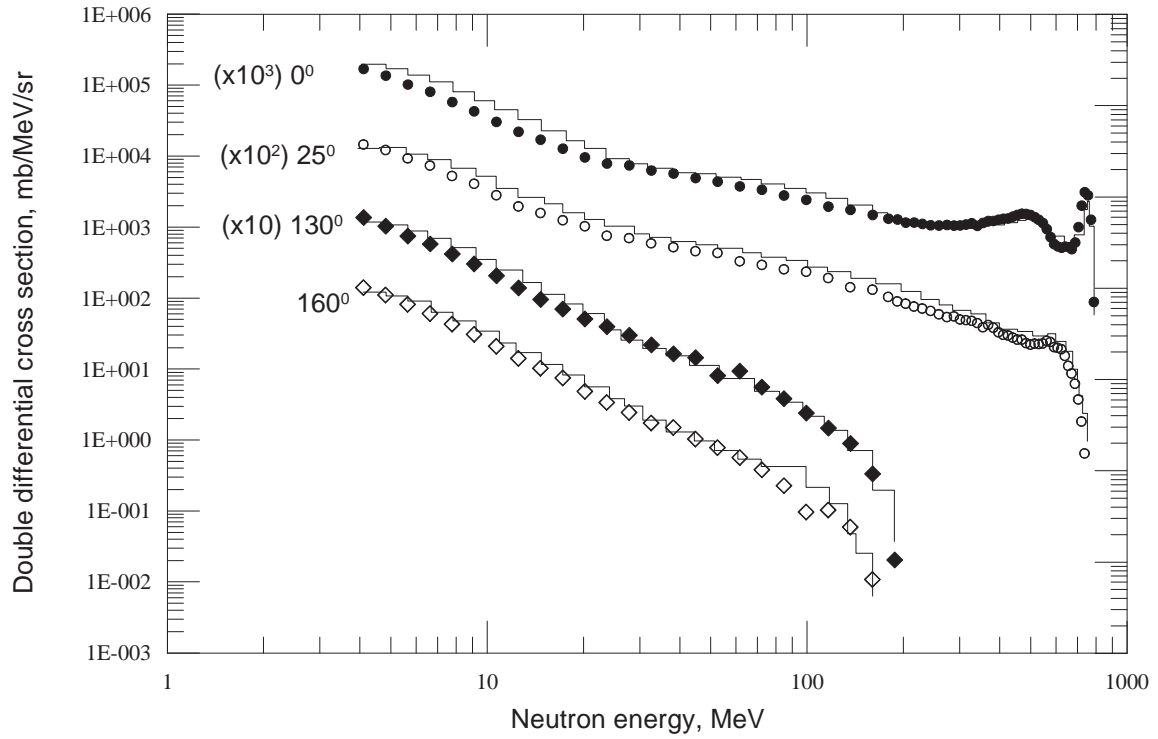Fig. 2. Total neutron yield as a function of target length

Fig. 3. $Pb(p, xn)X$ double differential cross sections at $E_p = 0.8$ GeV

References

1. A.I.Blokhin, I.I.Degtyarev et al., Proc. of the SARE-3 Workshop, KEK, 1997 // I.I. Degtyarev et al., IAEA Report INDC(CCP)-426, Vienna, 2001, p.161, p.171.
2. Y.K. Gambhir, S.H. Patil // Z.Phys. A321 (1985), p.161.
3. V.V. Uzhinskii, S.Yu. Shmakov // Yad. Fiz. 57 No. 8 (1994), pp.1532-1533.
4. K.K. Gudima et al. // Nucl. Phys. A401 (1983), p.329.
5. V.V.Uzhinskii, JINR preprint E2-96-192 (1996).
6. D.E. Cullen, Report IAEA-NDS-39, Rev. 9 (1996).

NUCLEAR REACTOR DATA

UDC 621.039.526+621.039.534

FUNDAMENTALS FOR THE DEVELOPMENT OF A LOW-ACTIVATION LEAD COOLANT WITH ISOTOPIC ENRICHMENT FOR ADVANCED NUCLEAR POWER FACILITIES

G.L. Khorasanov, A.I. Blokhin

National Research Centre - A.I. Leipunsky Institute for Physics and Power Engineering, Obninsk

FUNDAMENTALS FOR THE DEVELOPMENT OF A LOW-ACTIVATION LEAD COOLANT WITH ISOTOPIC ENRICHMENT FOR ADVANCED NUCLEAR POWER FACILITIES. The purpose of this paper is to study the prospects of new coolants for fast reactors and accelerator driven systems. The main focus is on their improvement using the isotopic tailoring technique to reduce post-irradiation activity. Calculations using the FISPACT-3 code show that irradiatinag natural lead (Pb-nat) for 30 years leads to the accumulation of long−lived toxic radionuclides, ^{207}Bi, ^{208}Bi and ^{210}Pb, which extends the cooling down period to the clearance level. This time can be shortened by using the lead isotope ^{206}Pb instead of Pb-nat. This substantially decreases the concentration of the most toxic polonium isotope, ^{210}Po. Calculations for lead activation in the hard proton-neutron ADS spectrum were performed using the CASCADE/SNT code. The time-dependent activity of the ^{207}Bi produced in Pb-nat and ^{206}Pb after irradiation for one year with a proton beam having an energy of 0.8 GeV and a current of 30 mA is given. The activity of ^{207}Bi is decreased by four orders of magnitude when ^{206}Pb is used instead of natural lead as a coolant for ADS targets. The production of such radiotoxic nuclides as ^{210}Po is also substantially diminished.

INTRODUCTION

This paper examines the radioactive waste generated by nuclear technology, which is one of the key problems - involving the long-term storage of fuel and materials, and the development of relatively clean energy sources which cause minimal environmental damage and maintain nature's radioactive balance - that the next-generation nuclear power industry will have to solve.

In the 21st century [1] Russia's large-scale nuclear power industry will be developing fast neutron reactors (FNRs) with a heavy, presumably lead, coolant, and proton accelerator driven systems (ADS). As noted in [2], spent heavy lead-bismuth or lead coolant differs from light sodium coolant in that the radionuclides accumulated in it have a long half-life, ranging from several decades to millions of years. Recently, for nuclear and thermonuclear reactors there has been a trend towards using structural and assembly materials with rapid decay rates - so-called low-activation materials. In the long term, this trend could lead to the conventional ferritic steels

in thermonuclear reactors being replaced with low-activation vanadium-chromium-titanium alloys, whose production technology is still under development. Enrichment of the ^{50}Ti isotope from its natural abundance of 5.4% to 95% in the natural titanium component of these materials can lead to a further several-fold increase in the decay rate of the activated materials [3, 4]. This approach is called isotopic tailoring and is suitable for chemical elements whose natural composition includes stable isotopes which generate long-lived radionuclides. Despite its high energy consumption and cost, isotopic tailoring can be economical in some cases: for example, when the cost of storing spent material is commensurable with the cost of enrichment of the initial material, or if significant damage is caused to the environment as a result of an accidental emission of radioactive waste into the atmosphere.

Ideas on the isotopic tailoring of materials for fission reactors were elaborated in [5, 6]. The first paper proposes enrichment of the ^{90}Zr isotope in structural material (zirconium) from its natural abundance of 51.5% to 99% in order to decrease its neutron activation in light water reactors; the second paper proposes enrichment of the ^{208}Pb isotope in lead coolant in order to improve the so-called void effect, which plays an important role in providing dynamic nuclear reactor safety.

Proposals for a low-activation coolant based on the ^{206}Pb isotope were made and substantiated at the end of the 90s by the present authors and their colleagues [7-13]. The present paper gives a brief overview of their results and describes how isotopic tailoring can be used to obtain low-activation coolants for FNRs and accelerator driven systems.

1.   MAIN PREREQUISITES AND DEFINITIONS

1.1.   Method for analysing the activity of lead and nuclear reaction products

The FISPACT computer code was used to analyse the activity of lead and the nuclear reaction products resulting from irradiation of lead in the FNR neutron spectrum. The FISPACT-3 version [14] has been widely used for several years to calculate the activation of structural materials in a D-T fusion reactor. The activation of materials is estimated both for fast neutrons where $E_{n\ max}$=14.5 MeV, and for intermediate neutrons with their minimum energy of $E_{n\ min}$≅1 eV. This means that the FISPACT-3 program can also be used to calculate the activation of structural materials for BOR-60 and BN-600 type reactors whose neutron spectra are within the spectral range of a D-T fusion reactor.

The modern EAF-99 [15] and FENDL-2/A [17] activation data libraries were used to carry out calculations in the framework of the FISPACT-3 code. These libraries contain 12 468 excitation functions for nuclear reactions of 766 isotopes induced by neutrons with an energy of up to 20 MeV. We should note that some data from the Russian ADL-3 library [18] are included in the EAF-99 and the FENDL-2/A libraries.

The activity decay of lead and individual nuclear reaction products for cooling periods of up to 10^3 years was calculated on the basis of the data given in the EAF-99 decay data library [16] and the FENDL-2/D library [17]. In all the calculations the specific activity was measured

in SI units: becquerel/kg. The neutron spectrum which was incorporated into the FISPACT-3 program corresponded to the neutron spectrum of a BOR-60 reactor.

The FISPACT-3 program can also be used to calculate the dose rate received by workers or members of the population who come in contact with radioactive material. This was measured in SI dose units: sievert/h.

1.2. Neutron spectra, fluxes and fluences used in the calculations

The neutron spectrum characteristic of the central area of a BOR-60 fast reactor was used in the calculations. The spectrum is in the 20 eV to 14.5 MeV neutron energy range, with a wide maximum in the 0.1 to 2.0 MeV region. In most calculations, the integral neutron flux with energy $E_{n\,min}$ to $E_{n\,max}$ was:

$$\Phi = \int_{E_{n\,min}}^{E_{n\,max}} \Phi(E)dE = 5 \cdot 10^{15} \text{ n/cm}^2\text{/s}.$$

The annual neutron fluence was $F = 1.6 \cdot 10^{23}$ n/cm^2, while the maximum fluence corresponding to an exposure time of 30 years was $F \cong 5 \cdot 10^{24}$ n/cm^2. The calculations were carried out for 1 kg of material. After irradiation, the activity of the material was calculated for cooling periods of 10^{-8} to 10^3 years.

1.3. Isotopic composition of natural lead

Lead is currently considered to be a likely coolant for FNRs and accelerator driven systems. Another candidate is the already well-accepted bismuth-lead eutectic (56% Bi, 44% Pb), which has a lower melting temperature ($t_{melt}=125^o$C) than lead ($t_{melt}=327^o$C). In support of their choice, the advocates of lead point to the abundant world supplies of lead (about 10^8 tons) and its relatively low cost on the world market (about \$1/kg). The neutron and physical characteristics of natural lead are rather favourable for FNRs; the neutron capture cross-sections are about 100 mbarn for intermediate neutrons and about 2-3 mbarn for fast neutrons. The elastic and inelastic neutron scattering cross-sections in natural lead are likewise not large (< 1 barn), which means that natural lead can, on the whole, be considered a low-moderation and low-absorption FNR coolant [19].

Natural lead, which is extracted from galena ores, is a mixture of four stable isotopes: ^{208}Pb, ^{207}Pb, ^{206}Pb and ^{204}Pb. The doubly magic (on account of its number of protons, Z=82, and neutrons, N=26) ^{208}Pb accounts for more than half of this mixture. The isotopic composition of natural lead given in [20] is as follows: $\%^{208}$Pb/^{207}Pb/^{206}Pb/^{202}Pb = 52.4/22.1/24.1/1.4.

1.4. Occupational radiation safety standards for radioactive lead and its transmutation products

The NRB-96 radiation safety standards [21] are a fundamental document regulating the permissible dose limits and levels for the effect of ionizing radiation on workers and the population.

The following are exempt from the NRB-96 regulations:

- radiation generators, provided that the equivalent dose rate at a distance of 0.1 m does not exceed 1.0 µSv/h;

- radiation generators with a radiation energy below 5 keV;

- radioactive substances with a specific or total activity below that subject to regulation.

The specific activity of radioactive substances is measured in Bq/kg, and their total activity in Bq. The levels of specific and total activity in a location at any time, below which radioactive substances are exempt from radiation monitoring, are given in NRB-96.

The most rigorous NRB-96 regulation, which sets a permissible specific activity of no more than $1 \cdot 10^4$ Bq/kg, applies to all alpha and hard gamma ray emitters with an energy of around 1 MeV. These include the radioactive products of lead irradiation: ^{210}Po, ^{207}Po, ^{205}Po, ^{203}Po, ^{206}Bi, ^{207}Bi, ^{208}Bi, ^{210m}Bi and ^{210}Pb.

Highly toxic radioisotopes with a permissible specific activity no greater than $1 \cdot 10^4$ Bq/kg can be divided into ultra-short-lived, short-lived and long-lived nuclides.

The ultra-short-lived include isotopes with $T_{1/2} < 1$ day: ^{202m}Pb, ^{203m}Pb, ^{204m}Pb, ^{207m}Pb, ^{209}Pb, ^{204}Bi, ^{203}Po, ^{205}Po and ^{207}Po.

The short-lived group consists of nuclides with 1 day $< T_{1/2} < 20$ years: ^{205}Bi, ^{206}Bi, ^{208}Po and ^{210}Po.

We will consider nuclides with $T_{1/2} > 20$ years as long-lived isotopes. They include: ^{210}Pb, ^{207}Bi, ^{208}Bi, ^{210m}Bi and ^{209}Po.

It should also be noted that, according to the established standards [21], the permissible equivalent dose rate must not exceed 25 µSv/h for hands-on-recycling or 10 mSv/h for remote recycling of process material.

2. LONG-LIVED RESIDUAL ACTIVITY OF FNR LEAD COOLANT

One of the pressing challenges in materials science today is the development of structural materials for nuclear technology that do not require disposal after 30 years of operation in an accelerator driven system and the subsequent 50 years of cooling. The ideal liquid metal coolant for an advanced FNR must satisfy these conditions as well. Considering that the volume of coolant in one full-size FNR is 10^3 m^3, and that in a favourable world nuclear power industry development scenario 10^2-10^3 FNR units would be required, the volumes of spent FNR coolant in the future could reach 10^5-10^6 m^3, which is equivalent to 10^6-10^7 tons of non-ferrous metal.

Let us now turn to analysis of the residual radioactivity of an FNR lead coolant. Figure 1 shows the results of the decay calculations of natural lead after irradiation in a BOR-60 FNR neutron spectrum for one year and with extension of this period to 30 years. It can be seen that the irradiation time has practically no impact on early coolant activity; in both cases it is high, measuring about $1 \cdot 10^{14}$ Bq/kg. However, after decay to ~$1 \cdot 10^{11}$ Bq/kg, the decay patterns differ considerably. Coolant which has been irradiated for 1 year has an activity of ~$1 \cdot 10^5$ Bq/kg after a cooling period of 100 years, which is close to the specific activity level at which it would be exempt from the NRB regulations. On the other hand, coolant which has been irradiated for 30 years decays significantly more slowly and has an activity of ~$5 \cdot 10^7$ Bq/kg after a cooling period of 100 years. This is linked to the accumulation of stable ^{209}Bi in lead and to the subsequent production of the long-lived radionuclides ^{207}Bi, ^{208}Bi, ^{210}Bi^m and ^{210}Po. The main source of bismuth-209 is the ^{209}Pb nuclide, formed by radioactive capture of a neutron by the nucleus of ^{208}Pb, which makes up more than 52% of the natural lead isotope mixture. Capture of another neutron can transform ^{209}Pb into the ^{210}Pb radioisotope but this process is less likely to occur than beta decay of ^{209}Pb. As a result, extended FNR operation can lead to the production and accumulation of the stable ^{209}Bi isotope in its lead coolant. The rate at which bismuth is produced in 1 kg of natural lead, calculated using the FISPACT-3 code for a BOR-60 reactor, is shown in Fig. 2. It can be seen that it is about 0.1 g/kg/year, and hence after only 10-30 years, 1-3 grams of ^{209}Bi per 1 kg of natural lead accumulates in an FNR.

As a comparison, we would like to point out that the bismuth-209 admixture in C00 lead, which is to be used in the BREST reactor, does not exceed 0.5 g/kg. If no provision is made for impurity extraction from the coolant during operation, bismuth-209 and its associated radionuclides accumulate in proportion to the time lead is used in the FNR. The results of the calculations on bismuth-209 production from irradiation of individual lead isotopes in the reactor are also given in Fig. 2. In coolant composed entirely of lead-206, 10^4 times less bismuth-209 is produced than in natural lead.

Bismuth-209 eventually leads to the accumulation in lead of such isotopes as ^{207}Bi and ^{208}Bi through the (n,2n) and (n,3n) reactions. Figures 3 and 4 show the induced activity of ^{207}Bi and ^{208}Bi for up to 30 years of irradiation in the BOR-60 FNR. Both of these radionuclides are long-lived and quite dangerous. The half-life of ^{207}Bi is 31.55 years, and its gamma radiation energy is 1.5 MeV. The ^{208}Bi radionuclide has a very long half-life ($T_{\frac{1}{2}}$=3.68$\cdot 10^5$ years) and gamma radiation energy of up to 2.7 MeV. The radiation safety standards establish that the permissible specific activity of ^{207}Bi and ^{208}Bi must not exceed $1 \cdot 10^4$ Bq/kg on account of their

high radiotoxicity. As can be seen from Figs 3 and 4, these permissible radioactivity levels are reached within as little as 2 years of natural lead irradiation in an FNR, and after 30 years of irradiation in the reactor, they are exceeded several-fold. In the [206]Pb isotope, [207]Bi and [208]Bi production occurs much more slowly and their activity remains below the permissible $A < 1 \cdot 10^4$ Bq/kg even after 30 years of irradiation in an FNR.

The alpha-active [210]Po isotope is another dangerous radionuclide produced in lead. Its production is also linked to the accumulation of bismuth in lead. As is seen in Fig. 5, the specific activity of [210]Po reaches the very high level of $A = 1 \cdot 10^{11}$ Bq/kg after prolonged irradiation in an FNR. So much [210]Po is produced in natural lead that, despite its relatively short half-life of $T_{1/2} = 138$ days, spent lead achieves clearance from radiation monitoring of the polonium-210 radionuclide only after 100 years. On the other hand, if the [206]Pb isotope is used instead of natural lead, [210]Po activity decreases by 4 orders of magnitude and this type of coolant achieves clearance from polonium-210 monitoring within only 2 to 3 years of decommissioning.

24-hour release in curies ($1 \text{ Ci} = 3.7 \cdot 10^{10}$ Bq) and the relative hazard posed by radionuclides in a beyond-the-design accident in a BREST-type reactor [22]

	Radionuclides						
	Zn	As	Cd	I	Cs	Hg	Po
Release, curie	500	300	100	60	100	1200	3
Relative hazard	0.1	0.044	0.006	0.16	0.08	0.2	0.4

Polonium accumulation is fraught with special danger in the event of a so-called beyond-the-design accident in an FNR involving rupture of the reactor vessel and containment. The potential radiological hazard of the polonium released each day as a result of a beyond-the-design accident is assessed in [22]. These data are given in the Table.

The release of radioactivity given corresponds to level 5 on the International Nuclear Event Scale for nuclear power plants - accidents with an environmental risk, and the radiotoxicity of the 3-curie release of polonium-210 is approximately equivalent to the total hazard posed by all the other radionuclides entering the coolant as a result of leaking fuel elements. As follows from Fig. 5, enrichment of the lead-206 isotope in the coolant would lead to a drop in [210]Po activity to $5 \cdot 10^6$ Bq/kg and would allow for a serious beyond-the-design accident with a release of radionuclides into the atmosphere to be classified as a nuclear power plant event with a lower environmental risk.

Figure 6 shows the radiotoxicity of 1 kg of irradiated natural lead and individual lead isotopes caused only by the gamma activity of the radionuclides produced in the course of 30 years. The radiotoxicity is expressed in dose equivalent rate units (Sv/h); the toxicity limits for hands-on (25 µSv/h) and remote (10 mSv/h) material processing are indicated. It can be seen that spent coolant made of lead-206 can be processed manually only one year after decommissioning, while coolant made of natural lead can only undergo remote processing and then only 100 years after it has been unloaded from the reactor.

3. TARGET WITH LOW POLONIUM AND BISMUTH YIELD FOR AN ACCELERATOR DRIVING A SUBCRITICAL FAST NEUTRON REACTOR

Lead is currently considered one of the most likely materials for the targets of powerful proton accelerators which create an additional neutron "intensification" for subcritical FNRs. It is planned to use lead as a coolant removing the scattered power of the beam, P=10-20 MW, as well as an efficient convertor of accelerated protons into fast neutrons with a particle conversion coefficient of K=20-30 neutrons/protons. Activation of such a target is caused by nuclear disintegration by high-energy protons, by fission of lead nuclei induced by secondary fast neutrons, by radiative neutron capture (n,γ), and by proton and neutron reactions of the (p,xn) and (n,xn) type, and others. A wide spectrum of secondary nuclides with masses ranging from m=3 to m=210 are formed. This could include long-lived alpha emitters (^{210}Po, ^{210m}Bi, ^{210}Pb) and emitters of hard gamma rays (^{207}Bi, ^{208}Bi).

The calculations of the activation of a proton accelerator lead target were carried out using the SNT program [23]. The program can be used to calculate nuclide production in lead which is placed in neutron and proton spectra. The proton reaction cross-sections for proton energies up to 100 MeV were taken from the MENDL library, and the neutron reaction cross-sections at neutron energies up to 150 MeV from the IAEF-99 library. The proton and neutron spectra corresponded to beam dissipation at a proton energy of E=0.8 GeV and a current of I=30 mA in a lead target with a diameter of D=0.5 m and length of L=1.0 m. The irradiation time was chosen as T=1 year. The total activity of the target is the sum of the activities of the large number of radionuclides produced, including ^{3}H, ^{194}Au, ^{194}Hg, ^{193}Pt, ^{205}Pb, ^{202}Pb, ^{204}Tl, and others. However, there are only a few radionuclides, chiefly ^{202}Tl, ^{207}Bi, ^{195}Au and ^{208}Bi, which are the main contributors to the overall gamma toxicity of a natural lead target. All the other radioisotopes are characterized either by a low level of gamma toxicity or by a complete lack of gamma toxicity, as is the case, for example, with the lead isotopes ^{202}Pb and ^{205}Pb with low-energy beta radiation. The time dependence of the residual gamma toxicity of a natural lead target is shown in Fig. 7. It can be seen that for a cooling period of up to 1 year the toxicity of the target is mainly determined by the gamma activity of the ^{202}Tl radionuclide, and in the following 200-300 years the main contribution to toxicity is made by ^{207}Bi.

In addition to the aforementioned channel of ^{207}Bi isotope production through the ^{209}Bi(n,3n)^{207}Bi reaction, there is a new channel for generating this radionuclide in a lead target irradiated by fast protons based on a reaction with proton participation: ^{208}Pb(p,2n)^{207}Bi. In the proton-neutron spectrum of the lead target of an accelerator driven device, ^{207}Bi production is mainly due to the (p,xn) reaction. Hence, the specific activity of ^{207}Bi is of the order 1·10^{10} Bq/kg and significantly exceeds the specific activity of the ^{210}Po produced, which is A=5·10^{7} Bq/kg. In natural lead targets, therefore, the problem of gamma-toxic ^{207}Bi accumulation can be more significant than the accumulation of alpha-toxic ^{210}Po [7, 9].

It follows from the above that in the targets of accelerator driven devices, as in FNR coolants, the heavy lead ^{208}Pb isotope is the main source of the most dangerous isotopes in natural lead. Removing it, with enrichment of the lead with lighter isotopes, especially ^{206}Pb, can lead to a decrease in the induced radiotoxicity. Figure 8 shows the time dependencies of the alpha activity of a number of polonium isotopes in a target made of natural lead and of ^{206}Pb. It

can be seen that the natural lead target achieves clearance from radiation monitoring of polonium radionuclides only 20-30 years after irradiation, whereas the target enriched with [206]Pb achieves clearance from radiation monitoring of polonium-210 more or less straight away after the beam is switched off.

4.   COST OF LEAD COOLANT WITH ISOTOPIC ENRICHMENT

The main criterion in favour of using enriched lead-206 in FNRs is that the total cost of the coolant starting with the cost of obtaining it, the cost of maintaining its quality, and, finally, the cost of its removal and the elimination of radwaste, which includes temporary storage, transport and, possibly, disposal - is economical.

Let us determine the maximum acceptable cost of coolant material for an FNR and say the overall cost of the coolant should be no more than 20% of the capital costs of a nuclear power plant. Assuming a capital cost per unit of power of $2 million/MW(e), the cost of a BREST-300 type power reactor is about $600 million. The maximum possible cost of a coolant in this scenario is then $120 million. Let us also assume that the FNR under consideration has the minimum necessary amount of coolant. As shown in [24], in an average reactor, designed correctly in terms of coolant minimization, the required amount of coolant is 0.7 t/MW(th). Thus, the minimum quantity of coolant in an FNR with a thermal power of 700 MW is 500 tons, and the corresponding highest acceptable cost of coolant material would be of the order of $240/kg. Thus, the cost of lead-206 product with 90% enrichment should not exceed $240/kg and, in this case, enriched lead-206 may be used as a low-activated material for coolants in advanced nuclear power facilities.

The current price of lead-206 product with 90% enrichment is about $10 thousand/kg. This is determined by the cost of separating lead in a cascade of gas centrifuges and by the costs for maintenance and renewal of the centrifuges. In the long run, the cost of the isotope separation process could be significantly reduced by operating the centrifuge in a mode with an input of excess process gas and an output of gas with a relatively high amount of the required isotope. Such an operating mode of the centrifuge is economical, provided that the cost of the feed is low and the abundance of the required isotope in the initial isotope mixture is high. Natural lead meets these requirements since it does not cost more than $1/kg, and its natural abundance of lead-206 is 24%.

The economics and expediency of using lead-206 as a coolant require further detailed calculations and investigation. If using materials with a modified initial isotopic composition becomes acceptable for nuclear technology, then tons of such material could be obtained using the large separative capacities already developed for uranium enrichment. Thus, for example, the Urenco consortium (Great Britain), with a separative capacity of $5 \cdot 10^6$ separative work units per year, has an annual production potential of lead-206 with 90% enrichment of 500 tons.

We note it is recommended that next-generation reactors be designed in such a way as to reduce the costs of radwaste disposal after a reactor is decommissioned. Currently, the cost of radwaste disposal, including temporary storage, packaging, transport and burial, is $20/kg [25]. At these prices, the disposal of sodium coolant (800 t) and reactor vessel materials (3800 t) from the BN-600 FNR (Zarechnyi) costs $90 million. On the other hand, for an FNR with the same

capacity but with lead coolant, which is 11.7 times heavier than sodium coolant, the cost of storage and disposal alone would require up to $200 million, which is commensurable with the cost given above for obtaining low-activation lead coolant enriched in the lead-206 isotope.

CONCLUSION

Under the Strategy for the Development of Russia's Nuclear Power Industry [1], it is envisaged to start using a heavy liquid metal coolant, presumably, lead, in future advanced fast reactors. It is recommended that next-generation reactors include design solutions to reduce the cost of radwaste disposal after a reactor is decommissioned. In fast reactors radwaste can be formed due to nuclear fuel combustion and neutron activation of coolant and structural materials. The cost of the disposal of large amounts of activated material can reach hundreds of millions of dollars.

Our goal was to predict the activation of chemically-pure natural lead, which is a mixture of stable lead isotopes, after prolonged use in fast reactors and targets of accelerator driven devices. We also aimed to indicate possible ways of reducing coolant activation in future nuclear power facilities.

The calculations we carried out show that prolonged use of natural lead in a fast reactor, for 10 to 30 years, leads to the production of 1 to 3 g of the stable bismuth isotope ^{209}Bi in it per 1 kg of lead, due to neutron radiative capture by the ^{208}Pb nucleus and the subsequent beta decay of the ^{209}Pb nucleus.

The bismuth produced is the source of the alpha-active isotopes ^{207}Po and ^{210m}Bi, as well as the long-lived gamma-active isotopes ^{207}Bi and ^{208}Bi. The production of ^{210}Po poses a particular hazard since, in case of an accident with rupture of the reactor vessel and a release of nuclides into the atmosphere, its radiotoxicity is equivalent to the harmful effects of all the other radionuclides put together, including ^{131}I and ^{137}Cs. After 30 years of operation the coolant achieves clearance from radiation monitoring of ^{210}Po only after a cooling period of 100 years. Several hundred years of cooling would be required for another radionuclide, ^{207}Bi, to decay to a safe level.

In accelerator driven devices, nuclear reactions involving protons are an additional channel for the production of ^{207}Bi and ^{208}Bi in lead targets which are irradiated by fast protons. These reactions make such a significant contribution that ^{207}Bi accumulation can be regarded as a problem in targets made of natural lead for accelerator driven subcritical fast reactors.

Thus, despite the widespread view that lead is a low activation material, after prolonged use in fast reactors and accelerator driven devices, it would require a cooling period of many years and, possibly, disposal. Taking into account the fact that the amount of lead coolant in large nuclear power facilities can be as much as several thousand tons, it is potentially very harmful in view of its induced activity as well as the prospect of the removal of a large amount of non-ferrous metal.

The analysis carried out has shown that the heavy lead isotope ^{208}Pb, which comprises 52.4% of the natural lead isotope mixture, is the main source of the production of radiotoxic polonium and bismuth isotopes. Depletion of this heavy isotope in natural lead would mean that a coolant could be obtained with a fast rate of radioactive decay which does not require lengthy cooling and disposal.

In view of the practical difficulties involved in extracting bismuth and polonium from lead while the coolant is in operation, we considered the possibility of reducing its activation by changing lead's initial isotopic content. The calculations we carried out show that high enrichment of natural lead in ^{206}Pb, which has an abundance of 24.1% of the natural lead isotope mixture, leads to a substantial reduction in polonium and bismuth radionuclide production and that a coolant of this type achieves clearance from radiation monitoring significantly earlier than natural lead.

In this way, enrichment of ^{206}Pb in a lead coolant would eliminate or ease the problem of the radwaste generated by nuclear power facilities. At the same time, the cost of lead enrichment must be commensurable with the cost of storage, processing, transport and possible disposal of radwaste.

The technology for separating lead isotopes has been developed in Russia, which has one third of the world's uranium enrichment capability using gas centrifuge cascades. Gaseous lead compounds exist and have been tested. A technique for obtaining kilogram quantities of lead isotopes has been developed. The current high cost of lead-206 product with 90% enrichment, which is about $10 000/kg, could be reduced several-fold if there was a large increase in demand for isotopic production and improvements in technology.
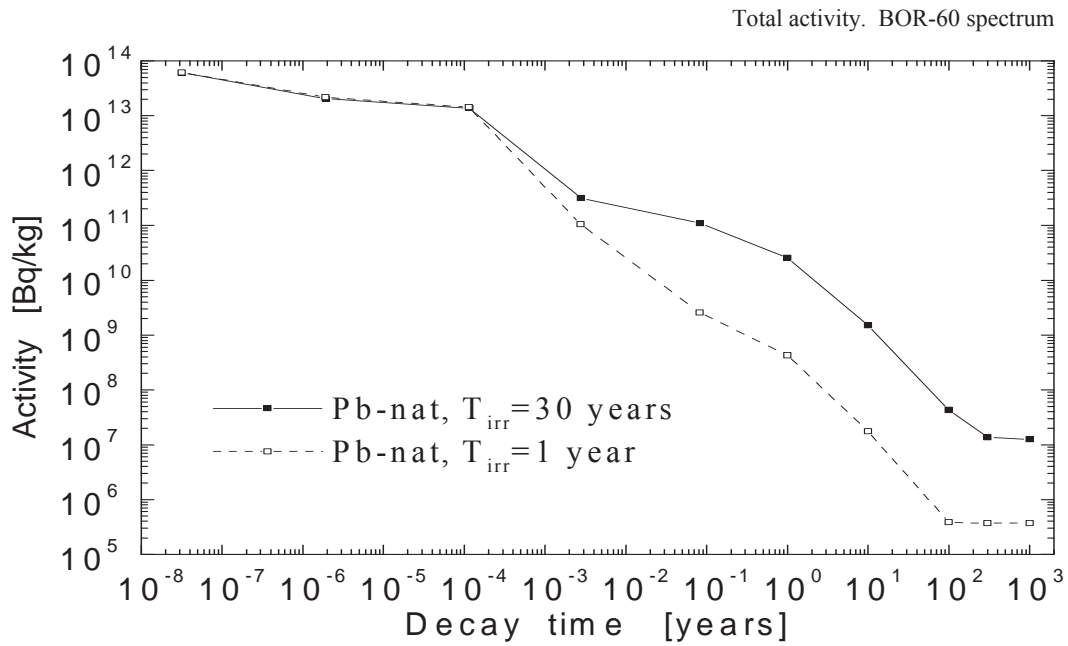
Total activity. BOR-60 spectrum

Fig. 1. Total specific activity decay (Bq/kg) of natural lead after irradiation in an FNR core for 1 year (dotted line) and 30 years (continuous line).

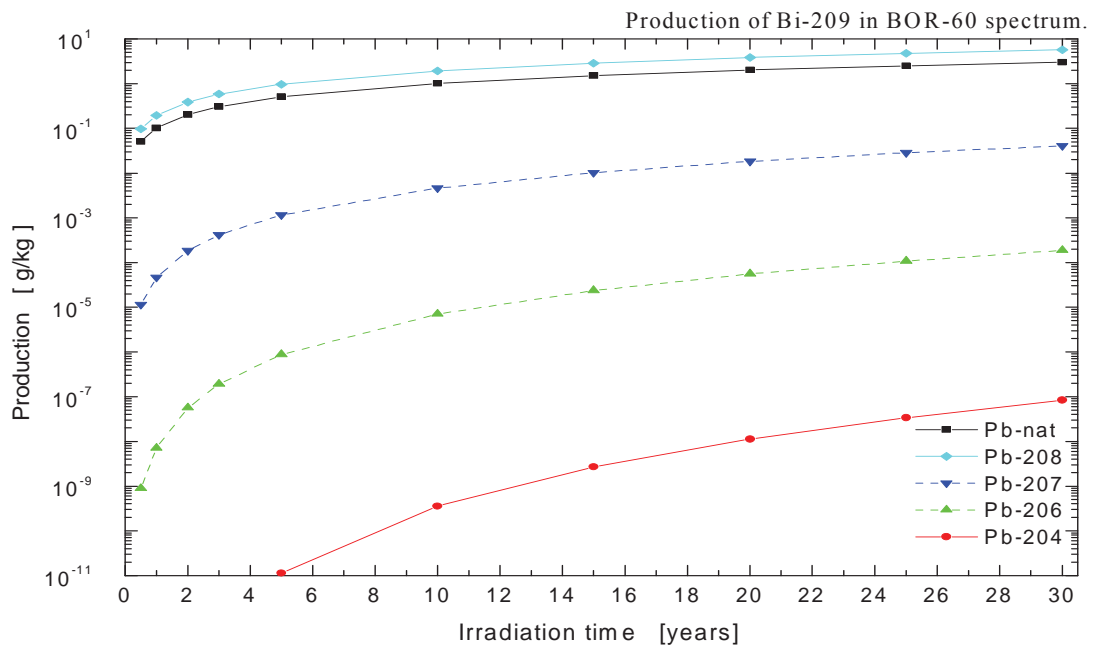Production of Bi-209 in BOR-60 spectrum.

Fig. 2. Amount of stable bismuth-209 (g/kg) produced in natural and enriched lead during irradiation in an FNR core.

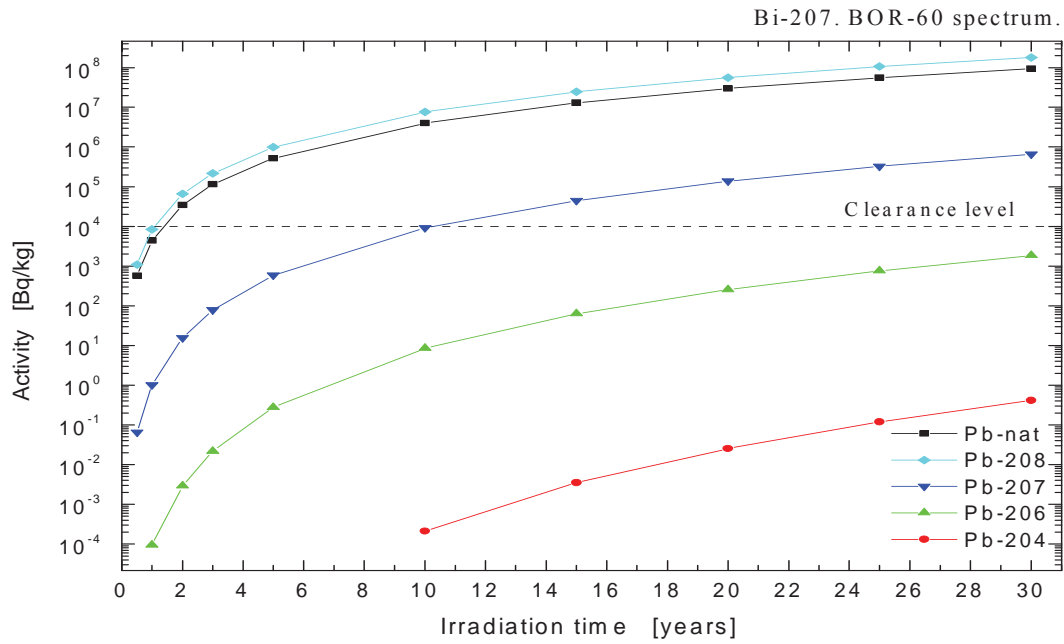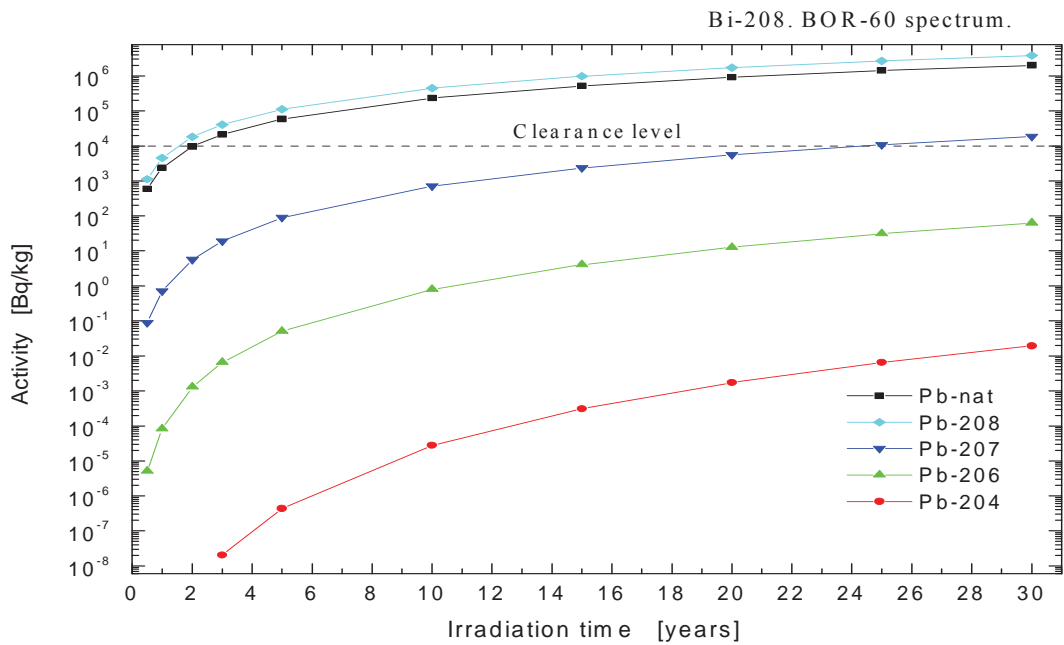Fig. 3. Specific activity of bismuth-207 (Bq/kg) induced in natural and enriched lead during irradiation in an FNR core. Dotted line - clearance level of a substance from radiation monitoring.

Fig. 4. Specific activity of bismuth-208 (Bq/kg) induced in natural and enriched lead during irradiation in an FNR core.
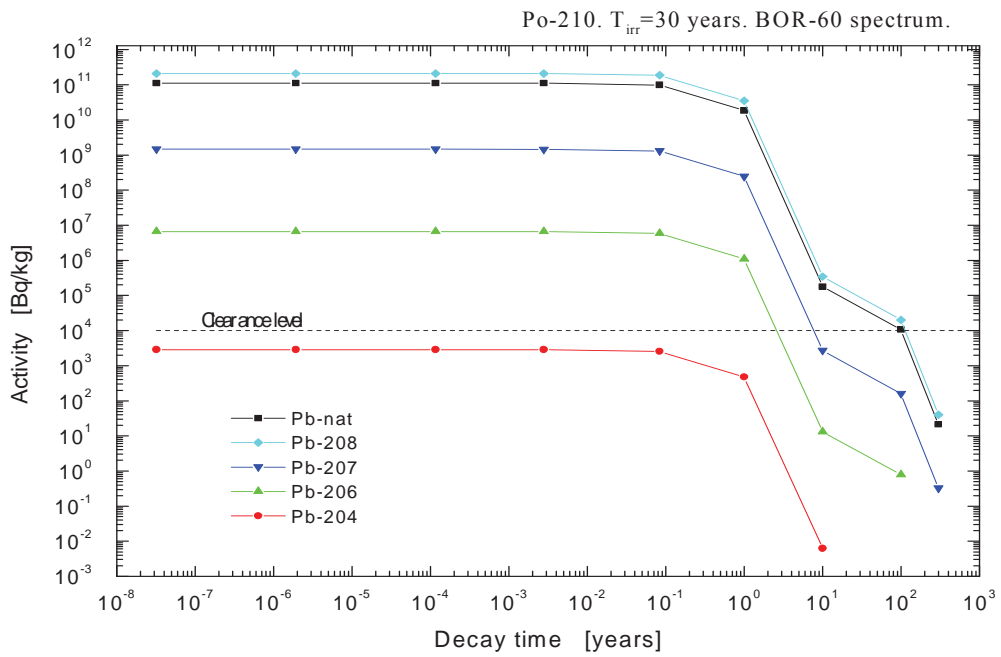
Po-210. T_{irr}=30 years. BOR-60 spectrum.

Fig. 5. Specific activity decay of polonium-210 (Bq/kg) induced in natural and enriched lead after irradiation in an FNR core for 30 years.
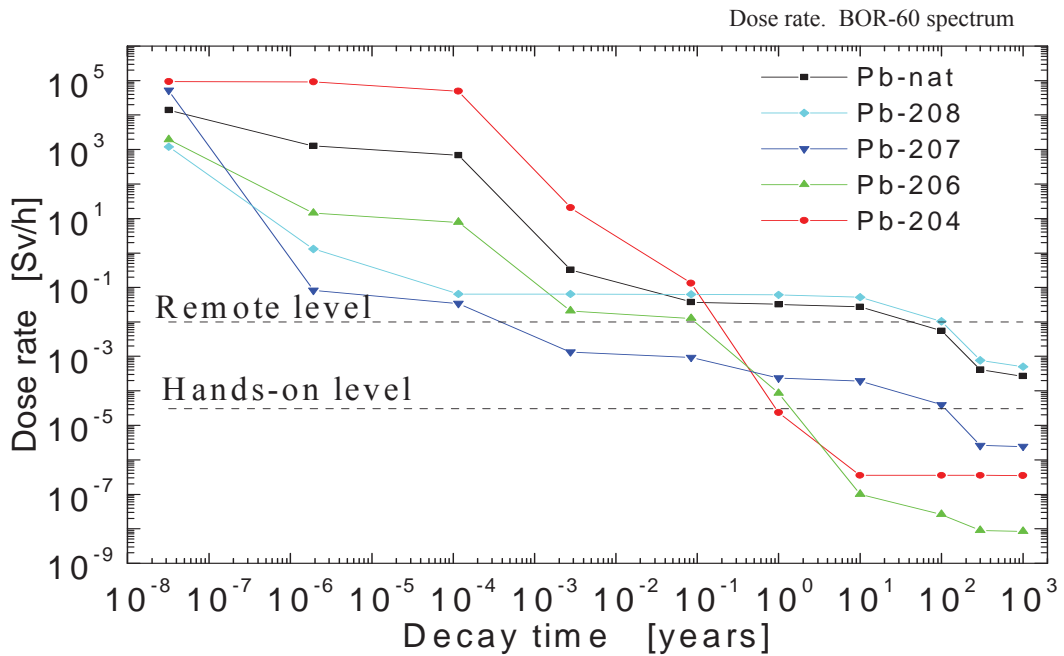
Dose rate. BOR-60 spectrum

Fig. 6. Decay of total dose rates (Sv/h) generated by 1 kg sources of natural and enriched lead after irradiation in an FNR core for 30 years. Dotted line - permissible dose rate limits for hands-on (lower line) and remote (upper line) processing.
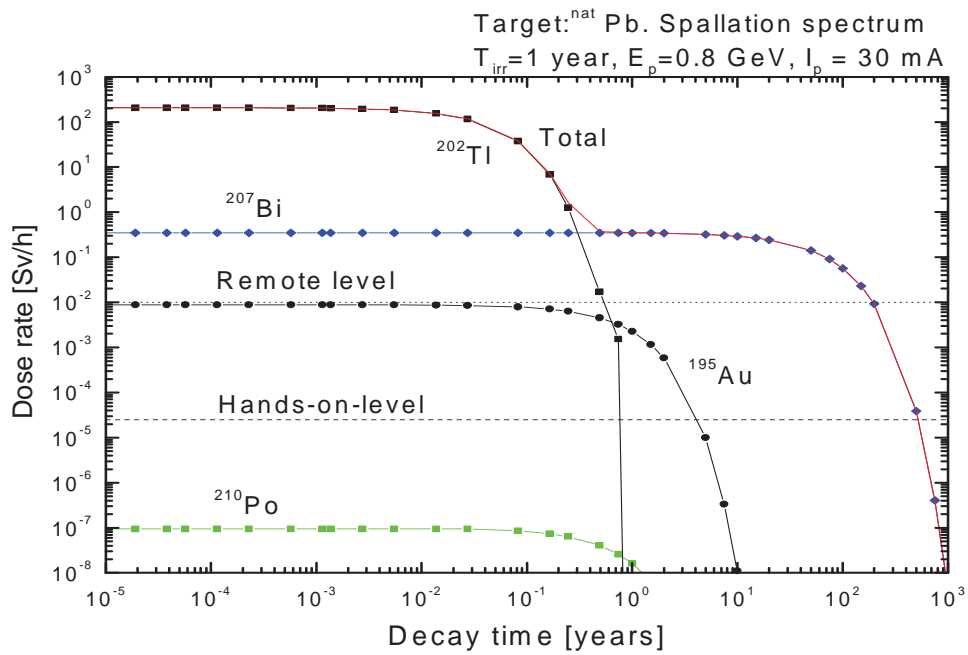
Fig. 7.   Decay of total dose rate and its main components (Sv/h) generated by a 1 kg source of natural lead after irradiation for 1 year by a proton beam with an energy of 0.8 GeV and a current of 30 μA.
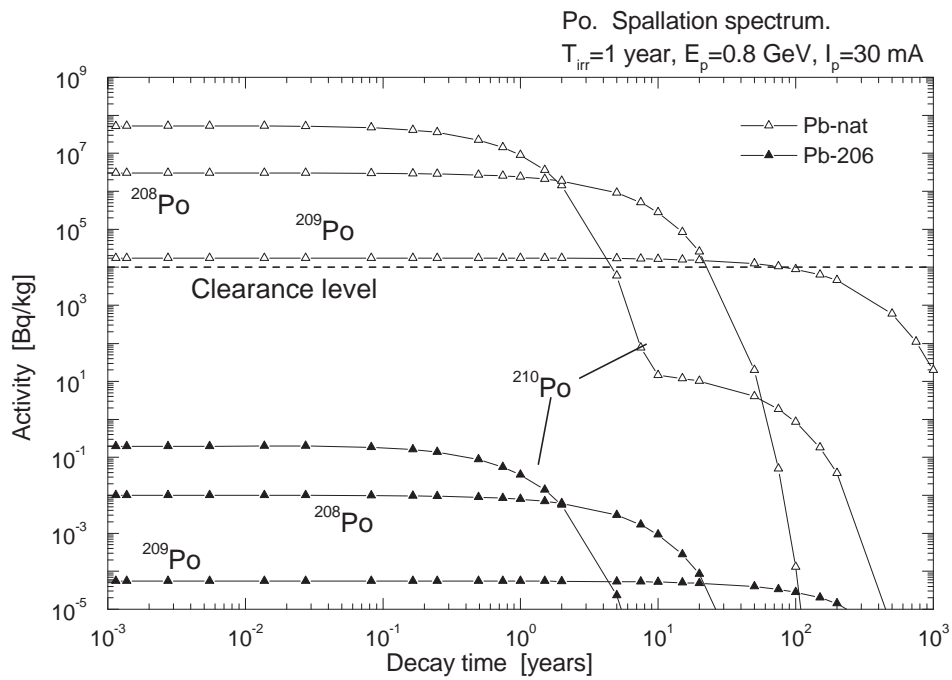

Fig. 8.   Specific activity decay for polonium-210, -209, -208 (Bq/kg) induced in natural lead and lead-206 after irradiation for 1 year by a proton beam with an energy of 0.7 GeV and a current of 30 μA.

REFERENCES

1. Strategy for the development of Russia's nuclear power industry in the first half of the 21st century. Bulletin of the Public Information Centre, Central Research Institute of Management, Economics and Information, Moscow, 2000, No. 6, pp 4-7 [in Russian].

2. Usanov V.I. et al., Dolgozhivushchie radionuklidy natrievogo, svintsovo-vismutovogo: svintsovogo teplonositelei v bystrykh reaktorakh. Atomnaya ehnergiya, 1999, v. 87, No. 3, pp 204-210.

3. Golovin I.N., Kadomtsev B.B., Sostoyanyie i perespektivy upravlyaemogo termoyadernogo sinteza. Atomnaya ehnergiya, 1996, v. 81, No. 5, pp 364-372.

4. Lyakishev N.P. et al., Prospect of development and manufacturing of low activation metallic materials for fusion reactor. Journal of Nuclear Materials, 1996, v. 233-237, pp 1516-1522.

5. Apseh V.A. et al., Otsenka snizheniya aktivatsii tsirkoniya v legkovodnykh reaktorakh putem izmeneniya ego nachal'nogo izotopnogo sostava. Izvestiya vuzov. Yadernaya ehnergetika, 1997, No. 5, pp 30-35.

6. Shmelev A.N. et al., Bezopasnost' bystrogo reaktora-vyzhigatelya dolgozhivushchikh aktinoidov, izvlechyonnykh iz radioaktivnykh okthodov. Atomnaya ehnergiya, 1992, v. 73, pp 450-454.

7. Khorasanov G.L. et al., Lead and tin targets for reducing polonium waste. In: Proceedings of the Int. Conf. on Accelerator Driven Transmutation Technology and Applications ADTTA '99, June 7-11, 1999, Prague, Czech Republic, Paper #Tu-O-E8.

8. Khorasanov G.L. et al., Low-activation materials with isotopic tailoring for future NPPs. In: Proceedings of the Int. Conf. on Future Nuclear Systems GLOBAL '99, Aug. 29–Sept. 2, 1999, Jackson Hole, Wyoming, USA, Paper #345.

9. Khorasanov G.L. et al., Bi-207 accumulation problem in lead targets for ADS. In: Proceedings of the Int. Conf. on Accelerator Breeder Systems and Advanced Nuclear Power Industry, 12-14 October, 1999, Moscow, Institute for Theoretical and Experimental Physics, pp 200-203 [in Russian].

10. Khorasanov G.L. et al., Low-activation coolant based on the lead-206 isotope for advanced accelerator breeders. In: Proceedings of the 4th All-Russia (International) Scientific Conference "Physical and chemical processes for the selection of atoms and molecules", 4-8 October, 1999, Zvenigorod, Moscow: Central Research Institute of Management, Economics, 1999, pp 262-267 [in Russian].

11. Khorasanov G.L. et al., High-enriched lead-206 for small nuclear power industry. In: Proceedings of the 5th All-Russia (International) Science Conference "Physical and chemical processes for selection of atoms and molecules", 2-6 October, 2000, Zvenigorod; Moscow: Central Research Institute of Management, Economics and Information, pp 186-189 [in Russian].

12. Khorasanov G.L. et al., Molten lead enriched with isotope Pb-206 as a low-activation coolant for emerging nuclear power systems. In: Proceedings of the 8th Int. Conf. on Nuclear Engineering ICONE-8, April 2-6, 2000, Baltimore, Maryland, Paper #ICONE‑8385.

13. Khorasanov G.L. et al., High enriched lead-206 for small nuclear power plants. In: Proc. of the 9th Int. Conf. on Nuclear Engineering ICONE-9, April 8-12, 2001, Nice, France, Paper #359.

14. Forrest R.A., Sublet J-Ch., FISPACT-3 user manual. Report AEA/FUS/227, 1993.

15. Sublet J-Ch., Kopecky J. and Forrest R.A., The European Activation File: EAF-99 cross section library. EASY Documentation Series UKAEA FUS 408 (1999). EURATOM/UKAEA Fusion Association, Culham Science Centre, Abingdon, Oxfordshire, OX14 3DB, UK.

16. Forrest R.A., Sublet J-Ch., The European Activation File: EAF-99 decay data library. EASY Documentation Series UKAEA FUS 409 (1999). EURATOM/UKAEA Fusion Association, Culham Science Centre, Abingdon, Oxfordshire, OX14 3DB, UK.

17. Pashchenko A.B., Summary report on the IAEA advisory group meeting on completion of FENDL-1 and start of FENDL-2, Del-Mar, USA, 1995. Report IAEA/INDC(NDS)‑352, 1996.

18. Grudzevich O.T. et al., ADL-3 library catalogue. Voprosy atomnojnauki i tekhniki. Ser.: Yadernye konstanty, 1993, No. 3-4, pp 3-180.

19. Table of simple integral neutron cross section data from JEF-2.2, ENDF/B-VI, JENDL-3.2, BROND-2 and CENDL-2. JEF Report 14, NEA OECD, Paris, France, 1994, p. 235.

20. Golashvili T.V. et al., Handbook on nuclides. Moscow, Central Research Institute of Management, Economics and Information, 1995, p. 440 [in Russian].

21. Radiation Safety Standards (NRB-96). Hygiene regulations. Moscow, Information and Publishing Centre of the State Committee of the Russian Federation for Epidemiology Control, 1996, p. 127 [in Russian].

22. Orlov V.V. et al., Deterministic safety of BREST reactors. In collected papers: Heavy liquid metal coolants in nuclear technologies, Obninsk. Institute for Physics and Power Engineering, National Research Centre of the Russian Federation, 1999, vol. 2, pp 440-449.

23. Korovin U.A. et al., Programma dlya rascheta izotopnogo sostava i navedennoi aktivnosti obluchennykh materialov. Voprosy atomnoj nauki i tekhiki. Ser.: Yadernye konstanty, 1992, No. 3-4, pp 117-121.

24. Grigor'ev O.G. et al., Demand for bismuth in serial use of the SVBR-75 nuclear facility to solve different tasks. In collected papers: Heavy liquid metal coolants in nuclear technology, Obninsk: Institute for Physics and Power Engineering, National Research Centre of the Russian Federation, 1999, v. 2, pp 556-563.

25. The NEA Co-operative Program on Decommissioning. OECD, Paris, 1996.